# Design, Analysis and Development of Photovoltaic and Concentrating Photovoltaic Cooling Systems with Earth Water/Air Heat Exchanger

**THESIS**

Submitted in partial fulfilment of the requirements for the degree of

**DOCTOR OF PHILOSOPHY**

by

**SANJEEV JAKHAR**

**ID NO. 2013PHXF0002P**

Under the Supervision of

**Dr. MANOJ KUMAR SONI**


BITS Pilani
Pilani | Dubai | Goa | Hyderabad

**BIRLA INSTITUTE OF TECHNOLOGY & SCIENCE**

**PILANI-333031 (RAJASTHAN) INDIA**

**2017**

***Dedicated***

*to*

***my parents and my wife***

Birla Institute of Technology & Science, Pilani
Pilani Campus

# CERTIFICATE

This is to certify that the thesis entitled **"Design, Analysis and Development of Photovoltaic and Concentrating Photovoltaic Cooling Systems with Earth Water/Air Heat Exchanger"** submitted by **Sanjeev Jakhar,** ID. No. **2013PHXF0002P** for award of Ph.D. degree of the Institute embodies original work done by him under my supervision.

Signature (Supervisor):_____

**Dr. Manoj Kumar Soni**

Assistant Professor, Department of Mechanical Engineering,

BITS Pilani, Pilani campus

Date: May 16, 2018

# ACKNOWLEDGEMENT

First and foremost, I praise God, the almighty for providing me this opportunity and granting me the capability to proceed successfully and with his blessings, only I have accomplished this huge task.

I offer respectful obeisance unto the lotus feet of **Dr. Manoj Kumar Soni** for all their valuable guidance, excellent direction, everlasting encouragement and inspiration given to me without which the present work would not have been possible. It was indeed my privilege to work under the supervision of him. I feel indebted to him for not only teaching me each and every aspect of the art of doing research, but also other important aspects of life. Their kindness and patience have really given me courage and assurance and their friendliness has given me hope during the difficult time I faced.

I am grateful to **Prof. Souvik Bhattacharyya,** Vice-Chancellor and **Prof. B. N. Jain**, Ex-Vice-Chancellor, BITS Pilani, **Prof. A. K. Sarkar,** Director and **Prof. G. Raghurama**, Former-Director, BITS Pilani, Pilani Campus for permitting me to pursue my research work at the Institute. I also express my sincere thanks to **Prof. S. K. Verma**, Dean, Academic Research Division (ARD) and **Dr. Hemant R. Jadhav**, Associate Dean, ARD for their motivation, constant support and encouragement.

I am highly indebted to my Doctoral approval committee (DAC) members **Dr. Hitesh Dutt Mathur,** Associate Professor, Department of Electrical and Electronics Engineering, Pilani Campus and **Dr. Pratik N Sheth,** Assistant Professor, Department of Chemical Engineering, Pilani Campus for fruitful discussions and suggestions and sparing their time for evaluation of this thesis. I would also like to acknowledge **Dr. Srikanta Routroy**, Convener, Departmental Research Committee, Associate Professor, Mechanical Engineering Department, Pilani Campus who has provided valuable comments during the departmental seminars.

I would also like to express my gratitude and thanks to **Prof. K. S. Sangwan**, Faculty-in-charge BITS workshop and **Dr. Anshuman**, Unit Chief, Estate Management who provided extraordinary support for fabrication and installation of experimental set-up, without this, the dream of developing the experimental set-up would not have come true. I thank **Prof. P. Srinivasan**, (Head of Department) and entire faculty and staff of Department of Mechanical Engineering, BITS-Pilani, Pilani Campus for their kind moral support and assistance.

I am also thankful to **Prof. (Dr.) Christoph Hermann** and **Dr. Gerrit Posselt**, TU Braunschweig and **Prof. (Dr.) Robert F. Boehm** Distinguished professor and Director of the Center for Energy Research, University of Nevada, Las Vegas, USA who invited me to their university and given me the opportunity to work as visiting scholar. I am also indebt to DST for giving me the prestigious fellowship for my research visit.

My gratitude knows no bounds for **Mr. Nikhil Gakkhar** (Scientist-B, Ministry of New and Renewable Energy, Govt. of India) and **Mr. Nilesh Purohit** for their unstinting guidance, many valuable suggestions and kind help at various stages of the work. I cherish all the moments spent with my friends and highly talented Research Scholars, **Mr. Vikrant Bhakar, Dr. Yogesh K. Bhateshvar, Mr. Narpat ram Sangwa, Mr. Kailash Choudhary, Ms. Nitesh Sihag, Mr. Kapil Choudhary, Mr. Sorabh Sharma, Mr. Pankaj Munjal and Mr. Tridev Mishra.** I have learnt a lot from each and everyone. I thank them for always there for me and making my time memorable in BITS Pilani. I wish them very bright future. I also thank the non-teaching staff **Mr. Ramu Saini**, **Mr. Bhim Singh**, **Mr. Parvat Singh, Mr. Dhanna Ram and Mr. Mahender Saini** for their valuable help at each stage of the experimental work. My sincere thank to all those persons whom I miss to acknowledge, who had directly or indirectly helped me to accomplish this task.

Last but not the least, I would like to thank my family; to my father, **Late Shri Om prakash Jakhar** and mother, **Ms. Bimla Devi**. I also thank my uncle **Mr. Keshar Dev Jakhar** and aunt **Ms. Shanti Devi**. I am deeply indebted to all the pains taken by them to make my dream come true. Thank you for giving me the confidence and courage to make the choices I have made. I would also thank my parents-in law. My sincere thank to my loving brothers and sister, **Mr. Prem Kumar, Mr. Manohar Lal** and **Ms. Chhavi Jakhar**. Their constant love and care empowered me to accomplish my thesis and also ignited me to take more challenges in my life. My words fail to express my gratitude and appreciation to my wife **Mrs. Santosh Thory** for all that she silently endured during the difficult times and way she always supported me and stood by my side. I also wish to thank my son **Mr. Manav Jakhar** for his love, affection and unending patience during the duration of this work.

Sanjeev Jakhar

May 2018

# ABSTRACT

The world's energy consumption is increasing day by day and with increase in demand, the generation is also increasing. Most of the energy generated from conventional sources of energy like fossil fuels, etc. With constant consumption of these non renewable energy sources, these will be depleted within few decades. Further with the use of these fuels, the environmental issues like global warming are also increasing. Thus, to tackle such problems, there is a dire need to use alternative sources like renewable energy sources. Among all the available renewable sources, solar energy is abundantly available. This solar energy can easily be converted directly into electricity by using photovoltaic (PV) and concentrating photovoltaic (CPV) systems. However, the main drawback of such systems is that with increase in temperature, their efficiency decreases. The PV and CPV cells will also exhibit long-term degradation, if the temperature exceeds a certain limit, and the life-span would reduce rapidly. Hence, a suitable cooling technology is required for such systems to achieve better performance.

In the present study, a novel geothermal based cooling technology is developed for the cooling of PV and CPV system, which are named as earth water heat exchanger (EWHE) and earth air heat exchanger (EAHE). For the development of such technology, the simulations were carried out in TRNSYS by coupling EWHE with unglazed PV panels. The simulation results showed that the performance of the coupled (unglazed PV/T+ EWHE) system hardly depends on the EWHE pipe material and pipe diameter. Thus, instead of using expensive galvanized iron (GI) and steel pipes, cheaper pipe material like high-density polyethylene (HDPE) could be used with smaller diameters, like 12 mm, to achieve optimum performance. Following this, the system design was carried out for CPV/T system coupled with EWHE and was compared with existing literature. The comparative study showed that EWHE could be used for CPV/T cooling instead of conventional cooling systems. The simulations were also carried out in TRNSYS for climatic conditions of Pilani, Rajasthan which gave the results that such system could be used for lower concentrations, like 6 Suns.

Further simulation studies were carried out on glazed PV/T systems with EWHE cooling by developing one dimensional mathematical model using MATLAB vR12a. The analytical models were developed for two types of glazed PV/T systems i.e. tube-and-sheet and broad water channel. To validate these two models, two experimental set-ups were developed along with EWHE cooling. The experimentation was carried out on these two set-ups to validate the proposed model. It is found that the results from the experiments are in good agreement

with the simulated one. It was observed that, with the use of EWHE cooling, the electrical efficiency of tube-and-sheet PV/T system is increased by 1.5% as compared to without cooling. Further to identify the grey areas for the improvement, exergetic analysis of these coupled systems has been carried out in terms of exergy losses and exergy destructions. The total maximum exergetic efficiency of coupled system (EWHE+PV/T) at the mass flow rate of 0.033 kg/s was found as 24.80% and 23.26% for tube-and-sheet and broad water channel systems respectively. At the end, a rooftop PV/T system coupled with EAHE cooling was also designed and simulated for combined electrical power and space heating of buildings. The simulations were carried out for three climatic conditions i.e. Las Vegas (USA), Pilani and Ajmer (India). It was found out that the results in Indian condition were more prominent because of higher cell temperature (up to 55 ºC) even during peak winters.

The EWHE system along with PV and CPV could be used for the semi-arid regions of western Rajasthan which is blessed with high solar insolation. This system will be very much helpful in summer as outside temperature reach up to 48 °C, leaving very small scope for utilization of thermal energy. While rejecting heat to the ambient will also be great challenge during that period. Thus the proposed PV/T and CPV/T coupled with EWHE system could be a better solution. The current research is an attempt to narrow the gap of utilizing geothermal energy and its untapped potential.

# TABLE OF CONTENTS

**CHAPTER 6: CONCLUSION AND FUTURE SCOPE OF THE WORK**

# LIST OF TABLES

# LIST OF FIGURES

# NOMENCLATURE

$A_c$: Area of collector ($m^2$)

$A_{IPVTS}$: Area of broad water channel ($m^2$)

$A_{PV/T}$: Area of broad air channel ($m^2$)

$B$: Width of absorber or channel (m)

$C_{air}$: Specific heat of air (J/kg K)

$C_w$: Specific heat capacity of water (J/kg K)

$D_{out}$: Outer diameter of PV/T collector tubes

$D_{in}$: Inner diameter of PV/T collector tubes

$dx$: Element length of flow pipe (m)

$\dot{E}x$: Exergy rate (W)

$F'$: Plate collector efficiency factor

$F_R$: Flow rate factor

$f$: Friction factor for smooth pipes

$G(I)$: Global solar radiation ($W/m^2$)

$h$: Specific enthalpy (kJ/kg)

$h$: Convection heat transfer coefficient between water and inner surface of EWHE pipe ($W/m^2 K$)

$h_o$: Convective heat transfer coefficient between glass cover of PV and the ambient ($W/m^2 K$)

$h_{rad}$: Radiative heat transfer coefficient between PV and the ambient ($W/m^2 K$)

$h_{tube}$: Heat transfer coefficient between PV/T collector pipe and flowing water ($W/m^2K$)

$hp_1$: Penalty factor which is due to PV cell material, glass and EVA

$hp_2$: Penalty factor which is due to the interface of tedlar and air flow in between

$I$: Current (A)

$k$: Thermal conductivity (W/m K)

$k_s$: Thermal conductivity of soil (W/m K)

$l$: Length (m)

$m_w$: Mass flow rate of water (kg/s)

$m_{air}$: Mass flow rate of air (kg/s)

$Nu$: Nusselt number

$P$: Pressure (Pa)

$PF_1$: Penalty factor due to the glass cover of PV Panel

$PF_2$: Penalty factor due to the absorber plate below PV panel

$pr$: Prandtl number

$Q$: Heat transfer (W)

$Re$: Reynold number

$r_s$: Radius of soil annulus (m)

$r_o$: Outer radius of EWHE pipe (m)

$s$: Specific entropy (kJ/kg K)

$T$: Temperature (K)

$t$: Thickness (m)

$U_{aw}$: Overall heat transfer coefficient from absorber to water flow (W/m$^2$ K)

$U_b$: Overall heat transfer coefficient from back surface of PV/T (W/m$^2$ K)

$U_{tw}$: Overall heat transfer coefficient from tedlar to water flow (W/m$^2$ K)

$U_{tair}$: Overall heat transfer coefficient between the tedlar and air flow (W/m$^2$ K)

$U_{c,amb}$ : Overall heat transfer coefficient from solar cell to ambient through glass cover (W/m$^2$ K)

$U_{ct}$: Conductive heat transfer coefficient from solar cell to tedlar (W/m$^2$ K)

$U_{gt}$: Overall heat transfer coefficient from glass to tedlar through solar cell (W/m$^2$ K)

$U_T$: Overall heat transfer coefficient from PV/T to surroundings (W/m$^2$ K)

$U$: Overall heat transfer coefficient in EWHE system (W/m$^2$ K)

$V$: Velocity of wind (m/s)

$V$: Voltage (V)

$v_w$: Velocity of water (m/s)

$v_{air}$: Velocity of air (m/s)

$W$: Tube spacing (m)

***Subscripts***

a: absorber

adh: adhesive

amb: ambient

airi: inlet temperature of the PV/T

airo: outlet temperature of the PV/T

airi1: onlet temperature of the EAHE

airo1: outlet temperature of the EAHE

ba: back surface of absorber

bt: Rear surface of tedlar

c: cell

convec: convection

des: Destruction

e: electrical

FF: fill factor

g: glass

in:  Inlet

ins: insulation

m: module

out: Outlet

oc: open-circuit

p: pipe

ref: Reference temperature

R: thermal resistance

s: soil

sc: short-circuit

ted: tedlar

th: thermal

w: water

w,avg: Average temperature of water

wi: Inlet temperature of PV/T

wo: Outlet temperature of PV/T

wi1: Inlet temperature of EWHE

wo1: Outlet temperature of EWHE

***Greek letters***

$\alpha$:  Absorptivity

$(\alpha\tau)$: Product of transmissivity and absorptivity

$\beta$: Packing factor

$\varepsilon$: Effectiveness of EWHE system

$\mu$: Dynamic viscosity of water (N s/$m^2$)

$\eta$: Efficiency (%)

ω:  Uncertainty in the result

$\Psi$ : Specific exergy (kJ/kg)

$\rho$: Density (kg/$m^3$)

$\tau$ :  Transmissivity

# LIST OF ABBREVIATIONS

BIPV/T: Building integrated photovoltaic thermal system

BICPV/T: Building integrated concentrating photovoltaic thermal system

CPV: Concentrating photovoltaic

CPV/T: Concentrating photovoltaic/thermal

EAHE: Earth air heat exchanger

EWHE: Earth water heat exchanger

IPVTS: Integrated photovoltaic thermal system

Mtoe : Million tonnes

PV: Photovoltaic

PV/T: Photovoltaic/thermal

PCM: Phase change material

RTD: Resistance temperature detector

SCs: Solar cell

STC: Standard test conditions

# CHAPTER 1
# INTRODUCTION

## 1.1 Energy Scenario

The energy consumption in the world has increased over the decades. In 1973, the primary energy consumption was 6,101 million tonnes (Mtoe) and it has grown up to 13,699 Mtoe in the year 2014. Electrical energy is a high grade form of energy which is being used directly in day to day life. And the demand of electricity is increasing at the rate of 3% per year due to globalization and the increase in technology for human comfort [1]. If the current trend of global energy use-demand continues, the supply of fossil fuels is predicted to be exhausted within the next centuries. A report by International energy agency in 2001, estimated that with the existing rate of consumption, the oil reserves will last up to the year 2100 and the coal reserves will exhaust in the next 170-200 years [2]. Burning fossil fuels releases stored greenhouse gases and lead to an increase in global warming. This disturbs the global carbon cycle, and leads to an increase in atmospheric $CO_2$ levels. The intergovernmental panel on climate change also estimated that the global average atmospheric temperature has increased by 0.6 °C in the last century and with the existing pace of carbon emissions, it will increase by 1.4 to 5.8 °C by 2100. The developed nations have signed a pact to decrease their carbon emissions in coming years. The major challenges lie with developing nations like India, which has a 18% population of the world. With this huge population, the energy consumption is increasing tremendously and it has doubled the figure in the year 2000. The total current electricity generation capacity of India is 330.15 GW out of which 69% are still fossil fuel based power plants [3].

The fossil fuel plants are one of the major pollutants and in order to reduce the emission levels, it is important and crucial to find the alternative sources of energy to overcome the use of conventional fossil fuels. A serious efforts are required to reduce the carbon emissions, especially by conventional power plants to have minimal impact on our environment. In recent times, there has been a significant revival of interest in renewable energy to tackle the above problems. These renewable energy sources are clean, abundantly available throughout the world and have minimum impact on the environment. Among various renewable energy sources, the solar energy is an abundant energy source which can meet the energy demand of the world for years to come.

## 1.2 Solar energy

The Sun is the primary source of energy for life on Earth. Being a hot gaseous matter, the effective temperature of the Sun's surface is 5778 K which radiates 63 MW/$m^2$ energy in all the directions. The Earth receives only $1.7\times10^{14}$ kW of energy. It is estimated that 84 minutes of solar radiation falling on the earth would cover the energy demand of the world for the whole year. India, on an average, has 300 sunny days per year and receives an average hourly radiation of 200 MW/$km^2$. The India energy portal estimated that around 12.5% of India's land mass, or 413,000 $km^2$, could be used for harnessing solar energy [4]. Solar energy in general and photovoltaic (PV) in particular can provide a good source of producing clean energy for such areas. The area could be further increased by the use of rooftop solar PV systems. The solar PV growth in India has been slow since its inception, but gained pace after the announcement of Jawaharlal Nehru national solar mission and later national solar mission. For instance, the overall cumulative capacity of solar power in the country during 2009 was 9.13 MW but it has grown to 9012.85 MW in year 2016-17 and expected to grow up to 1,00,000 MW by 2022 as per the target of national solar mission [5]. The graphical representation of installed solar power capacity in MW till 2016-2017 in India is shown in Fig.1.1

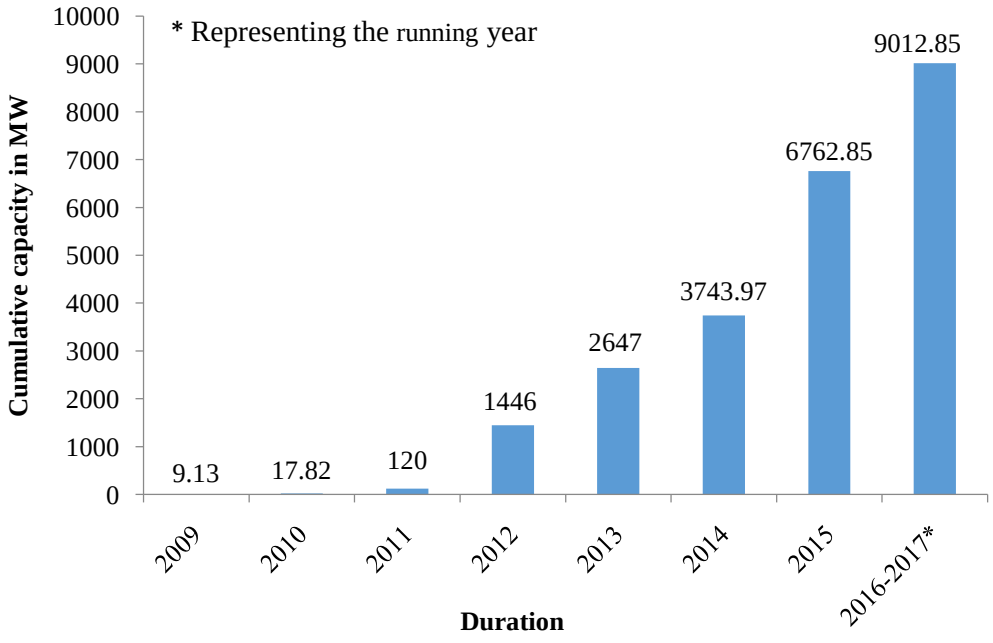


**Fig. 1.1**. India's installed solar power capacity in MW [5]

### 1.2.1 Photovoltaic systems

Solar energy can be harnessed to produce electricity in two ways, PV and concentrating solar power (CSP). The PV technology works on the PV effect which was first discovered by the physicist Edmund Becquerel in 1839 who recommended that sunlight can be converted directly into electricity using semiconductor devices known as PV cells. The PV effect works on the principle of photon energy where photons with less than 1100 nm of wavelength has ample energy to break the bond in the semiconductors, creating a free electron and a free hole. These movements of electrons generate electricity when connected with external loads [6].

The PV cells are made-up of semiconductor materials having high absorption characteristics of solar radiation matching with the solar spectrum. PV system uses various semiconductor materials and technologies such as crystalline silicon, cadmium telluride, gallium arsenide, chalcopyrite films of copper indium selenide, etc. Now silicon solar cells (SCs) represent 40% of the world, SCs production and yield efficiencies varies between 9 to 18%. PV technology can be thin films or wafer based technology [7]. The PV technology has seen worldwide growth of 40% from 2000 to 2014. According to the reports of Fraunhofer Institute for Solar Energy Systems, during the year 2014, the annual production of PV systems was 47.5 GWp, out of which almost 91% (43.1 GWp) were based on silicon wafer based PV modules. Despite huge demand and production, the wafer based technology put forth few challenges, which includes a thicker wafer, high material processing requirement, high embodied energy, complex manufacturing techniques, etc. for high efficiency SCs. Due to these factors, research work on thin film technology is also growing. In both the cases, the SCs are tested at standard test conditions (STC) set by National Renewable Eenergy Laboratory which includes solar radiation as 1000 $W/m^2$, 25°C module temperature and 1.5 air mass [8]. With increase in demand, the mass production of SCs lead to decrease in cost and improved the quality to be incorporated in different applications. For instance, earlier the PV systems were used for space applications like satellites, but now it is being used for various applications such as calculators, watches, grid connected and off grid solar power plants.

A number of PV panels can be connected in series or parallel to build a desired PV array system for grid connected and large stand-alone power plant. A stand-alone PV systems are being used in the areas where electric grid is not easily accessible. The electrical energy from

the stand-alone PV system can be stored in batteries. This type of system consists of PV panel, charge controller, batteries and an inverter as shown on Fig. 1.2. The grid connected PV system consists of inverter/power conditioner, dump load and utility grid as shown in Fig.1.3. The power generated from the grid connected PV systems need to be used immediately or to sell to any electricity company.

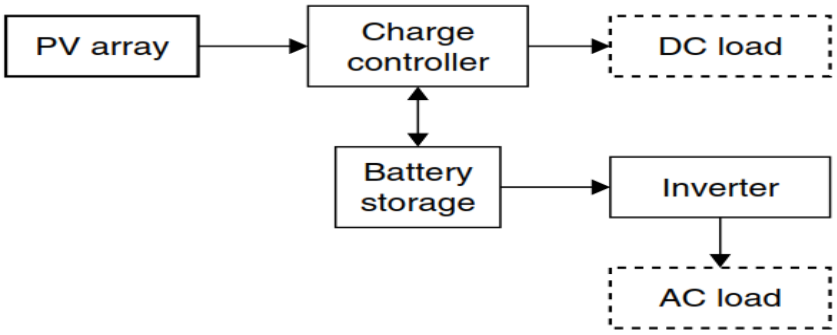


**Fig. 1.2.** Stand-alone PV system

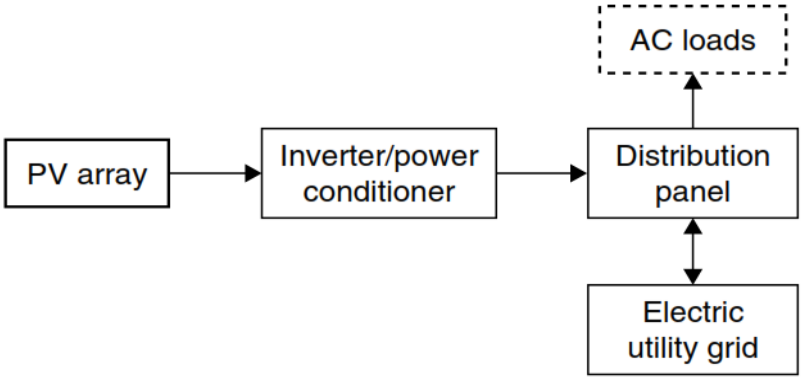


**Fig. 1.3.** Grid-connected PV system

### *1.2.1.1 Photovoltaic module characteristic curve*

The PV module which is used in the solar power plant need to be tested for its efficiency and performance characteristics. The SCs are characterized by a PV module characteristic curve which is the current-voltage (I-V) curve as shown in Fig. 1.4. A typical I-V curve represents values of voltage and current under constant solar insolation and ambient temperature. This curve provides the required information of the PV module. The commonly used parameters of the I-V curve include electrical, thermal and physical characteristics of a SCs [9].

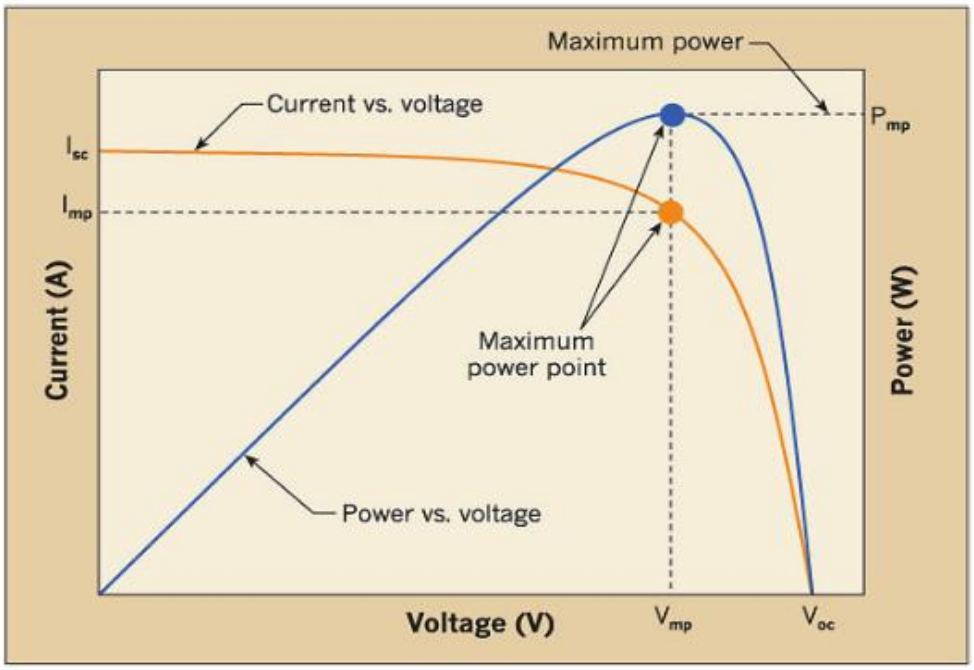


**Fig. 1.4** PV module characteristic curve [9]

The main parameters of I-V curve are explained as below:-

*Short circuit current ($I_{sc}$)*

It is the maximum current that PV module will produce corresponding to zero voltage.

*Open circuit voltage ($V_{oc}$)*

It is the maximum voltage that PV module will produce corresponding to zero current.

*Maximum power*

It represents the maximum power obtained from the I-V curve at a constant solar insolation and ambient temperature conditions.

*Fill Factor (FF)*

It is the ratio of the maximum power to the product of open circuit voltage and short circuit current. This factor represents the quality of PV panel.

*PV panel efficiency ($\eta_e$)*

The instantaneous efficiency of the PV module is defined by the ratio of maximum power that can be obtained by the incident solar energy G (I) over that panel area ($A_{PV}$). Mathematically, it is represented as:

$$\eta_e = \frac{FF\ I_{sc}V_{oc}}{A_{PV}\ G(I)} \qquad (1.1)$$

### 1.2.2 Concentrating photovoltaic system

The PV cells are flat and occupies a large area as the efficiency depends upon the same. The cost of the PV is still higher as compared to conventional sources of power generation due to the large size of panels. The output from PV panel can be increased by increasing the intensity of solar radiation on it. This can be achieved by using cheaper concentrating mirrors or lenses which concentrate solar radiation to a smaller area, thus reducing the required SCs area for the same output. These CPV systems are classified according to the concentration ratio (CR) of solar radiation incident on it. This ratio indicates the number of times the solar light is concentrated and it is usually known as 'Suns' and denoted by symbol '×'. According to concentration ratio, CPV systems can be classified into three categories:

- Low CPV system: The system which concentrates the sunlight between 1 to 40 times, i.e. 1-40× or 1-40 Suns.
- Medium CPV system: The system which concentrates the sunlight between 40 to 300 times, i.e. 40-300× or 40-300 Suns.
- High CPV system: The system which concentrates the sunlight between 300 to 2000 times, i.e. 300-2000× or 300-2000 Suns [10].

The CR of a system depends upon various factors like aperture area, acceptance angle, geometry, etc. There are four main concentrating systems which can be categorized by the way they focus the Sun's rays and the technology used to receive the Sun's energy. These systems are classified by their focus geometry as either line-focus concentrators (parabolic trough concentrator and linear Fresnel concentrator) or as point-focus concentrators (parabolic dishes and Scheffler systems)[11]. The advantages and disadvantages of the CPV system are as follows:

**Advantages**

- Required less PV material for the same output as compared to normal PV system.
- Achieved high electrical efficiency up to 40% with multi-junction SCs.
- Low energy payback time.
- Low cost of electricity per watt of manufacturing capital.

**Disadvantages**

- Tracking is required.

- Proper cooling is required to maintain the uniform cell temperature.
- Lack of technology standardization.

### 1.3 Problem statement

In the both cases of PV and CPV systems, only 6 to 35% of the total solar insolation is converted into electrical energy while the small portion is reflected back and remaining is converted into heat. This results in an increment in the SCs operating temperature, which in turn reduces the bond energy and the band gap of SCs, resulting in degradation in its performance. The SCs will also exhibit long-term degradation if they are exposed to higher temperatures for long duration, reducing the lifespan rapidly [12]. Research studies show that the operating temperature is one of the key factors that influence the performance of the SCs. The correlations between PV operating temperature and its efficiency has been discussed by Skoplaki and Palyvos [13]. They concluded that for most of the normal PV cells with a base temperature of 25°C, the average decrease in efficiency is of the order of 0.45% per degree rise in operating temperature. Nishioka et al. [14] presented the relation between temperature coefficients and conversion efficiency of triple junction SCs and found the conversion efficiency to be decreased by 0.248% at 1 Sun and 0.098% at 200 Suns for per degree rise in operating temperature. These two studies show that the temperature control is very important and crucial factor to improve the efficiency and life span of the SCs.

The rise in operating temperature of SCs can be controlled by using cooling technologies. The cooling technology which can be active or passive is an important aspect in case of CPV rather than normal PV because of higher CR and hence solar insolation. The selection of cooling technology depends upon various parameters like area available for cooling, fluid flow rate and heat transfer coefficient. It should be reliable, easy to operate and efficient in nature. The design of the cooling system for SCs depends upon global solar radiation and CR. From the past few years a significant amount of work has been done on different active and passive SCs cooling techniques by many researchers. The existing system of SCs uses heat pipe, water, phase change material, liquid immersion, microchannel heat sink, nanofluid, PV/T and CPV/T as cooling methods to keep the SCs temperature under the operational limit. Another cooling approaches which are used to cool down the system other than SCs are also discussed by various researchers. One of them is geothermal cooling, which is used for air conditioning and can be utilized for other applications too.

## 1.4 Principle of geothermal cooling

Earth behaves as a huge collector-cum-storage medium of solar energy and can be used as daily or seasonal thermal storage medium. Because of the large heat capacity and insulation potential, the ground possesses many advantages for various applications. The average typical thermal capacity of the soil is 920 J/kg K and average volumetric density around 1800 kg/$m^3$. Thus, each cubic meter of the ground, or rock bed, could store about 1.67 MJ/kg of energy. It is studied over time that the thermal losses from an underground reservoir are quite small and the annual heat losses amount to 10% of the total annual energy stored. Because of the large thermal capacity of the earth, the effect of diurnal variation does not observe beyond the depth of 0.5 m and for seasonal variation the depth is up to 3 meters [15-16].

According to American society of heating, refrigerating and air-conditioning engineers (ASHRAE), beyond this depth or more, the earth's temperature remains fairly constant throughout the year, and is approximately equal to the average annual ambient air temperature. The ground can therefore be used as a heat sink for cooling, especially during peak summers in dry and semi-arid regions like Rajasthan and Gujarat of India, where due to high solar insolation the ambient temperature reaches about 48 ºC. For such areas, geothermal cooling may be considered to be a very good alternative for cooling purpose. Based on the principle of geothermal energy, earth air heat exchanger (EAHE) systems have been used by some researchers for air conditioning. Besides air conditioning, this technique may be used for cooling of SCs. However, the challenges with EAHE is that it requires a large surface area for effective heat transfer because of low thermal conductivity and low heat carrying capacity of air. The required surface area may be reduced by using water as a cooling medium because of its high heat transfer capacity, thus it makes it as earth water heat exchanger (EWHE) systems. In the EWHE system hot water (exiting of PV panels) is sent into the pipes that are buried in the underground. When hot water flows through EWHE, heat is transferred from the hot water to the earth as a result the temperature at the outlet of the EWHE is much lower than that of at the inlet and ambient. The outlet water from EWHE can be directly used for solar cell cooling of PV and CPV systems.

## 1.5 Objectives of the present research work

With recent advancement in the cooling technologies of PV and CPV systems, the published literature in this area is growing tremendously. Still, the available literature has a huge scope

for further research. Among the many gaps in existing research on the PV and CPV cooling techniques, some of them have been addressed in the present thesis. Based on the literature review done, the following issues have been considered and addressed:

1. The present work discusses the aspects of a novel cooling technology termed as EWHE for the PV and CPV systems. The proposed configuration is unique and is applied for the first time to investigate the performance of PV and CPV systems for a semi-arid region in India. Two aspects for semi-arid regions are important to note here; first, the population density in such regions is low and second, the average ambient temperature during operating hours of PV and CPV from morning to evening usually is above 48 $^{o}$C during the summer period. This implies that the demand of hot water in such regions is directly satisfied by the ambient itself. Moreover, the adoption of EWHE allows nearly constant inlet water temperature to the PV/T and concentrating photovoltaic/thermal (CPV/T) system of the order of soil temperature at a depth of 3 m i.e. 27 to 29 $^{o}$C which is average annual ambient air temperature. This water temperature is much lower as compared to that reported in the literature. This low temperature (27 to 29 $^{o}$C) of water is the result of EWHE i.e. geothermal cooling and will help in improvement in the efficiency of the PV/T and CPV/T system. The already existing systems of PV/T cooling are not feasible for arid and semi-arid regions as continuous supply of cold water was not available for the cooling of PV panel due to high ambient temperature. In the current system the heat is rejected at ambient temperature.
2. Literature shows the availability of models for PV/T and CPV/T systems however a model which couples PV/T and CPV/T cooling with EWHE is not available. For the same, an analytical expression for characteristic equations of different type PV/T collectors coupled with EWHE have been derived and simulated in MATLAB.
3. An experimental set-up was developed and experimental studies were carried out to validate the theoretical models of tube-and-sheet PV/T and broad water channel PV/T systems coupled with EWHE cooling. Further, the effect of major parameters such as mass flow rate, EWHE pipe length, diameter, material and SCs temperature, etc. have been studied for the both systems.
4. Further to identify the grey areas of the improvement, second law thermodynamic analysis of coupled (EWHE+PV/T) system has been carried out in terms of exergy losses and exergy destructions.

5. Design and analysis of rooftop PV/T air system coupled with EAHE cooling for combined electrical power and space heating of buildings has been done. The simulations were carried out for three climatic conditions i.e. Las Vegas (USA), Pilani and Ajmer (India). The importance of the analysis lies during the winter where the ambient temperature drops to 0 °C while PV surface temperature reaches up to 55 °C during peak time.

### 1.6 Thesis organization

This thesis report is organized into six chapters.

**CHAPTER 1: INTRODUCTION**

In this chapter, the background and status of solar energy is presented. A brief description of PV system, CPV system and geothermal cooling is also presented. Furthermore, the problem statement, objectives of the present research and organization of the thesis have been presented.

**CHAPTER 2: LITERATURE REVIEW**

In this chapter, an exhaustive literature review on different PV and CPV cooling techniques and geothermal cooling has been given. A brief discussion on different PV and CPV coolings and research gap has been presented. Furthermore, this chapter also presents the problem to be investigated and gray areas for the present research.

**CHAPTER 3: MODELLING AND SIMULATION**

This chapter deals with the modelling and simulation of unglazed PV/T system with EWHE cooling. A detailed TRNSYS model was developed to investigate the transient performance of the unglazed PV/T system with EWHE cooling followed by its parametric study. Also a detailed TRNSYS model was developed to investigate the transient performance of the CPV system coupled with EWHE. The parametric study has also been carried out. For the same, a case study has been taken from the literature and analysis was carried out to replace the conventional heat exchangers with EWHE. Further a detailed thermodynamic model of glazed PV/T system coupled with EWHE has been developed and analyzed using the first law analysis. The study has been carried out on two types of glazed PV/T collectors which

include (a) tube-and-sheet absorber system and (b) broad water channel system. Furthermore a mathematical model is developed for rooftop photovoltaic thermal system with EAHE for combined electrical power and space heating.

**CHAPTER 4: EXPERIMENTAL STUDIES**

This chapter exhibits the detailed of experimental test set-up of glazed tube-and-sheet and broad channel PV/T systems with EWHE cooling along with instrumentation and experimental procedure used in the study. It also presents the uncertainty analysis of the system. At the end, an exergetic assessment model of the glazed PV/T systems coupled with EWHE cooling has been given. The exergetic equations were developed for the coupled system based on exergetic losses and exergy destructions. The exergetic efficiencies have been evaluated and reported using the thermodynamic model and second law analysis.

**CHAPTER 5: RESULTS AND DISCUSSION**

In this chapter, the theoretical and experimental results for glazed PV/T systems coupled with EWHE cooling have been discussed. It also presents the comparison of difference along with statistical analysis.

**CHAPTER 6: CONCLUSION AND FUTURE SCOPE OF THE WORK**

The conclusions of the study, future work and recommendations based on the study has been presented and discussed in this chapter.

# CHAPTER 2
# LITERATURE REVIEW

PV and CPV cooling systems received some attention in the late 70s and early 80s, but they did not end up enjoying wide acceptance, either due to poor cooling performance or because of other associated problems such as operational issues, lower reliability and high pumping power. Since then a lot of work has been done for the improvement in the performance of the PV and CPV cooling system. Many researchers have developed and studied different PV and CPV cooling systems. Most of the studies on such cooling systems focused on its performance investigation and enhancement of cooling effect. Whereas, some researchers determined the performance of these systems coupled with other systems like solar water heater and solar distillation to see the feasibility of using it as a part of hybrid systems. Most of these systems have been developed as experimental units, whereas, analytical and numerical estimation has also been performed to simulate these systems.

## 2.1 Concentrating photovoltaic cooling systems

The various types of cooling technologies which have been implemented for CPV systems are discussed in the following sections. The classification is made according to the type used.

### 2.1.1 Heat Pipe cooling

Heat pipes are hollow metal pipes whose inner surface is lined with a porous wick material which is soaked in a liquid coolant that transports heat by evaporating and condensing in a continuous cycle. Heat pipes can be classified according to their geometry, function and the methods used to transport the liquid from the condenser to the evaporator [17] . Because of their high thermal conductivity and high heat transfer characteristics, heat pipes have been extensively used for cooling of small electronic equipments. They are good alternatives to large heat sinks, especially in laptops where space is limited [18]. Singh et al.[19] developed a miniature loop heat pipe with the flat disk shaped evaporator for thermal management of compact electronic equipments. The materials used for loop are copper with nickel wick and water is used as the working fluid. They showed that the system can dissipate maximum heat load of 70 W with evaporator temperature below 100±5 °C limits.

From the literature, it is also observed that heat pipe cooling is also used by some researchers on PV and CPV systems. Russell [20] has patented a CPV system with heat pipe to maintain

constant temperature of SCs. The system contains linear Fresnel lenses focusing solar energy onto a string of SCs mounted on the heat pipe of circular cross-section, along its length, as shown in Fig. 2.1. Several pipes were arranged next to each other to form a panel. The heat pipe has an internal wick elongated lengthwise of the tube that draws out the liquid up to the evaporator. The heat was removed from the heat pipe by an internal liquid coolant flowing through the U shaped pipe maintaining a uniform temperature along the pipe.

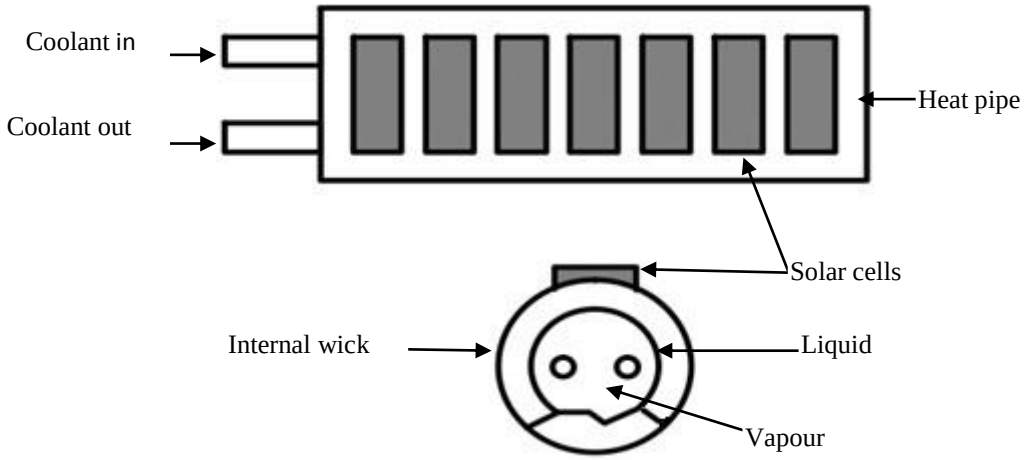


**Fig. 2.1.** Heat pipe cooling system for PV as proposed by Russel [20]

The role of heat pipe for thermal management of CPV cells has been experimentally investigated by Akbarzadeh and Wadowski [21]. In their experiment heat pipe was made up of flat copper pipe having a finned condenser and SCs were mounted vertically on them at the end. The system was designed for 20 Suns concentration with parabolic trough collector of size 1 m×0.8 m. An experiment was conducted for a period of four hours. It was found that the surface temperature of SCs was maintained within 46 °C, as opposed to 84 °C in the same conditions but without heat pipe. It was reported that the power output was increased from 10.6 W to that of 20.6 W when heat pipe cooling was applied. Cheknane et al. [22] examined the role of gravity dependent copper heat pipe on silicon based CPV system with up to 500 Suns. As shown in Fig. 2.2, the gravity dependent heat pipe consisted of a sealed copper cylinder filled with a small amount of working fluid. The SCs were attached at the lower end of the heat pipe, and receive radiation from Fresnel lens concentrator. The working fluid is vaporized by the heat from SCs and the vapour rises up in the tube. The vapour gets condensed on the pipe walls by rejecting heat to the ambient air though large fins, which are mounted on the walls as shown in Fig. 2.2. The condensate flows by gravity down the tube walls through wick structure, back to the pool. The system used water or acetone as the

working fluids and it was reported that the efficiency was more when acetone was used compared to that of water.

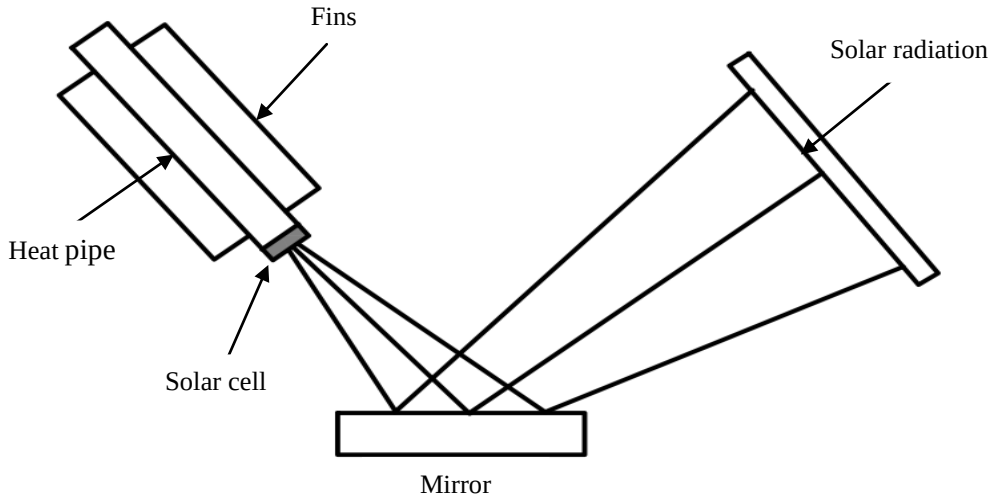


**Fig. 2.2.** A Schematic drawing of gravity assisted heat pipe and test set-up [22]

Anderson et al. [23] designed a copper-water heat pipe with aluminum fins to cool a 30 Suns CPV system. They did CFD analysis to find optimum fin sizes and spacing for a heat input of 40 W/cm$^2$ with heat rejection by natural convection. Heat pipe was designed for different working fluids like water, ammonia, methanol, pentane, and toulene. They found that the water is the best working fluid among the others. Huang et al. [24] designed a method to fabricate a novel hybrid-structure flat plate (NHSP) heat pipe for a beam radiation of 930 W/m$^2$ CPV system. They used a sintered wick structure and a coronary-stent-like rhombic copper mesh to support the structure. They observed that the thermal resistance of NHSP heat pipe was less as compared to conventional heat pipes. They also reported that the NHSP heat pipe is proven to be better cooling technology for CPV system, which can increase photoelectric conversion efficiency by approximately 3.1%, compared to an aluminum substrate. Lee and Baek [25] proposed a CPV cooling system using an insulated aluminium thermal absorber (width: 80 mm, length: 50 mm, height: 30 mm) having two heat pipes with distilled water as the working fluid. Triple junction (InGaP, InGaAs and Ge) SCs of 10×10 mm was placed on the thermal absorber. Their results showed that the CPV cell temperature was 29.3, 33.3, 37.2 and 41.2 °C for 500, 600, 700 and 800 Suns respectively. They found electrical and thermal efficiency as 20% and 77% respectively. Farahat [26] has suggested the use of controlled gas heat pipes for cooling of PV cells. He used two types of evaporator

shapes, i.e. round and square. He showed that the heat pipe cooling method can be successfully applied to the PV system.

### 2.1.2 Liquid immersion cooling

Russell [27] has patented a liquid immersion cooling system. In his design, he used optical concentrators focusing sunlight on an elongated pipe which is filled with electrically nonconductive thermally conductive liquid. He placed SCs inside the pipe and immersed in liquid having a refractive index suitable for concentrating the light onto the SCs array. Koehler [28] proposed a new system where the SCs are submerge in a circulating dielectric coolant liquid, the heat was transferred from SCs surfaces while the cooling water was circulated around them. He recommended that local boiling on the PV cells can be achieved, which results in a uniform temperature across the surface and higher heat transfer coefficient. Similar research has been done by Abrahamyan et al. [29]. They used an isotropic liquid dielectric as glycerin, butanol, acetone, dioxane, toluol, isopropyl alcohol and deionized water. Their experimental results showed that thin film of thickness 1 to 4 mm of dielectric increased the SCs efficiency by 40 to 60%. Wang et al. [30] also contributed to an enhanced efficiency of silicon SCs by using dielectric liquid immersion technique. Zhu et al. [31] proposed a liquid immersion cooling method for densely packed SCs under high CR. They found that the module was cooled to 35-45 °C for water flow velocity of 2.0-2.7 m/s at 16 °C inlet temperature of silicon oil. Their results showed that convective heat transfer coefficient can go beyond 3000 W/($m^2$ K) for a given range of velocities and found that experimental values were higher than simulated ones due to electricity to light conversion efficiency variation.

Liu et al. [32] developed an experimental system to dissipate heat from both the front and back surfaces of SCs by dielectric liquid immersions. They used a long arc xenon lamp as a source and dimethyl-silicon oil as the dielectric fluid. They observed that the temperature of cells can be reduced to 30 °C corresponding to 1000 W/($m^2$ K) heat transfer coefficient. They also achieved a uniform temperature distribution for the module in turbulent flow with a maximum temperature difference of less than 3 °C. Han et al. [33] proposed a direct liquid immersion cooling system for CPV cells. They used deionized water, isopropyl alcohol, ethyl acetate, and dimethyl silicon as immersion liquids. The SCs were encapsulated between two sheets of 100×100 mm square and 3.3 mm thick Borofloat glass. They observed rise in efficiency from 8.5 to 15.2% for 1.5 mm thick liquid layer over the cell surface for 30 Suns,

and concluded that the fluid inlet velocity and flow mode also influenced the SCs temperature. Zhu et al. [34] designed a liquid immersion cooling system to eliminate the contact thermal resistance of back cooling for 250 Suns. They designed a system for ambient conditions of 900 W/$m^2$ and 17 °C with inlet water temperature at 31 °C. They obtained 49 °C as peak temperature and 45 °C as uniform temperature of PV cell. They found a convective heat transfer coefficient to be approximately 6000 W/($m^2$ K).

A three dimensional simulation model for a cylindrical liquid immersion solar receiver was developed by Xiang et al. [35]. The system used a dish type concentrator with 250 Suns. The influences of inlet velocity and module geometric parameters were investigated by them. They found that the inlet velocity is inversely proportional to cell temperature. They observed that cell module, with fin height 4 mm with eleven fins, has the best thermal performance. Han et al. [36] investigated the performance and long-term stability of silicon CPV SCs through three separate liquid immersion tests. They concluded that it was difficult to achieve stable electrical performance of the cell with 9 mm liquid film when immersed in deionized water. Sun et al. [37] designed a narrow rectangular channel receiver to reduce the liquid holdup with 9.1 Suns. The width of the channel was 6 cm and 5 cm for the upper and lower part respectively. They used silicon SCs of 5 cm × 4 cm with an active area of 19.5 $cm^2$. They maintained the cell temperature in the range of 20-31 °C at 910 W/$m^2$ DNI with 15 °C inlet temperature of silicon oil as a coolant. They found a convective heat transfer coefficient to be approximately 1000 W/($m^2$ K) for the Reynold's number of 13,602. They also concluded that the electrical performance of the SCs was stable when immersed in the silicon oil and no degradation found even after 270 days of operation. Xin et al. [38] conducted an experimental study on cooling of triple-junction SCs (GaInP/GaInAs/Ge) immersed in dimethyl silicon oil upto depth varying from 1 mm to 30 mm under 500 Suns. They observed cell temperature of 78.92 °C, 71.91 °C, 82.43 °C and 115.69 °C at depth of 1 mm, 2.5 mm, 5 mm and 10 mm respectively with a mass flow rate of 0.00138 kg/s and concluded that silicon oil thickness should not be less than 2.5 mm.

### 2.1.3 Microchannel heat sink cooling

Edenburn [39] presented a cost analysis of a CPV system with heat sink cooling for optimizing the cost of cooling geometry for CRs of 50, 92 and 170 Suns. Their results showed that SCs can maintain below 150 °C on extreme days at 92 Suns. They concluded that the cost of heat sink increases with increase in lens area. Araki et al. [40] presented a

simple module structure in which Fresnel lens focus the sunlight onto SCs. The SCs are mounted onto an aluminum plate with a heat conductive epoxy and copper sheet. Their setup consists of heat spreader and a metal plate, where temperature rise was controlled by 3 mm thick aluminium sheet. They conducted experiments for two different CR and found that 18 °C rises in SCs temperature under 500 Suns and 21 °C rise under 400 Suns above the optimum temperature. They suggested that the effective thermal contact between the SCs and the metal plate is important to maintain low temperature of SCs. Chou et al. [41] investigated the thermal performance of the high CPV system using ANSYS simulation tool where they used 160 μm thick SCs (6.7×5.5 mm) and 3000 μm thick aluminium plate (535×257 mm) as a heat sink for cooling of CPV system. They discussed different design parameters like the thickness of heat sink, thermal conductivity of test board and solder paste of SCs assembly. Their experimental results showed the maximum junction temperature of 44.25 °C with corresponding thermal resistance of 1.56 °C/W. They concluded that the maximum junction temperature decreases as the aluminium thickness increases and found stable when thickness was more than 20 mm.

Kermani et al. [42] fabricated and investigated a novel manifold microchannel heat sink for cooling of a CPV system with CR of 1000 Suns. The heat sink distributed the coolant into alternate inlet and outlet channels in a direction normal to it, thus resulting in a greater heat transfer dissipation rate because of lower pressure drop across the surface to be cooled. They found maximum heat transfer coefficient and heat flux of 75 W/cm$^2$ for channel hydraulic diameter of 36 μm with aspect ratio of 10 and equal fin width of 20 μm. Min et al. [43] designed a thermal model for CPV cells with aluminium plates with black coating as heat sink to maintain the SCs temperature. The area of SCs was 700 times smaller than the heat sink area. Their outdoor experiment confirmed decrease in SCs temperature with an increase in the heat sink area for a fixed concentration. They showed that the required heat sink area increases linearly with the CR in order to maintain the constant temperature of SCs. They observed SCs temperature of 37 °C with a heat sink at 400 Suns and which otherwise would have been about 1200 °C without cooling. Alvarado et al. [44] did a CFD analysis of the fluid flow and heat transfer performance of heat sinks on conventional configuration with a single continuous channel and novel flow field configurations which include symmetric bifurcation flow distributors and parallel flow channels. For CR of 40 to 50 Suns they concluded that the novel flow field configurations showed better heat transfer performance for application in heat sink. Further an attempt has been made by Maio et al. [45] to control the flow of water in

a multi mini-channel heat sink integrated with a shape memory polymer. They used two configurations, open and obstructed, of water flow for the numerical steady state analysis. Their analysis showed that by using shape memory polymer, coolant flow in multi-channel heat sink can be regulated thus reduces the pumping power by 26%. Natarajan et al. [46] presented a numerical study to predict the SCs temperature for CPV system with CR of 10 Suns. They did 2-D simulation of SCs with fins and without fins. Their results showed that in 4 fins of 1 mm thickness and 5 mm height each with 4mm spacing in between can be effectively used to reduce the SCs temperature to 49.6 °C.

Lee et al. [47] simulated a 3D copper cooling block for CPV to investigate the effects of various parameters like working fluid properties, inlet fluid velocity and cooling block geometry. In their model cooling block of dimensions 350×175×20 mm was selected. They used square pin fins of width 5 mm and height 15 mm in cooling block. Their results showed that for higher inlet velocity (up to 3.5 m/s), the CPV and cooling block temperature has been reduced by 8.36% and 10.55% respectively. Their graphical representation showed that the temperature of CPV decreases with increase in inlet velocity for both 10.38 and 15.19 mm fin spacing, and with large temperature gradient in the latter case. They also concluded that coolant with lower viscosity had a superior cooling performance and for low inlet velocity, smaller spacing between fins is required. Linderman et al. [48] presented a study on Alpha-2 CPV system having E19 high efficiency PV module which was mounted on same rotational axis. In their system CPV had six parabolic concentrator rows and Alpha-2 receiver was made similar to E19 PV with folded fin heat sink beneath the PV module. They introduced a new cell packaging concept with an additional 0.37 gram of aluminium per watt of receiver and concluded that this system could maintain 8 °C lower cell temperatures for CPV. Using 3D finite element model, Gualdi et al. [49] proposed a thermal analytical model to determine the limits of passive cooling of CPV system. In their system the area for cooling was equal to the area of the concentrator, and the lower plate of SCs was made of aluminium having thermal conductivity of 200 W/(m K) and thickness of 3 mm. They stated that their graphical results could be used to obtain equivalent thermal resistance which was required to achieve the temperature below 80 °C cell temperature for a 10 $mm^2$ SCs area having CR more than 400. They concluded that natural convection of ambient air is sufficient to maintain the cell temperature below 80 °C with CR more than a thousand. Collin et al. [50] developed a methodology to calculate the thermal performance of a receiver as a part of cooling component for CPV. In their system a receiver was used in between SCs and heat sink to

draw most of the heat at the backside of the cell. The performance was calculated by measuring the thermal resistance with and without spreading of heat in the receiver. They concluded that the variation of heat depends on material, thickness and configuration of the receiver.

A novel design of heat sink for the CPV cooling system was proposed by Reddy et al. [51] for the CR of 500 Suns. In their design, an array of microchannels which were enclosed in the parallel flow channel was numerically simulated with the help of commercial CFD software ANSYS13. From the analysis, they observed high heat transfer in the microchannels over heat generations spots. They found a lower pressure drop of 8.5 kPa because of parallel flow channels and the estimated rise in temperature of 10 K in the CPV module of 12×12 $cm^2$. Liao et al. [52] proposed a hybrid power generation system, using a CPV module and a thermoelectric generator which used heat sink for the dual purpose of cooling and additional electricity generation. They numerically calculated maximum power output of 240 W for optimum value of thermal conductance between the CPV and thermoelectric generator of 120 W/K, CR of 5 Suns, and current of 17 A. Their results showed that CPV-thermoelectric generator hybrid system has more electrical power output and higher efficiency than normal CPV or thermoelectric generator system.

Wu et al. [53] presented a theoretical model of glazed and unglazed PV/thermoelectric generator using nanofluid cooling with CR up to 6 Suns. They analyzed the effects of various parameters like CR, load resistance, wind velocity and figure of merit. They numerically analyzed that the efficiency of unglazed PV/thermoelectric was higher than that of glazed one with a figure of merit of 0.0021 $K^{-1}$, while for the figure of merit 0.0085 $K^{-1}$ the efficiency difference between them slowly decreased with increasing CR. Their results show that the power output of unglazed system increased from 50 to 440 W as the CR increased up to 5.5 Suns with figure of merit, wind velocity and flow rate of nanofluid as 0.0085 $K^{-1}$, 2.5 m/s and 0.01 m/s respectively. They also concluded that nanofluid cooling had a superior performance than water cooling. The manifold microchannel heat sink was further explored by Sarangi et al. [54] to study its geometric parameters and concluded that the manifold microchannel heat sink has an optimal heat transfer performance at a manifold inlet to outlet length ratio of 3. Yang and Zuo [55] designed a novel multi layer manifold microchannel cooling system (length 98 mm, width 220 μm, depth 1.5 mm) where they used three silicon SCs (17 mm × 17 mm). Their experimental results showed that CPV cells temperature decreased from 44.1 to 20.4 °C for flow rate of 0.00535 to 0.0232 kg/s with 28 Suns. They observed that there is no

change in CPV cell temperature beyond 0.0232 kg/s flow rate. They found the heat transfer coefficient and pressure drop of 8235.84 W/($m^2$ K) and at most 3 kPa respectively due to multiple inlet/outlet manifolds.

### 2.1.4 Phase change material cooling

Phase change material (PCM) system referred to as latent heat storage technique whereby a large amount of heat energy can be stored in a relatively small mass of PCM. The PCM has ability to keep relative stable temperature during heat absorption because of its phase transition (melting and freezing), which has received much attention in thermal management of buildings, electronics equipment and thermal storage systems. Kandasamy et al. [56] Tan and Tso, [57]. Maiti et al. [58] performed an experiment on V-trough PV system to enhance the solar insolation. They used paraffin wax as a PCM with melting range of 56-58 °C and integrated it to the rear of the module to moderate its temperature rise. They solved the problem of low thermal conductivity of the PCM by using packed aluminium metal turnings. They performed experiment for both indoor and outdoor conditions using 0.06 m thick aluminium housing containing the PCM bed. They found that in the outdoor testing, PV module temperature could be reduced from 78 to 62 °C with the PCM and in indoor experiment temperature could be maintained at 65 to 68 °C for three hours whereas in its absence the temperature rose beyond 90 °C within 15 min.

Tan et al. [59] presented a numerical method to study the PCM melting characteristics using four different fin shapes: straight fin, T-shape fin, Y-shape fin and cross-shape (+) fin configurations in a rectangular encapsulation. They compared these four fin shape configurations with the conventional eight straight fins and found that the geometry of fins affect the formation of natural convection currents in liquid PCM. Further a system design of sustainable thermoelectric power generator based on solar concentrator and PCM heating/cooling was presented by Tan et al. [60] . They used system as shown in Fig. 2.3. They used two gravity assisted type of heat pipes for conveying the transmitted heat from the cold side of the thermoelectric module to the PCM thermal storage tank. They used paraffin wax as PCM for absorbing the heat at 60 Suns. Their indoor experimental results showed that concentrated thermoelectric generator PCM system was able to generate about 4 W of thermo electricity using two thermoelectric cells with a maximum temperature difference of 70 °C.

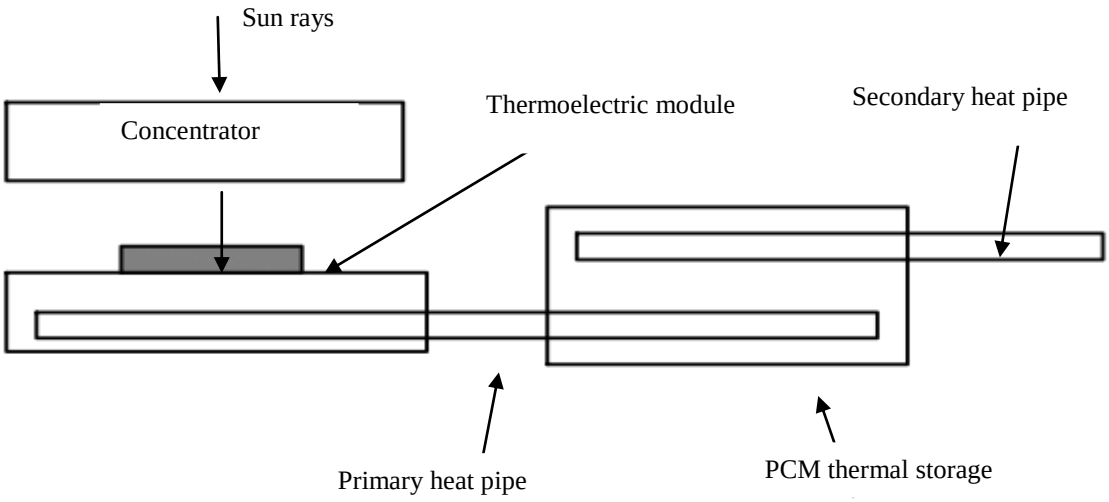


**Fig. 2.3.** Schematic diagram of concentrated thermoelectric generator-PCM system [60]

### 2.1.5 Concentrating photovoltaic/thermal system

CPV/T system is a hybrid solar system having CPV and solar thermal components which produce both electricity and heat as a coupled system. Research work done on different types of CPV/T systems is discussed in the following sections.

#### *2.1.5.1 CPV/T air system*

Air type collectors use air as a cooling medium. Othman et al. [61] proposed a theoretical model and conducted experiments on a hybrid double-pass PV/T air collector with a compound parabolic concentrator (CPC). The reason for the use of the CPC was stated to be, the lesser requirement for SCs to generate electricity and heat hence reducing the cost of the system. They used fins at the back of the PV panels to increase the heat transfer from PV to flowing air. Their results showed a drop in the fill factor of PV from 0.54 to 0.42 when the radiation intensity was increased from 400 W/m$^2$ to 700 W/m$^2$. They observed that the combined efficiency of the system was varied from 39% to 70% with the solar radiation intensity of 500 W/m$^2$. They also observed a decline in the electric power at elevated air flow temperatures, thus suggested a trade-off between electrical output and hot air production. Jian and Mingheng [62] proposed a CPV/T system with CPC and fins to dissipate heat to the flowing air. The system used by them was as shown in Fig. 2.4. It has low iron glass cover; through which radiation was concentrated on to SCs by the CPC. They carried out experimental studies from June 2009 to August 2009 and reported that the thermal, electrical

and system efficiency of the hybrid PV/T system increases with increasing the air mass flow rate, the length of the system and the packing fraction of the system.

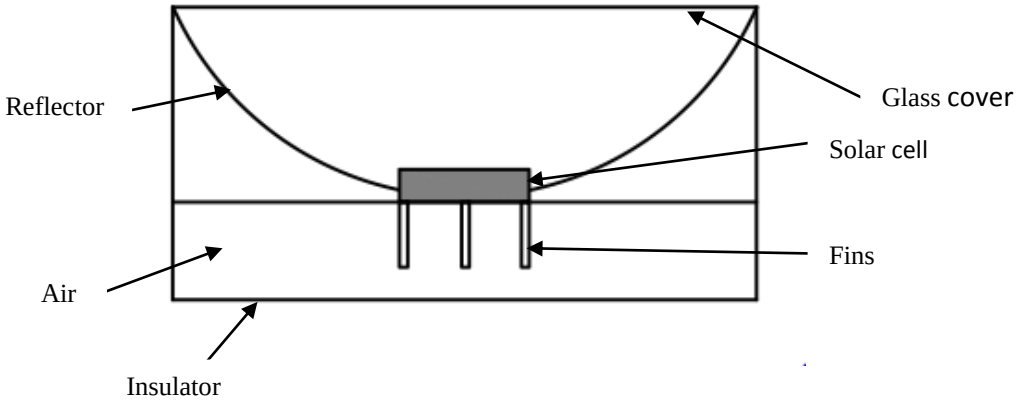


**Fig. 2.4.** Schematic diagram of the concentrating PV/T system [62]

Cuce and Cuce [63] presented a numerical and experimental study to analyze the air cooling effect of silicon PV cells. Their results showed that the PV cell temperature was maintained at 29 °C, when air at 15 °C with velocity of 5 m/s was supplied. Amri and Mallick [64] presented a mathematical heat transfer model for cooling the GaInP/GaAs/Ge triple-junction SCs with 100, 150 and 200 Suns. In this system air was forced to flow within a duct behind the 1.5 mm thick aluminium plate which was attached to SCs. They assumed external wall of the duct to be adiabatic. They found that maximum cell temperature can be reduced by as much as 50% at medium CR. They also showed that maximum cell temperature and the CR are highly dependent on channel width, air inlet velocity, thicknesses and thermal conductivities of the SCs holders and accessories.

### *2.1.5.2 CPV/T water cooling system*

Water type collectors use water as a cooling medium and produce the combined heat and electrical power from one system. Water with its suitable optical properties makes it compatible with PV modules as it can absorb light mainly in infrared radiations which are of longer wavelengths. In the field of water cooling Chenlo and Cid [65] designed a CPV system using linear Fresnel lenses, having concentration of 24 Suns, with water flowing through a galvanized steel pipe. The SCs were soft soldered to a copper-aluminum-copper sandwich, to accommodate for the difference in the thermal expansions between cells and the steel tube. Their experimental results showed 10.2% overall efficiency at beam radiation of

890 W/m$^2$ with an inlet water temperature of 28 °C. Horne [66] patented a CPV cooling system where paraboloidal dish was used to concentrate the solar radiation on vertical cells, lying on a set of rings. Water was transported up to the receiver by a central pipe and then flowed behind the cells for cooling. He found out that the water not only cooled the cells, it also acted as a filter by absorbing a significant amount of ultraviolet radiation that would otherwise have reached the cells. Lasich [67] invented an active cooling system with water circulation for densely array CPV with 200 Suns. The system was capable of dissipating heat flux of 500 kW/m$^2$ from the SCs and maintained it at around 40 °C temperature for normal operating conditions. His system was designed such that water flowed through small but parallel channels in thermal contact with the SCs. Kolhe et al. [68] designed and manufactured a CPV system with 8.5 Suns and water cooling system. The effect of water flow rate on performance was analyzed and they concluded that with increase in water flow rate, the electrical efficiency and thermal efficiency increases rapidly. They also observed that the electrical output of the water cooled CPV was 4.7 to 5.2 times higher than that of PV module without concentration and cooling. They found that the efficiency of the CPV mainly depends on the heat extraction rate and water flow rate.

Chong and Tan [69] constructed and tested an automotive radiator cooling system for effective heat dissipation from CPV module with 377 Suns. They simulated a cooling block made of copper with multiple water channels to mount the CPV panel on it. They conducted experiments for six hours and observed improvement in the conversion efficiency of CPV module from 22.39% to 26.85%, while the CPV cell temperature was observed to decrease from 59.4 °C to 37.1 °C. Correia et al. [70] invented a novel CPV system in which a reflector was used to concentrate the incident radiation on PV cells where only 5% the reflector area could produce the same amount of electrical energy as by the conventional solar panel. They found that this design can reduce the material cost of PV cell for same output and pumped power to transfer the generated thermal energy into a working fluid. Tan et al. [71] proposed a CPV cooling system based on the solar trough concentrator. Their designed used a metal cavity as a separate heating stage with one dimensional tracking device for increasing the temperature of working coolant. The metal cavity was placed after SCs during the experimentation. Their results showed that temperature of liquid was increased up to 12.06 °C with one cycle in the long metal cavity, but further temperature was raised up to 62.8 °C with 30 closed cycles thus inferred the increased thermal efficiency. They found the maximum power of SCs was 3.47529 W, with the cell temperature of 23 °C. Kuo and Lo [72]

investigated water cooling on the GaAs CPV cell. They found that the water cooling increased the efficiency and power capacity of PV by 2.29 to 3.37% and 2 to 15% respectively. Chaabane et al. [73] developed a 3D water cooled CPV model to investigate the effects of parameters like number of pipes, flow rate of water, etc. Their numerical results for the two connected water cooling pipes estimated the electrical efficiency between 7.39 and 8.38% for the flow rate between 0.0035 kg/s and 0.05 kg/s and thermal efficiencies between 22.5 and 45.9%. When they increased number of water pipes from two to six, they observed the increase in electrical efficiency in the range of 8.05 to 8.96%, while thermal efficiency from 46.8 to 63.2% for the same water mass flow rate. They maintained the SCs temperature of about 42.5 °C with 1020 $W/m^2$ solar insolation. Coventry [74] presented another variation on line focusing PV/T collector and named it as CHAPS (concentrating heat and power system). Their system consists of rows of cells cooled by liquid flowing through an internally finned aluminum pipe. The system with 37 Suns had thermal and electrical efficiency as 58% and 11% respectively. He observed low thermal efficiency than those reported in other research studies because of low heat losses from the CHAPS system, due to its smaller area. Mittelman et al. [75] designed and analyzed a CPV/T collector to produce both electricity and desalinated water using multiple effect evaporation with 200 Suns. They also designed a thermal storage system to provide round the clock operation of the desalination plant. Their experimental results showed that the electrical and thermal efficiencies depend upon coolant exit temperature and the total efficiency was found to be around 80%. They compared the thermal efficiency of the system with conventional desalination system on the economic conditions and found that it is valid for places with higher electricity price and lower solar collectors cost.

The hybrid CPV approach was explored by Sonneveld et al. [76] with a CR of 25 Suns. Their system consists of a Fresnel lens greenhouse chamber ($6\times6$ $m^2$) which allows diffuse solar radiation to pass through trapping all DNI. They used water as cooling medium as well as pre-heater liquid for waste heat. They estimated annual electrical and thermal energy production as 29 $kWh/m^2$ and 518 $MJ/m^2$ respectively, with combined efficiency of 67%. Similar research for CPV cooling and water heating has been reported by Kerzmann and Schaefer [77]. Ong et al. [78] have worked on the similar system, where they have done modelling and experimental study of a hybrid CPV/T with water desalination system. They found that the system was able to convert 85% of the solar irradiation into useful energy. Further three types of SCs array were investigated on parabolic trough CPV/T system by Li

et al. [79]. They conducted experiments for five hours with a super cell array, GaAs cell array and a concentrating silicon cell array. They observed that the average electrical efficiencies for three type SCs array were found to be 3.63%, 8.94%, and 3.67% respectively. They concluded that the concentrating silicon cell array was better in terms of performance-price ratio for low or middle CR. Xu et al. [80] simulated a tree shaped cooling channel system with heat recovery, using the COMSOL software for a Fresnel lens CPV/T system with 50 Suns. They designed the system in which SCs were attached to tree shaped cooling water channel by utilizing a thin-film thermal cladding. They used the channel structure as shown in Fig. 2.5. They compared pressure drop, effective heat transfer coefficient and electrical efficiency of tree shaped network with straight channel. They found that the tree shaped network channel maintained 10 °C lower temperature of PV cell as compared to straight channel, hence increased the life span and reliability of the system. Renno and Petito [81] proposed a CPV/T system for a domestic application with 900 Suns. They used a system with Fresnel lenses and parabolic mirrors with water and glycol as the cooling fluid to cool the cells. They observed the fluid outlet temperature from CPV/T to be 90 °C, which was used to drive an absorption heat pump (AHP) for summer cooling. Kunnemeyer et al. [82] designed a V-trough CPV/T solar collector to optimize both electrical and thermal efficiency. The V-trough was fabricated from a mirror finish stainless steel with a fluid channel in the center as shown in Fig. 2.6. They noticed shading problem on absorber in the early morning and afternoon. Their results showed that the combined thermal and electrical efficiency was around 35% and suggested that it can be increased by improved cooling. Helmers et al. [83] proposed an energy balance model for CPV/T system to calculate both electrical and thermal efficiency. They observed that thermal efficiency decreased as the temperature increased due to thermal losses. They concluded that for CR above 300, with mean fluid temperature up to 160 °C, theoverall efficiency of the system was 75%. Kosmadakis et al. [84] designed and numerically analyzed a CPV/T system coupled with an organic Rankine cycle (ORC) in which the heat removed from CPV was supplied to the boiler of an ORC for additional power production as shown in Fig. 2.7. They used refrigerant R-245fa (Critical Point: $T_{cr}$=154.05 °C, $P_{cr}$=36.4 bar) as the working fluid in ORC. They observed increased power generation with increase in CR (2-100 Suns). They further compared this integrated system with a standalone system which does not incorporate an ORC and found out the annual efficiency of standalone system was 6.56% lower than the efficiency of the integrated CPV-ORC system.

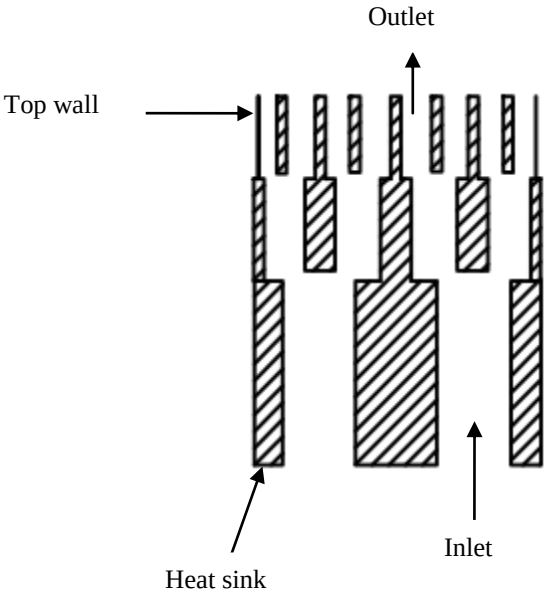


**Fig. 2.5.** Sketch of tree shaped network channel [80]

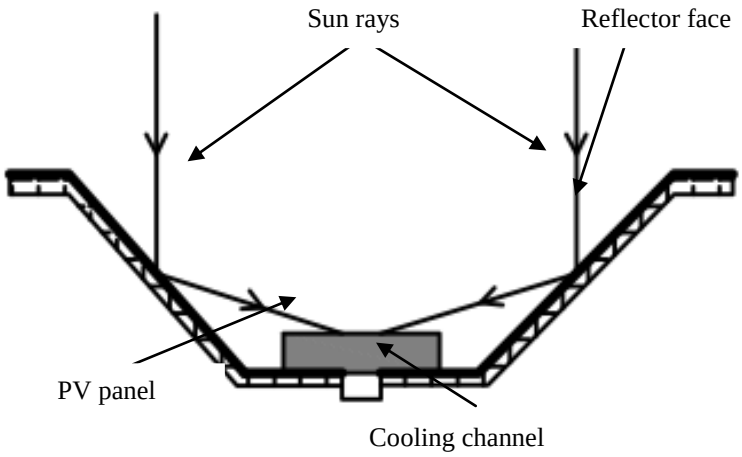


**Fig. 2.6.** Configuration of V-trough concentrator [82]

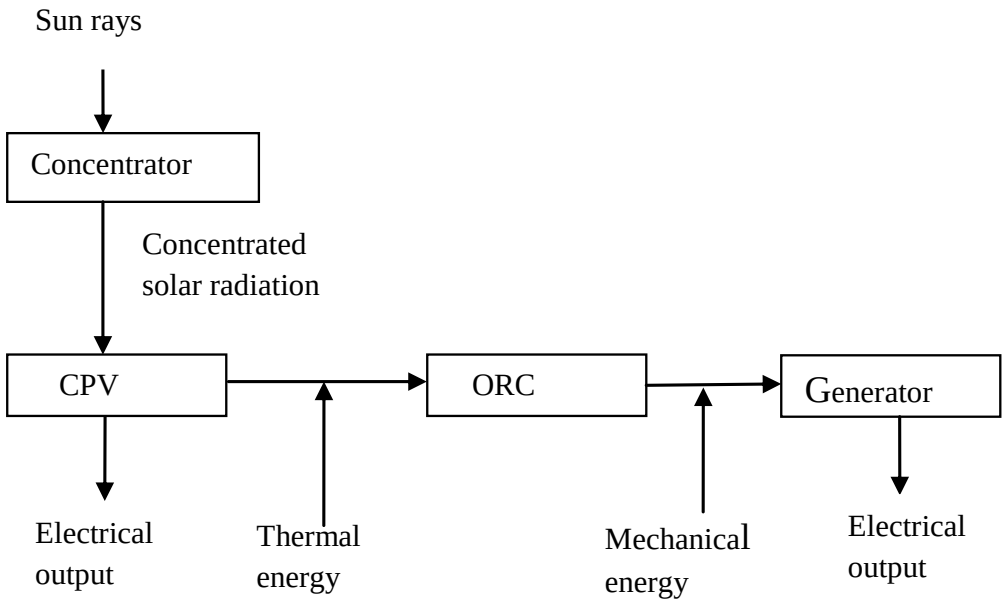


**Fig. 2.7.** Basic operation principle of the CPV-ORC system [84]

Xu et al. [85] conducted an outdoor experimental study on point focus Fresnel CPV/T system (CR of 1090) with triple junction SCs (InGaP/GaAs/Ge). They used a heat sink having the tubes with ID and OD of 26.4 mm and 34 mm respectively for the cooling. They found the instantaneous electrical and thermal efficiency of 28% and 54% respectively at DNI of 700 $W/m^2$ with 25 °C inlet temperature of water as a coolant. They also observed that the cell temperature maintained between the range of 60 to 90 °C for the DNI from 300 to 700 $W/m^2$. A numerically and experimentally U-shaped solar energy collector model of a CPV/T system was developed by Hussain and Lee [86] to analyze the electrical and thermal efficiencies by varying the mass flow rates. Their design consisted of a triple junction SCs (GuInp, GuAs, Ge) with a copper receiver tube to carry the coolant and silicon on glass Fresnel lens as a concentrator with dual axis tracking system. Their results showed the maximum overall efficiency of 76% for optimum flow rate of 2 lpm, at 900 $W/m^2$. Bahaidarah et al. [87] presented a numerical and experimental study to analyze the electrical, thermal and optical performance of a V-trough PV cooling system with 2 suns. The V-trough was fabricated from a glass mirror of thickness 5 mm with a reflectivity around 79%. Their results showed that the PV cell temperature was reduced from 47.1 to 39.20 °C in the month of March, while it reduced from 62.8 to 53.7 °C in the month of September.

#### *2.1.5.3 Building integrated concentrating photovoltaic thermal system*

Building integrated concentrating photovoltaic thermal system (BICPV/T) consists of a PV array, which acts as building envelope and dissipates heat through natural as well as forced convection. Such systems can also be operated with liquid as the working fluid. Baig et al. [88] performed both experimental and numerical analyses on BICPV system with 3.6 Suns. In their analyses they used a dielectric based cross compound concentrator made from clear polyurethane material and silicon cells, which were soldered using thin tip plated copper strips. At 0° incidence angle, they found the maximum cell temperature of 59 °C which further dropped to 26 °C incident angle of 60°. Baig et al. [89] carried out modelling and indoor experiments to evaluate the performance of BICPV. Their system consists of a dielectric based symmetric elliptical hyperboloid (SEH) concentrator with CR of 6, attached to silicon SCs between two glasses. In their simulation they took 10 $W/m^2$ and 7 $W/m^2$ convective heat transfer coefficients as the boundary conditions for exterior and interior surfaces respectively. At 0° incidence angle, they found the cell temperature of 45 °C and concluded that the temperature dropped with increasing incidence angle. Candanedo et al. [90] carried out an experimental study on an open loop air based BIPV/T system and derived convective heat transfer correlations from experimental observations. In their system the heated air was drawn through a channel below PV array by a variable speed fan as shown in Fig. 2.8. They suggested that this hot air may be used for ventilation, space heating and air to water heat exchanger to heat water. Their experimental results showed Nusselt number for top surfaces to be in the range of 6-48 for Reynolds numbers ranging from 250 to 7500 and for bottom surfaces it was in the range of 22-68 for Reynolds numbers ranging from 800 to 7060. Similarly Jubayer et al. [91] developed a correlation for exterior convective heat transfer coefficients for BIPV/T system and compared with boundary layer theory.

### 2.1.6 Jet impingement cooling

Jet impingement is an attractive cooling technique due to its potential of achieving high heat transfer rates. This cooling method has been used extensively in industrial applications such as annealing of metals, cooling of gas turbine blades, cooling in grinding processes [92]. Royne and Dey [93] proposed a jet impingement technique for cooling the densely packed PV cells. In their setup water flows through a plenum chamber in the normal direction to heated surface through stainless steel orifice plate, which was welded at the bottom of the plenum chamber. The heater consisted of thick stainless steel foil which was clamped and

stretched tightly between two aluminum bus bars. A model was also developed by them to predict the pumping power of different device shapes and they found that a higher number of nozzles per unit area improved the performance. They used Huber and Martin models for different concentration level. They found that PV cell temperature drops from 60 to 30 °C at 200 Suns and from 110 to 40 °C for 500 Suns in both models. Barrau et al. [94] conducted an outdoor experiment on hybrid jet impingement/microchannel cooling system for densely packed CPV cells. They used a dummy SCs (size 29.75 mm × 29.75 mm, thickness 2 mm) made of brass instead of real SCs for the testing. They obtained uniform temperature at 0.049 kg/s for the both CR of 373 and 537. They found low thermal resistance around $6.2\times10^{-5}$ $km^2/W$ for the same flow rate. Using experimental results they correlated the flow rate and CR as a function of temperature.

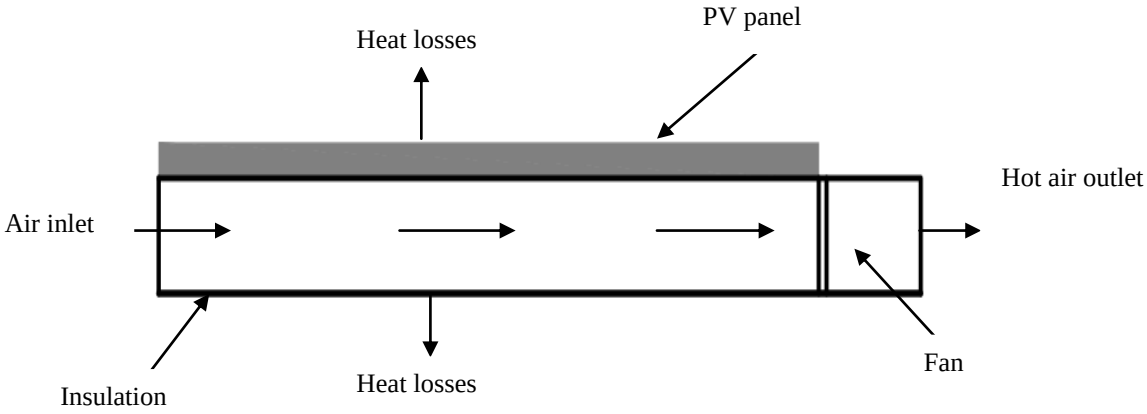


**Fig. 2.8** Schematic of a typical air based open loop BIPV/T system [90]

## 2.2 Photovoltaic cooling techniques

The various types of cooling technologies which have been implemented for PV systems are discussed in the following sections. The classification is made according to the type used.

### 2.2.1 Photovoltaic/thermal system

PV/T systems are formed by combining thermal collectors with PV panel through which excess heat can be dissipated to the cooling fluid so that the temperature of the SCs can be maintained within the limits. Such PV/T system provides thermal as well as the electrical output and are called as hybrid system. The PV/T systems are divided into two sub-systems: a solar sub-system and a cooling sub-system. The solar sub-system consists of the solar

collectors, a thermal storage, an electrical storage, an inverter, controllers and a regulator to distribute DC power from the collector array to/from the battery array. The cooling sub-system consists of a heat recovery cycle, fans, controllers, etc., A typical PV/T systems is shown in Fig. 2.9 [95].

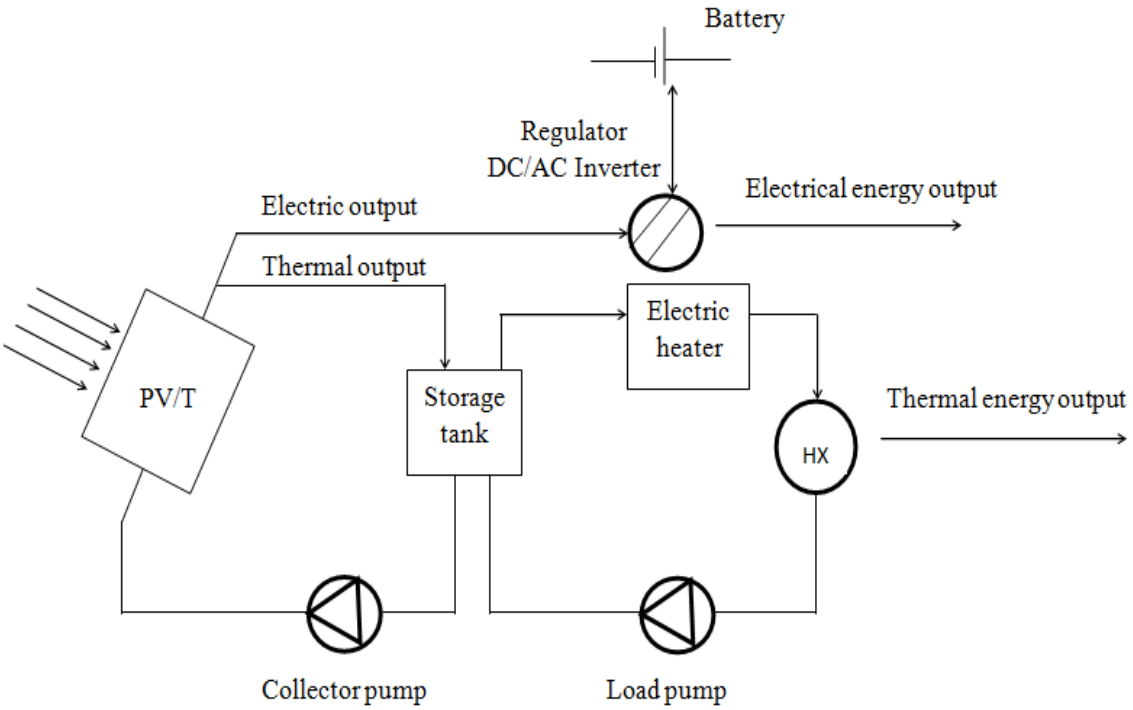


**Fig. 2.9.** Configuration of the PV/T system [95]

The research work on PV/T systems was started from mid 1970's. The research on such system were done by various researchers. The PV/T cooling systems classified in two types on the basis of cooling medium which used to remove the heat.

1. Air type
2. Liquid type

### *2.2.1.1 PV/T air systems*

Air type PV/T systems use air as the cooling medium. Hegazy [96] presented four different models of forced air type PV/T system, as shown in Fig.2.10.

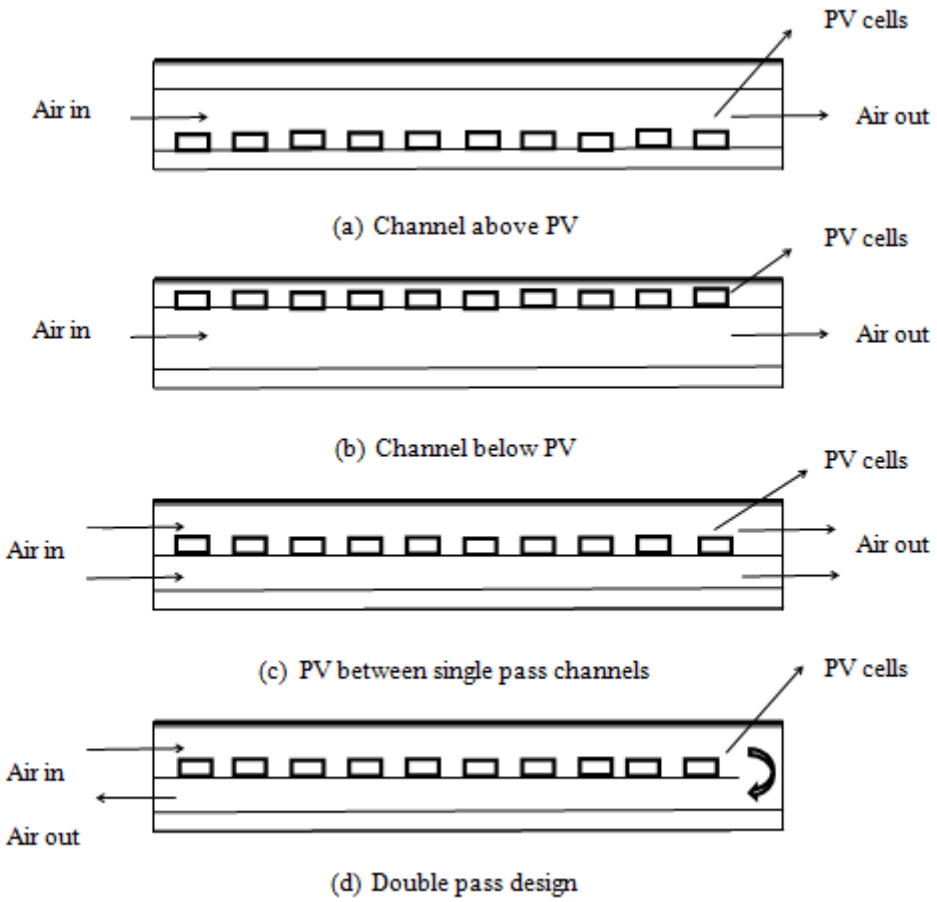


**Fig. 2.10.** Schematics of the various PV/T models by forced convection [96]

Tiwari et al. [97] presented an analytical model and experimental results to predict performance of a PV module along with an air duct. They performed the analyses for three modes. The first mode was the natural mode, without air flow below tedlar. The second mode was a forced mode using a single fan. The third mode was a forced mode with two fans. They found a close agreement between analytical and experimental results with a correlation coefficient (r) of between 0.97 to 0.99 and a root mean square percent deviation (e) between 7.54% to 13.89%. Joshi et al. [98] performed an analytical and experimental study to evaluate the performance of hybrid PV/T air collector system. They compared the performance of glass-to-tedlar and glass-to-glass PV/T systems using the analytical and experimental results. Their results showed that the PV back surface temperature and thermal efficiency were higher for glass-to-glass system as compared to glass-to-tedlar system. They found the inverse correlation-ship between the overall thermal efficiency and the length of the duct in both cases. Solanki et al. [99] developed a cost effective PV/T solar air heating setup for the indoor conditions. Their experimental setup had three PV modules (mono crystalline silicon

SCs) of glass to tedlar type. Their experimental results showed that with the increase in mass flow rate, efficiency increases and reaches towards the steady state condition. They found thermal and electrical efficiency 42% and 8.4% respectively, and the overall efficiency was found to be 50%. They concluded that this set-up can be used by SCs manufacturers to optimize different types of SCs in order to optimize.

A thermodynamic analysis of the PV/T system coupled with greenhouse air heater and dryer was carried out by Barnwal and Tiwari [100]. In their experimental set-up, two PV/T systems were mounted on the south roof of a greenhouse for heating and to run a DC air fan. The DC air fan was mounted on the higher end of the east wall to remove the humid air and drying of the greenhouse. Their results showed that the overall exergetic efficiency (11.4-13.2 %) was lower than the thermal efficiency of the PV/T system coupled with air heater. They concluded that this type of hybrid systems could be used in the remote areas of developing countries.The performance of PV/T air collector was optimized in terms of the net output exergy by Sarhaddi et al. [101]. They optimized the various thermal and electrical parameters of PV/T air system like front and back surface temperature of PV, inlet and outlet air temperature of PV/T, short-circuit current and voltage and maximum power point current. Further, they developed the novel equations for the exergetic efficiency of air collector and simulated in MATLAB. The observed marginal effect on exergetic efficiency of the system by variation in inlet air temperature of PV/T and duct length. They found the maximum exergetic efficiency of the PV/T system as 11.12%. Kamthania et al. [102] estimated the performance of PV/T double pass facade system for combined power and space heating. They used semi transparent PV panels which were mounted on the building. In their system, the ambient air was heated through a PV by using forced convection and reheated by another channel. The hot air, then used for the space heating. Their results showed that the annual thermal and electrical energy from the system were 480.81 kWh and 469.87 kWh respectively. They concluded that room temperature was increased by 5 to 6 °C with the PV/T double pass facade system.

A theoretical model of PV/T air system was developed by the Gholampour and Ameri [103] to investigate the effect of the various parameters like environmental, operational and dimensional. They concluded that the second law analysis is necessary for making good design decisions. They also concluded that the packing factor of the PV panel is crucial factor to determine the output and with an increase in packing factor both energy and exergy efficiency increases. Singh et al. [104] discussed the application of genetic algorithm with

multiple objective functions to improve the efficiency of an existing PV/T system. They incorporated conventionally parameters in optimization like geometry of the PV panel, flow channel, velocity of the air and inlet temperature of the PV/T system. They used two objective functions for the genetic algorithm as overall exergetic efficiency and the overall thermal efficiency of the PV/T system. They selected two cases for the study as case I: optimized the overall exergetic efficiency and case II: optimized of the overall thermal efficiency. They found that the electrical efficiency of the system during the first case was observed to be 14.15%, while the thermal efficiency was 11.88%. The electrical efficiency during this case II was observed to be 14.08%, while the thermal efficiency was 19.48%. They found an improvement of 4.6% in the overall exergetic efficiency and 13.14% in the overall thermal efficiency due to optimization. Two PV panels (poly-Si and mono-Si) were tested numerically and experimentally with the backside convection cooling arrangement for the Mediterranean climatic conditions by Nizetic et al. [105]. Apart from experimental study they did also a CFD analysis to obtain a sensitivity analysis of PV panels and they achieved a good agreement between the CFD and experimental results. They found out that due to flow separation there is an increase in average panel temperature by 5 to 9 °C which results in degradation of panel electrical efficiency from 2.5 % to 4.5 %. It is also observed that the efficiency may improve if flow separation is removed.

#### *2.2.1.2 Liquid type PV/T systems*

Liquid type PV/T systems use liquid as a cooling medium. The coolant in these systems passes through channels which are incorporated into the back of PV modules. Hegazy [96] presented four different models of forced water type PV/T system, as shown in Fig. 2.11. Water with its suitable optical properties makes it compatible with PV modules as it can absorb light mainly in infrared radiations which are longer wavelengths. Huang et al. [106] discussed a PV/T system for water heating and compared it to a conventional solar water heater and found that the primary energy saving efficiency of the system was about 60%, which is higher than the conventional solar water heater. Tripanagnostopoulos et al. [107] (2002) discussed the feasibility of hybrid PV/T solar systems. They concluded that the system performance can be improved by the use of an additional glazing, and a booster diffuse reflector or both. Their results showed 45% thermal energy with both additional glazing and booster diffuse reflector. They found a 13.3% increase in electrical efficiency when PV/Insulator was replaced by the PV/Water. Zondag et al.[108] presented different designs of PV/T systems to evaluate their performance. The highest annual efficiency was achieved with

channel underneath the transparent PV design followed by sheet-and-tube with 2% lesser efficiency. Though the latter design is little less efficient, but was considered as better alternative owing to its ease of manufacturing.

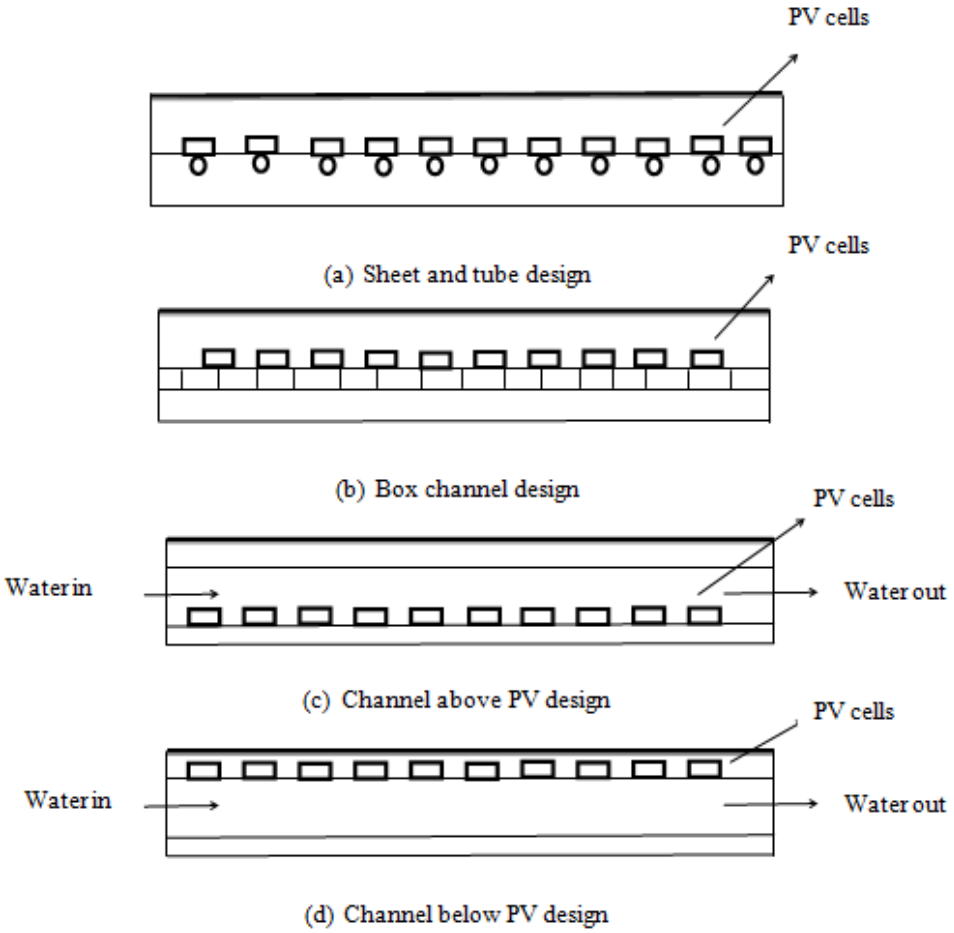


**Fig. 2.11.** Cross-sections of some common PVT/ water collector designs [96]

Vokas et al. [109] presented a theoretical approach on hybrid PV/T systems for domestic heating and cooling. They found that the thermal efficiency of the PV/T system was 9% lower than the efficiency of the conventional solar collector which tells that the proposed model is feasible and cost effective. They concluded that the thermal energy produced by a PV/T system can be used for the domestic heating and cooling. A numerical model of PV thermosyphon collector with fins was developed and validated with experimental data by Chow et al. [110]. Their experimental design had an aluminum plane box, type PV/T system with fins. They used two approaches for the performance investigation, first was tested through the reduced temperature analysis and second considering the summer and cold climate zones of China. Their results showed that the electrical and thermal efficiency of the system were 11.5% and 57.4%, respectively, with the fully covered absorber surface by PV

module. They concluded that their results are very good and could be used in PV potential domestic sector. Dubey and Tiwari [111] designed an integrated combined system which produced both electricity and hot water. Their system was supplied 200 liters hot water. They also derived an analytical expression for characteristic equation for PV/T flat plate collector for different condition as a function of design and climatic parameters. Their experimental results showed a significant increase in the efficiency from 33% to 64% due to increase in glazing area. They suggested that such system may be installed in remote areas to provide both hot water and electricity. Kumar and Tiwari [112] designed a proto type experimental system to evaluate the performance of hybrid PV/T and the solar still system. They used two designs for the hybrid solar stills system the first was a single slope passive system and second was single slope active system. The experimental study was conducted for three water depths of 0.05 m, 0.10 m, and 0.15 m for each of the still. Their results showed that the active solar still produced a maximum yield of 7.22 kg with water depth of 0.05 m. While the passive solar still produced only a maximum yield of 2.26 kg for the same water depth. They concluded that the hybrid active solar still produced 3.2 times higher daily yield as compared to passive solar still during in summer season. They also concluded that the new active solar still design provided a better electrical output and a 20% higher overall thermal efficiency as compared to the passive solar still.

Bilbao and Sproul [113] conducted an experiment on the PV/T system for developing countries. They considered two identical PV panels in their experimental set up in which one panel was converted to a PV/T-water module using a polycarbonate back sheet collector, while the other panel was kept unchanged as a control. Their experimental results showed that PV/T prototype has 5% more electricity than the control PV panel when effective cooling was provided. Li et al. [114] performed an experimental investigation on electrical and thermal performances of a semi-transparent PV/T System with water cooling. Their systems not only provide the electrical power and hot water, but also provide the natural illumination to the building. They calculated PV and thermal efficiency about 11.5% and 39.5%, respectively, to illustrate the performance of the PV/T system. Evola and Marletta [115] have calculated the optimum inlet temperature of water to the PV/T system to maximize the total exergy generated in the system. They suggested that this ideal temperature lies within the range usually occurring in solar thermal systems and could be attained in practical applications. They also performed a thermo economic analysis to calculate the price of thermal energy generated from the PV/T system in terms of exergy content. They concluded

that the price of the thermal energy generated from the PV/T system should be in the range of 1 to 10 c€/kWh.

Yazdanpanahi et al. [116] experimentally investigated the second law efficiency of PV/T water system. Using experimental analysis, they validated their one dimensional analytical model of the PV/T system. They found good agreement between theoretical and measured experimental results. They pointed out the errors in the calculations of exergetic efficiency performed by various researchers where they observed exergetic efficiency is similar to the value of electrical efficiency of the PV/T system at standard test conditions. Their results showed that the exergetic efficiency was 13.95% with a 0.002 kg/s flow rate. Nizetic et al. [117] was conducted an experimental study to cool both sides of PV panel using the water spray technique. For cooling, they used various nozzles on the front and back side of the 50 W monocrystalline PV panel. Their results showed that the PV panel temperature decreased from 54 °C to 24 °C and effective increase in electrical efficiency was measured as 5.9 % with cooling. No maintenance cost was observed as the water spray cooling system itself performed the cleaning effect, thus provided an insight on the economical aspect of such systems.

#### *2.2.1.3 Building integrated photovoltaic thermal system*

Building integrated photovoltaic thermal system (BIPV/T) consists of a PV array, which acts as building envelope and dissipates heat through natural as well as forced convection. Anderson et al. [118] designed a BIPV/T system and analyzed with the use of a modified Hottel-Whillier model. They showed that the BIPV/T system can be made of lower cost materials, such as pre-coated colour steel, without decrease in efficiency. They concluded that by increasing the ratio of the cooling tube width to spacing, the electrical efficiency decreases. They found that the fin spacing, the thermal conductivity between the PV cells and their supporting structure, and the lamination method had a significant influence on both the electrical and thermal efficiency. Agrawal and Tiwari [119] developed an analytical model to compare the performances of BIPV/T and the simple BIPV system. The parameters for the comparison were chosen as energy, exergy and life cycle cost. The study was conducted on mono-crystalline silicon, poly-crystalline silicon, crystalline silicon, amorphous silicon, cadmium telluride and copper indium gallium selenide based PV modules for the weather conditions of New Delhi, India. They found that the mono-crystalline silicon BIPV/T system produced the maximum annual electrical energy output as 15131 kWh. While, the least

annual electrical energy output was 6066 kWh, provided by the amorphous silicon system. They also found that the maximum thermal energy was produced by the amorphous silicon system as 20615 kWh and the least thermal energy was produced by the mono-crystalline silicon system as 16764 kWh. The reason for this was cited as higher solar insolation of the systems providing higher electrical output. From their results, it was observed that the BIPV/T system has a 17 to 20% higher energy efficiency and a 1.5 to 2% higher exergetic efficiency as compared to a simple BIPV system operating in the same climatic conditions. This was attributed to the cooling effect of the air.

Agrawal and Tiwari [120] developed an analytical model and conducted experiments to study the performance of a BIPV/T system. The analyses were conducted for four configurations. The first configuration had all rows of the BIPV/T system connected in parallel. The second configuration had three rows of the BIPV/T system connected in parallel, each having two rows in the series. The third configuration had two rows of the BIPV/T system connected in parallel, each having three rows in the series. The fourth configuration had all the rows of the BIPV/T system connected in the series. They observed that the series connected BIPV/T produced the yield optimum results for constant mass flow rate of air. While, the parallel arrangement system was reported to perform best when constant velocity of air flow was maintained. They found that the annual electrical exergy and annual thermal exergy of the system were 16209 kWh and 1531 kWh respectively. Yang and Athienitis [121] conducted an experiment on a BIPV/T system with glazed air collector and single inlet. They further simulated this system with multiple air inlets and found increase in thermal efficiency by about 5%. They observed that by adding a vertical glazed solar air collector, thermal efficiency was improved by 8% and it was more significant with wire mesh packing in the collector where it achieved 10%. Wang et al.[122] investigated the performance of the BIPV/T system under frame shadows. In a BIPV/T system an air layer exists between SCs and glazing glass which decreased the heat loss and increased the thermal efficiency of the system. However, a frame was used to support the glazing glass resulted in casting a shadow on the SCs. Hence, they investigated the effects of this shadow on the performance of the BIPV/T system. They found that this shadow decreased the PV efficiency to 2.6% for the Hefei China conditions. They also concluded that 70.15 kWh/$m^2$ was a total electrical loss due to this shadow. Gupta et al.[123] has been carried out the exergetic analysis of building integrated semitransparent PV/T system. The design was considered, the room below a constant room temperature. They derived the energy balance equations for the SCs, room air,

room floor temperature and SCs efficiency. It has been observed that SCs and room air temperature was decreased as an increase in the number of air changes. Their results showed that the daily thermal exergy, overall thermal exergy and thermal energy of the system were increased by 6.28%, 1.15% and 26.81% respectively with the increase in air changes from 0 to 4. They found good agreement between theoretical and experimental results with a correlation coefficient of 0.97.

### 2.2.2 Phase change material cooling

As discussed earlier the PCM has ability to keep the relative stable temperature during heat absorption because of its phase transition (melting and freezing). Huang et al.[124] investigated a numerical model to moderate the rise in temperature of BIPV system and validated the same with experimental data. In their work PCM was attached to the rear surface of a PV cell, thus allowing convection to take place on the surface of the PV. They suggested that the PCM transient temperature should be higher than the ambient temperature and lower than 25 °C to maintain the same temperature on the front of PV cell. They resolved the problem of low thermal conductivity of the PCM by using aluminium fins. Fig. 2.12 shows the system used by them, it shows the front wall (with two fins attached) and rear wall of the PV/PCM system. They concluded that fins enable a more uniform temperature distribution within the PV/PCM system as compared to a system without fins. Further the performance of a different internal fin arrangement with two PCMs was investigated and compared by Huang et al. [125]. The two PCMs used were RT25 with a melting temperature of 25 °C and GR40 with a melting temperature of 40 °C. The PCMs were packed in the aluminium structure with 31 fins of 27 mm wide with an insolation of 750W/$m^2$. Their experimental results showed that GR40 was less efficient compared to RT25 as GR40 maintained the PV temperature below 51 °C while RT25 maintained below 32 °C for the same conditions. Their results showed that fin spacing of 8 to 12 mm was beneficial as compared to that of 4 to 8 mm. With increased fin spacing requires less fin material while temperature difference was observed to be 0.9 °C higher as compared to lower spacing. An experiment with BIPV to evaluate the performance of five different PCMs in four different PV/PCM systems was carried out by Hasan et al. [126] with one Sun. During the experiment they observed a temperature drop of 18 °C in first 30 minutes, which reduced down to 10 °C in next 5 hours. Biwole et al.[127] presented a detailed CFD modelling of heat and mass transfers in coupled PV/PCM system. In the simulated system they found that the PV temperature of below 40 °C for 80 minutes simulation run with one Sun, while the same

temperature was reached by the panel within only 5 minutes, without PCM. The main focus of their study was to optimize the design of PV/PCM finned system and they found that the cooling fins in the PCM provide a faster attenuation of the operating temperature.

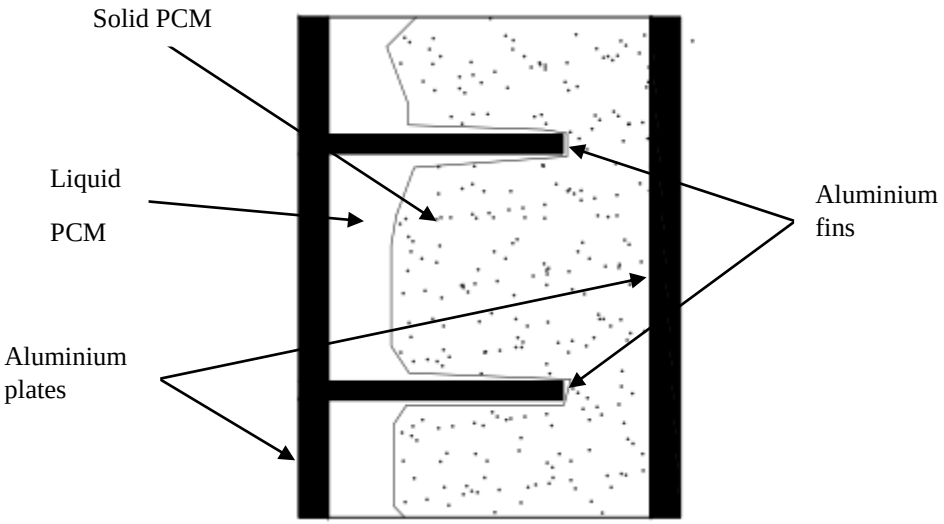


**Fig. 2.12.** PV/PCM system with aluminium fins [124]

## 2.3 Summary of literature review

A detailed summary of various cooling technologies discussed above is provided in Table 2.1. In Table 2.2 a comparative study of different cooling systems is presented. The parameters for various cooling technologies are different as per their applications, as presented in Table 2.1. Some parameters which are applicable to one cooling technology are not applicable for other. Considering the wide range of cooling technologies, it is difficult to compare them on common grounds. Furthermore, the literature lacks the information on all these aspects together. In Table 2.1, the experimental and theoretical work for various types of the cooling system of PV and CPV has been presented. From the Table 1, it is observed that, various types of cooling systems were used for CR ranging from 1-1000. In case of heat pipe cooling technology, maximum temperature obtained was 40 °C higher than the ambient conditions. Experimental work has also been done using fins on the heat pipe to improve the cooling capacity. From the literature, it has been inferred that such type of cooling is preferred for low and medium concentration levels. In case of water cooling technologies, the maximum cooling effect (which is the difference of SCs temperature with and without cooling) with a temperature drop of 50 °C was observed. Even in case of PV/T, CPV/T and jet impingement, water is preferred as the coolant instead of other fluids. Such type of

cooling system can be used for a higher range of CR, as discussed in Table 2.2. However the main challenges in such systems are leak proof designs with lower pumping power.

When air is used as coolant media in PV/T and CPV/T, the cooling effect is quite low as compared to the liquid coolant due to the lower heat capacity of the air and hence needs more surface area. However, such system can be hybridized for space heating purposes. In case of liquid immersion technologies, the heat transfer coefficient can go up to 6000 W/($m^2$ K). Such type of cooling is quite effective as heat is transferred from both front and rear surfaces of the SCs. The main application for such system is that it can be used in densely packed CPV systems. However, salt deposition is the main challenge in such technology. In microchannel heat sink cooling technology, both air and water have been used as coolant but water is more effective coolant than air as discussed previously. Such cooling technology has low thermal resistance and can sustain high CR up to 1000 Suns as presented in Table 2.1. But the main challenge in the design of the heat sink is to minimize the pressure drop across its length. This limitation can be overcome by using a tree shaped network channel in the design. In PCM based cooling technology, most of the work has been done for PV. The main advantage of such a cooling system is that it stores large amount of heat at constant temperature, which may be used for some thermal applications and it does not use electrical power. It is also evident from the literature that a limited amount of work has been done using PCM with CPV in contrast with the work done with silicon cell technology, which dominates the commercial market as of date.

**Table 2.1.** A summary of the cooling system reviewed

| Author | Type of Cooling | CPV cell material | CPV cell temperature (°C) | Cooling effect (Temperature change) ΔT(°C) | Concentratio -n ratio (Suns) | Type of concentrator | Flow conditions | Heat transfer coefficient ($W/m^2 K$) | Location | Ambient Conditions | | |
|---|---|---|---|---|---|---|---|---|---|---|---|---|
| | | | | | | | | | | DNI ($W/m^2$) | Ambient temp. (°C) | Wind speed (m/s) |
| Akbarzadeh and Wadowski (1996) | Heat pipe cooling | Polycrystalline | 46 | 38 | 20 | Linear trough | | | Australia | | | |
| Farahat (2004) | Heat pipe cooling | | | | | Parabolic dish | 35 l/m | | Egypt | 1000 | 20 | |
| Cheknane et al. (2006) | Gravity dependent heat pipe | Silicon cells | | | Up to 500 | Fresnel lens | | | Algerie | | | |
| Anderson et al. (2008) | Heat pipe cooling with fins | | 40 (higher than ambient) | 170 | 30 | | | 3.88 | Lancaster (UK) | | 25-30 | |
| Huang et al .(2012) | NHSP heat pipe | III-V multijunction | | | | Fresnel lens | | 3561 and 991 | South Taiwan | 930 | 35 | 3.1-3.5 |
| Lee and Baek (2015) | Heat pipe cooling | Triple junction (InGaP, InGaAs and Ge) | 29.3, 33.3, 37.2, 41.2 | | 500, 600, 700, 800 | Fresnel lens | | | Korea | | | |
| Chenlo and Cid (1987) | Water cooling | Monocrystalline | 28 | 15 | 24 | Fresnel lens | | 1150 | Madrid (Spain) | 890 | | |
| Lasich (2006) | Water cooling | | 40 | 40 | 200 | Parabolic dish | | | Australia | | | |
| Kolhe et al. (2012) | Water cooling | | 49 | | 8.5 | Optical type | | | China | 900 | 32.5 | 0.25 |
| Chong and Tan (2012) | automotive radiator cooling | Multijunction Cells | 37.1 | 22.3 | 377 | Non imaging planer | 0.583kg/s | 1967 | Kuala lumpur (Malaysia) | 300-950 | 30-36 | 3 |
| Chaabane et al. (2015) | Water cooling | Monocrystalline | 42.15 | 17 | | | 0.0035 kg/s-0.05 kg/s | | Tunisia | 1024 | Chaabane et al. (2015) | Water cooling |
| Conventry (2005) | Water cooling (CPV/T) | Monocrystalline silicon cells | | | 37 | Parabolic trough | | | Camberra (Austraia) | 1000 | 25 | 0.21 |
| Mittlemen et al. (2009) | CPV/T -MEE desalination | Multijunction Cells | 10-30 higher than coolant outlet temp. | | 200 | | | | Israel | 900 | | |

| Author | Type of Cooling | CPV cell material | CPV cell temperature (°C) | Cooling effect (Temperature change) ΔT(°C) | Concentratio -n ratio (Suns) | Type of concentrator | Flow conditions | Heat transfer coefficient ($W/m^2 K$) | Location | Ambient Conditions | | |
|---|---|---|---|---|---|---|---|---|---|---|---|---|
| | | | | | | | | | | DNI ($W/m^2$) | Ambient temp. (°C) | Wind speed (m/s) |
| Li et al. (2011) | Forced water circulation (CPV/T) | Super cell, GaAS and silicon cell | | 23.6[1] | 28.8 & 30.8 | Parabolic trough | 40 l/h | | China | 900-960 | | |
| Sonneveld et al. (2011) | Water cooling (CPV/T) | Monocrystalline Si- cells | | 3.4[2] | 25 | Fresnel lens | 18.6kg/s | | Netherland | 630-792 | | |
| Ong et al. (2012) | Water circulation (CPV/T-Desalination) | Multijunction Cells | | 50[3] | | High concentration | 1.9-5.63 l/min | | Switzerland | 525 | | |
| Xu et al. (2012) | Water circulation in tree shaped network | Silicon cells | 47.7 | 22 | 50 | Fresnel lens | 1.59 l/h | 3000-1200 for 25-250 mm cell | Newyork (US) | | | |
| Renno and Petito (2013) | CPV/T-AHP for summer cooling | lnGap/lnGas/Ge | | 67[4] | 900 | Fresnel lens & parabolic mirror | 0.0138-0.055kg/s | | South Italy | | | |
| Kunnemeyer et al. (2013) | Water circulation (CPV/T) | Polycrystalline cells | | | 1.2 | V-trough | | | New Zealend | 555 | [5] | |
| Bahaidarah et al. (2015) | Water circulation (CPV/T) | Monocrystalline | 39.20 and 53.7 | 7.9 and 9.1 | 2 | V-trough | 0.6-1 l/m | | Saudi Arabia | 963 | | |
| Xu et al. (2015) | Water circulation (CPV/T) | InGaP/GaAs/Ge | 60-90 | | 1090 | Fresnel lens | 0.33 $m^3$/h | | China | 300-700 | 15-17 | 1 |
| Hussain and Lee (2015) | Water circulation (CPV/T) | GuInp Gu As Ge | | | | SOG Fresnel lens | 0.5, 2, 4 l/m | 5 convective | South Korea | 900 | 25 and 30 | |
| Tan et al. (2014) | Water circulation | Crystalline-silicon | 23 | | | parabolic trough | | | China | 896 | 15.1 | 0.3 |

[1]Coolant inlet temperature was 18.0 °C while outlet temperature was 41.6 °C.
[2] The inlet temperature was taken as 12.4 °C while outlet was observed as 25.8 °C.
[3] The cooling water temperature changes from 25 °C to 75 °C.
[4] Coolant water temperature rises from 40 °C to 107 °C.
[5] Air mass was taken as 1.5.

| Author | Type of Cooling | CPV cell material | CPV cell temperature (°C) | Cooling effect (Temperature change) ΔT(°C) | Concentratio -n ratio (Suns) | Type of concentrator | Flow conditions | Heat transfer coefficient ($W/m^2 K$) | Location | Ambient Conditions | | |
|---|---|---|---|---|---|---|---|---|---|---|---|---|
| | | | | | | | | | | DNI ($W/m^2$) | Ambient temp. (°C) | Wind speed (m/s) |
| Baig et al. (2014) | CBIPV | | 26 | 33 | 3.6 | 3D cross compound parabolic | | 10 for exterior, 7 for interior | Penryn UK | 1000 | | |
| Helmers et al. (2014) | Water circulation | | | | 300 | | 0.133 kg/s | | Germany | 850 | 20 | 3 |
| Kosmadakis et al. (2011) | CPV/T-ORC | | 80 | 60 | 2 to 100 | | | 8.8 | Athens, Greece | 1000 | 25 | 2.0 |
| Jian and Mingheng (2010) | Air circulation (CPV/T) | Silicon cells | | | 5 & 7 | Compound parabolic | | | China | 1000 | | |
| Cuce and Cuce (2013) | Air circulation | Silicon cells | 29 | 16 | | | 5 m/s | | Nottingham (UK) | 1000 | 15 | |
| Amri and Mallick (2013) | Air active circulation | GalnP/GaAs/Ge | 150 for 100 suns | 90 for 100 Suns | 100,150 &200 | | 8,16,32 m/s | | Saudi Arabia | | 27 | |
| Abrahamyan et al. (2002) | Dielectric liquid immersion (DLI) | Silicon cells | | | | | | | Armenia | 800 | | |
| Wang et al. (2009) | Dielectric liquid immersion | Silicon cells | | | | | | | China | | | |
| Zhu et al. (2010) | Liquid immersion | Monocrystalline silicon cells | 45 | 15 | 250 | | 2.0-2.7 m/s | 3000 | China | | | |
| Han et al. (2011) | DLI | Silicon cells | | | 10, 20 and 30 | Optical | 0.56-1.11l/s | 1000 | China | | 25 | |
| Han et al. (2013) | DLI | Silicon cells | | | 10,20 and 30 | Optical | | | China | | | |
| Zhu et al. (2011) | DLI | | 49 | 31 | 250 | Dish concentrator | 2.23m3/h, 1.05 m3/h | 6000 | Las Vegas (US) | 940 | 17 | 2.0-2.7 |
| Xiang et al. (2012) | Liquid immersion with fins | | 38 | | 250 | | 0.04-0.80 m/s | | China | | | 0.32 |
| Liu et al. (2011) | DLI | Silicon cells | 30 | [6] | 47 | Long arc xenon lamp | | 1000 | China | | | |

[6] Author mentioned that the total heat removed from the module was 44.3 $kW/m^2$.

| Author | Type of Cooling | CPV cell material | CPV cell temperature (℃) | Cooling effect (Temperature change) ΔT(℃) | Concentratio -n ratio (Suns) | Type of concentrator | Flow conditions | Heat transfer coefficient ($W/m^2 K$) | Location | Ambient Conditions | | |
|---|---|---|---|---|---|---|---|---|---|---|---|---|
| | | | | | | | | | | DNI ($W/m^2$) | Ambient temp. (℃) | Wind speed (m/s) |
| Sun et al. (2014) | liquid immersion | Silicon cells | 20-31 | 11 | 9.1 | linear flat mirror | | 1000 | China | 910 | | |
| Xin et al. (2015) | liquid immersion | Triple-junction (GaInP/GaInAs/Ge) | 78.92℃, 71.91℃, 82.43℃ and115.69℃ | | 500 | Fresnel lens | 0.00138 kg/s | | China | 500 | | |
| Edenburn (1980) | Natural convection heat sink | | 150 for 90 suns | | 50,92 & 170 | Point focus Fresnel lens | | | US | | | |
| Araki et al. (2002) | Natural convection heat spreader | Multijunction cells | 18 and 21 more than ambient | | 400 & 500 suns | Fresnel lens | | | Japan | 600 | | 0.3-2.8 |
| Chou et al. (2007) | Heat sink | | 44.25 | [7] | 350 | | | 4.64 | Taiwan | 910 | 30.5 | |
| Kermani et al. (2009) | Manifold micro-channel heat sink | Silicon cells | | [8] | 1000 | | 0.0011 kg/s | 65480 | Abu Dhabi | 1000 | | |
| Min et al. (2009) | Heat sink | Triple junction Galnp/GaAs/Ge) | 37 | 1163 | 400 | Fresnel lens | | Convective =5 | China | | 27 | |
| Alvarado et al. (2011) | Micro-channel heat sink | | Maximum 70 | [9] | 40 -50 | | 0.00015-0.00030 kg/s | | US | | | |
| Lee et al. (2012) | Heat sink with fins | | 130 and 160 for 10.38 fin spacing | [10] | 255 | | 1.5-3.5 m/s | | Malaysia | | | |
| Gualdi et al. (2013) | Heat sink | Multijunction cells | below 80 | | 400 | | | | France | 1000 | | |
| Reddy et al. (2014) | Micro-channel heat sink | Multijunction cells | Min. 40 | 4.53[11] | 500 | Square parabolic dish | 0.105l/s | | India | 550 | | |

[7] Heat dissipation power was observed as 8.79 W.
[8] The author discussed the heat flux as 75 $W/cm^2$.
[9] It was stated that the heat flux to be 41.5 $kW/m^2$.
[10] Heat flux was observed as 255 $kW/m^2$.
[11] Coolant inlet and outlet temperature was 40 °C and 44.53 °C respectively.

| Author | Type of Cooling | CPV cell material | CPV cell temperature (°C) | Cooling effect (Temperature change) ΔT(°C) | Concentratio -n ratio (Suns) | Type of concentrator | Flow conditions | Heat transfer coefficient ($W/m^2 K$) | Location | Ambient Conditions | | |
|---|---|---|---|---|---|---|---|---|---|---|---|---|
| | | | | | | | | | | DNI ($W/m^2$) | Ambient temp. (°C) | Wind speed (m/s) |
| Liao et al. (2014) | Thermoelectric hybrid | Polycrystalline cells | | | 5 | Fresnel lens | | | China | 800 | | |
| Wu et al. (2015) | Thermoelectric hybrid | | | | up to 6 | | 0.01 m/s | | China | 1000 | 25 | 2.5 |
| Natarajan et al. (2011) | Heat sink with fins | Silicon cells | 51.9 for three fins | 16.4 | 10 | Fresnel lens | | 5 for sides, 14.8 for back plate | Edinburgh (UK) | 1000 | 20,30,40,& 50 | 1 & 4 for top & bottom of SCs Respectively |
| Yang and Zuo (2015) | manifold microchannel | Silicon cells | 20.4 | 23.7 | 28 | long-arc xenon lamp | 0.00535 to 0.0232 kg/s | 8235.84 | China | | | |
| Huang et al. (2004) | PCM with fins | | 36.4 | 50.2 | | | | 12.5 | Ireland (UK) | 750 | 20 | |
| Huang et al. (2006) | PCM with different internal fins | Silicon cells | 32 for RT25 51 for GR40 | 30 | | | | | Ireland (UK) | 750 | 23±1 | |
| Hasan et al. (2010) | PCM system | | | 18 | | | | | Ireland (UK) | 500,750,1000 | 20±1 | |
| Maiti et al. (2011) | PCM system with paraffin wax | Silicon cells | 62 (outdoor exp.); 65 (indoor exp.) | 16 for outdoor exp. & 25 for indoor exp. | | | | | India | 30-43 | | 1.5 |
| Tan et al. (2012) | PCM with CTEG | Thermoelectric cell module | 78 | 78 | 60 | | | | Australia | | 20 | 2 |
| Biwole et al. (2013) | PCM with fins | Silicon cells | 40 | | | | | Indoor-5 Outdoor-10 | France | 1000 | 20 | |
| Royne and Dey (2007) | Jet impingement cooling | Silicon cells | 30 for 200 Suns and 40 for 500 Suns | | 200 and 500 | | | [12] | Australia | | | |

[12]It was observed that the heat transfer coefficient for 200 suns was found as $27x10^3$ $W/(m^2 K)$ (using martin model) and $28x10^3$ $W/(m^2 K)$ (using huber model) while for 500 Suns it was $38x10^3$ $W/(m^2 K)$ (using martin model) and $37x10^3$ $W/(m^2 K)$ (using huber model).

**Table 2.2** Comparative study of different cooling systems

| Type of cooling | Advantages | Disadvantages | Challenges in the construction | Application |
|---|---|---|---|---|
| Heat pipe coolings | ✓ Passive heat exchange device<br>✓ It can transfer heat across long distances<br>✓ Easy to integrate<br>✓ It can accept heat at very high heat fluxes | ✓ High cost<br>✓ Dependent on atmospheric conditions like wind speed<br>✓ Corrosion problem<br>✓ Generation of non condensable gas | ✓ More complex design<br>✓ Leakage of refrigerant<br>✓ Choice of pipe material | ✓ Used for high wind speeds convection<br>✓ For low and medium concentration level |
| Hydraulic (water) cooling and Jet impingement cooling | ✓ Higher thermal conductivity and heat capacity<br>✓ Higher heat transfer coefficient<br>✓ Higher mass flow rate<br>✓ Very low thermal resistance can be achieved in Jet impingement cooling | ✓ High cost due to pumping power<br>✓ Corrosion problem<br>✓ Higher maintenance cost<br>✓ Life cycle is low<br>✓ In case of impingement cooling disturbances occur when water from one jet meets the water from neighboring jet | ✓ Leak proof design to avoid liquid ingress<br>✓ Minimizing pressure drop that depends on flow path<br>✓ Direct contact of liquid to the PV panel<br>✓ Suitable design of an array of jets in case of Jet impingement cooling | ✓ Jet impingement cooling can be apply to larger dimensions and for high concentration level due to low thermal resistance<br>✓ It could be alternatives of heat sink |
| PV/T and CPV/T system (Air and water) | ✓ Higher heat transfer rate in liquid than air<br>✓ Produces both thermal and electrical energy<br>✓ Hot air can be used for space heating<br>✓ Higher temperature reduction in case of water | ✓ Low temperature reduction in case of air<br>✓ Low mass flow rate of air<br>✓ Pumping power required in case of water<br>✓ Initial cost is high | ✓ Mounting of tanks and its supporting structures<br>✓ Leak proof design<br>✓ Design a proper channel for water flow to rear side of panel | ✓ Can be used for providing both thermal and electrical energy<br>✓ Can be hybridized with other sources like desalination, ORC, space heating etc. |
| Phase change material cooling | ✓ Passive heat exchange<br>✓ Large amount of heat energy can be stored<br>✓ Compatibility, reliability, maintenance-free and high cooling capacity<br>✓ No electricity consumption | ✓ Higher cost<br>✓ Some PCMs are toxic and have fire safety issue<br>✓ Disposal problem after end of life cycle | ✓ The design criterion must take care of the volume<br>✓ increase upon melting of wax | ✓ It can be used for high heat fluxes<br>✓ It can be used for thermal storage applications |
| Liquid immersion cooing | ✓ For back cooling, it eliminates the contact thermal resistance<br>✓ Heat can be transferred from both front and rear surfaces | ✓ More complicated system design<br>✓ High cost | ✓ Salt deposition can be a problem<br>✓ Leak proof design reduired<br>✓ Supporting<br>✓ structures and tank increases weight | ✓ Most suitable for densely packed CPV |
| Microchannel heat sink cooling | ✓ Low thermal resistance<br>✓ Low power requirement<br>✓ Remove a large amount of heat in a smaller area | ✓ Pressure drop limitations<br>✓ Undesirable uneven temperature distributions along the streamline | ✓ Maintain low contact thermal resistance between the substrate and heat sink | ✓ It can be used for high concentration level due to its low thermal resistance |

A comparative assessment of all the cooling technologies with respect to CR used and cell temperature is shown in Fig. 2.13. Minimum temperature of 20.4 °C was obtained for microchannel heat sink for 28 Suns, while maximum temperature of 78.92 °C was obtained using liquid immersion technology for 500 Suns. Maximum heat transfer coefficient of 38000 W/($m^2$ K) was observed in case of jet impingement cooling technology for CR of 500. In CPV, the best cooling technologies cited in the literature are, microchannel heat sink, liquid immersion and jet impingement. Most of the research work for cooling technologies used silicon cells, which still dominates the market as shown in Fig. 2.14. This presents a lot of scope for exploring their applications with multi junction SCs. The research outcomes may also be utilized towards efficient commercial advancements.

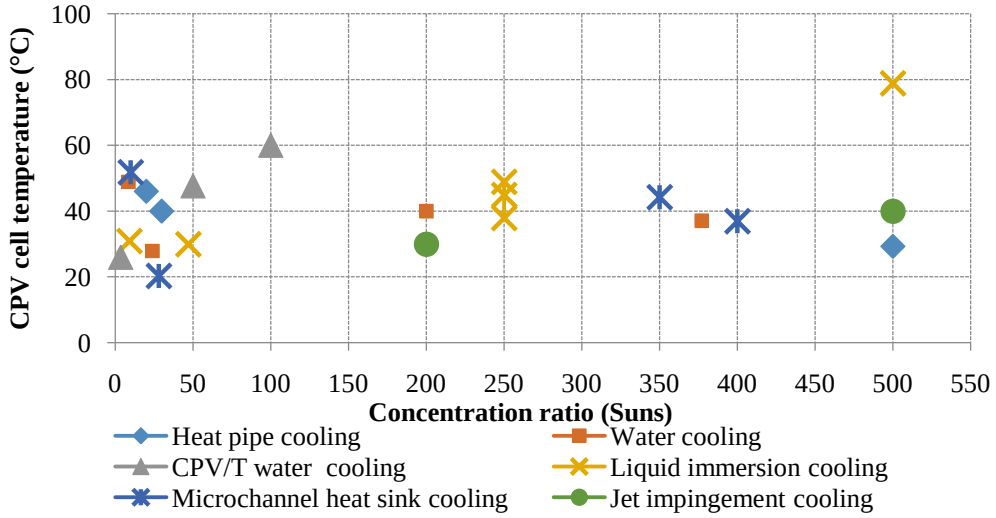


**Fig. 2.13.** Comparison of maintained SCs temperature of various cooling technologies

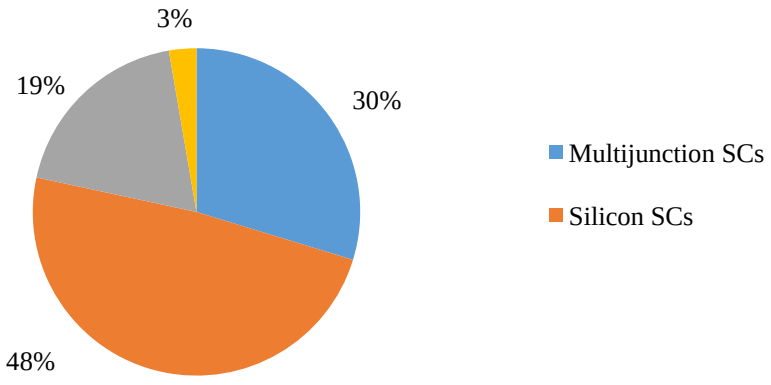


**Fig. 2.14.** Distribution of cell materials used in literature for different cooling technologies

Other cooling approaches which are used to cool down the system other than PV and CPV are also discussed by various researchers. One of the technology is geothermal cooling, which is discussed in the next section.

### 2.4 Geothermal cooling

Geothermal systems are widely used to exchange thermal energy due to the high thermal capacitance of earth. One of the applications is an air conditioning system which uses a geothermal system to dissipate excess heat. Such principle can also be used for PV and CPV systems cooling. The soil temperature at a depth of about 3-3.5 m remains constant throughout the year and is equal to the average annual ambient air temperature [16]. Based on the nature of heat transfer fluid taken for the system, it is termed as earth air heat exchanger (EAHE) system, when air is the working fluid or earth water heat exchanger (EWHE) system when water is the working fluid.

#### 2.4.1 Earth air heat exchanger

With early research work in the late 1970s and early 1980s, EAHE systems were not widely accepted due to poor system performance or technical issues like growth of microorganism in the air tube. With the advancement and push towards green technologies, the interest in development of EAHE has grown. Various researchers have developed and studied EAHE from different angles of investigations. The broad area for the research includes performance investigation, enhancement of cooling/heating effect, coupling it with other systems to make as hybrid system, etc. Such hybrid systems were analyzed analytically and tested experimentally to explore their cooling/heating potentials at different locations. Sodha et al. [128] investigated the effect of length, radius of pipe and air mass flow rate on the seasonal cooling potential of an EAHE system. They also investigated the most effective combination of these parameters for maximum cooling potential considering given mass flow rate and material of the pipe. Calculations were made for hot-dry and composite climates typified by Jodhpur and Delhi in India, respectively. In their set-up a fixed amount of air was passed through a single pipe or ‘m’ number of pipes. They found that the necessary blower power for number of pipes was much larger than that required for a single pipe. Sharan and Jadhav [129] analyzed the performance of a single pass EAHE system in cooling and heating mode. They used the 50 m long, 100 mm nominal diameter and 3 mm wall thickness mild steel pipe for the EAHE system which was buried at 3 m depth. The

ambient air with 11 m/s velocity was circulated with the help of 400 W blower. They found out that the EAHE system reduced the hot ambient temperature by 14 $^{o}$C in the month of May while the basic soil temperature was 26.6 $^{o}$C. Ajmi et al. [130] developed a theoretical model of an EAHE system for predicting its cooling potential and outlet air temperature in a hot, arid climate of Kuwait. It was observed that EAHE system with pipe length of 60 m, pipe diameter 0.25 m and air flow rate of 100 kg/h reduced the indoor temperature of a domestic building and its cooling load by 2.8 $^{o}$C and 1700 W respectively. They concluded that EAHE system has the potential for reducing cooling energy demand of buildings by 30% over the peak summer season. Kumar et al. [131] used the concept of goal-oriented genetic algorithm to design a tool for evaluating and optimizing various aspects of EAHE behaviour. They investigated the effects of various parameters on EAHE outlet temperature like ambient temperature, ground upper surface temperature and ground temperature at a certain depth and impact of humidity. They found that the outlet temperature of EAHE was significantly affected by ambient air temperature and ground temperature at a certain depth. Chel and Tiwari [132] investigated the performance and life cycle cost analysis of the EAHE system for the adobe structures for the composite climate of New Delhi (India). They found that the outlet air temperature of EAHE was higher by 5 ºC to 15 ºC as compared to ambient temperature during the winter season and was lower as compared to ambient values during summers with a payback period of less than 2 years. Bansal et al. [133] developed a transient and implicit model based on CFD to forecast the cooling capacity and thermal performance of the EAHE systems. Their results showed that the outlet temperature of EAHE was decreased by 8 °C to 12.7 °C with the flow velocity range of 2 m/s to 5 m/s. Their results showed that the hourly cooling of the system was found in the range of 1.2 MWh to 3.1 MWh. They also found that the COP of the system was varied from 1.9 to 2.9 with an increase in velocity from 2.0 m/s to 5.0 m/s.

Jakhar et al. [134] experimentally investigated the thermal performance of EAHE with solar air heating duct for the winter heating. They found out that the heating capacity of EAHE system got increased by 1217.62-1280.75 kWh when it was coupled with solar air heating duct with a substantial increase in room temperature by 1.1-3.5 °C. They also concluded that the COP of the system was increased up to 4.57 when assisted with solar air heating duct, thus the heating capacity of EAHE can be significantly increased by coupling it with solar air heating duct. Jakhar et al. [135] developed a model for the EAHE with solar air heating duct using TRNSYS

17 in which they optimized the pipe length as 34 m and soil depth as 3.7 m to achieve optimized outlet temperature. It was also observed that increase in flow velocity results in decrease in EAHE outlet temperature, while room temperature was found to increase for higher velocities (5 m/s). They achieved the COP the system as 6.304 with solar air heating duct.

### 2.4.2 Earth water heat exchanger

Compared to EAHE, EWHE system would require less area as the heat transfer fluid is water. Such systems are similar to geothermal heat pump embedded horizontally underground within the soil. In world scenario, a very few research work has been done to investigate the performance of EWHE system. Joen et al. [136] presented an analytical model for comparison the performance of EAHE and EWHE systems. Their design included a EWHE system buried at a depth of 0.12 to 0.17 m and connected to a compact heat exchanger to transfer the heat from water to air. They investigated the effects of various parameters like pipe length, pipe diameter and flow rate of water. They calculated that the soil resistance is more dominant in case of EWHE and required small diameter tubes for effective heat transfer. Their results revealed that the large surface area and large diameter tubes of EAHE could be replaced with the help of EWHE system. Chel et al. [137] investigated the performance of an integrated system of EWHE, water air heat exchanger (WAHE) and air to air heat exchanger (AAHE) with the help of TRNSYS 17. Their EWHE system consists of a serpentine type flexible pipe length, diameter and thickness of 150 m, 30 mm and 5 mm respectively. The inlet ambient air was circulated to EAHE followed by WAHE to gain excess energy from hot water. The high temperature air was then transferred for space heating through AAHE. Results showed that the EWHE and AAHE had an impact of 7% and 66% respectively on the decrease of the yearly heating consumption of the building. They found that the integrated system together could reduce the annual heating consumption of the building by 72 %. There was a drastic reduction of the overheating time above 25 ºC due to the EWHE integration in the building having annual ventilation air cooling contribution of 602.6 kWh/year. Shah et al. [138] investigated the performance of the EWHE system for the ventilation of swine finishing barn Raleigh, North Carolina. EWHE system was comprised of 154 m long PVC pipe of 35 mm diameter, buried in flat land with dry soil at a depth of 3.2 m. The outlet of EWHE was connected to a tube and the fin type heat exchanger to transfer the energy from water to air. Their results revealed that the COP, the temperature change

of building and energy produced were 8.2, 3.2 ºC and 4.3 kW respectively, with 8 h continuous operation of EWHE during summer season. While it was only 6.7, 2.2 ºC and 3.4 kW with 12 h continuous operation of EWHE during winter season. They concluded that the EWHE system could be cost-effective for the greenhouse and zone cooling in all over the world.

### 2.5 Gray areas identified for further research

The presented literature review identified many vital areas for further research. The following can be the key points for future research work:

1. Most of the research work of CPV cooling used silicon cells while only a few have used multijunction SCs. This presents a very good potential for multijunction cells for exploring their applications in CPV with cooling.
2. The integration of the CPV with other energy conversion systems may be done to increase combined efficiency. More research on the coupling of CPV along with ORC, AHP or desalination systems could provide a new prospective in this area.
3. Rooftop BICPV/T system for buildings could be a prominent research area in comparison to the roof top BIPV systems. The hybrid system could be used for electricity generation as well as space heating with low CR CPV systems.
4. Application of micro and nano technologies for PV and CPV cooling may provide a new perspective in this area. Efficient design to reduce pressure losses and pumping power in such technologies will play an important role for PV and CPV cooling.
5. Liquid immersion cooling, which can be used for higher CR has a problem of salt deposition. The reduction in salt deposition is a challenge and has a very good research potential. Similarly the use of PCM for PV and CPV cooling for continuous supply of thermal energy could provide new research insight in this field.
6. It is clear from the above literature review that no attempt has been made to use the technique of EAHE and EWHE for cooling of PV and CPV systems. Thus, the geothermal cooling (EAHE and EWHE) system along with PV and CPV may be used for arid and semi-arid regions with high solar insolation where the ambient temperature reaches up to 50 °C during peak summer. This leaves very small scope for utilization of thermal energy and rejecting heat to the ambient is also a challenge. Thus, the EAHE and EWHE coupled system could be a better solution to reject excess heat.

7. Performance of EWHE system is affected by various geometrical and physical parameters like mass flow rate of water, pipe diameter, pipe material and length of the pipe, etc. Hence, it is desirable to assess the performance of EWHE coupled with PV and CPV based on geometrical and physical parameters.
8. Feasibility study of PV and CPV coupled with EWHE cooling based on exergetic analysis has not been carried out in the literature and hence it is desirable to assess the system performance based on second law of thermodynamics.
9. No attempt has been made to use the BIPV/T system coupled with EAHE for combined electrical power and winter heating of buildings during winter season. So there is need to investigate the performance of such coupled systems.

# CHAPTER 3

# MODELLING AND SIMULATION

## 3.0 Modelling and simulation of the PV/T and CPV/T systems with geothermal cooling

This chapter presents TRNSYS and MATLAB modelling of unglazed and glazed PV/T system coupled with EWHE cooling for the climatic and ground conditions of Pilani (Rajasthan). An analysis has been carried out by varying its operating parameters for these systems. The purpose of TRNSYS modelling is to understand the transient behavior of unglazed PV/T system coupled with EWHE cooling in hot and dry climatic conditions of Pilani (Rajasthan) with variation of key parameters. Besides, the results of TRNSYS modeling have also been used to decide the design of glazed PV/T system coupled with EWHE cooling. For the same, a detailed thermodynamic model has been presented using the first law of thermodynamics and energy balance. The analysis has been carried out on two types of glazed PV/T collectors which included tube-and-sheet collector and broad water channel collector. At the end a mathematical model is also developed for a rooftop photovoltaic thermal system with earth air heat exchanger (EAHE) for combined electrical power and space heating.

## 3.1 Modelling and simulation of unglazed PV/T system coupled with EWHE cooling

### 3.1.1 Description of the proposed system

The schematic diagram of the proposed coupled system is shown in Fig. 3.1. It consists of an unglazed PV/T, EWHE, valves and pump connected in series. In the unglazed PV/T system copper tubes are bonded to an absorber plate which is fixed underneath the PV panels as shown in Fig. 3.1 (b). The whole unglazed PV/T is enclosed in a casing and insulated from the sides and back. The back side of PV panel consists of copper tubes which carries water to take away the excess heat from the panel thus resulting in an increase in its own temperature. The outlet of PV/T is connected to EWHE through pipes and valves. It comprises of 30 m long horizontal high density polyethylene (HDPE) pipe, buried in soil at a 3.5 m depth. In the EWHE, heat is transferred from hot water (PV/T outlet) to the soil. As a result, the water temperature at the

outlet of EWHE is much lower than the ambient during the peak summer period. The outlet from the EWHE is then sent back to PV/T inlet through copper tubes for cooling and works continuously which decreases the PV panel temperature and increases the efficiency.

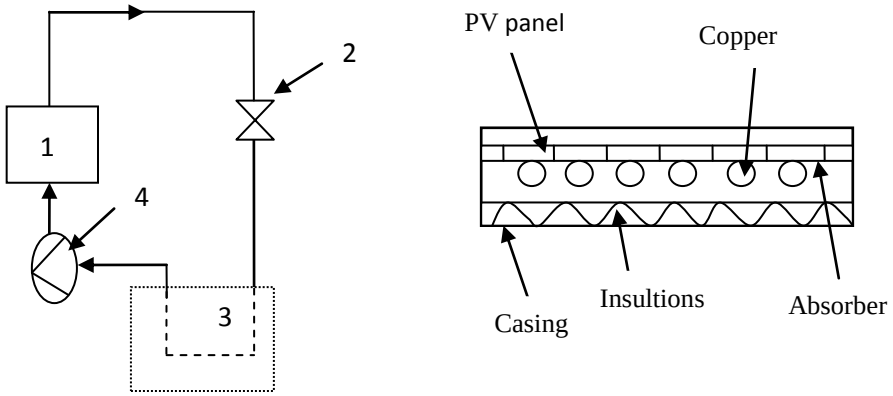


1. PV/T system 2. Valves

3. EWHE 4. Pump

(a) (b)

**Fig. 3.1.** (a) Schematic diagram of proposed system (b) Cross-sectional of unglazed PV/T system

### 3.1.2 Description of the TRNSYS software

TRNSYS is a tool which is used for modelling and simulation of complex systems to identify its transient behavior. The systems may be thermal (solar, refrigeration, etc.) or electrical (PV, wind, etc.) and can be solved using an inbuilt set of equations using a modular approach. The basic equations related to each component are subroutine through FORTAN language. Theses subroutines are called as *Types* and works as a single system component. The complex system can be made by joining all the *Types* together within the proper sequence. One of the advantages of this tool is that, the standard library has an extensive set of more than 150 components and models. Each component is denoted by *'Type X*' where 'X' denotes the number. For instance, *'Type 3'* represents a variable speed pump and can be used directly to solve the case of variable speed pump.

This software was developed in 1970 by University of Wisconsin-Madison for their internal purpose but was commercialized in 1975. Due to its vast set of library and adaptability to

incorporate every sub-component of renewable energy, it is widely supported by the researchers in this area, where they could develop their own model by writing the equations in the FORTRAN and easily interfaced with the existing components. Each model has an input and output parameters, which are correlated by a set of algebraic and first order differential equations. Using time dependent input in the inbuilt model, the components are interconnected through a flowchart. The connection is made in such a way that the output of one component is the input for another. After running the simulation, it gives the time dependent output of the entire system or component wise. TRNSYS provides the flexibility to user for incorporating their components as per the special requirements. Further, these components can easily be connected to the external softwares like EES, Fluent, MATLAB etc.

### 3.1.3 Simulation methodology

In the current work, the transient modelling and simulation of unglazed PV/T with EWHE cooling was carried out using TRNSYS (v17.0). The adopted simulation methodology for this work is explained using the following steps:

1. The problem definition needs to be defined. It is very important to understand as much as possible about the problem being simulated in order to accurately define it. This stage involves collecting all the necessary data required for the simulation including design parameters, fluid properties and flow specifications, etc.
2. The simulation of unglazed PV/T system coupled with EWHE cooling requires climatic data such solar radiation, wind velocity, ambient temperature, relative humidity, etc. Weather data for Pilani, Rajasthan (India) has been generated using inbuilt Meteonorm files provided within TRNSYS. The weather component is taken as *Type15-3* under TMY3 library.
3. The component for unglazed PV/T collector is created using PV/T collectors (*Type560*) in the electrical library which is termed as TESS library in the software.
4. Within the ground heat pump library of TRNSYS, EWHE (Type 952) is a horizontal heat exchanger model which interacts thermally with the ground. It considers convection between the inner surface of buried pipe to flowing water, conduction within the buried pipe and conduction between the external surface of buried pipe and earth.
5. For a closed loop cycle and to circulate the heat transfer fluid, a pump is required, so

form the Hydronics TESS library, a variable speed pump (*Type3*) which can also vary the mass flow rate, is taken.

6. To fix the upper and lower temperature limits of PV/T and EWHE, a controller is also used which is denoted by *Type2* component and is connected in between PV/T and EWHE.
7. The output results can be extracted by number of components which includes simulation output, simulation summary and printer components. In this work *Type65* is taken from the TESS library.
8. At the end, all the system components are linked and interconnected as per the system requirement in a form of flow chart. As mentioned above, the output of one *Type* is the input for another, thus the simulation can be run for the desired period of time.
9. Having obtained the solution, the user can then analyze the results in order to check that the solution is satisfactory and to determine the required flow data. If the results obtained are unsatisfactory, the possible source of error needs to be identified, which can be an incorrect wrong component link, wrong input parameters and a conceptual mistake in the formulation of the problem.

Fig. 3.2 represents the simplified simulation model with all major components of the coupled system under consideration for this research. As shown in Fig. 3.2 the component for the unglazed PV/T is connected to pump, which is further connected to EWHE to make it as a close loop. PV/T is a hybrid collector which produces both electrical and thermal energy. Within the ground heat pump library of TRNSYS, EWHE is a horizontal heat exchanger model which interacts thermally with the ground. In the closed loop simulation, the excess waste heat of unglazed PV/T is dissipated to the earth by EWHE. Furthermore, the weather data component is connected with PV/T to provide the climatic data of the local conditions. And the following standard TRNSYS component models (*Types*) were used in the simulation:

- Type 560- unglazed PV/T collector
- Type 3- Variable speed pump
- Type 952- Earth water heat exchanger
- Type 15 - Weather data processor
- Type 65- Online plotter
- Type 28- Simulation summary
- Type 25- Printer

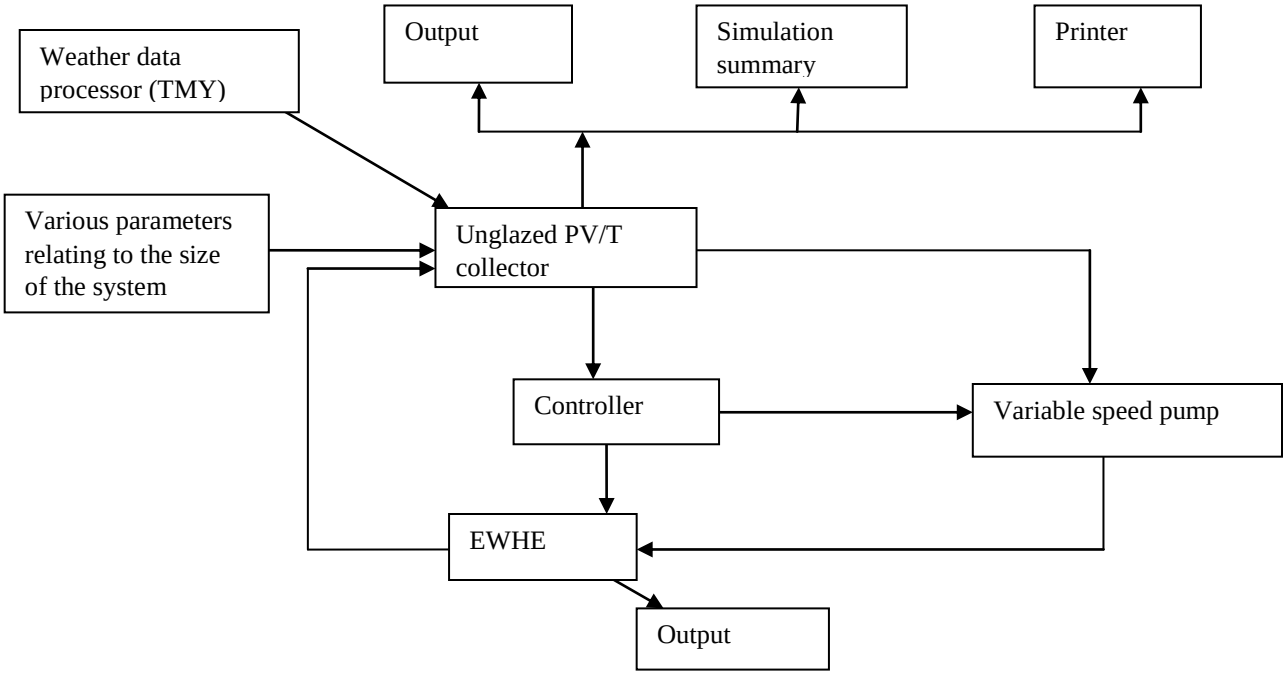


**(a)**

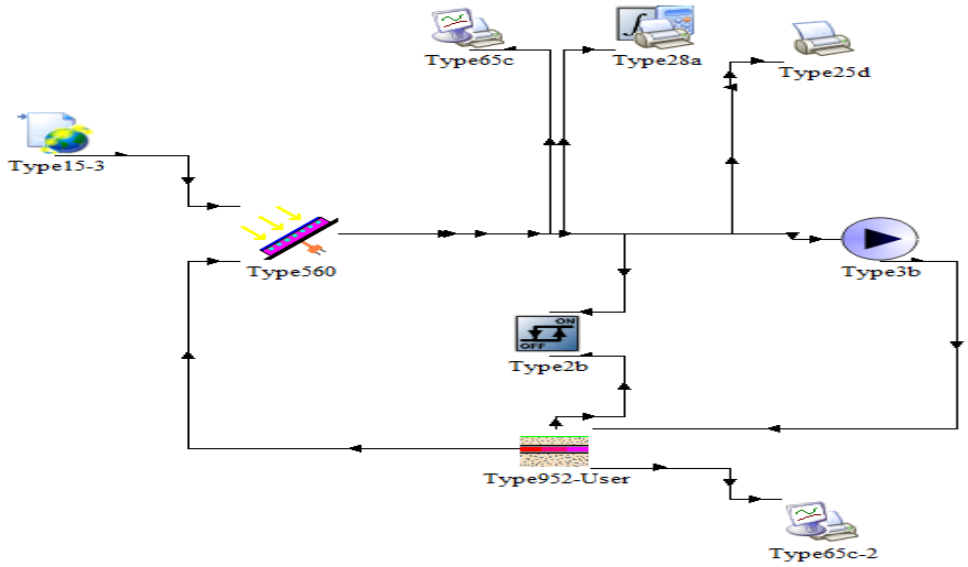


**(b)**

**Fig. 3.2.** (a) Schematic diagram for the unglazed PV/T with EWHE cooling (b) TRNSYS flow diagram

### 3.1.4 Description of the main components used in simulation

In this section, the values of all parameters which used for the simulation of major TRNSYS components are presented.

*(a) Unglazed PV/T component*

The unglazed PV/T system provides the combined electrical and thermal energy from one system. In this system the copper tubes are mounted on the rear side of PV panel with water as a heat transfer fluid (HTF). The HTF takes away the excess heat from the panels thus resulting in a decrease in panel temperature. To design PV/T, various parameters are required, which involves physical parameters like length, width, tube spacing, etc. The user can also provide their parameters as per the design to run the simulation. In the present case, PV/T has been designed by taking different parameters to achieve optimum value. Table 3.1 shows all design and input parameters which were taken to optimize using trial method.

**Table 3.1.** Design and input parameters of unglazed PV/T system

| S. No. | Parameter name | Parameter description | Value | Unit |
|---|---|---|---|---|
| 1 | Collector length | The length of the collector (direction along the tubes) | 1.20 | m |
| 2 | Collector width | The width of the collector (direction across the tubes) | 1.59 | m |
| 3 | Absorber plate thickness | Thickness of the absorber tube | 0.001 | m |
| 4 | Thermal conductivity of absorber plate | Thermal conductivity of absorber plate (plate bonded to the tubes) | 385 | W/m K |
| 5 | Number of tubes | The number of identical water tubes bonded to the absorber plate | 20 | - |
| 6 | Tube diameter | The diameter of the water tubes bonded to the absorber plate | 0.012 | m |
| 7 | Bond thickness | The average thickness of the bond between the tube and the absorber plate | 0.0015 | m |
| 8 | Bond thermal conductivity | The thermal conductivity of the bond between the absorber plate and the tubes | 385 | W/m k |
| 10 | PV cell reference temperature | The reference temperature at which the efficiency of the PV cell is provided | 25 | $^{o}$C |
| 11 | PV cell reference radiation | The reference total incident solar radiation at which the efficiency of the PV cell is provided | 1000 | W/m$^2$ |
| 12 | PV efficiency at reference condition | The efficiency of the PV cells in converting incident radiation to electricity at the provided reference condition | 12 | % |
| 13 | Inlet flow rate | The flow rate of water entering the PV/T collector array | 0.006-0.026 | kg/s |

*(b) EWHE system*

EWHE is a horizontal ground heat exchanger model which interacts thermally with the ground. The model being used to design EWHE as it behaves as a heat sink and heat source in summer and winter respectively. Table 3.2 represents all the input parameters, both physical and thermal, for the design of this system.

**Table 3.2.** Design and input parameters of EWHE system

| S. No. | Parameter name | Parameter description | Value | Unit |
|---|---|---|---|---|
| 1 | Length of buried pipe | The length of the buried horizontal pipe | 10-60 | m |
| 2 | Inner diameter of pipe | The inner diameter of the buried pipe containing the heat transfer fluid | 0.01-0.0227 | m |
| 3 | Outer diameter of pipe | The outer diameter of the buried pipe containing the heat transfer fluid. | 0.012-0.025 | m |
| 4 | Buried pipe material | High density polyethylene (HDPE), Galvanized Iron (GI) and Steel pipe | - | |
| 5 | HDPE pipe thermal conductivity | The thermal conductivity of buried HDPE pipe | 0.40 | W/m K |
| 6 | GI pipe thermal conductivity | The thermal conductivity of buried GI pipe | 16 | W/m K |
| 7 | Steel pipe thermal conductivity | The thermal conductivity of buried steel pipe | 54 | W/m K |
| 8 | Density of water | The density of the working water flowing through the horizontal buried pipe | 1000 | $kg/m^3$ |
| 9 | Thermal conductivity of water | The thermal conductivity of the working water flowing through the horizontal buried pipe | 0.555 | W/m K |
| 10 | Thermal conductivity of soil | The thermal conductivity of the soil in which the horizontal pipe is buried | 0.80 | W/m K |
| 11 | Density of soil | The density of the soil in which the horizontal pipe is buried | 1700 | $kg/m^3$ |
| 12 | Specific heat of soil | The specific heat of the soil in which the horizontal pipe is buried | 0.82 | kJ/kg K |
| 13 | Average surface temperature | The average surface temperature during the year. This temperature will be used as the deep earth temperature for the calculations | 27 | ºC |
| 14 | Depth of buried pipe | The depth of buried pipe from the ground surface | 3.5 | m |

### 3.1.5 Results and discussion

As mentioned earlier, the performance of unglazed PV/T panel coupled with EWHE cooling was analyzed by using TRNSYS (v17.0) software. The climatic condition for the simulation of the

coupled system is taken as that of Pilani, Rajasthan which has a semi-arid climate and has a high ambient air temperature and high solar radiation during the peak summer. The simulation was conducted for 10 hours of system operation, which is average sunshine duration during the peak summer period. For the simulations, 21$^{st}$ June, the equinox day, was selected and the climatic data were taken from inbuilt meteonorm files in TRNSYS. The simulation study was carried out to estimate the effect of burial depth over a period of year, for the local conditions of Pilani, Rajasthan. Since the earth acts as a heat sink for the higher temperature, as the depth increases the soil temperature converges to annual average ambient temperature. Fig. 3.3 shows the ground temperature variation for different depths. It is found that with increase in depth from 0.5 m to 3.5 m, the average temperature over the year varies from 9.5 °C to 44.7 °C for 0.5 m depth while it remains within the range of 22.5 °C to 27.7 °C for 3.5 m depth. Fig. 3.3 reveals that the temperature of soil at the depth of 3.5 m is not at all affected by the diurnal variation of ambient temperature and solar radiation. Considering this small variation in temperature, the depth of 3.5 m is taken for the simulations. At first, the investigation has been carried out for a selected material by taking a fixed pipe length (30 m), pipe diameter (0.012 m) and mass flow rate (0.014 kg/s). Further the parametric study has been carried out.

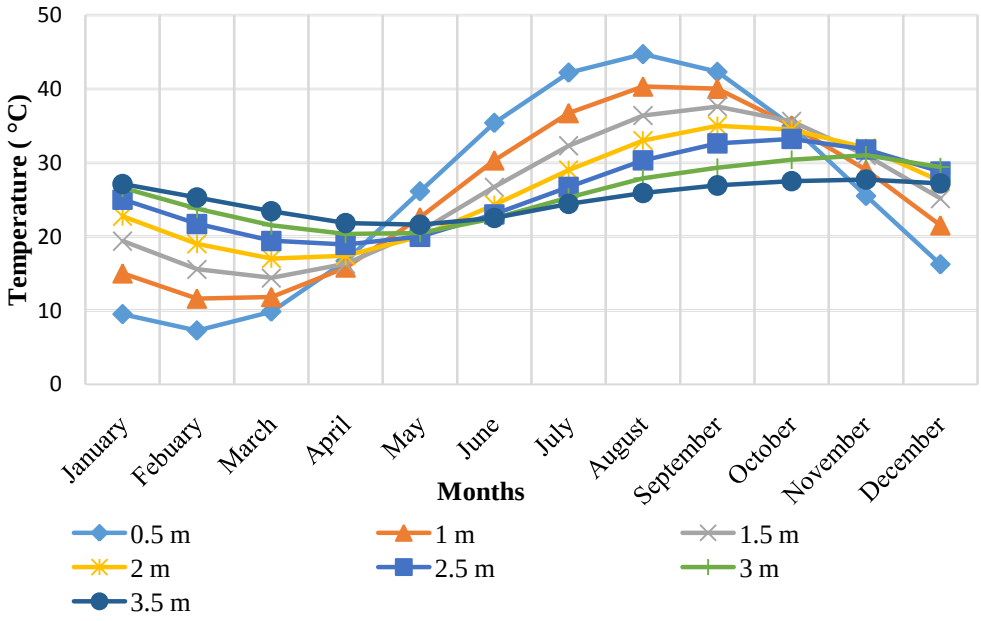


**Fig. 3.3.** Simulated annual ground temperature range at different depths for Pilani, Rajasthan (India)

The variations of ambient temperature and global solar radiation intensity during the simulation day are shown in Fig. 3.4. It reveals that the ambient temperature and solar radiation ranges between 239-997.58 W/m$^2$ and 33.40-39.58 °C respectively for the Pilani, Rajasthan. Fig. 3.5 shows the hourly variation of PV panel temperature without cooling and with cooling at cooling water flow rates of 0.014 kg/s. From the simulation results it was observed that the PV panel temperature varies between 35.43 °C to 79.31 °C without cooling for 10 hours of system operation. On the other hand, the PV panel temperature drops with the EWHE cooling the and it ranges between 28.97 °C to 49.18 °C for the flow rate of 0.014 kg/s. This was observed that during the morning (at 9 AM) the solar radiation is less, thus the temperature difference of with and without cooling is less (10.25 °C). But with an increase in solar radiation, at 2 PM, the difference increases to 30.13 °C. And in the evening, the morning trend follows. Thus, it was observed that the EWHE cooling is more effective during morning and evening.

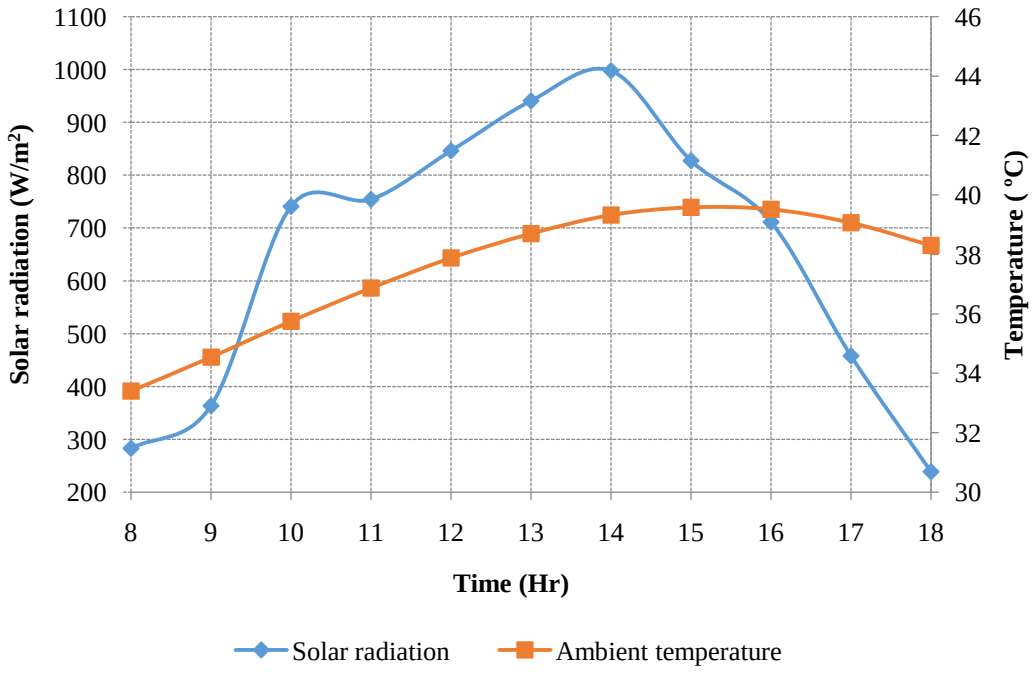


**Fig. 3.4.** Intensity of solar radiation and ambient air temperature of June, 21 for the Pilani, (Rajasthan)

Fig. 3.6 reveals the PV power output for mass flow rates of 0.014 kg/s. The PV power remains within the range of 39.4 W to 140.3 W without any cooling, over the period of 10 hours. However, with cooling, it varied from 38.3 W to 161.58 W for same mass flow rate. It can be

observed that the PV power increased by 21.28 W with EWHE cooling for the same mass flow rate as compared to without any cooling. It was observed that the power was less in the morning and evening because of lower solar radiation and maximum during afternoon. The simulated results of PV electrical efficiency for both configurations (without cooling and with cooling) at a flow rate of 0.014 kg/s have been presented in Fig. 3.7. In case of without cooling, the electrical efficiency varied from 8.73% to 10.59% due to high cell temperature. Further, with EWHE cooling the efficiency was varied from 10.54% to 11% at the same flow rate. It is found that the electrical efficiency of the system is increased by 0.23% to 1.87% with EWHE cooling as compared to without cooling. Further, it was noticed that in case of cooling, only 0.23% of efficiency increases at 6 PM, which is quite marginal. Thus EWHE could be turned off to avoid power loss by pump. It was also noticed that PV efficiency increases during the morning and evening period and decreases during peak sunshine hours. This is due to the change in the temperature of PV panel throughout the day. At higher temperature, the PV panel efficiency decreases.

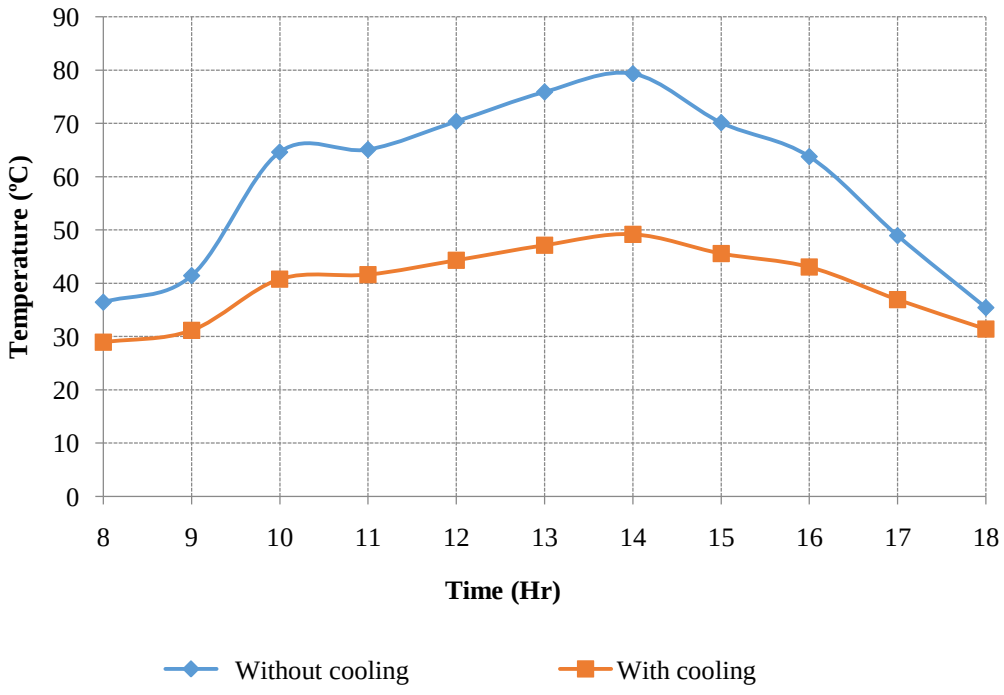


**Fig. 3.5.** PV panel temperature without cooling and with cooling for mass flow rate of 0.014 kg/s

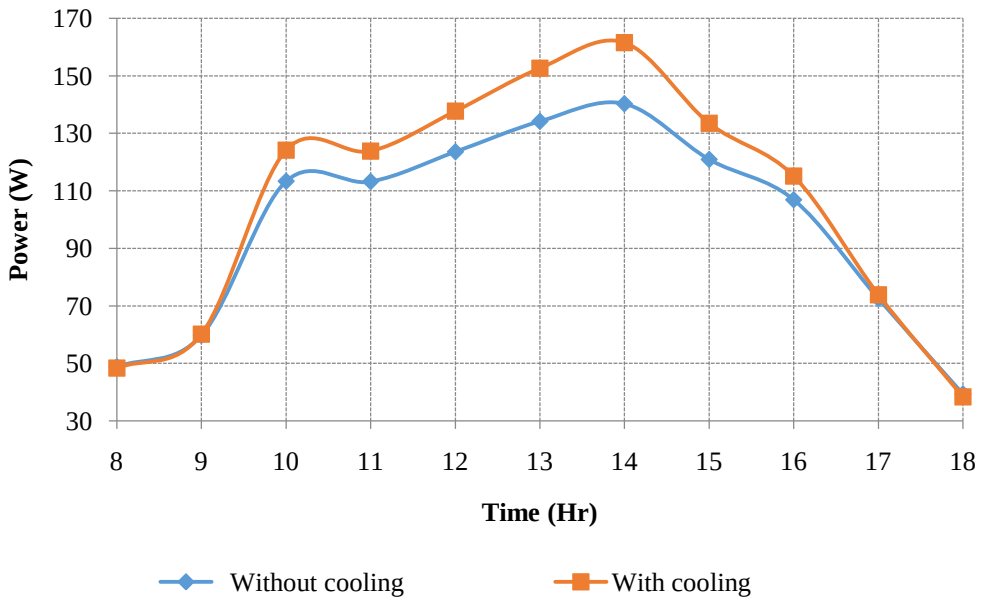


**Fig. 3.6.** PV power output without cooling and with cooling for mass flow rate of 0.014 kg/s

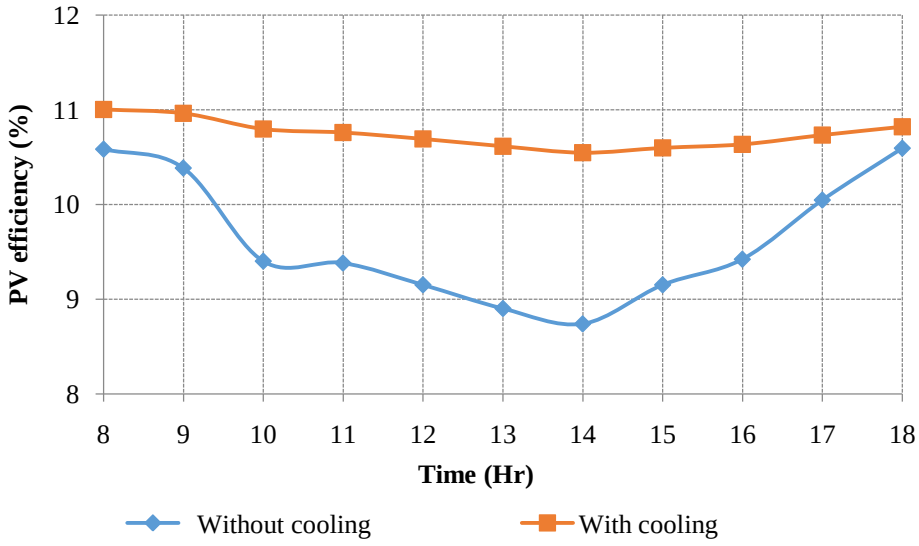


**Fig. 3.7.** PV electrical efficiency without cooling and with cooling for mass flow rate of 0.014 kg/s

### 3.1.6 Validation of TRNSYS simulation results

Validation of TRANSYS simulation results obtained is important to verify the accuracy of the developed model. From the literature review, it is observed that there is hardly any study on unglazed PV/T coupled with EWHE using water as a heat transfer fluid. Studies on various PV/T systems and their applications varies and depends on the ambient conditions, solar radiation,

wind velocity, etc. Hence it would be difficult to compare them on a common basis. Similarly, studies based on EWHE depend on soil properties and thus the location cannot be generalized. Moreover, sufficient amount of research has been done on EAHE. Some researchers have done work using EAHE for air conditioning. One of the experimental study was performed on the hybrid EAHE [139] for the conditions of Ajmer (India). In their experimental analysis, they used the thermal and physical parameters of various materials like soil density, soil thermal conductivity, soil specific heat and pipe thermal conductivity as 2050 kg/m$^3$, 0.52 W/m K, 1.840 kJ/kg K and 0.16 W/m K respectively. Experimental study done by Misra et al. [139] is simulated in TRNSYS on a model of EAHE to determine the precision of results for the same properties of materials. The variation of EAHE outlet air temperature with length of EAHE pipe from both simulation and experimental analysis are shown in Fig. 3.8. It is observed from the Fig. 3.8 that the simulated results are within the close agreement with the experimental results with a variation of 0.8 to 7.93%. This error may occur due to the improper insulation of pipes, variation in the coefficient of friction of materials used in simulation, and irregularities such as fitting and joints in the experimental setup. So the comparison of simulated model and experimental results in the literature with air as heat transfer fluid is showing small error for the same climatic conditions, it is expected that the study for the EWHE will also follow the same pattern with more precise results. Thus the coupled system of EWHE and PV/T would provide better results in the present simulation.

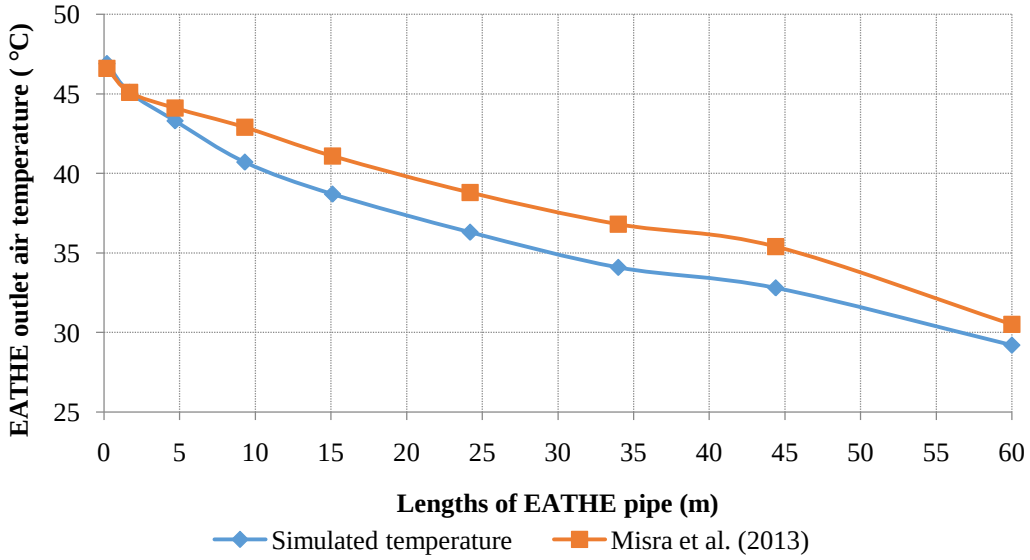


**Fig. 3.8.** Simulated EAHE model validation with experimental results in the literature

### 3.2 Parametric analysis of unglazed PV/T system coupled with EWHE cooling

It is observed from the literature review that the various parameters of the EWHE pipe such as length, diameter, and pipe material along with the mass flow rate of cooling water significantly affect the thermal performance of EWHE system. In this analysis these important parameters of EWHE pipe greatly affect the performance of the unglazed PV/T system coupled with EWHE and these have been considered during TRNSYS simulations.

#### 3.2.1 Methodology

The methodology for system design and its parametric variation for the EWHE is discussed in this section. The simulation of unglazed PV/T coupled with EWHE system is carried out for 10 hours of system operation which is average sunshine hours as a conservative estimate during the peak summer period (June 21). To optimize the design parameters of such coupled system, the parametric simulation was performed for different mass flow rates for a fixed diameter and length of the HDPE pipe. This analysis gives the optimum flow rate of 0.018 kg/s for a 30 m HDPE pipe length and diameter of 12 mm. For three different EWHE pipe materials, i.e. galvanized iron (GI), HDPE and steel pipe, the simulation was carried out it shows that the performance of the coupled system hardly depends on the buried pipe material. Thus, among all the pipe materials discussed here, HDPE pipe is considered for the performance analysis as it is economical as compared to other two. With HDPE as pipe material, the variation in pipe length is analyzed for a particular diameter and flow rate. Further the variation in pipe diameter is carried out by keeping the pipe length and mass flow rate constant.

#### 3.2.2 Effect of mass flow rate of cooling water

The effect of mass flow rate on the performance of unglazed PV/T along the EWHE pipe length of 30 m and a diameter of 25 mm for the HDPE pipe is shown in Fig. 3.9. It reveals that the temperature of PV goes up to 79.31 °C without any cooling. In case of EWHE cooling scenario, the PV temperature decreases significantly and it varies with different mass flow rates, i.e. 29.99 °C - 53.82°C for 0.01 kg/s, 28.54 °C - 47.13 °C for 0.018 kg/s and 28.33 °C - 46.29 °C for 0.026 kg/s. It is observed that with increase in mass flow rate the PV temperature decreases and becomes almost same for 0.018 kg/s, 0.022 kg/s and 0.026 kg/s. For the practical applications, 0.018 kg/s flow rate could be used as with increase in mass flow rate the pumping power required also increases. Fig. 3.10 reveals the PV power output for different mass flow rates. The PV power

over 10 hours remains within the range of 39.4 W to 140.3 W without cooling and it varies from 38.29 W to 163.46 W with cooling for 0.018 kg/s flow rate. It can be observed that the PV power increased by 23.16 W with EWHE cooling for the same mass flow rate as compared to without cooling. As the PV panel temperature reduced, electrical efficiency increases significantly and it increase in flow rate of cooling water as higher heat transfer coefficient causes the high heat removal rate from the PV/T system. Thus, in order to have a maximum electrical efficiency and power of the PV/T system, the mass flow rate needs to be optimized within a suitable range.

The effect of mass flow rate of the fluid on the performance of unglazed PV/T outlet temperature is shown in Fig. 3.11. It reveals that with increase in mass flow rate the outlet temperature of PV/T decreased as expected. The exit temperatures obtained after 06 hour simulation are 54.63 °C for 0.006 kg/s and 46.85 °C for 0.026 kg/s respectively. Moreover Fig. 3.11 depicts that the temperature difference between 0.018 kg/s and 0.022 kg/s flow rates is merely 0.63 °C for the same conditions. Considering the small variation in temperature for these flow rates, it can be concluded that the 0.018 kg/s flow rate may be sufficient for the PV/T system.

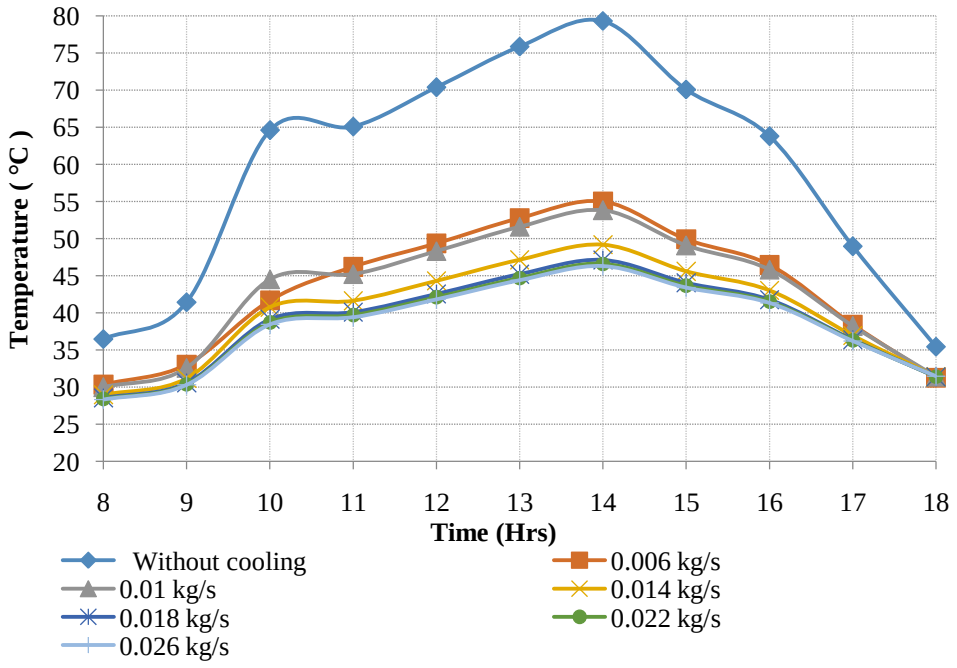


**Fig. 3.9.** PV panel temperature without cooling and with cooling for different mass flow rates

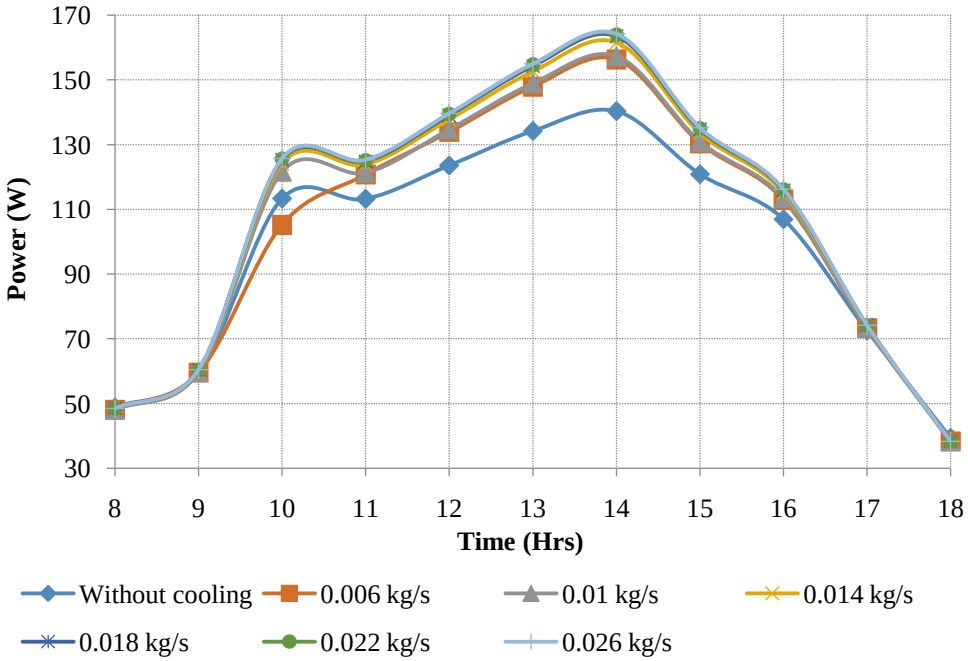


**Fig. 3.10.** PV power output without cooling and with cooling for different mass flow rates

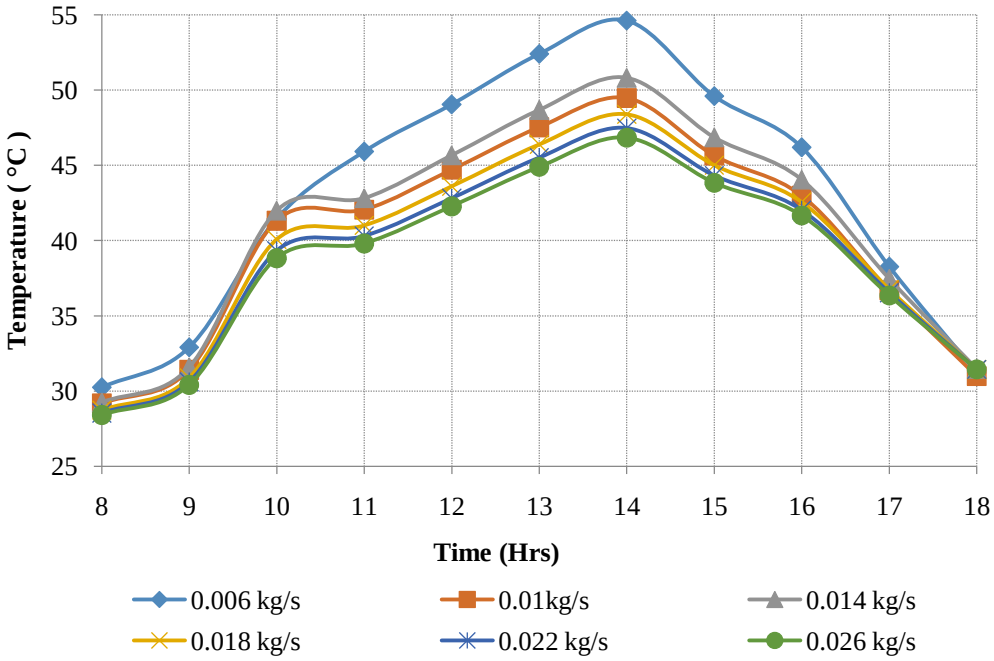


**Fig. 3.11** PV/T outlet temperature for different mass flow rates

### 3.2.3 Effect of EWHE pipe material

Fig. 3.12 shows the PV temperature for three different EWHE pipe materials (i.e. GI, HDPE, steel) for the diameter and length of 12 mm and 30 m respectively with flow rate of 0.018 kg/s. It reveals that the temperature difference of PV panel for HDPE and GI is mere 1.04 °C, while in the steel and HDPE pipe is around 1.5 °C, for the same simulation conditions. Fig. 3.13 shows the PV power output for three different pipe materials for flow rate of 0.018 kg/s. It is observed from the Fig. 3.13 that the difference in power output is just 0.97 W for HDPE and steel pipe, here in the analysis power consumed by pump is not considered. This small variation is due to the small coefficient of friction and lower thermal conductivity of HDPE pipes, while that of higher thermal conductivity and higher coefficient of friction for steel and GI. The higher heat transfer due to one better property is compensated by another poor property. Hence there is marginal variation in the outlet temperature and power output for all three materials. Thus, it can be concluded that the selection of pipe materials out of three materials have small impact on the performance of the unglazed PV/T coupled EWHE system. The same has also been discussed in literature for EAHE [140]. This validates the selection of the HDPE pipe as it is much cheaper than the other two.

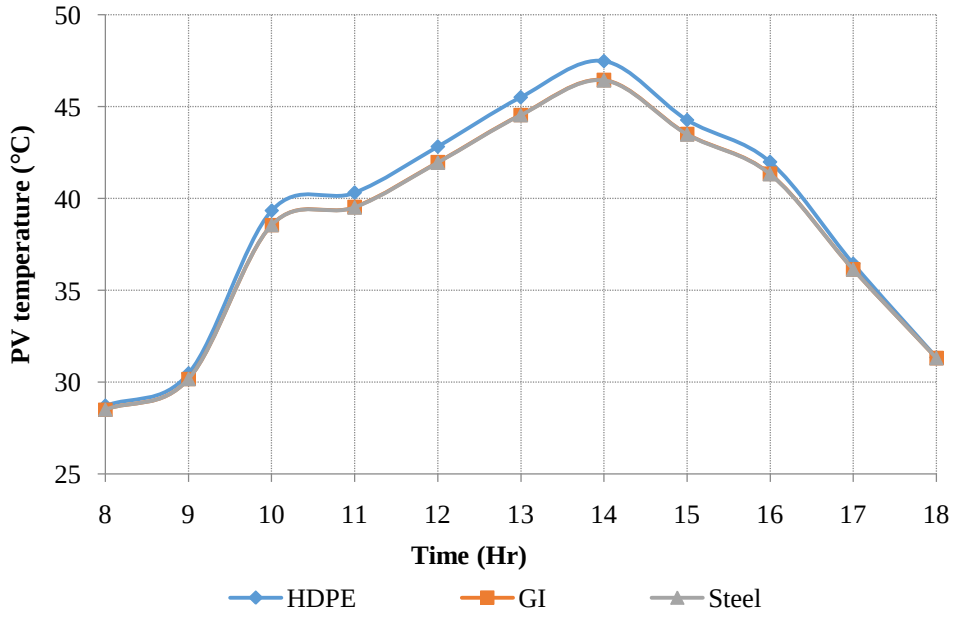


**Fig. 3.12.** PV temperature vs different pipe material (pipe ϕ 12 mm, length = 30 m, flow rate = 0.018 kg/s)

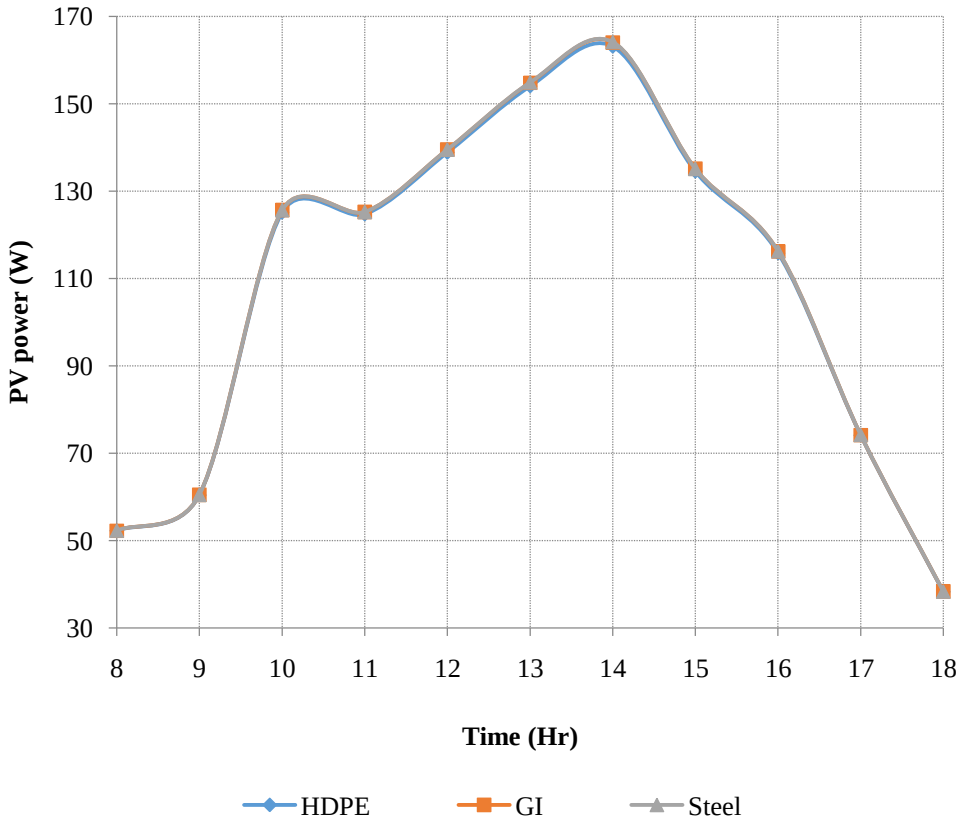


**Fig. 3.13.** PV power vs different pipe material (pipe ϕ 12 mm, length = 30 m, flow rate = 0.018 kg/s)

### 3.2.4 Effect of EWHE pipe length

Further, the hourly variation of PV temperature is estimated for the different pipe lengths for HDPE pipe diameter (12 mm) and flow rate of 0.018 kg/s and has been represented in Fig. 3.14. From the Fig. 3.14, it is observed that the PV temperature decreases with increase in pipe length from 10 to 60 m. It also observed that during peak sunshine hour, for the pipe length up to 50 m the maximum PV temperature drops drastically and with increase in pipe length beyond 50 m this temperature drop is gradually. From the Fig. 3.15, it is observed that for a variation in pipe length from 10 to 50 m, the maximum PV power ranges from 151.64 W to 167.36 W at peak sunshine hour. However, for the pipe length of 60 m the Maximum PV power is 168.60 W, which is just a 1.24 W increase in power output for 10 m increase in pipe length as compared to 40 m. Thus the pipe length of 40 m would be sufficient for such coupled systems.

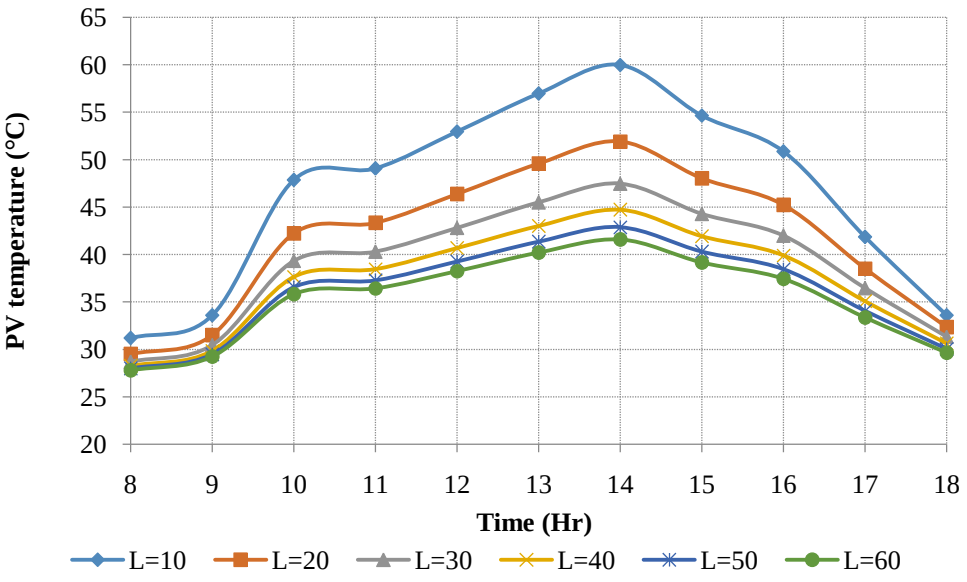


**Fig. 3.14.** PV temperature vs different pipe lengths (pipe ϕ 12 mm, flow rate= 0.018 kg/s, pipe material=HDPE)

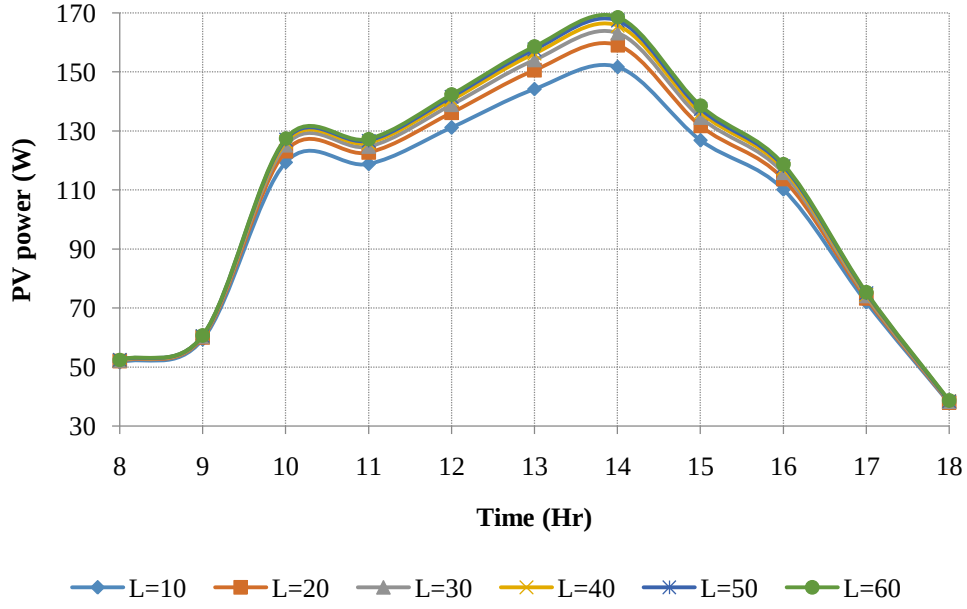


**Fig. 3.15.** PV power vs different pipe lengths (pipe ϕ 12 mm, flow rate=0.018 kg/s, pipe material=HDPE)

### 3.2.5 Effect of EWHE pipe diameter

The variation of PV panel temperature with respect to time for various diameters with flow rate of 0.018 kg/s and pipe length of 50 mm is represented in Fig. 3.16. With the increase in the pipe diameter the PV temperature decreases gradually over a period of time. Initially during the first

hour of simulation the PV temperature drop, is less for smaller diameters while it is more in case of larger diameters. At the peak simulation hour the PV temperature in all the pipe diameters exhibits an almost similar temperature drop, with variation of just 1.05 °C between 12 mm to 25 mm pipe diameters. Fig. 3.17 depicts the variation of PV power output with respect to time for various pipe diameters with flow rate of 0.018 kg/s and pipe length of 50 m. It is observed that at 1400 hours, for 12 mm and 25 mm pipe diameter PV power output is 167.36 W and 168.30 W respectively, which is a very small variation. From the analysis, it is observed that the variation in pipe diameters hardly affects the PV power output. Thus, it is concluded that 12 mm pipe may be considered for the practical applications because of economic reasons. The analysis of the results of TRNSYS simulation of PV/T coupled with the EWHE system as discussed above provides the optimum values of various parameters.

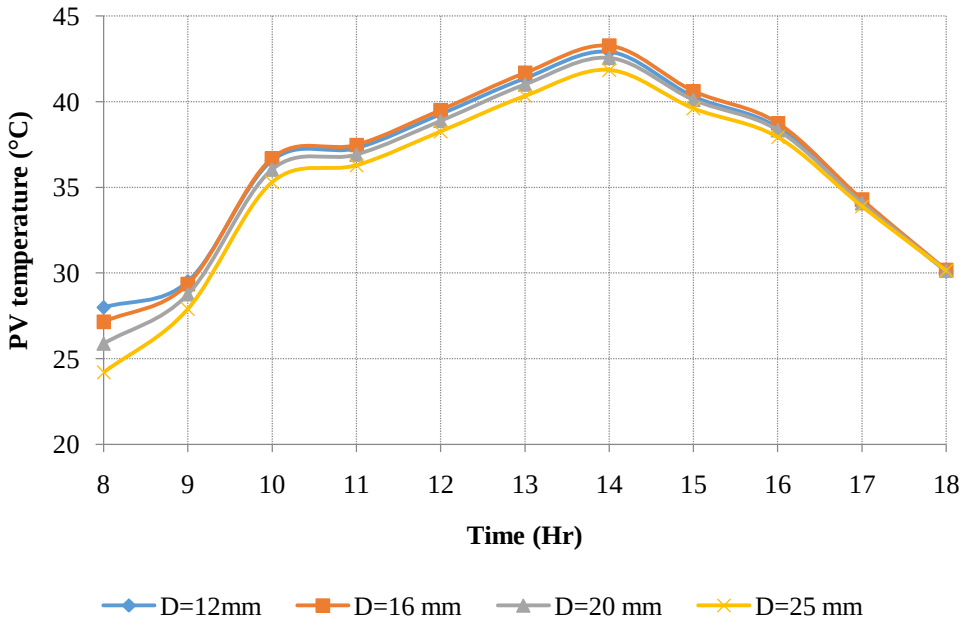


**Fig. 3.16.** PV temperature vs different pipe diameters (length=50 m, flow rate=0.018 kg/s, pipe material=HDPE)

The variation of all the parameters combined together is represented in 3D surface plot using MATLAB and represented in Fig. 3.18 and Fig. 3.19. The variation in PV panel temperature with respect to variation in pipe diameter, pipe length and mass flow rates is shown in Fig. 3.18. The comparative variation shows the direct correlation of each parameter with respect to PV panel temperature. Similar to this, another 3D surface plot has been mapped in Fig. 3.19 which depicts the variation in PV power output with respect to variation in pipe diameter, pipe length

and flow rates. It is observed that there is marginally temperature variation and power output for the flow rate of 0.022 kg/s, pipe diameter of 25 mm and pipe length of 60 m as compared to flow rate of 0.018 kg/s, pipe diameter of 12 mm and pipe length of 50 m. Thus the latter case may be considered for practical application owing to economical reason.

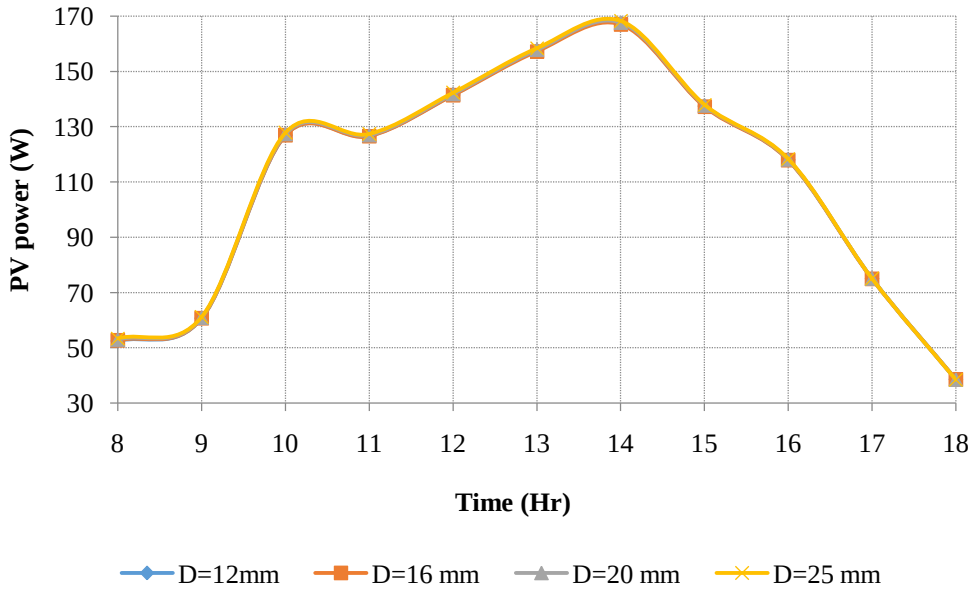


**Fig. 3.17.** PV power vs different pipe diameters (length=50 m, flow rate=0.018 kg/s, pipe material=HDPE)

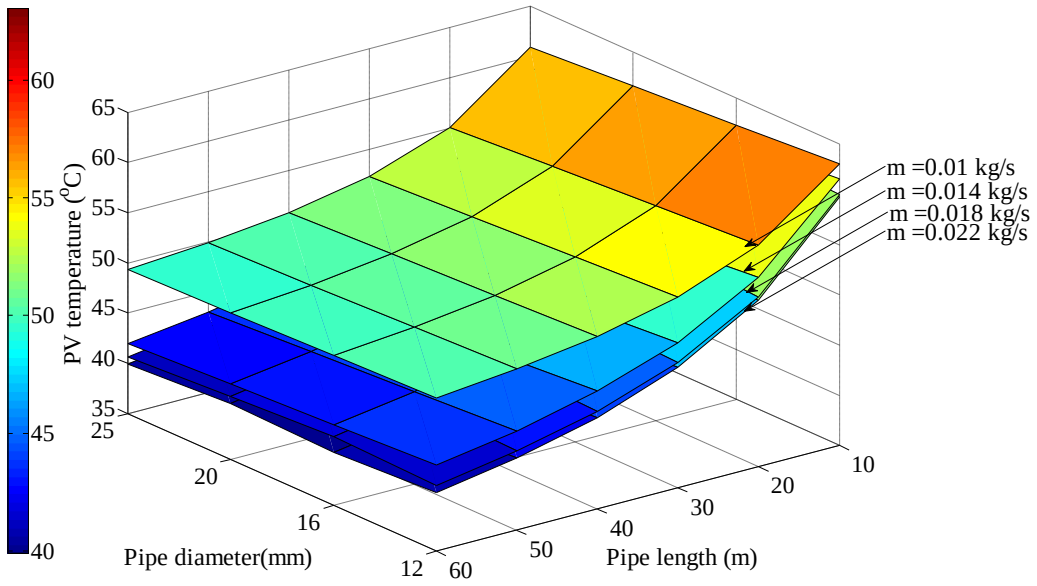


**Fig. 3.18.** PV temperature for different mass flow rates at different pipe diameter and lengths (material=HDPE)

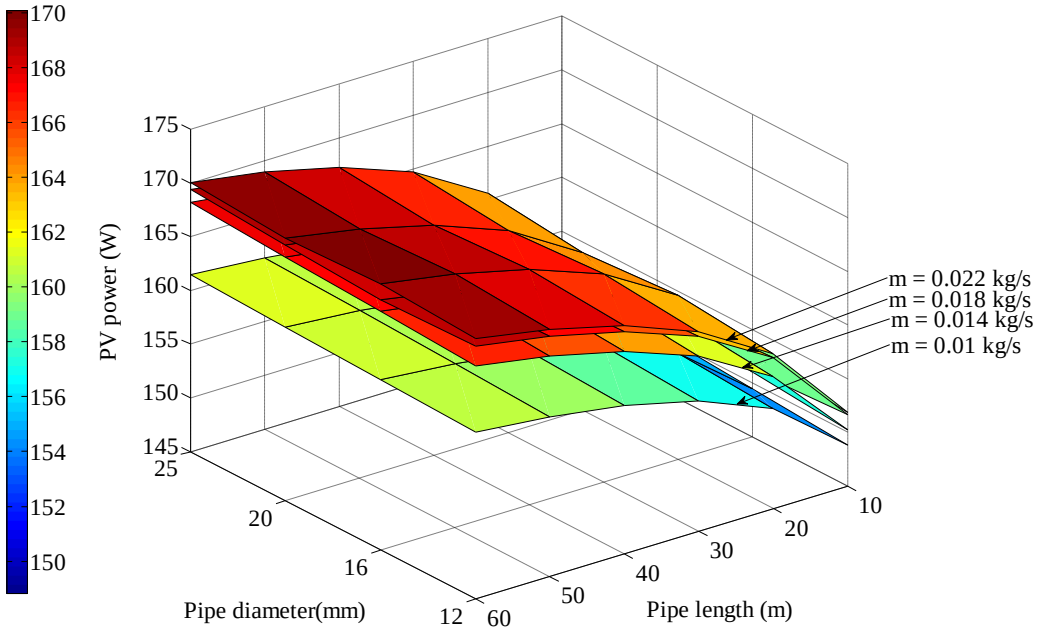


**Fig. 3.19.** PV power for different mass flow rates at different pipe diameter and lengths (material=HDPE)

## 3.3 Modelling and simulation of the CPV/T system coupled with EWHE cooling

As discussed in previous section, unglazed PV/T system coupled with EWHE could be used for semi-arid regions for better performance. Similarly, from the literature, it was found out that such EWHE could also be coupled with CPV/T system. No study has been carried out to perform CPV cooling with EWHE. Thus, in this section, the design, modelling and simulation has been carried out for CPV/T system with EWHE cooling. The methodology adopted for modelling and simulation of EWHE cooling is shown in this section

### 3.3.1 Methodology for the design and analysis of the EWHE system for CPV cooling for Pilani

In this section, the methodology of variation in design parameters for the buried pipe dimensions is discussed. The various parameters were analyzed by simulating their performance on TRNSYS. The simulation conditions were taken for Pilani Rajasthan (India) and the simulation was performed for the duration of 10 hours operation which is average sunshine hour during summer period. The parametric simulation was performed for three pipe materials i.e. GI, HDPE and steel pipe. For different pipe material, by keeping length, flow rate and diameter constant

simulation were carried out and observed that the temperature variation between all three materials is almost similar with the temperature difference of ±1.61 °C. Among three materials, HDPE pipe is taken for the performance analysis because of it is cheaper as compared to other two. For HDPE pipe by keeping diameter and length of the pipe as fixed value, the mass flow rate is varied and outlet temperature for each case is determined. This analysis gives the optimum flow rate for a given condition. By keeping this flow rate as constant for HDPE pipe the analysis is carried forward by changing the length of the pipe for a particular diameter. In the final analysis the effects of different HDPE pipe diameters are estimated for the fixed length and flow rate.

Further, to discuss the applicability of such system, by replacing the cooling system given in the literature of CPV with the proposed system, the results obtained were compared with the existing literature. For the analysis, two references [80,141] have been taken and the values of outlet temperature of CPV/T system were taken as inlet for EWHE system. From the analysis, it has been estimated that the cost of the proposed system is quite inexpensive as compared to the conventional system used in the literature.

And the following standard TRNSYS component models (*Types*) were used in the simulation:

- Type 77-Simple ground temperature model
- Type 952- Earth water heat exchanger
- Type 3- Variable speed pump
- Type 15 -Weather data processor
- Type 65- Online plotter

Type 952 is important models in ground heat pump library of TRNSYS which models a ground horizontal heat exchanger that interacts thermally with the ground. It considers conductive heat transfer to the soil and convective heat transfer within the pipes. For the simulation, the physical and thermal parameters of the system taken are shown in Table 3.3.

**Table 3.3.** Design and input parameters of EWHE system

| S. No. | Parameter name | Parameter description | Value | Unit |
|---|---|---|---|---|
| 1 | Inlet temperature of water | The EWHE inlet temperature of cooling water | 90 | ºC |
| 2 | Length of buried pipe | The length of the buried horizontal pipe. | 50, 60, 70, 80, 90 | m |
| 3 | Inner diameter of pipe | The inner diameter of the buried pipe containing the heat transfer fluid. | 0.0227-0.046 | m |
| 4 | Outer diameter of pipe | The outer diameter of the buried pipe containing the heat transfer fluid. | 0.025-0.05 | m |
| 5 | Buried pipe material | HDPE, GI and Steel pipe | - | |
| 6 | HDPE pipe thermal conductivity | The thermal conductivity of buried HDPE pipe | 0.40 | W/m K |
| 7 | GI pipe thermal conductivity | The thermal conductivity of buried GI pipe | 16 | W/m K |
| 8 | Steel pipe thermal conductivity | The thermal conductivity of buried steel pipe | 54 | W/m K |
| 9 | Density of water | The density of the working water flowing through the horizontal buried pipe | 1000 | $kg/m^3$ |
| 10 | Thermal conductivity of water | The thermal conductivity of the working water flowing through the horizontal buried pipe | 0.555 | W/m K |
| 11 | Thermal conductivity of soil | The thermal conductivity of the soil in which the horizontal pipe is buried | 0.80 | W/m K |
| 12 | Density of soil | The density of the soil in which the horizontal pipe is buried | 1700 | $kg/m^3$ |
| 13 | Specific heat of soil | The specific heat of the soil in which the horizontal pipe is buried | 0.82 | kJ/kg K |
| 14 | Average surface temperature | The average surface temperature during the year. This temperature will be used as the deep earth temperature for the calculations | 27 | ºC |
| 15 | Depth of buried pipe | The depth of buried pipe from the ground surface | 3.5 | m |
| 16 | Mass flow | Mass flow rate of cooling water | 0.008, 0.02, 0.04, 0.05 | kg/s |

### 3.3.2 Results and discussion

The performance of EWHE system is analyzed by varying different parameters, which includes the type of pipe material, length and diameter of pipe and mass flow rate of fluid within the pipe. As mentioned in the previous section the burial depth of 3.5 m is taken for the simulations. It is important to mention here that the inlet temperature of EWHE for each case was taken as 90 °C, which is assumed to be an outlet temperature of CPV as discussed in the literature [81, 20]. Fig. 3.20 reveals that the EWHE exit temperature for three different pipe materials for pipe length of

90 m, diameter of 25 mm and flow rate of fluid as 0.02 kg/s. It is concluded that the temperature difference of the fluid at outlet of EWHE for GI and Steel pipes is mere 0.2 °C while in the HDPE and Steel pipe is around 1.6 °C, for same inlet conditions. This small variation occurs because of less coefficient of friction for HDPE pipes. Although the GI and steel pipes have high thermal conductivity as compared to HDPE pipes, the coefficient of friction is quite high in these two. This causes the temperature at the outlet as marginally lower than the HDPE pipe. From this estimation, it can be concluded that in EWHE system, the properties of these materials have small impact on the performance of the system. The HDPE pipe is selected for the study as it is much cheaper as compared to GI and steel pipe.

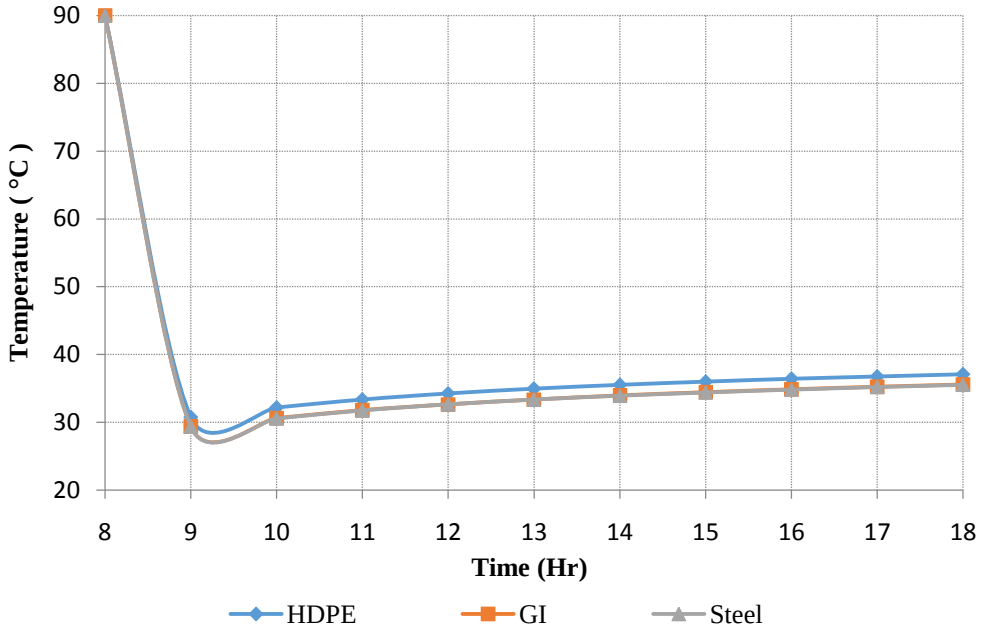


**Fig. 3.20.** EWHE outlet temperature vs different pipe material (pipe ϕ25 mm, Length=90 m, Flow rate=0.02 kg/s)

The effect of mass flow rate on the performance of EWHE along the fixed length of 90 m and diameter of 25 mm for HDPE pipe is shown in Fig. 3.21. It reveals that with increase in mass flow rate the outlet temperature of EWHE increases as expected. This is evident from the fact that with increase in mass flow rate, the Reynolds number increases, which in turns increases the Nusselt number and hence the convective heat transfer coefficient. But with the increase in flow rate of fluid, the contact time to which fluid is in contact with the ground is reduced significantly. Thus the later effect is dominant and so the temperature drop at higher flow rate will be less as compared to lower flow rate. The maximum temperature drops observed for 0.008 kg/s but it is

very low flow rate so for the analysis the mass flow rate varied from 0.02 to 0.05 kg/s. By keeping the mass flow rate of 0.02 kg/s for HDPE pipe, with diameter as 25 mm, the effect of variation of length is estimated. The results obtained by the varying length from 50 m to 90 m are shown in Fig. 3.22. It reveals that with an increase in length the temperature drop increases as expected. For the pipe length of 90 m, the outlet temperature is obtained as 31.9 °C for the inlet of 90 °C. The standard sizes of HDPE pipe available in the market are selected for analysis ranging from 25 mm to 50 mm. The effect of variation in diameter from 25 mm to 50 mm of HDPE pipe at the flow rate of 0.02 kg/s and 90 m length is shown in Fig. 3.23. It is observed that with increase the pipe diameter the outlet temperature decreases gradually over a period of time. After four hours of EWHE operations the temperature drop will be more for HDPE pipe with a maximum diameter of 50 mm.

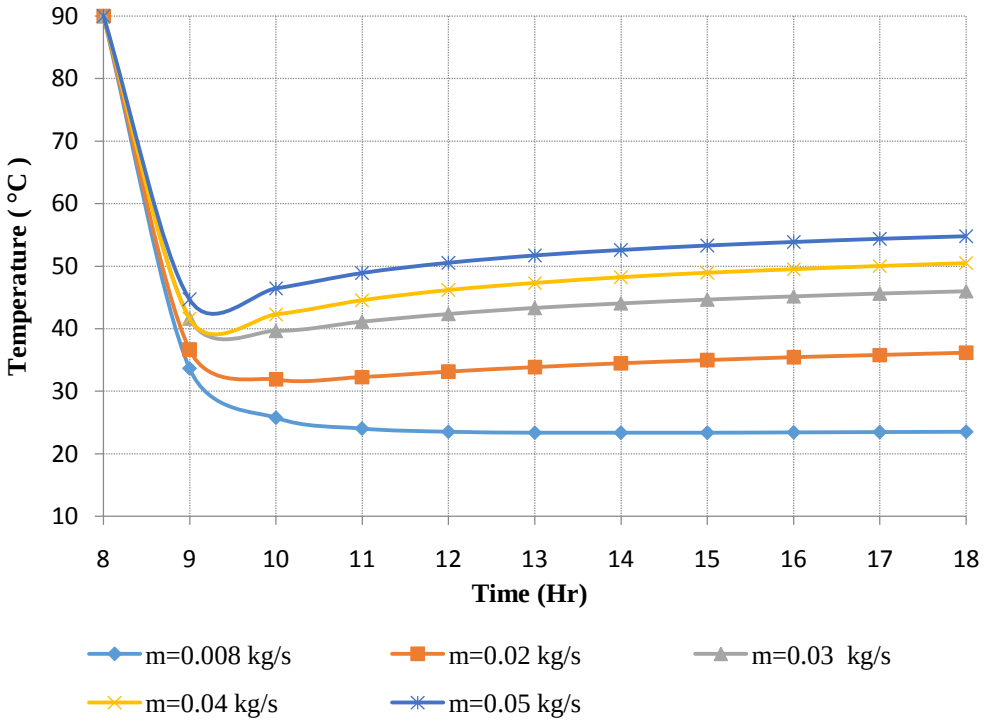


**Fig. 3.21.** EWHE outlet temperature vs mass flow rate (pipe ϕ 25 mm, Length= 90 m, Pipe material= HDPE)

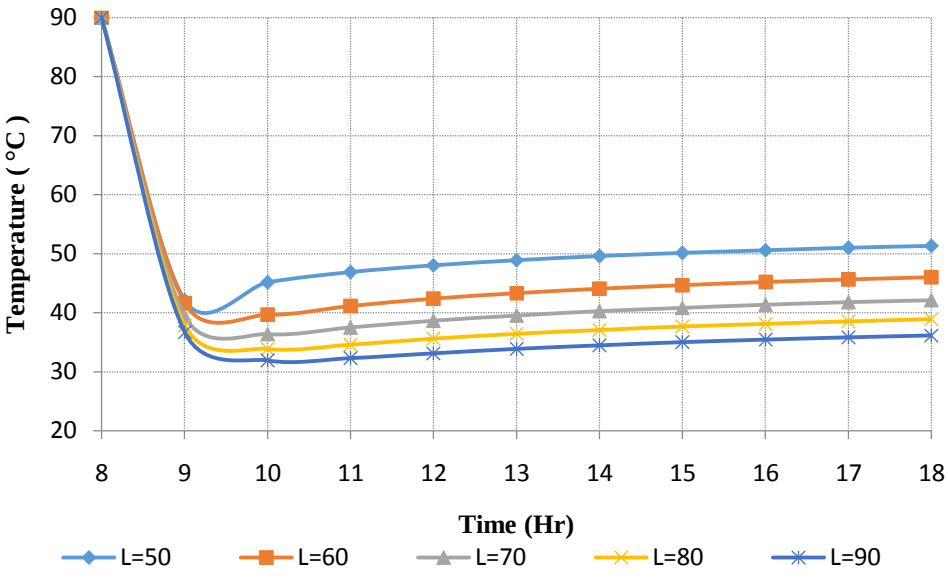


**Fig. 3.22.** EWHE outlet temperature vs pipe length (pipe ϕ 25 mm, flow rate = 0.02 kg/s, Pipe material= HDPE)

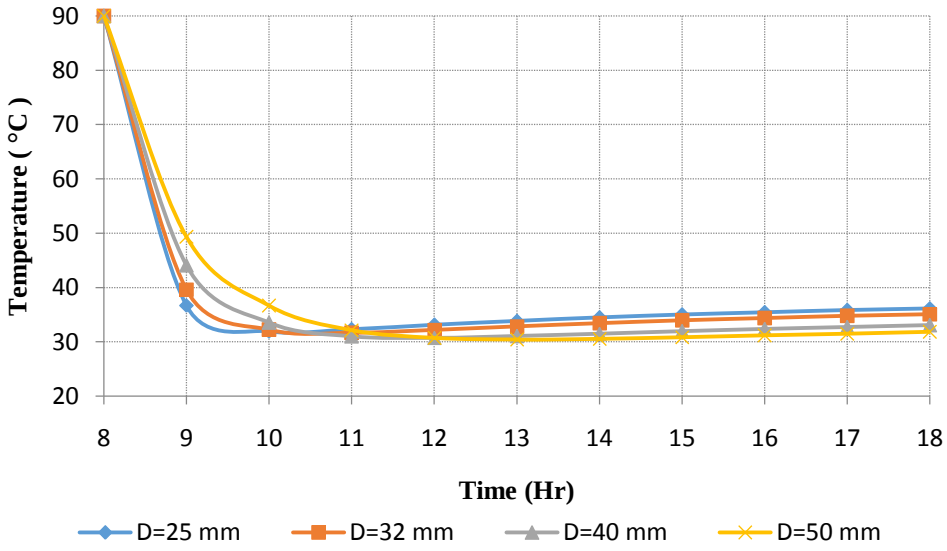


**Fig. 3.23.** EWHE outlet temperature vs pipe diameter (Length=90 m, flow rate= 0.02 kg/s, Pipe material= HDPE)

### 3.3.3 Applicability of EWHE system for CPV cooling

In this section, the usability of such EWHE system to replace the cooling system given in the literature of CPV has been identified. For the analysis, a CPV/T system with storage tank is

taken from the literature [80, 141]. Xu et al. [80] designed the CPV/T system in which solar cells were attached to straight and tree shaped cooling water channel by utilizing a thin-film thermal cladding. They used inlet temperature of 25 °C, CR of 50 suns and flow rate of 0.00045 kg/s and 0.00044 kg/s for straight and tree shaped channel to achieve CPV/T outlet temperature of 58.7°C and 55°C for respective cases. These outlets of the CPV/T system are simulated as the inlet for the proposed system to identify the appropriate length of EWHE for the same cooling effect. It is observed from the Table 3.4, that it would take EWHE system of 4 m and 5 m length for the respective cases to achieve the temperature drop up to inlet temperature of 25°C. The cost comparison shows that it is economical than the reference cases and could be a better and cheaper option. The Table 3.4 also shows the comparative study with the existing system of Li et al. [141] where they used CR of 16.92 and flow rate of 0.012 kg/s for four different solar cells, i.e. Crystalline Silicon (CS), Polycrystalline Silicon (PS), Super Cell Array (SCA) and GaAs cell array. In their system they used the CPV/T system connected to storage tank heat exchanger for hot water applications. This system is modified in the present study and simulated for the same inlet temperature and direct normal irradiance to achieve the same outlet temperature as shown in Fig. 3.24. The results obtained with the proposed EWHE system are shown in Table 3.4, which indicates that the maximum length of 60 m would be sufficient to achieve the same cooling effect. The proposed system is cheaper as compared to reference cases. The EWHE system along with CPV may be used for the semi-arid regions of western Rajasthan which is blessed with high solar insolation.

**Table 3.4** Applicability of EWHE system with existing literature

| Author | Concentration ratio (CR) (Suns) | CPV cells material | Flow rate (kg/s) | Water outlet temp. from CPV/T (EWHE Inlet) °C | Water outlet temp. from EWHE (CPV/T inlet) °C | Pipe length required for EWHE (meter) |
|---|---|---|---|---|---|---|
| Xu et al. (2012) | 50 (Straight) | Monocrystalline silicon | 0.00045 | 58.70 | 24.20 | 5 |
| | 50 (Tree) | | 0.00044 | 55.00 | 24.30 | 4 |
| Li et al. (2011) | 16.92 | CS and PS | 0.012 | 48.50 | 25.50 | 60 |
| | 16.92 | SCA | 0.012 | 47.00 | 25.70 | 58 |
| | 16.92 | GaAs | 0.012 | 42.50 | 26.00 | 52 |

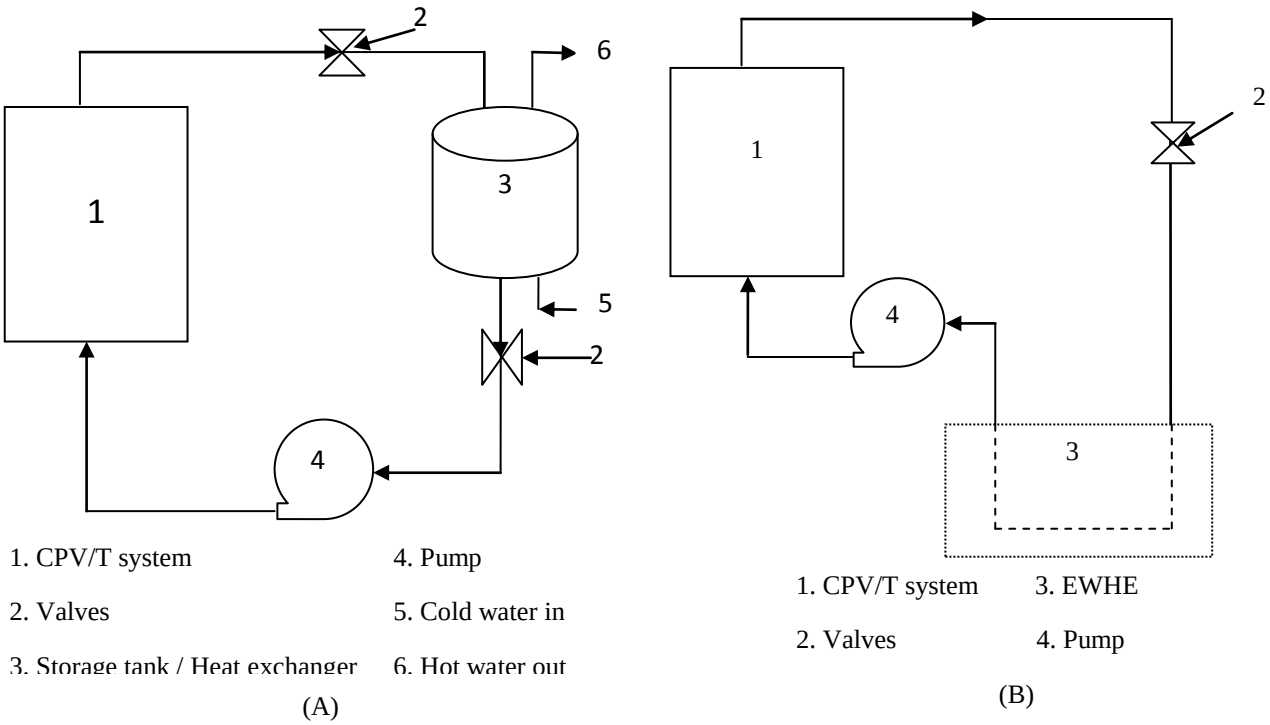


**Fig. 3.24.** Schematic diagram of (A) Conventional CPV/T cooling system (B) Proposed CPV/T cooling system with EWHE

### 3.4 Design and analysis of CPV/T system with EWHE cooling for Pilani

In the previous section, the feasibility of EWHE was tested for CPV cooling. It was also concluded in the previous section that the such EWHE system could be used for the CPV cooling for the semi-arid regions. Thus a modelling and simulation of CPV/T system coupled with EWHE cooling (closed system) has been performed using TRNSYS, for climatic condition of Pilani, Rajasthan. This section discusses the simulation and result analysis of such coupled system.

#### 3.4.1 Description of the proposed system

The schematic diagram of the CPV/T system coupled with EWHE is shown in Fig. 3.25. The coupled system includes EWHE, CPV/T system, valves and pump all connected in sequence.

The copper tubes are joined with adhesive on the absorber plate which was mounted on the back side of CPV panel. These copper tubes carry water to take away excess heat from the panel causing temperature increase of water. With the help of pipes and valves, the outlet of CPV/T is connected to EWHE. EWHE has HDPE pipe buried at a depth of 3.5 m and transfer heat from hot water to earth. Due to this, at outlet, the water temperature is quite less than the ambient, during summers. This is sent back to copper tubes for cooling of CPV/T system in a continuous way and resulting in a decrease in CPV temperate and increase in efficiency.

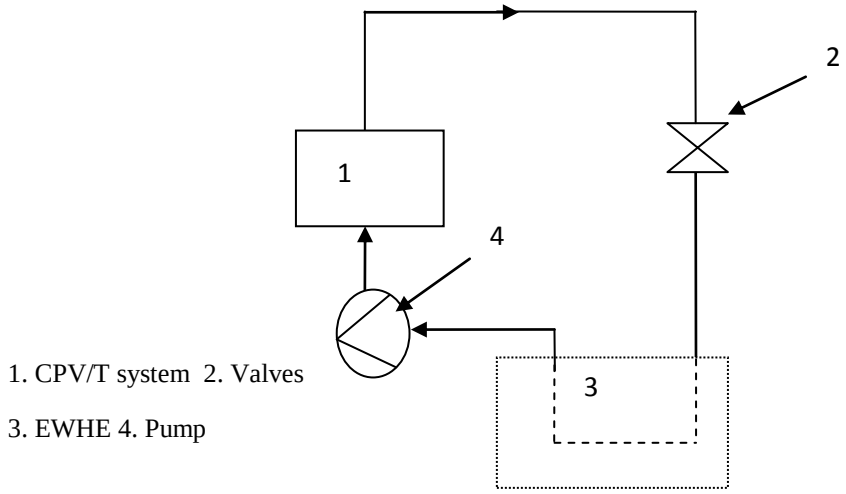


**Fig. 3.25.** (a) Schematic diagram of proposed CPV/T coupled with EWHE cooling system

### 3.4.2 Simulation methodology

In the current work, the transient modelling and simulation of CPV/T with EWHE cooling was carried out using TRNSYS (v17.0). The adopted simulation methodology for this work is explained using the following steps:

1. The simulation of CPV/T system coupled with EWHE cooling requires climatic data, such solar radiation, wind velocity, ambient temperature, relative humidity, etc. Weather data for Pilani, Rajasthan (India) has been generated using inbuilt Meteonorm files provided within TRNSYS. The weather component is taken as *Type15-3* under TMY3 library.
2. The component for CPV/T collector is created using CPV/T collectors (*Type50*) in

the electrical library (TESS)

3. Within the ground heat pump library of TRNSYS, EWHE (*Type952*) is a horizontal heat exchanger model which interacts thermally with the ground.
4. For a closed loop cycle and to circulate the HTF, a pump is required, so form the Hydronics TESS library, a variable speed pump (*Type3*) which can also vary the mass flow rate, is taken.
5. To fix the upper and lower temperature a limit of CPV/T and EWHE, a controller is also used which is denoted by *Type2* component and is connected in between CPV/T and EWHE.
6. The output results can be extracted by number of components which includes simulation, output, simulation summary and printer components. In this work *Type65* is taken from the TESS library.
7. In the end, all the system components are linked and interconnected as per the system requirement in a form of flow chart. As mentioned above, the output of one TYPE is input for another, thus the simulation is run for the desired period of time.
8. With the obtained results, the user can check for the accuracy of the results. The satisfactory required flow of data proves the authentication of the results. In case of any error, of unsatisfactory results, user needs to check the possible source of error which could be wrong components link, wrong input parameters or a conceptual mistake in the formulation of the problem.

Fig. 3.26 represents the simplified simulation model with all major components for the coupled system under consideration for this research. As shown in Fig. 3.26 the component for the CPV/T is connected to pump, which is further connected to EWHE to make it as a close loop. CPV/T is a hybrid collector which produces both electrical and thermal energy. Within the ground heat pump library of TRNSYS, EWHE is a horizontal heat exchanger model which interacts thermally with the ground. In the closed loop simulation, the excess waste heat of CPV/T is dissipated to the soil by EWHE. Furthermore, the weather data component is connected with CPV/T to provide the climatic data of the local conditions. And the following standard TRNSYS component models (*Types*) were used in the simulation:

- Type50- CPV/T collector
- Type3- Variable speed pump

- Type952- Earth water heat exchanger
- Type15 - Weather data processor
- Type65- Online plotter
- Type28- Simulation summary

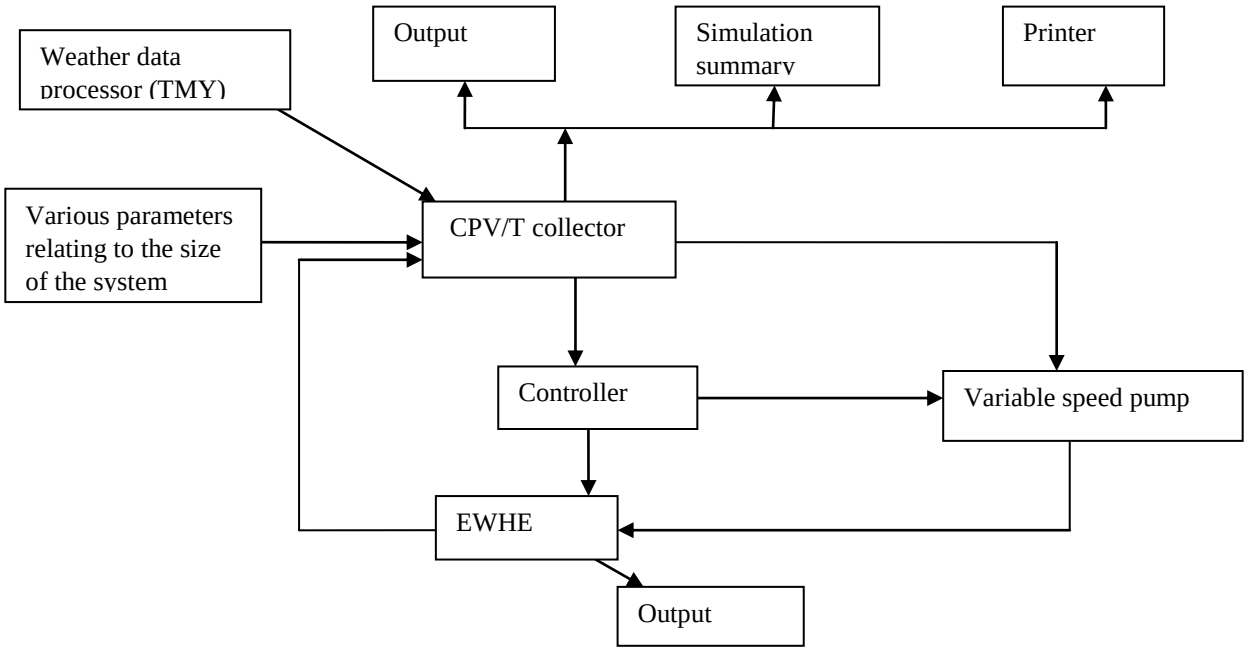


**(a)**

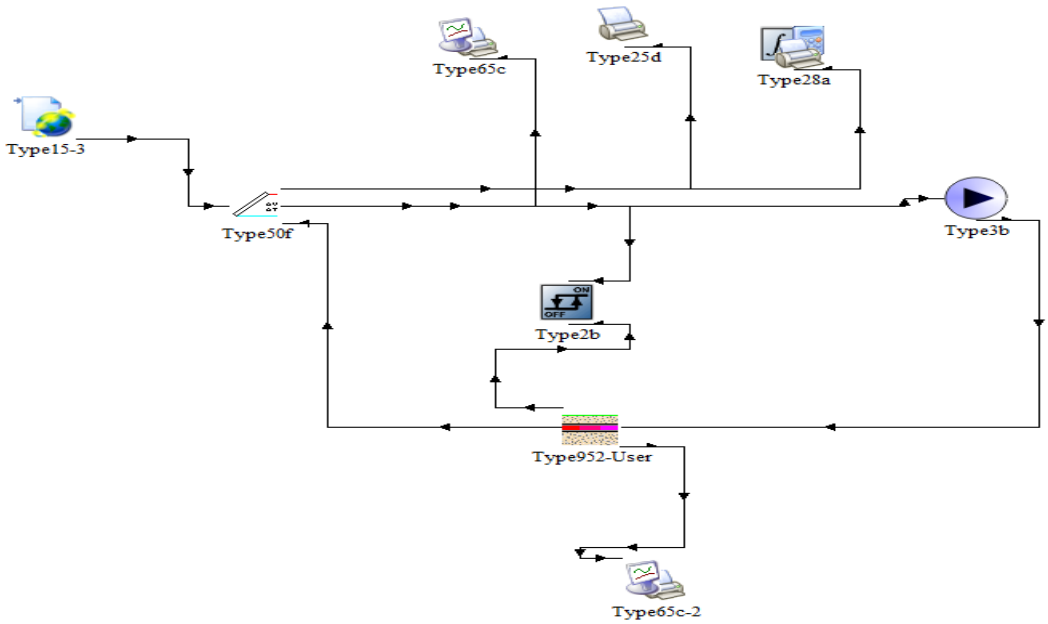


**(b)**

**Fig. 3.26.** (a) Schematic diagram for the CPV/T with EWHE cooling (b) TRNSYS flow diagram

### 3.4.3 Description of the main components used in simulation

In this section, the values of all parameters which used for the simulation of major TRNSYS components are presented.

*(a) CPV/T component*

The CPV/T system provides the combined electrical and thermal energy from one system. In this system the copper tubes are mounted on the rear side of the CPV panel with water as a HTF. The HTF takes away the excess heat from the panels thus resulting in a decrease in panel temperature. CPV/T design needs various physical parameters like length, width, tube spacing, etc. and thermal parameters like heat transfer coefficients, etc. For design of the CPV/T different parameters were taken to optimize and are show in Table 3.5.

**Table 3.5.** Design and input parameters of CPV/T system

| S. No. | Parameter name | Parameter description | Value | Unit |
|---|---|---|---|---|
| 1 | Collector area | The area of collector surface that intercepts solar radiation | 5 | $m^2$ |
| 2 | Concentration ratio | The area of the collector's aperture divided by the area of the absorber | 2-6 | Suns |
| 3 | Plate absorptance | The solar radiation absorptance of the collector's plate | 0.9 | - |
| 4 | Fin efficiency area ratio | The fin efficiency area ratio of the collector | 0.96 | - |
| 5 | Back loss coefficient for no-flow condition | The heat transfer coefficient for thermal losses from the back and sides of the collector | 1.2 | $W/m^2$ k |
| 6 | Tube diameter | The diameter of the water tubes bonded to the absorber plate | 0.012 | m |
| 7 | Thermal conductance between cells and absorber | This parameter accounts for contact resistance between the PV cells and the collector absorber plate. Set this value high to indicate good thermal conductivity between the two | 101250 | W/K |
| 8 | Cover plate transmittance | The solar spectrum transmittance of the collector's transparent covers | 0.9 | - |
| 9 | Water specific heat | The specific heat of the water flowing through the CPV/T collector array | 4.19 | kJ/kg K |
| 10 | PV cell reference temperature | The reference temperature at which the efficiency of the PV cell is provided | 25 | ºC |
| 11 | Number of glass covers | The number of identical transparent covers on the collector | 1 | |
| 12 | Absorber plate emittance | The collector plate emittance (infra-red wavelength range) | 0.9 | |
| 13 | Inlet flow rate | The flow rate of water entering the PV/T collector array | 0.006-0.026 | kg/s |

*(b) EWHE*

The optimized parameters required for EWHE are already discussed in Section 3.3.1 and Table 3.3.

### 3.4.4 Results and discussion

The simulation of the proposed system ran for 10 hours, which is mean sunshine hours during the peak summer period (June 21). The parameters for the EWHE system were taken from the Section 3.3.2 which gives the optimized value of length as 90 m, burial depth 3.5 m, tube diameter 25 mm and mass flow rate as 0.02 kg/s. However, for CPV/T collector the pipe diameter of 12 mm was taken due to the fact that with higher diameters, say 25 mm, the CPV/T performance decreases, as mentioned in the literature. Thus, for EWHE system the pipe diameter was taken as 12 mm and the simulation was performed for mass flow rate of 0.06 kg/s, 0.01 kg/s, 0.014 kg/s, 0.018 kg/s, 0.022 kg/s, 0.026 kg/s and 0.03 kg/s by taking climatic conditions from the meteonorm files inbuilt in TRNSYS.

The temperature variation of CPV/T system for different mass flow rates in case of cooling and without cooling is shown in Fig. 3.27. It is observed that the temperature of CPV/T system ranges from 122.48 °C to 416.36 °C with 3 Suns in case of without cooling when there is no flow. With EWHE cooling scenario, the CPV panel temperature decreases drastically and it varies between 64.71 °C - 128.51°C, 43.43 °C - 91.40 °C, 38.49 °C- 79.87 °C and 37.05 °C- 76.48 °C for mass flow rates of 0.006 kg/s, 0.018 kg/s, 0.026 kg/s and 0.03 kg/s respectively. It shows that with an increase in the mass flow rate, the CPV/T temperature decreases. The maximum temperature drop is observed for 0.03 kg/s and it remains almost constant for flow rate of 0.026 kg/s and 0.022 kg/s. Since 0.03 kg/s is a high flow rate that is high pumping power, so 0.022 kg/s may be selected for the practical applications as the temperature variation in these three flow rates are almost similar. When the simulation is carried out for the 3 suns, with the simulation time of 10 hour duration, it is observed that in case of without cooling there is no CPV power output from 9 am to 5 pm due to high cell temperature. However the power is obtained for simulations of early morning (8 am) and late evening (6 pm). The CPV power output for same CR with different mass flow rates in case of EWHE cooling is shown in Fig. 3.28. It is found out that in case of EWHE cooling the CPV produces power for the entire simulation duration. For the flow rate of 0.022 kg/s, the power output varies from 137.98 W to

722.43 W. It is also observed that the CPV power gradually increases as mass flow rate increases. However, during the peak hours the lower mass flow rates (0.006 kg/s, 0.01 kg/s) experiences lesser power output. The reason for the same is that they carried away the less heat due to lower heat transfer coefficient and thus resulting is less CPV temperature drop. This causes the variation in CPV power for lower and higher flow rates with peak output obtained at 1400 hrs for later case.

For the mass flow rate of 0.022 kg/s, the effect on the performance of CPV for the CR varying from 2 to 6 Suns is estimated. The results are shown in Fig. 3.29 and Fig. 3.30. It is observed that with the increase in CR the maximum CPV temperature varies from 290.68 °C to 793.39 °C for CR variation of 2 to 6 respectively in case of without cooling at 1400 hrs. Similarly, it decreases with EWHE cooling and ranges between 36.79 °C - 72.53 °C, 43.92 °C - 95.49 °C and 50.97 °C - 117.12 °C for 2 Suns, 4 Suns and 6 Suns respectively. As discussed earlier, CPV does not produce electrical power without any cooling for CR of 2 to 6 Suns due to fact that CPV power depends on the operating temperature and without cooling the temperature is very high. The CPV power with cooling for different CR is shown in Fig. 3.30. It is observed that the power output is in the range from 134.15 W- 665.29 W, 140.59 W- 714.18 W and 145.24 W - 749.64 W for 2 Suns, 4 Suns and 6 Suns respectively. Thus, it is clearly seen that the high CR is beneficial for CPV cells, but at the same time the cooling is essential.

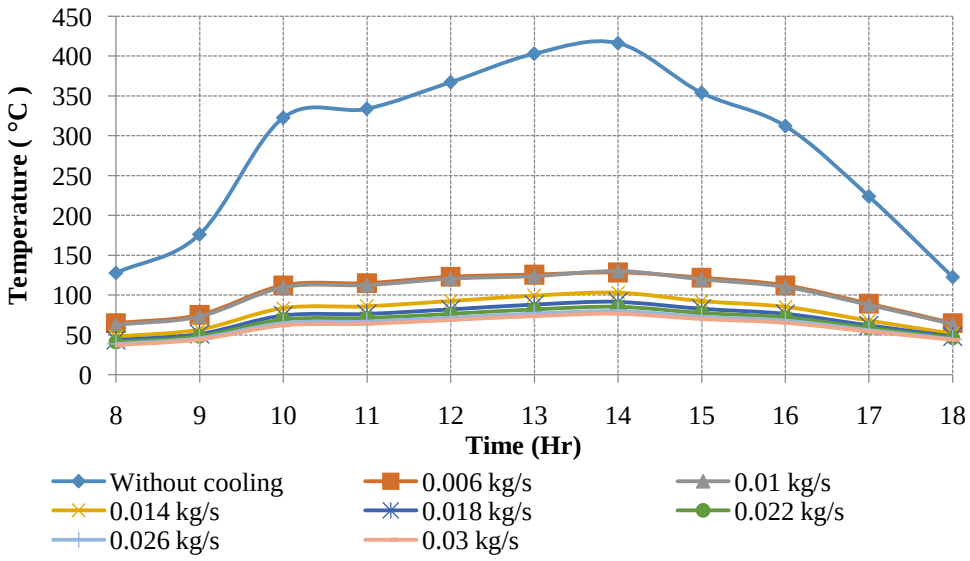


**Fig. 3.27.** CPV/T panel temperature with cooling and without cooling for various mass flow rates (Suns=3)

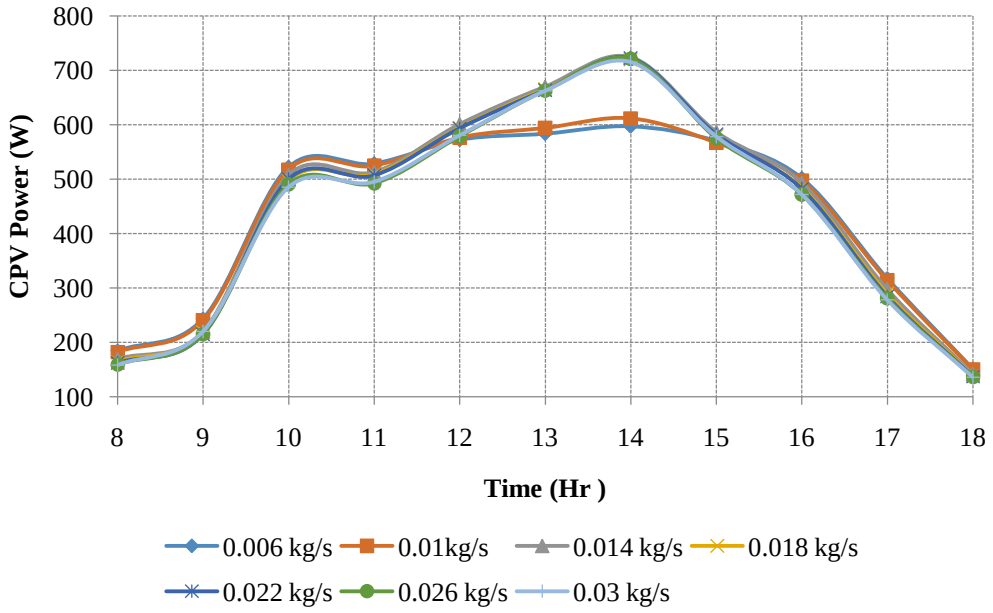


**Fig. 3.28.** CPV power output with cooling for different mass flow rates (Suns=3)

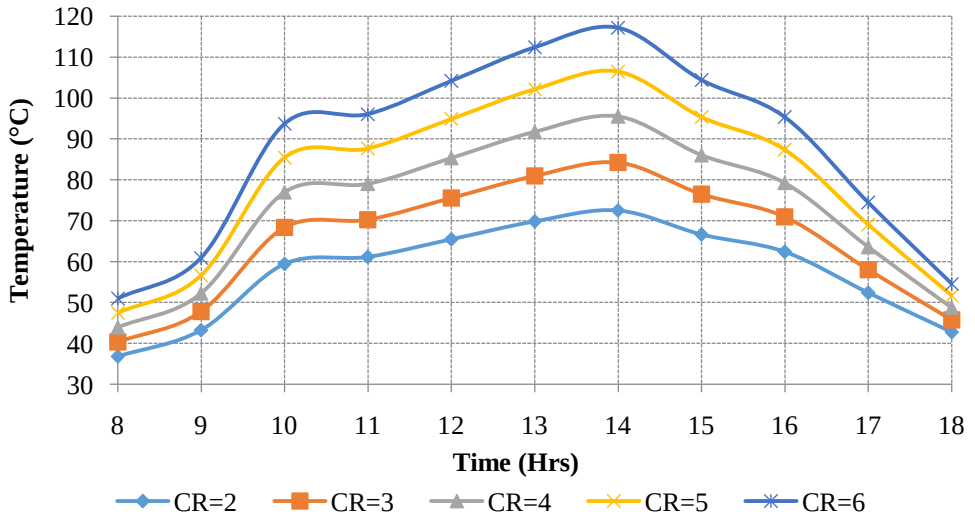


**Fig. 3.29.** CPV temperature with cooling for different concentration ratios (flow rate=0.022 kg/s)

The variation of CPV/T water outlet temperature at 3 Suns for different mass flow rates is shown in Fig. 3.31. It is observed that the outlet temperature of CPV/T decreases with the increase in mass flow rate, as expected. The outlet temperatures obtained after six hours of simulation (i.e. 1400 hrs) are 80.23 °C for 0.006 kg/s and 62.10 °C for 0.026 kg/s respectively. Moreover Fig.3.31 depicts that the temperature difference between 0.022 kg/s and 0.026 kg/s flow rates is

merely 1.9 °C for the same conditions. Considering the small variation in temperature for these flow rates, it can be concluded that the 0.022 kg/s flow rate may be sufficient for CPV/T system with 3 Suns. From the Fig. 3.29 and Fig. 3.31 it is also observed that the temperature of CPV cells is higher than CPV/T water outlet temperature with different mass flow rates which makes it possible to cool the CPV cells.

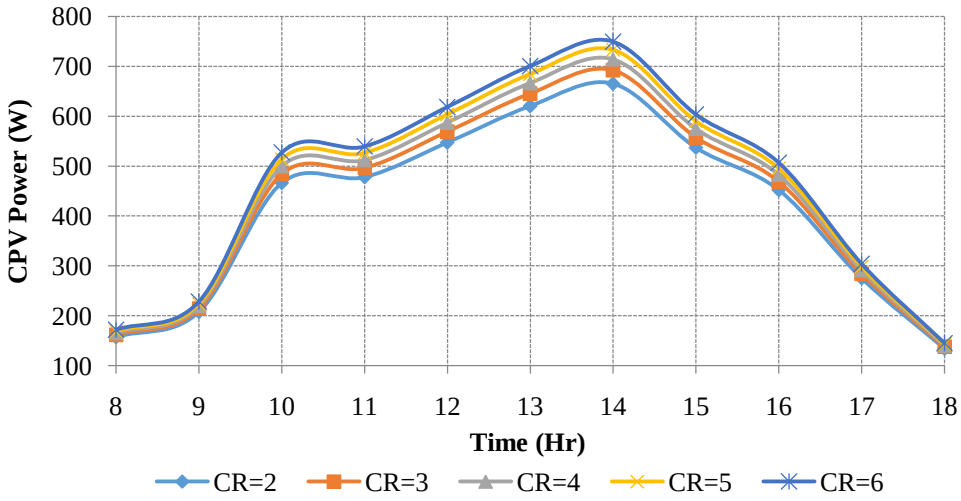


**Fig. 3.30.** CPV power output with cooling for different concentration ratios (flow rate=0.022 kg/s)

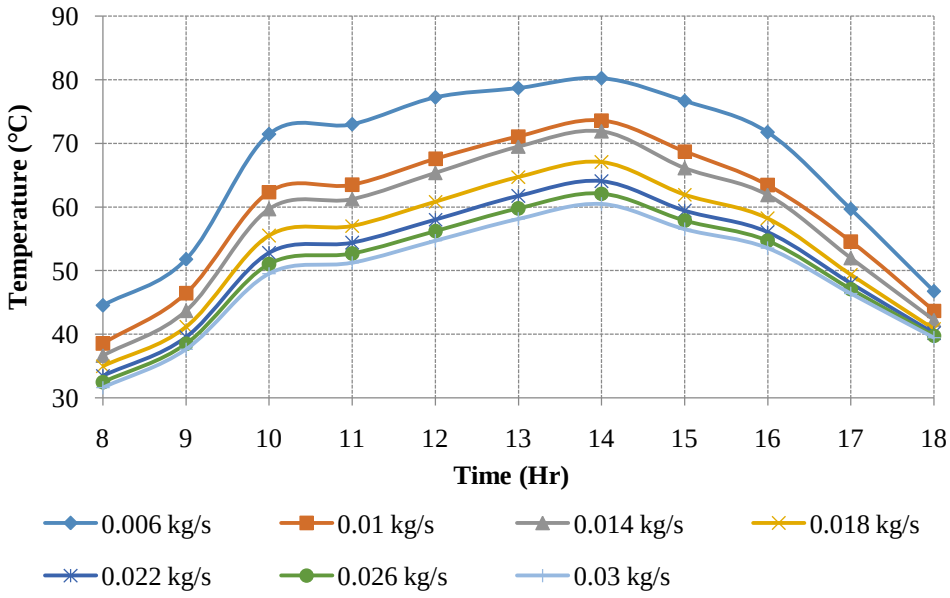


**Fig. 3.31.** CPV/T water outlet temperature for different mass flow rates (Suns=3)

## 3.5 Modelling and simulation of glazed PV/T system with EWHE cooling

As discussed above that the simulation of unglazed PV/T coupled with EWHE was carried out in TRNSYS, the software itself has its own limitations. It has inbuilt models which do not allow the user to perform parametric variation. Further, in PV/T collector only tube-and-sheet type model is available. Hence, to carry out the parametric variation, with different types of PV/T collectors, one dimensional mathematical equations were developed from the literature review and simulated in MATLAB. Here three different types of PV/T system were developed, viz. tube-and-sheet type, broad water channel type and broad air channel type PV/T collector. The analysis has been carried out by coupling all these PV/T collectors with geothermal cooling followed by experimental validation.

### 3.5.1 Tube-and-sheet PV/T system coupled with EWHE cooling

Such type of collector has absorber tube, bonded on the back side of PV panel with adhesive, and has pipes welded upon them. These pipes are of high thermal conductivity and carries HTF. The design and detail discussion on such collector is carried out in Chapter 4. In order to analysis the performance of the proposed system, the first law of thermodynamic analysis of PV/T coupled with EWHE has been done. In this section, an energy analysis is presented to evaluate the performance of the PV/T coupled with EWHE system.

#### *3.5.1.1 Tube-and-sheet PV/T system*

The assumptions for first law analysis of the PV/T system are as follows:

- The one-dimensional heat transfer is considered for the analysis.
- The Ohmic losses in the PV module are negligible.
- PV/T system is in quasi-steady-state.
- The heat capacity of the PV/T system is neglected.
- The temperature gradient across the PV module is neglected.

The energy balance of the PV/T system is carried out to derive the analytical expressions for the thermal and electrical efficiencies of the PV/T system. For the same the thermal resistance circuit

diagram is shown in Fig. 3.32 which includes all three thermal resistances, namely, convective, conductive, and radiative. The heat transfer resistances help in identifying the flow of energy and obtaining the thermal efficiency of the collector.

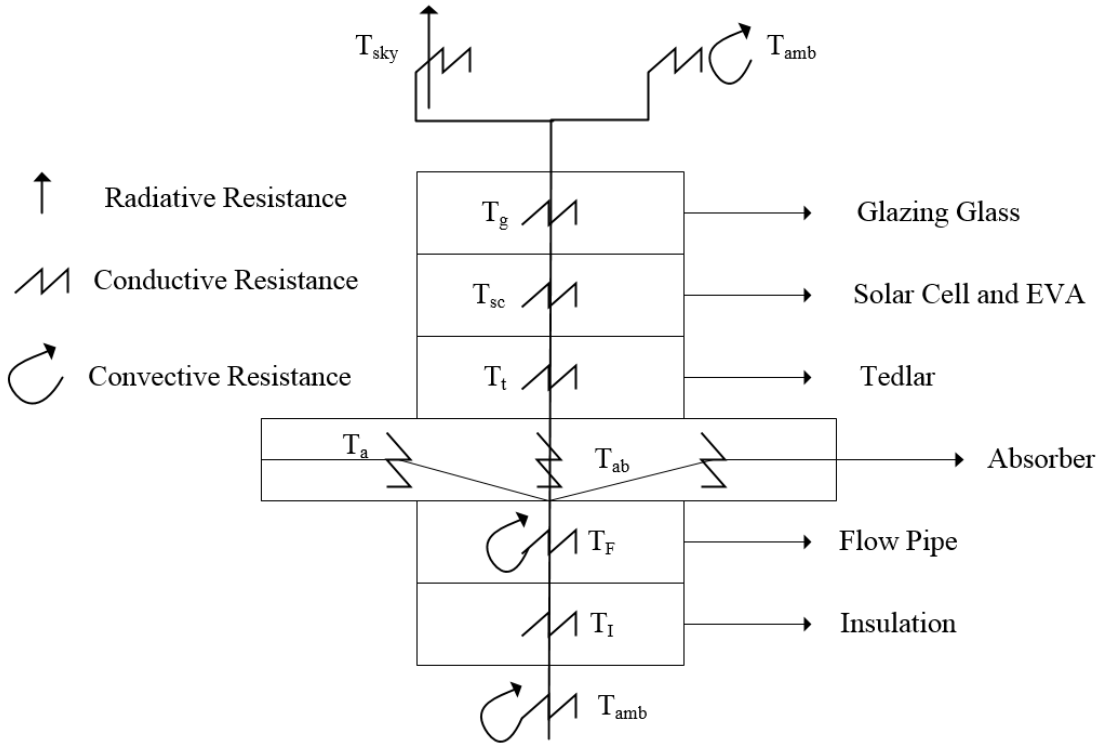


**Fig. 3.32.** Thermal resistance circuit diagram for PV/T system

(a) Energy balance for the PV module (glass to tedlar) is given by equation 3.1 [98]:

$$\tau_g \alpha_c \beta_c G(I) B dx + \tau_g (1-\beta_c)\alpha_{ted}\, G(I) B dx = \left[U_{c,amb}\,(T_c - T_{amb}) + U_{ct}(T_c - T_{ba})\right] B dx + \eta_{c,el}\beta_c \tau_g G(I) B dx \quad (3.1)$$

Where $T_c, T_{ba}, T_a, B, G(I)$, $\eta_{c,el}$, and $\beta_c$, are solar cell temperature, back surface temperature of absorber, ambient temperature, the width of absorber, global solar radiation, electrical efficiency of solar cell and packing factor of solar cell respectively.

The equation for the solar cell temperature obtained from equation (3.1) as:

$$\overline{T_c} = \frac{\tau_g[\alpha_c\beta_c + (1-\beta_c)\alpha_{ted} - \eta_{c,el}\beta_c]G(I) + U_{c,amb}\,T_{amb} + U_{ct}\,\overline{T_{ba}}}{U_{c,amb} + U_{ct}} \quad (3.2)$$

(b) For the back surface of tedlar the energy balance yields equation 3.3 [142]

$$U_{ct}(T_c - T_{ba})Bdx = U_{aw}(T_{ba} - T_w)Bdx \tag{3.3}$$

From equation (3.3), the expression for average absorber temperature is

$$\overline{T_{ba}} = \frac{PF_1(\alpha\tau)_{eff}\, G(I) + U_{gt}T_{amb} + U_{aw}\overline{T_w}}{U_{gt} + U_{aw}} \tag{3.4}$$

Where $PF_1$ is the penalty factor due to presence of solar cell material, glass and EVA and $U_{gt}$ is overall heat transfer coefficient from glass to tedlar [111].

$$U_{gt} = \frac{U_{c,amb} \times U_{ct}}{U_{c,amb} + U_{ct}} \tag{3.5}$$

$$PF_1 = \frac{U_{ct}}{U_{c,amb} + U_{ct}} \tag{3.6}$$

(c) The energy balance for water flowing in tube-and-sheet collector below the PV module yields equation 3.7 [143]

The energy balance of flowing in tube-and-sheet collector below the PV module is given by:

$$F' U_{aw}\left(T_{ba} - T_{w,avg}\right)Bdx = m_w C_w \frac{dT_{w,avg}}{dx}dx + U_{bc}\left(T_{w,avg} - T_a\right)Bdx \tag{3.7}$$

Now rearranging and integrating the both sides of the equation (3.7) with boundary conditions, $T_{fx=0} = T_{fi}$ $and$ $T_{fx=L} = T_{f0}$ , we got the expression for the outlet fluid temperature as:

$$T_{wo} = \left[\frac{PF_1\, PF_2(\alpha\tau)_{eff}\; G(I)}{U_T} + T_{amb}\right]\left[1 - \exp\left(-\frac{F' A_c U_T}{m_w C_w}\right)\right] + T_{wi}\exp\left[-\frac{F' A_c U_T}{m_w C_w}\right] \tag{3.8}$$

Where $PF_2$ is a penalty factor due to the presence of the interface between tedlar and cooling water through the absorber below PV module.

$$PF_2 = \frac{U_{aw}}{U_{aw} + U_{gt}} \qquad (3.9)$$

And the average fluid temperature is calculated by integrating equation (3.8) as: [143]

$$\overline{T_w} = \frac{1}{L_t}\int_0^{L_t} T_{wo}\, dx \qquad (3.10)$$

$$\overline{T_w} = \left[\frac{PF_1\, PF_2(\alpha\tau)_{eff}\; G(I)}{U_T} + T_{amb}\right]\left[1 - \left(\frac{1 - \exp\left(-\frac{F' A_c U_T}{m_w C_w}\right)}{\frac{F' A_c U_T}{m_w C_w}}\right)\right] + T_{wi}\left[\frac{1 - \exp\left(-\frac{F' A_c U_T}{m_w C_w}\right)}{\frac{F' A_c U_T}{m_w C_w}}\right] \qquad (3.11)$$

where $(\alpha\tau)_{eff} = \tau_g[\alpha_c\beta_c + (1-\beta_c)\alpha_{ted} - \eta_{c,el}\beta_c]$ (3.12)

By putting the expression of $\overline{T_w}$ from equation (3.11) in equation (3.4), we get an average absorber temperature $\overline{T_{ba}}$. After obtaining $\overline{T_{ba}}$, the expression for an average solar cell temperature $\overline{T_c}$ can be evaluated from equation (3.2). Further, according to Evans [144] and Schott [145] the solar cell efficiency ($\eta_c$) can be calculated as:

$$\eta_c = \eta_{STC}[1 - \beta_0(T_c - T_{STC})] \qquad (3.13)$$

Further the electrical efficiency of PV module can be calculated as follows [146]:

$$\eta_m = \beta_c \tau_g \eta_c \qquad (3.14)$$

The instantaneous thermal efficiency of the PV/T system is [146]:

$$\eta_{th} = \frac{m_w c_w\, (T_{wo} - T_{wi})}{A_c\; G(I)} \qquad (3.15)$$

And the instantaneous electrical efficiency of the PV/T system is calculated as:

$$\eta_e = \frac{FF\; I_{sc} V_{oc}}{A_c\; G(I)} \qquad (3.16)$$

### *3.5.1.2 EWHE system*

EWHE system is modeled as a combined heat transfer process, namely convection heat transfer between flowing water and inner surface of buried pipe and conduction heat transfer between the outer surface of buried pipe and the soil. The assumptions for writing the energy balance equations for EWHE system are as follows:

- One-dimensional heat transfer is considered for the analysis.
- The buried pipe soil is isotropic with homogenous thermal conductivity throughout.
- The soil temperature taken as equal to the annual average ambient air temperature.
- The pipe is of uniform circular cross-section area.
- The thermal effect of the surrounding soil vanishes after a distance equal to pipe radius from the buried piper outer surface.
- EWHE system is in quasi-steady-state.

The thermal resistance of the soil annulus is calculated as [147]:

$$R_{soil} = \frac{\ln\left(\frac{r_s}{r_o}\right)}{2\pi\, l_p k_s} \qquad (3.17)$$

The thermal resistance of the pipe thickness is calculated as [147]:

$$R_{pipe} = \frac{\ln\left(\frac{r_o}{r_i}\right)}{2\pi\, l_p k_p} \qquad (3.18)$$

For the calculation of the convection heat transfer coefficient the Reynolds number (Re) and Nusselt number (Nu) is given by:

$$Re = \frac{\rho v_w 2r_i}{\mu} \qquad (3.19)$$

The Nusselt number for laminar flow is given as:

$$Nu = 4.36, for\ Re < 2300$$

And Nusselt number for turbulent flow in a circular pipe for the ranges $0.5 < pr < 2000\ and\ 2300 <\ Re < 5 \times 10^6$ is given as [147]:

$$Nu = \frac{(f/8)(Re - 1000)Pr}{1 + 12.7\ (f/8)^{0.5}(Pr^{0.66} - 1)} \qquad (3.20)$$

Here $f$ is friction factor for smooth pipes and is calculated by Petukhov's relation [148]

$$f = (0.79 \ln Re - 1.64)^{-2} \qquad (3.21)$$

Now the thermal resistance due to convective heat transfer between flowing water and inner surface of buried pipe is calculated as [148]:

$$R_{Convec} = \frac{1}{2\pi r_i l_p h} \qquad (3.22)$$

Where $h$ is convective heat transfer coefficient and calculated as [148]:

$$h = \frac{Nu\ k_w}{2r_i} \qquad (3.23)$$

The total thermal resistance between flowing water and soil of EWHE system is calculated from

$$R_{total} = R_{soil} + R_{pipe} + R_{Convec} \qquad (3.24)$$

Then overall heat transfer coefficient is defined by

$$U = \frac{1}{R_{total}} \qquad (3.25)$$

For a pipe of constant temperature ($T_{pipesurface} = T_s$) the effectiveness of EWHE can be calculated as [130]

$$\varepsilon = 1 - e^{\left(-\frac{U}{m_w c_w}\right)} \qquad (3.26)$$

Then the temperature effectiveness is calculated as [130]

$$\varepsilon = \frac{T_{wi1} - T_{wo1}}{T_{wi1} - T_s} \qquad (3.27)$$

The outlet temperature of EWHE is calculated from the equation (28) as [130]

$$T_{wo1} = T_{wi1} - (T_{wi1} - T_s) \times \varepsilon \qquad (3.28)$$

The cooling potential of EWHE is given by

$$Q = m_w c_w (T_{wi1} - T_{wo1}) \qquad (3.29)$$

The design parameters used in the above equations are presented in Table 3.6.

**Table 3.6**. Design parameters of PV/T water collector with EWHE

| Parameter | Value |
|---|---|
| Diameter of PV/T collector tubes | 0.012 m |
| Tube spacing | 0.098 m |
| Thermal conductivity of insulation | 0.042 W/m K |
| Thickness of absorber plate | 0.002 m |
| Thermal conductivity absorber plate | 385 W/m K |
| Thickness of solar cell | 0.0003 m |
| Thermal conductivity of solar cell | 0.036 W/m K |
| Thickness of tedlar | 0.0005 m |
| Thermal conductivity of tedlar | 0.033 W/m K |
| Absorptivity of solar cell | 0.90 |
| Transmissivity of solar cell | 0.90 |
| Transmissivity of glass | 0.95 |
| Absorptivity of tedlar | 0.75 |
| Thickness of glass cover | 0.0032 m |
| Thermal conductivity of glass cover | 1 W/m K |
| EWHE pipe material | HDPE |
| EWHE pipe total length | 80 m |
| EWHE pipe diameter | 0.20 |

### 3.5.2 Broad water channel glazed PV/T system (IPVTS) coupled with EWHE cooling

This type of collector doesn't have any metallic absorber on the back side of PV panel. Instead of that, a broad water channel was developed using GI sheet through which water flows with direct contact with tedlar sheet. The detailed description for such system is mentioned in Chapter 4. The broad water channel PV/T system also known as integrated photovoltaic thermal system (IPVTS). The first law of thermodynamics is used to analyze the performance of the proposed IPVTS system coupled with EWHE. This section presents an energy analysis to evaluate the performance of the proposed system.

#### *3.5.2.1 Broad water channel PV/T (IPVTS) system*

The assumptions for first law analysis of IPVTS system are as follows:

- The 1-D heat transfer is considered for the analysis.
- The Ohmic losses in the PV panel are negligible.
- IPVTS system is in quasi-steady-state.
- The heat capacity of the IPVTS system is neglected.
- The temperature gradient across the PV module is neglected.

Analytical expressions for the thermal and electrical efficiencies of the IPVTS system have been derived using energy balance. The thermal resistance circuit diagram for the same is shown in Fig. 3.33. The diagram shows three different resistances namely, convective, conductive, and radiative. The thermal efficiency of the IPVTS is then obtained by identifying the energy flow through the heat transfer resistances.

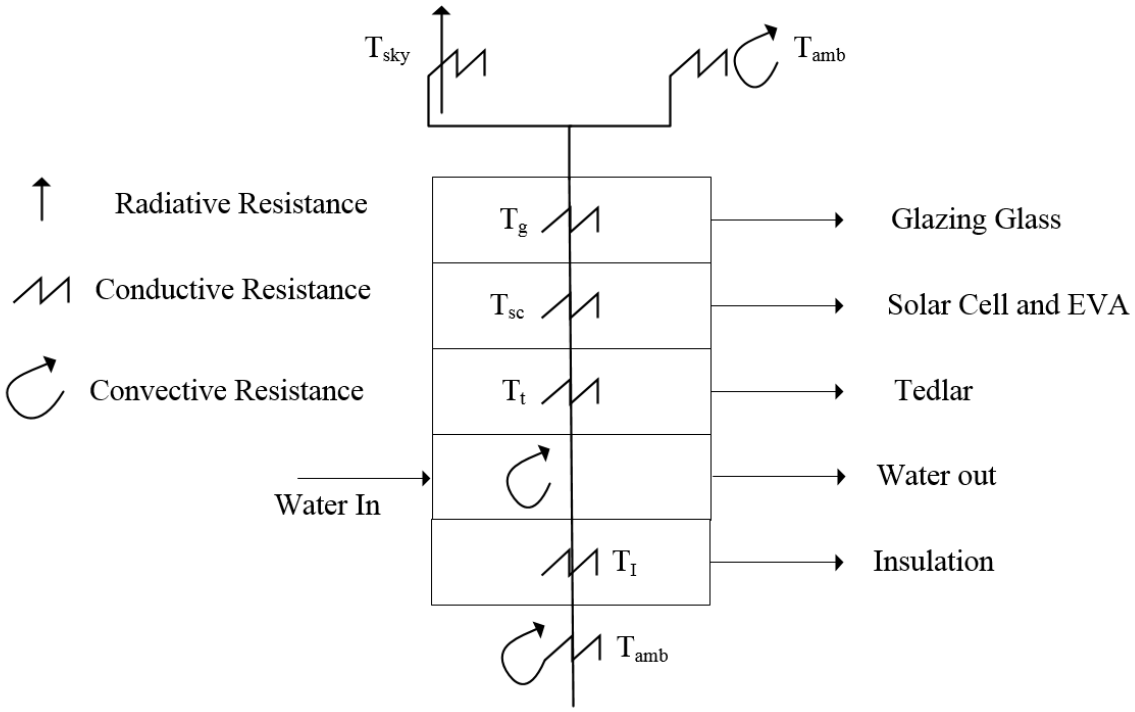


**Fig. 3.33.** Thermal resistance circuit diagram for IPVTS system

(a) Energy balance for the PV Panel (glass to tedlar)

The energy balance of PV panel would be same as equation (3.1). The SCs temperature was calculated using equation (3.2).

(b) For the rear surface of tedlar energy balance is given by equation 3.30 [142]

$$U_{ct}(T_c - T_{bt})Bdx = U_{tw}(T_{bt} - T_w)Bdx \qquad (3.30)$$

From equation (3.30), the expression for average absorber temperature is

$$\overline{T_{bt}} = \frac{PF_1(\alpha\tau)_{eff}\,G(I) + U_{gt}T_{amb} + U_{tw}\overline{T_w}}{U_{gt} + U_{tw}} \qquad (3.31)$$

where $PF_1$ is the penalty factor due to presence of SCs material, glass and EVA and $U_{gt}$ is overall heat transfer coefficient from glass to tedlar [111].

(c) The energy equilibrium of flowing in the broad water channel below the PV module is given by [143]; [149]:

$$U_{tw}\left(T_{bt} - T_{w,avg}\right)Bdx = m_w C_w \frac{dT_{w,avg}}{dx}dx + U_{bc}\left(T_{w,avg} - T_{amb}\right)Bdx \qquad (3.32)$$

Now rearranging and integrating the both sides of the equation (3.32) with boundary conditions, $T_{fx=0} = T_{fi}$ $and$ $T_{fx=L} = T_{f0}$ , we got the expression for the outlet water temperature as [98]:

$$T_{wo} = \left[\frac{PF_1\,PF_2(\alpha\tau)_{eff}\;G(I)}{U_T} + T_{amb}\right]\left[1 - \exp\left(-\frac{A_{IPVTS}U_T}{m_w C_w}\right)\right] + T_{wi}\exp\left[-\frac{A_{IPVTS}U_T}{m_w C_w}\right] \qquad (3.33)$$

where $PF_{2a}$ is a penalty factor due to the interface between cooling water below PV module and tedlar.

$$PF_2 = \frac{U_{tw}}{U_{tw} + U_{gt}} \qquad (3.34)$$

And the average fluid temperature is calculated by integrating equation (3.33) as [143,98]:

$$\overline{T_w} = \frac{1}{L_t}\int_0^{L_t} T_{wo}\,dx \qquad (3.35)$$

$$\overline{T_w} = \left[\frac{PF_1\ PF_2(\alpha\tau)_{eff}\ G(I)}{U_T} + T_{amb}\right]\left[1 - \left(\frac{1 - \exp\left(-\frac{A_{IPVTS}\ U_T}{m_w C_w}\right)}{\frac{A_{IPVTS}\ U_T}{m_w C_w}}\right)\right] + T_{wi}\left[\frac{1 - \exp\left(-\frac{A_{IPVTS}\ U_T}{m_w C_w}\right)}{\frac{A_{IPVTS}\ U_T}{m_w C_w}}\right] \quad (3.36)$$

$$\text{where } (\alpha\tau)_{eff} = \tau_g[\alpha_c\beta_c + (1-\beta_c)\alpha_{ted} - \eta_{c,el}\beta_c] \quad (3.37)$$

By putting the expression of $\overline{T_w}$ from equation (3.36) in equation (3.31), we got an average absorber temperature $\overline{T_{bt}}$. After obtaining $\overline{T_{bt}}$, the expression for an average SCs temperature $\overline{T_c}$ can be evaluated from equation (3.2). Further, according to [144] and [145] the SCs efficiency ($\eta_c$) can be calculated from equation (3.13). The electrical efficiency, thermal efficiency and instantaneous electrical efficiency of IPVTS system were calculated from equation (3.14), (3.15) and (3.16) respectively.

#### *3.5.2.2 EWHE system*

The same set of equations, as discussed in Section 3.5.1.2, were used for EWHE system

The design parameters used in the above equations are presented in Table 3.7.

**Table 3.7**. Design parameters of IPVTS water collector with EWHE

| Parameter | Value |
|---|---|
| Diameter of GI pipe of IPVTS | 0.012 m |
| Thermal conductivity of insulation | 0.042 W/m K |
| Thickness of solar cell | 0.0003 m |
| Thermal conductivity of solar cell | 0.036 W/m K |
| Thickness of tedlar | 0.0005 m |
| Thermal conductivity of tedlar | 0.033 W/m K |
| Absorptivity of solar cell | 0.90 |
| Transmissivity of solar cell | 0.90 |
| Transmissivity of glass | 0.95 |
| Absorptivity of tedlar | 0.75 |
| Thickness of glass cover | 0.0032 m |
| Thermal conductivity of glass cover | 1 W/m K |
| EWHE pipe material | HDPE |
| EWHE pipe total length | 80 m |
| EWHE pipe diameter | 0.21 |

## 3.6 Rooftop PV/T air collector coupled with EAHE system for combined power and space heating

In this work an analytical model of a PV/T air collector coupled with EAHE has been developed and validated with existing experimental data from the literature. The system is further analyzed and compared for different arid and semi-arid regions which includes Ajmer (India), Pilani (India) and Las Vegas (USA). The performance of the proposed coupled system was evaluated based on electrical efficiency of the PV/T system and outlet air temperature of PV/T and EAHE system. Further, to estimate the effect of major parameters like mass flow rate, collector channel depth, collector length, EAHE pipe length and solar radiations, a parametric assessment has been carried out using the first law of thermodynamics. An attempt has been made to explore the effectiveness of PV/T coupled with an EAHE system for its future developments.

### 3.6.1 Description of the PV/T air collector coupled with EAHE system

The schematic diagram of a glazed PV/T air system is shown in Fig. 3.34. It shows that a part of incident solar insolation is transformed into electrical power through SCs and the rest is thermal energy in the loss from the front and rear surfaces of the module. A channel was made on the back side of the PV/T system which allows the air to flow through. Both sides and the back of the PV/T system were well insulated to avoid any losses to the environment. Fig. 3.34 shows also the combined PV/T coupled with EAHE system. It can be seen from the Fig. 3.34 that the ambient air is first passed through an EAHE system so that thermal energy is transferred from the earth to the air which was then circulated to the back side of the PV/T system. This leads to cooling of PV cells by increasing the air temperature, and this hot air could be used for space heating. This is important to mention here that the purpose of the EAHE is not only to decrease the SCs temperature but also to provide for a space heating requirement. The ambient air, especially during winter, could directly be sent to cool down the PV temperature but is not suitable for space heating as the air has not heated up to the room comfort level. Due to above said reasons; an investigation is carried out for such a coupled system to identify the effectiveness and feasibility for different applications.

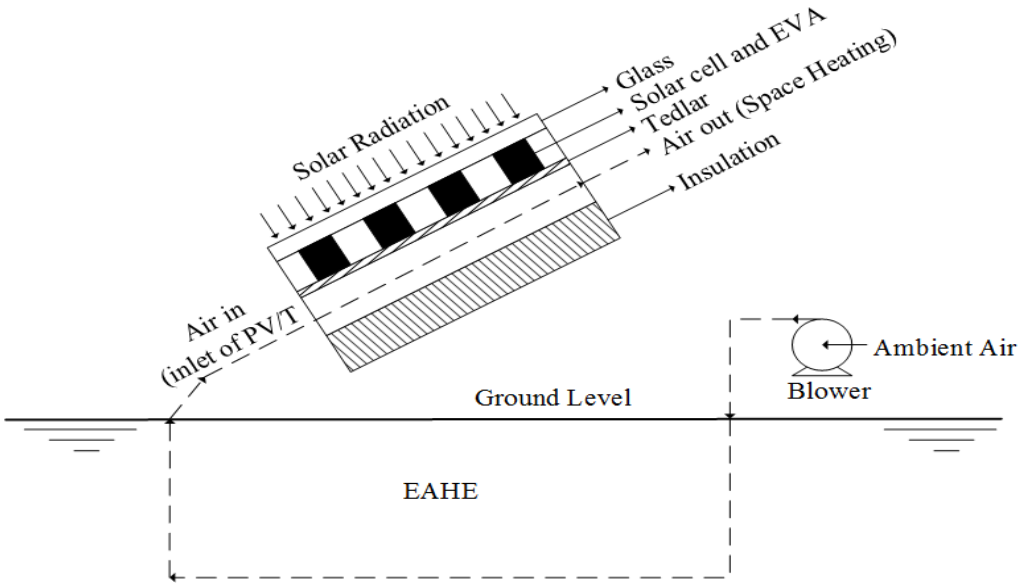


**Fig. 3.34.** Schematic diagram of the proposed PV/T coupled with the EAHE system

### 3.6.2 Thermal modelling of PV/T air collector coupled with EAHE system

For the performance analysis of the EAHE coupled with the PV/T air collector system, the energy balance was performed using the first law of thermodynamics. The current section provided the energy analysis to assess the performance of the coupled system.

#### *3.6.2.1 PV/T air system*

The assumptions for energy balance of the PV/T air system are as follows:

- One dimensional heat transfer is assumed in the present study.
- Ohmic losses are taken as negligible in the PV system.
- The PV/T system is taken at quasi-steady-state.
- The heat capacity of the PV/T is neglected.
- The temperature gradient across the PV system is also neglected.

To estimate the PV/T thermal and electrical efficiencies, an analytical expression for the energy balance has been derived. The thermal resistance diagram of the PV/T air system is shown in Fig. 3.35. It is shown there that all the three modes of the heat transfer are used in the energy

balance. The thermal efficiency of the PV/T system is calculated by estimating the resistance of air flow to the back side of the panel.

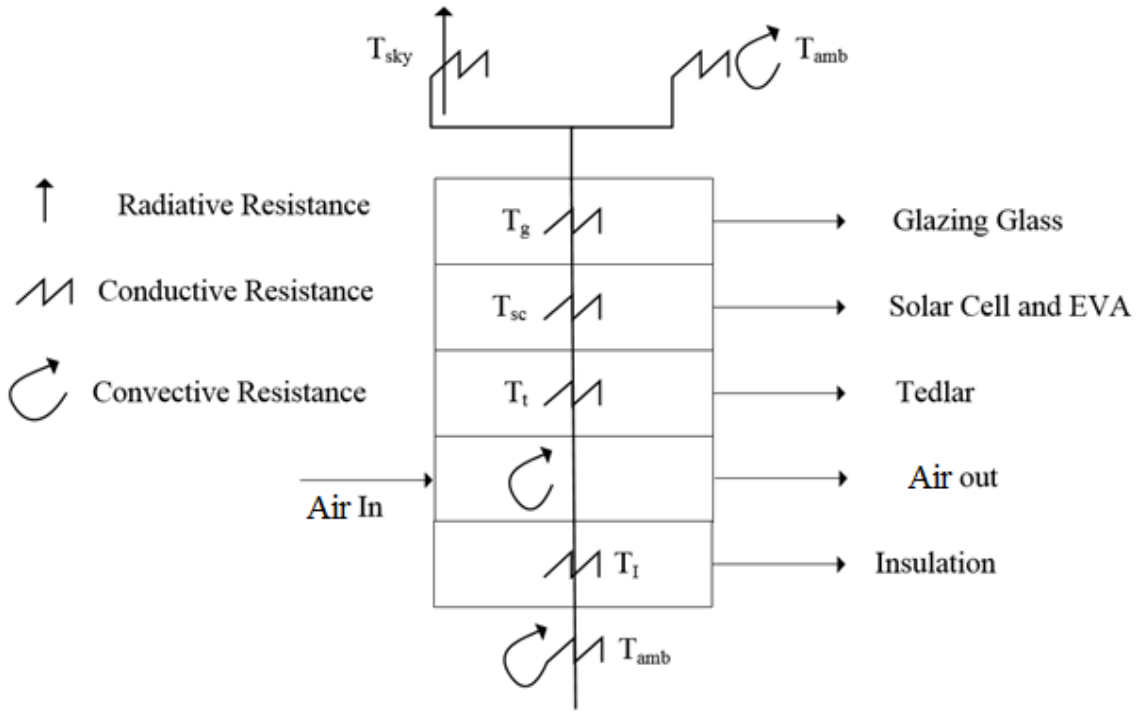


**Fig. 3.35.** Thermal resistance circuit diagram for PV/T air system

(a) Energy balance for the PV module is given by equation 3.38 (glass to tedlar)[98]:

$$\tau_g \alpha_c \beta_c G(I) B dx + \tau_g (1-\beta_c) \alpha_{ted} G(I) B dx = \left[U_{c,amb}\,(T_c - T_{amb}) + U_{ct}(T_c - T_{bt})\right] B dx + \eta_{c,el} \beta_c \tau_g G(I) B dx \quad (3.38)$$

where $T_c$, $G(I)$, $T_{bt}$, $T_{amb}$, $\eta_{c,el}$, $W$, and $\beta_c$, are PV cell temperature, global solar radiation, rear surface temperature of tedlar, ambient temperature, electrical efficiency of PV cell, the width of broad air channel and packing factor of SCs, respectively.

The formulation for the PV cell temperature calculated from equation (3.38) is:

$$\overline{T_c} = \frac{\tau_g [\alpha_c \beta_c + (1-\beta_c)\alpha_{ted} - \eta_{c,el}\beta_c] G(I) + U_{c,amb}\, T_{amb} + U_{ct}\, \overline{T_{bt}}}{U_{c,amb} + U_{ct}} \quad (3.39)$$

(b) For the back surface of the tedlar the energy balance yields equation 3.40 [142]

$$U_{ct}(T_c - T_{bt})Bdx = U_{tair}(T_{bt} - T_{air})Bdx \tag{3.40}$$

From equation (3.40), the expression for the average tedlar temperature is

$$\overline{T_{bt}} = \frac{hp_1(\alpha\tau)_{eff}\, G(I) + U_{gt}T_{amb} + U_{tair}\,\overline{T_{air}}}{U_{gt} + U_{tair}} \tag{3.41}$$

where $hp_1$ is a penalty factor which is due to PV cell material, glass and EVA and $U_{gt}$ is heat transfer coefficient between the glass and tedlar [111].

$$U_{gt} = \frac{U_{c,amb} \times U_{ct}}{U_{c,amb} + U_{ct}} \tag{3.42}$$

$$hp_1 = \frac{U_{ct}}{U_{c,amb} + U_{ct}} \tag{3.43}$$

(c) The energy balance for air flow on the back side of the PV/T air collector is calculated using this equation [143]:

$$U_{tair}\left(T_{bt} - T_{air\,,avg}\right)Bdx = m_{air}\,C_{air}\,\frac{dT_{air\,,avg}}{dx}dx + U_b\left(T_{air\,,avg} - T_{amb}\right)Bdx \tag{3.44}$$

Now rearranging and integrating both sides of the equation (3.44) with the boundary conditions, $T_{fx=0} = T_{fi}$ $and$ $T_{fx=L} = T_{f0}$ , the expression for the PV/T outlet air temperature as

$$T_{airo} = \left[\frac{hp_1\, hp_2(\alpha\tau)_{eff}\; G(I)}{U_T} + T_{amb}\right]\left[1 - \exp\left(-\frac{A_{PV/T}U_T}{m_{air}\,C_{air}}\right)\right] + T_{airi}\,\exp\left[-\frac{A_{PV/T}U_T}{m_{air}\,C_{air}}\right] \tag{3.45}$$

Where $hp_2$ is another penalty factor which is due to the interface of tedlar and air flow in between.

$$hp_2 = \frac{U_{tair}}{U_{tair} + U_{gt}} \tag{3.46}$$

The average cooling air temperature is calculated by integrating equation (3.45) as [143]

$$\overline{T_{air}} = \frac{1}{L_t}\int_0^{L_t} T_{airo}\, dx \qquad (3.47)$$

$$\overline{T_{air}} = \left[\frac{hp_1\, hp_2(\alpha\tau)_{eff}\; G(I)}{U_T} + T_{amb}\right]\left[1 - \left(\frac{1 - \exp\left(-\frac{A_{PV/T}U_T}{m_{air}\, C_{air}}\right)}{\frac{A_{PV/T}U_T}{m_{air}\, C_{air}}}\right)\right] + T_{airi}\left[\frac{1 - \exp\left(-\frac{A_{PV/T}U_T}{m_{air}\, C_{air}}\right)}{\frac{A_{PV/T}U_T}{m_{air}\, C_{air}}}\right] \qquad (3.48)$$

$$\text{where}(\alpha\tau)_{eff} = \tau_g[\alpha_c\beta_c + (1-\beta_c)\alpha_{ted} - \eta_{c,el}\beta_c] \qquad (3.49)$$

By putting the term of $\overline{T_{air}}$ from equation (3.49) in equation (3.41), we get an average tedlar temperature $\overline{T_{bt}}$. After obtaining $\overline{T_{bt}}$, the expression for an average PV cell temperature $\overline{T_c}$ can be given from the equation (3.39).

Further, according to Evans [144] and Schott [145] the PV cell efficiency ($\eta_c$) can be calculated as:

$$\eta_c = \eta_{STC}[1 - \beta_0(T_c - T_{STC})] \qquad (3.50)$$

The instantaneous thermal efficiency of the PV/T air system is calculated as:

$$\eta_{th} = \frac{m_{air}\, c_{air}\; (T_{airo} - T_{airi})}{A_{PV/T}\; G(I)} \qquad (3.51)$$

### *3.6.2.2 EAHE system*

The EAHE system is modelled using three heat transfer processes. The first is the conductive heat transfer process between the soil and outer surface of buried pipe. The second mode is also a conductive mode in between buried pipe from inner to outer surface. The third one is the convective heat transfer between the inner surface of buried pipe and the air flowing in the pipe. The assumptions taken for calculating the equations for EAHE system are as follows:

- The soil temperature is taken as an annual average ambient air temperature.
- The uniform circular cross section area is taken for buried pipe.

- The thermal effect of surrounding soil is insignificant after a distance equal to the buried pipe radius from its outer surface.
- The buried pipe soil is isotropic with homogenous thermal conductivity throughout.
- One dimensional heat transfer is assumed in the present study.
- The EAHE system is taken at quasi-steady-state.

The thermal resistance of the soil annulus is given as [147]:

$$R_{soil} = \frac{\ln\left(\frac{r_s}{r_o}\right)}{2\pi \, \mathrm{l_p} k_s} \qquad (3.52)$$

The thermal resistance of the buried pipe thickness is considered as:

$$R_{pipe} = \frac{\ln\left(\frac{r_o}{r_i}\right)}{2\pi \, \mathrm{l_p} k_p} \qquad (3.53)$$

The Reynolds number (Re) and the Nusselt number (Nu) are given by equations (3.54) and (55), respectively, which are used to calculate the convection heat transfer coefficient

$$Re = \frac{\rho v_{air} \, 2r_i}{\mu} \qquad (3.54)$$

The Nusselt number for laminar flow is given as:

$$Nu = 4.36, for \; Re < 2300$$

The Nusselt number for turbulent flow in a buried pipe for the ranges $0.5 < Pr < 2000 \; and \; 2300 < Re < 5 \times 10^6$ is given as[147]:

$$Nu = \frac{(f/8)(Re - 1000)Pr}{1 + 12.7\,(f/8)^{0.5}(Pr^{0.66} - 1)} \qquad (3.55)$$

Where $f$ is friction factor for smooth pipes and is uses Petukhov's relation [148]

$$f = (0.79 \ln Re - 1.64)^{-2} \qquad (3.56)$$

The thermal resistance due to convective heat transfer between flowing air and inner surface of buried pipe is calculated as:

$$R_{Convec} = \frac{1}{2\pi r_i l_p h} \qquad (3.57)$$

Where $h$ is the convection heat transfer coefficient and given as [148]:

$$h = \frac{Nu\ k_{air}}{2r_i} \qquad (3.58)$$

The overall thermal resistance between the flowing air and soil of the EAHE system is given as

$$R_{total} = R_{soil} + R_{pipe} + R_{Convec} \qquad (3.59)$$

Then overall heat transfer coefficient is calculated as

$$U = \frac{1}{R_{total}} \qquad (3.60)$$

For a pipe of constant temperature ($T_{pipesurface} = T_s$) the effectiveness of EAHE can be calculated as [130]

$$\varepsilon = 1 - e^{\left(-\frac{U}{m_{air}\, c_{air}}\right)} \qquad (3.61)$$

Then the temperature effectiveness of the EAHE system is calculated as

$$\varepsilon = \frac{T_{airi\,1} - T_{airo\,1}}{T_{airi\,1} - T_s} \qquad (3.62)$$

The EAHE outlet temperature is calculated from equation (3.63) as [130]

$$T_{airo\,1} = T_{airi\,1} - (T_{airi\,1} - T_s) \times \varepsilon \qquad (3.63)$$

The heating potential of the EAHE is given by

$$Q = m_{air}\, c_{air}\, (T_{airi\,1} - T_{airo\,1}) \qquad (3.64)$$

The design parameters used in the above equations are presented in Table 3.8.

**Table 3.8**. Design parameters of PV/T air collector with EAHE

| Parameter | Value |
|---|---|
| PV Module | Mono-crystalline silicon PV module, glass to tedlar type |
| Area of PV/T air collector | 1.272 $m^2$ |
| Maximum efficiency of PV module at STC | 11% |
| Thermal conductivity of insulation | 0.042 W/m K |
| Thickness of solar cell | 0.0003 m |
| Thermal conductivity of solar cell | 0.036 W/m K |
| Thickness of tedlar | 0.0005 m |
| Thermal conductivity of tedlar | 0.033 W/m K |
| Absorptivity of solar cell | 0.90 |
| Transmissivity of solar cell | 0.90 |
| Transmissivity of glass | 0.95 |
| Absorptivity of tedlar | 0.75 |
| Thickness of glass cover | 0.0032 m |
| Thermal conductivity of glass cover | 1 W/m K |
| EAHE pipe material | Polyvinyl chloride (PVC) |
| EAHE pipe total length | 10 m, 20 m, 30 m, 40 m, 50 m, 60 m |
| EAHE pipe diameter | 100 mm |
| Thermal conductivity of Pilani soil | 0.80 W/m K |
| Thermal conductivity of Ajmer soil | 0.52W/m K |
| Thermal conductivity of Las Vegas soil | 2.35 W/m K |
| Density of Pilani soil | 1700 $kg/m^3$ |
| Density of Ajmer soil | 2050 $kg/m^3$ |
| Density of Las Vegas soil | 1300 $kg/m^3$ |
| EAHE pipe thermal conductivity | 0.16W/m K |
| EAHE pipe buried depth | 3.5 m |

### 3.6.3 Model validation

From the literature survey, it is observed that no study has been performed which uses the PV/T air system with EAHE for space heating. The performance of the PV/T system depends upon ambient conditions like solar insolation and ambient temperature, etc. The analysis on PV/T air collector has been performed by various researchers on different ambient conditions. A study by Tiwari et al.[150] experimentally tested the PV/T air system for the composite weather of India (New Delhi) during the month of January. In their experimental study, the used design parameters included area of collector, width of collector, penalty factor and packing factor of PV module as 0.54 $m^2$, 0.45m, 0.89 and 0.83 respectively. Fig 3.36 shows the values of climatic conditions like solar insolation and ambient temperature during their experimentation. It was shown that the solar insolation and ambient temperature ranged between 134 $W/m^2$ to 546 $W/m^2$ and 13 °C to 20 °C respectively during the experimental day. The maintained flowing air

velocity over the PV/T air collector was 3 m/s, 3.17 m/s 3.3 m/s 3.33 m/s, 3.2 m/s, 2.97 m/s and 2.9 m/s for at time of 10 AM, 11 AM, 12 AM, 13 PM, 14 PM, 15 PM, 16 PM, respectively.

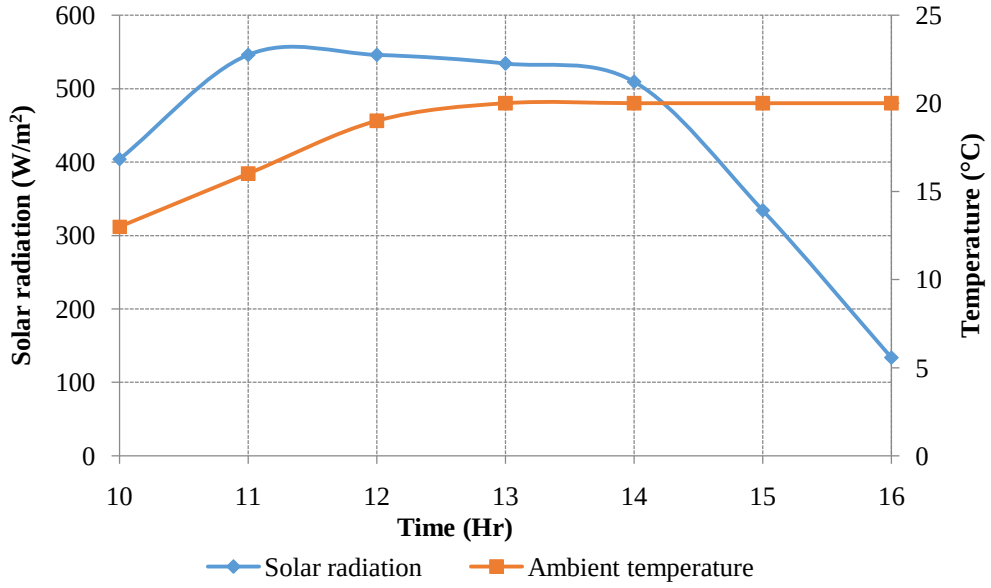


**Fig. 3.36.** Ambient conditions during experimental study of Tiwari et al. [150]

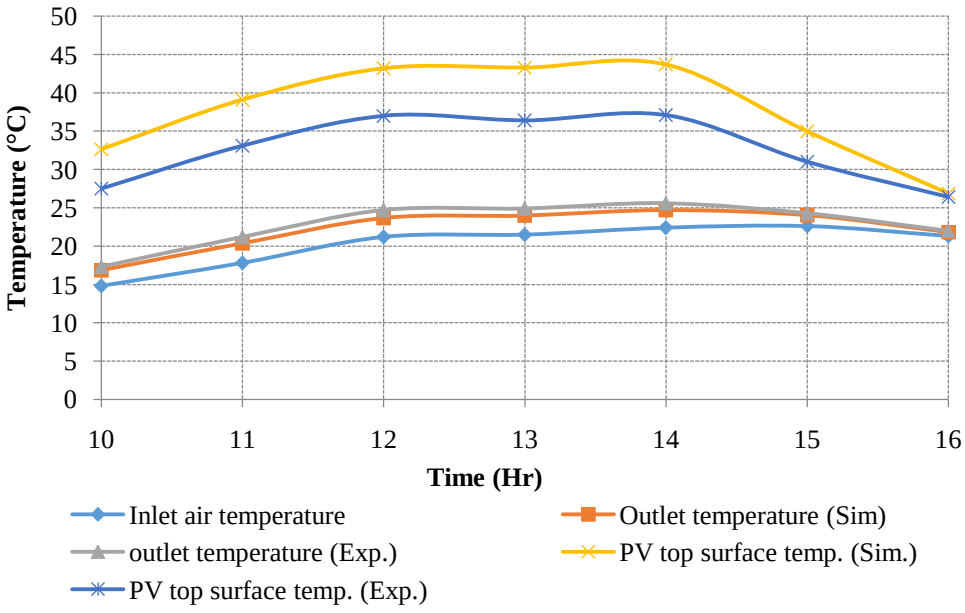


**Fig. 3.37.** Validation of simulated and experimental results of PV/T air system

The current study simulated the PV/T system using the experimental design parameters as discussed by Tiwari et al.[150]. The change in PV cell temperature and PV/T outlet temperature

from both the experimental and simulation study are shown in Fig. 3.37. It is seen that the simulated and experimental cell temperature ranges between 26.89 °C to 43.7 °C and 26.4 °C to 37.1 °C respectively. It also shows a good comparison between the simulated and experimental results. The mean square percent deviation was observed to be 11.5% and 2.9% for the PV cell temperature and the PV/T outlet temperature, respectively. Thus, by obtaining good agreement with the PV/T results, it was expected that the current coupled model of the PV/T air collector with the EAHE would also follow the same pattern and give more precise results.

# CHAPTER 4

# EXPERIMENTAL STUDIES

## 4.0 Experimental test set-up of PV/T systems coupled with EWHE cooling

This chapter deals with the development of experimental set-up of tube-and-sheet PV/T system and broad channel IPVTS system coupled with EWHE cooling, instrumentation used and experimental procedure adopted. The entire experimental set-up has been fabricated in Central Workshop, BITS Pilani, Pilani campus. Further, the EWHE cooling system has been developed by burying HDPE pipes at a depth of 3 m, in the backyard of SR Bhavan (Boy's hostel) BITS Pilani, Pilani campus (28.38°N, 75.61°E). Both the PV/T systems were coupled at this site with EWHE cooling to carry out the performance study. Pilani is situated at the border (near Haryana) of Rajasthan state. As far as the climatic conditions are concerned, Pilani has a semi-arid climate with high temperatures for most part of the year. The climate of Pilani is representative of a composite climate with three distinct seasons i.e. winter (November to March), summers (April to June) and monsoon (July to October).

## 4.1 Purpose and description of the experimental study

The main purpose of developing the experimental set-up was to perform test runs for PV/T cooling with EWHE system at different operating parameters. The experimentation was carried out for tube-and-sheet PV/T system as well as broad channel IPVTS system coupled with EWHE cooling. Results of this experimental analysis are used to validate the analytical MATLAB simulation model of two types PV/T systems integrated with EWHE cooling. The experimental measurements have been carried out during different clear days during peak radiations in September 2016 and experimental data were recorded at different interval of time. The measured data include global solar radiation, inlet and outlet temperature of PV/T and EWHE, temperature at various points at EWHE, PV panel front surface temperature, ambient temperature, wind speed, open-circuit voltage, short- circuit current, load voltage and load current.

## 4.2 Description and fabrication of PV/T water collectors

This section presented the description and fabrication of the tube-and-sheet PV/T system and broad water channel (IPVTS) system.

### 4.2.1 Tube-and-sheet PV/T system

Tube-and-sheet PV/T system has been fabricated in the Institute Central Workshop of the BITS Pilani, Pilani campus. For the fabrication, the dimensions of the tube-and-sheet were selected from literature followed by selection of the material for absorber and tubes. Behind the tube-and-sheet PV/T system, an absorber plate was fixed with epoxy upon which U-shaped pipes were welded. These pipes are made of copper and carries HTF. The cross sectional front view of the tube-and-sheet PV/T system is shown in Fig. 4.1. In the present study, the panel used is mono-crystalline silicon PV panel (Model: TATA BP Solar, 70 W, glass to tedlar type) having dimension 1.20 m × 0.53 m (L×W). The absorber consists the copper plate having the dimension of 1.16 m × 0.51 m and copper tube having the OD as 12 mm. These copper tubes were bend in U-shape as shown in Fig. 4.2 (a). The U-shape pipe bends were joined with straight long pipe using tungsten inert gas welding for making condenser type flow pipes as shown in Fig 4.2 (b). These condenser type flow pipes were welded on absorber plate at the appropriate location as shown in Fig. 4.2 (c). The pipe width spacing (center to center) between U shaped pipes was taken from the literature as 90 mm.

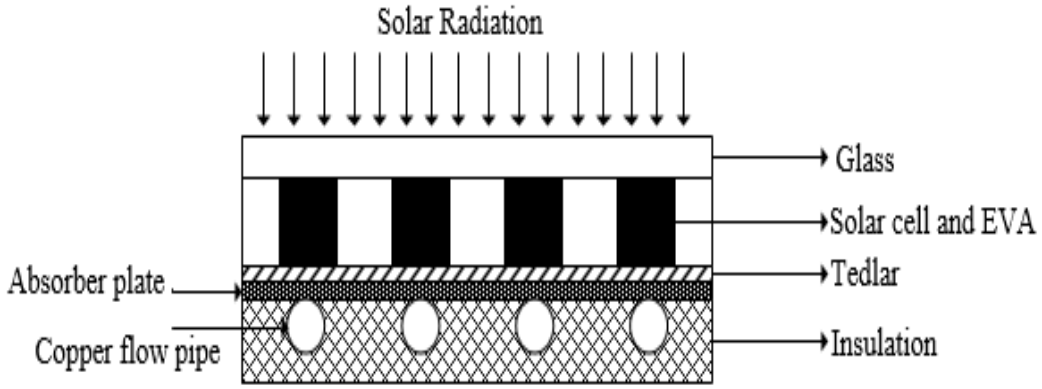


**Fig. 4.1**. Cut sectional front view of tube-and-sheet PV/T collector system

The tube-and-sheet collectors were integrated on the back side of PV module using omega bond epoxy adhesive (OB-101, thermal conductivity 1.04 W/m K) as shown in Fig. 4.3. It is important to mention here that for this study, the PV/T collectors were fabricated using two PV panels as otherwise the dimension of the single PV/T would be quite small for the performance evaluation.

(a) (b) (c)

**Fig. 4.2.** Fabrication of tube-and-sheet collector

**Fig. 4.3** Final tube-and-sheet PV/T water collector

Both PV/T collectors were insulated from the back sides with the thermocol layer of 0.04 m thickness to reduce heat losses, as per the cross sectional view (Fig. 4.1). These two PV/T systems were connected in series and termed as PV/T1 and PV/T2. The first one, PV/T1 was connected to PV/T2 by a copper pipe of diameter 0.012 m. The outlet of PV/T2 was connected to inlet of EWHE system which is described in next section. In PV/T, the tube-and-sheet collector

circulates the water beneath the PV panels which reduces the temperature of PV panels and hence, increases performance. The outlet hot water gets cool down in the EWHE system which can be supplied directly to inlet of PV/T1 for its cooling and completing the cycle as shown in Fig. 4.4. Three RTDs were mounted at the inlet and outlet of PV/T1 and outlet of PV/T2 to measure the water temperature at respective locations. The both PV/T collectors were installed on a mild steel frame at an inclination angle of 50º as shown in Fig. 4.5.

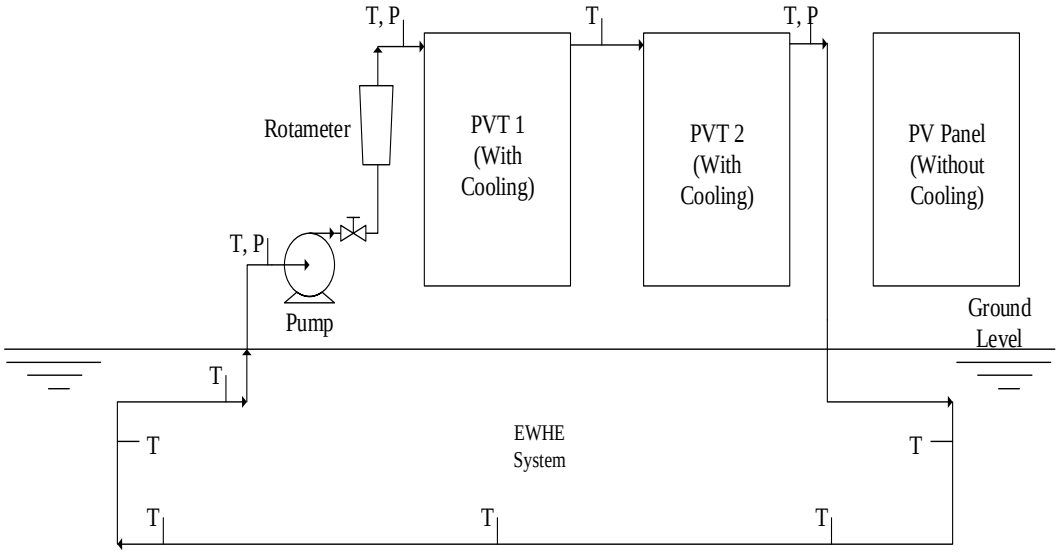


**Fig. 4.4.** Schematic diagram of tube-and-sheet PV/T coupled with EWHE experimental setup

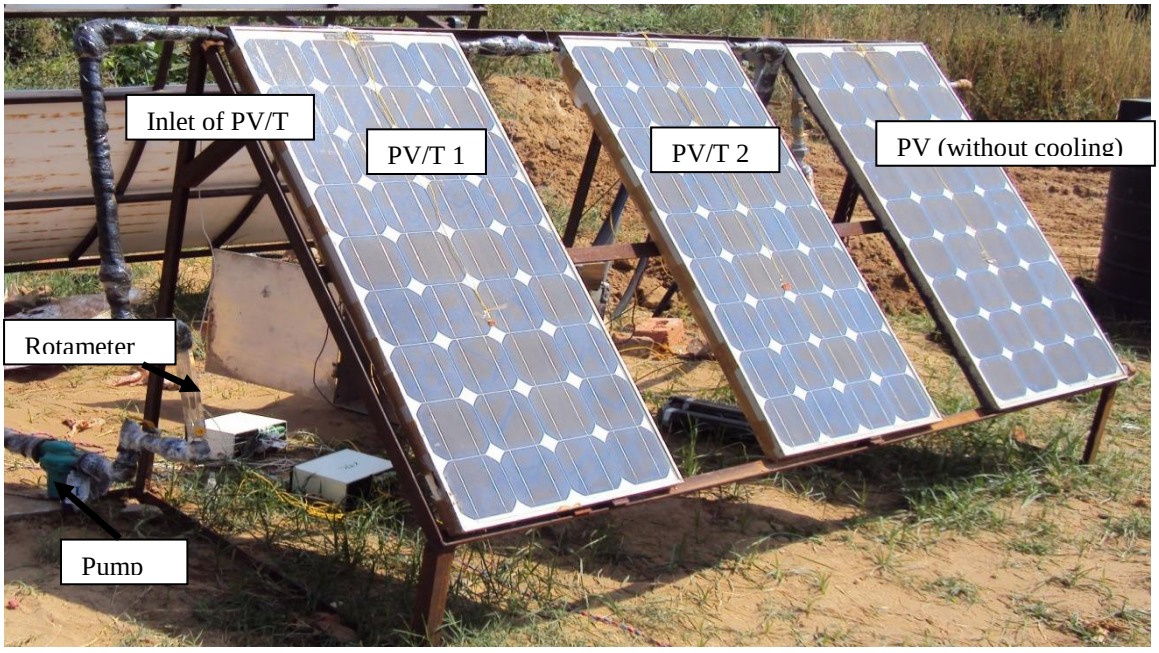


**Fig. 4.5.** On site experimental setup of tube-and-sheet PV/T system coupled with EWHE cooling

### 4.2.2 Broad water channel PV/T system (IPVTS)

In the IPVTS system, a broad channel is mounted on the back side of PV panel through which water flows down having direct contact with its rear surface. In the IPVTS also, two mono-crystalline silicon PV module (Model: TATA BP Solar, 70 W, glass to tedlar type) were taken and a broad channel was mounted on the back side of these two. For the development of broad channel, a galvanized iron (GI) pipe having OD 12 mm was selected and uniform hole were drilled in it, as shown in Fig. 4.6 (a). This GI pipe was then arranged on the back side of PV panel as shown in Fig. 4.6 (b). The entire assembly was then sealed with anti-leakage sealant (M-seal epoxy compound) to avoid any leakage. For the broad channel, an enclosure was made using GI sheets and was mounted on the back side of PV panel and was sealed with aluminium frame with silicon sealant to avoid water leakage. The boundaries of the enclosure were sealed to maintain pressure difference in-between and a separate pipe was provided at the bottom for the outlet of fluid. Similar to tube-and-sheet PV/T system, here also two PV panels were taken to develop two PV/T water collectors which were connected in parallel.

(a) (b)

**Fig. 4.6** (a and b). Fabrication of broad water channel collector (IPVTS)

To decrease the heat losses, back sides of both IPVTS were insulated using a thermocol layer of 0.04 m thickness, as shown in Fig. 4.7. Two IPVTS systems were connected in parallel in which

the GI pipe (OD=0.012 m) was uniformly distributed in half, in each of the system to provide a continuous supply of the heat transfer fluid as shown in Fig. 4.8. At the outlet, the fluid from both of the systems was converged to one single pipe, which was connected to the inlet of EWHE as shown in Fig. 4.9. Further at the outlet of EWHE a pump along with a flow meter was connected, to recirculate the cooling fluid back to both IPVTS systems.

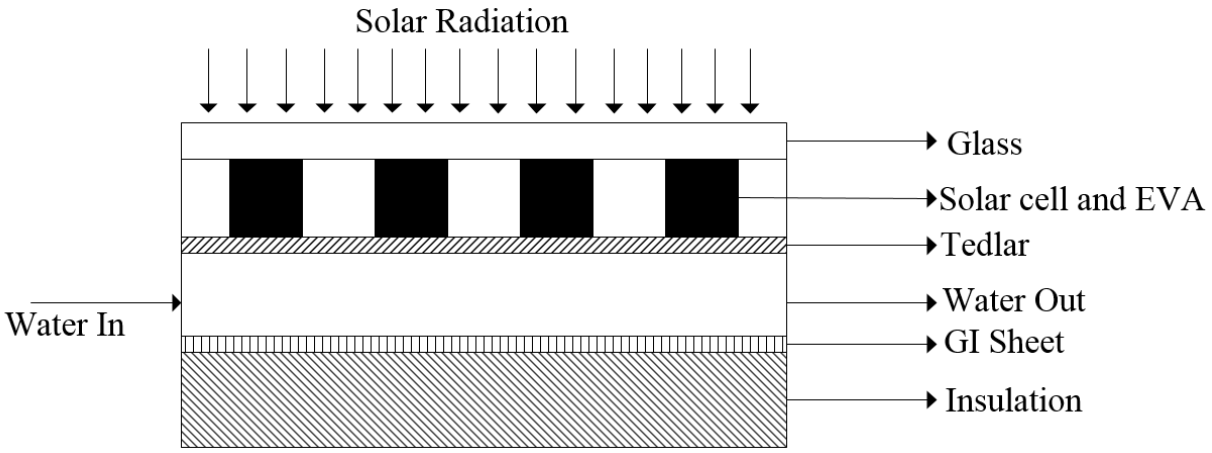


**Fig. 4.7**. Cut sectional front view of broad water channel PV/T system (IPVTS)

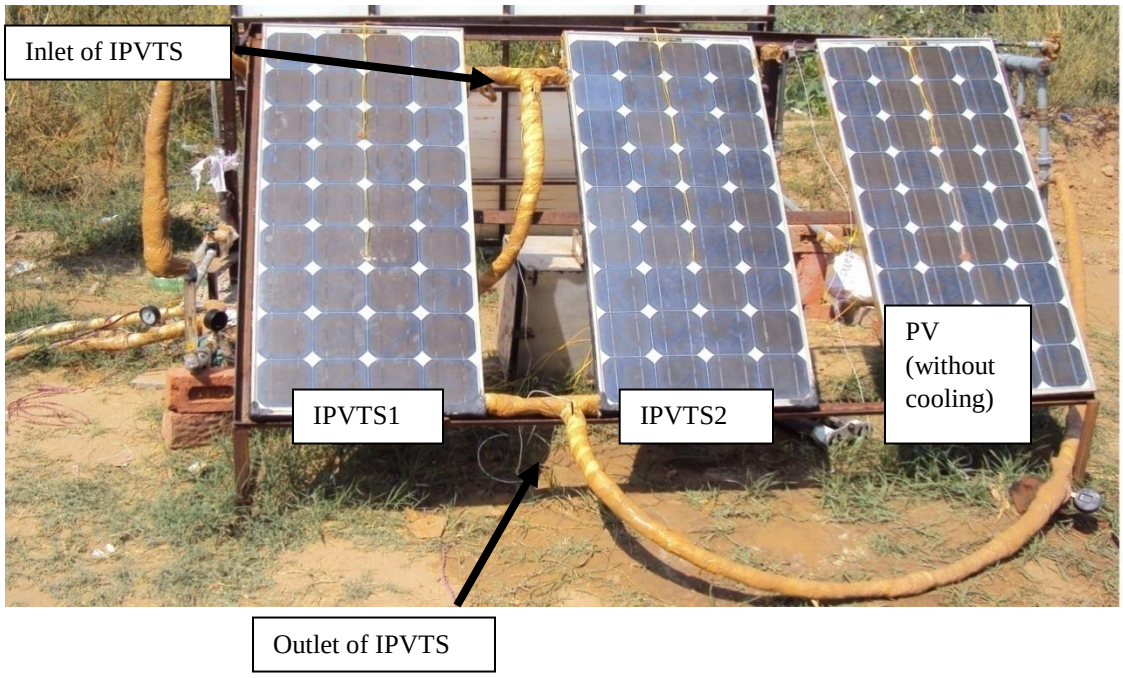


**Fig. 4.8.** On site experimental set-up of broad water channel PV/T system (IPVTS) coupled with EWHE cooling

In IPVTS, water was circulated underneath the PV panels using the broad water channel. This decreases the temperature of PV panels, thus improving their performance. Once the thermal

energy was absorbed by water from the channel, EWHE system was used to transfer that heat to the earth and cool down the water, making it suitable to be circulated for cooling again as shown in Fig. 4.9. Two RTDs were mounted at the inlet and outlet of IPVTS system to measure the water temperature at respective locations. The both IPVTS collectors were installed on a mild steel frame at an inclination angle of 50º as shown in Fig. 4.8. All the connecting pipes between IPVTS and EWHE were insulated with glass wool to prevent any loss of energy.

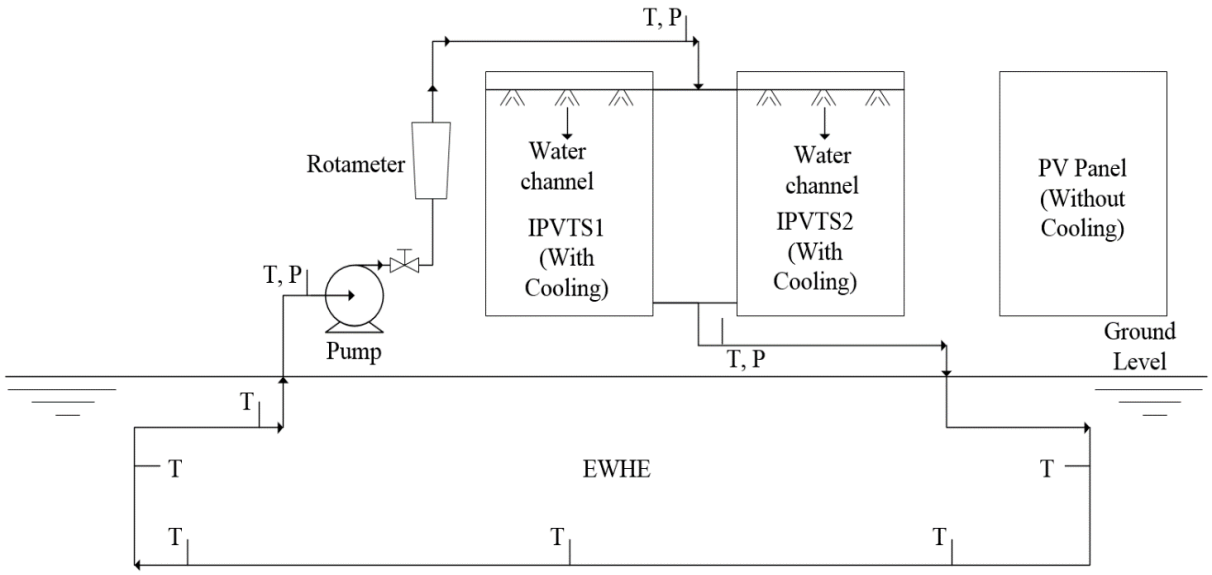


**Fig. 4.9.** Schematic diagram of broad water channel PV/T system (IPVTS) coupled with EWHE experimental set-up

## 4.3 Description of simple EWHE system

### 4.3.1 Site preparation and trenches excavation

EWHE system was set-up at the backyard of SR bhavan of the Institute. In order to finalize the depth of EWHE as 3.0 m, initially at the site a small pit of 3.0 m depth was excavated and temperature sensors (RTD Pt-100) viz. $T_1$-$T_6$ were placed into it at a depth of 0.5 m, 1 m, 1.5 m. 2.0 m, 2.5 m and 3.0 m respectively from the ground surface and refilled as shown in Fig. 4.10. Temperature indicated by the sensors was measured and recorded on an hourly basis for a fortnight, in order to observe the variation in the sub soil temperature. It was observed that the temperature of the soil at the depth of 3.0 m is not at all affected by the diurnal variation of ambient temperature and solar radiation and remained constant at 29.03 °C irrespective of time of the day. On the basis of observed values of undisturbed subsoil temperature, it was decided to

excavate the trench having a depth of 3.0 m for laying the EWHE pipe. It was observed that for all the experimental days, the soil temperature ($T_6$) observed at a depth of 3.0 m was almost identical with the variation from 29.03 °C to 29.06 °C. This temperature was almost 8 °C less than the ambient temperature. Earth where the EWHE was planned to be set up was almost flat at the ground surface. Before carrying out the excavation of trench, layout of EWHE pipe was marked with the help of lime stone powder, which also helped the operator of JCB excavating machine to follow the exact path.

**Fig. 4.10** Installation of RTDs at various depth of soil from the ground surface

**Fig. 4.11** Excavation work in progress and the trench excavated by excavation machine

Fig. 4.11 shows the excavation work in progress and the trench excavated by excavation machine. The size of the trench was 80 m × 1m × 3.0 m. After excavation of the trench, the base of the trench was leveled manually and wherever there was any waviness in the side walls of the trench at base it was leveled to maintain both side walls perfectly straight. This ensures a constant centre to centre distance between parallel pipes.

### 4.3.2 Laying of EWHE pipes and installing the temperature sensors

Laying of EWHE pipes was quite important as to maintain the uniformity in the pipes. Before laying down the pipes, the trench base was covered uniformly with loose and clean sand (10 cm thick), and maintained free from pebbles and small stones, etc. to provide the cushioning effect. Commercial HDPE pipes of 20 mm, 25 mm, 32 mm, 40 mm diameters and a GI pipe of 25 mm diameter were used in making EWHE. But it is important to mention here that for the present study, HDPE pipe of 20 mm diameter was used. Other large pipe diameters were not used due to small diameter (12 mm) of PV/T system. Thus for the present study, HDPE pipe of OD 20 mm is discussed here. The other pipes are left for the future scope of the work. A total horizontal length of 80 m of EWHE pipe was used, without use of any external bend. Fig. 4.12 shows the activity of laying the HDPE pipes in trench.

**Fig. 4.12** Laying activity of EWHE pipes

After the completion of laying of the pipes, RTD sensors were mounted along the length of pipe at different positions from inlet section. Fine holes were drilled on the pipe surface and temperature sensors were inserted into them up to the centre of the pipe. After that small clearance between sensor wire and pipe surface was packed with anti-leakage sealant (M-Seal).

Six RTD (Pt-100) temperature sensors viz. $T_7$ to $T_{12}$ were mounted along the length at horizontal distances of 15 m, 27 m, 38 m, 54 m, 67 m, and 80 m respectively to measure the water temperature across the pipe length. Fig. 4.13 shows the activity and position of RTD sensors placed along the length of pipe. Having mounted all the temperature sensors, all were tested by connecting them to temperature scanner and it was made sure that each and every sensor was working perfectly. Cables of all the RTD temperature sensors were taken out of trench by through of conduit pipes.

**Fig. 4.13.** Activity and position of RTD sensors placed along the length of EWHE pipes

For the current study, as OD of 20 mm was taken, the outlet of EWHE pipe was connected through a vertical pipe to a centrifugal pump. Further the outlet of the pump was connected to a flow meter (Rotameter, make JTM) along with a flow rate regulating valve and to inlet of IPVTS/PVT systems as shown in Fig. 4.9. The outlet of IPVTS/PVT system was connected to inlet of EWHE system to complete a cycle as shown in Fig. 4.9. PUF (Polyurithane foam) and glass wool insulation was provided on connecting pipes between PV/T and EWHE system in order to prevent thermal losses to the surroundings.

### 4.4 Instruments used in experimentation

For PV/T coupled with EWHE system, the accuracy and precision of instruments used (RTD, flow meter, etc.) is quite important for evaluation of its thermal performance. For the same, high quality and accurate calibrated instruments were used for measuring the different parameters viz. ambient temperature, intensity of solar insolation, mass flow rate of water, pressure, current and

voltage, etc. Description along with the specifications of the instruments, which played key role in the process of measurement, is given below.

### 4.4.1 Pyranometer and weather station

For the measurement of solar radiation, a pyranometer (make: Kipp and Zonen) with data logger was used. Pyranometer measures the global solar radiation at any desired inclination angle. Data logging system is also a part of pyranometer which automatically saves all the values at an interval of one minute. Pyranometer is powered directly from data logger and there is no need of external power source. This time interval can further be changed by programming of the same. The dry bulb temperature of ambient air and wind speed were taken from the weather station installed in the institute. Technical specifications of the pyranometer are shown in Table 4.1.

**Table 4.1.** Technical specifications of the pyranometer

| | |
|---|---|
| Make | Kipp & Zonen |
| Model | CMP 11 |
| Serial number | 140443 |
| Sensitivity | 9.39 μv/W/$m^2$ |
| Impedance | 30 Ω |
| Uncertainty of the WRR | ±0.3% |

### 4.4.2 Resistance temperature detectors

RTD's are sensors used to measure temperature by correlating the resistance of the RTD element with temperature. Most RTD elements consist of a length of fine coiled wire wrapped around a ceramic or glass core. The element is usually quite fragile, so it is often placed inside a sheathed probe to protect it. The RTD element is made from a pure material whose resistance at various temperatures has been documented. The material has a predictable change in resistance as the temperature changes; it is this predictable change that is used to determine temperature. Commonly RTD elements used are Nickel (Ni), Copper (Cu) or Platinum (Pt). Among various commercial available variants, Platimum RTD is most stable and reproducible temperature sensor having linear positive temperature coefficient from -200 to 800 °C with resistance variant as 100-ohm or 1000-ohm. In the current study, Pt-100 having least count of 0.1 ˚C was used as RTD. These RTDs were placed at the specified positions to measure the temperature across the

pipe length. To ensure the proper working of the RTDs, during installation, the resistance between the elements was checked with the help of digital multimeter.

### 4.4.3 Centrifugal pump

Centrifugal pump was used to augment the flow of water through PV/T and EWHE. Firstly it takes water from EWHE system and circulated it through PV/T system. Pump was installed at the outlet of the EWHE (i.e. Inlet of PV/T), therefore it is a push through system. Centrifugal pump used in the experimental study is shown in Fig. 4.14. Speed of the pump was regulated through a regulating switch which was on the back side of pump. Pump used for the experiment was quite compact and did not occupy much larger space. The specifications of the pump are shown in Table 4.2.


**Fig. 4.14** Centrifugal pump used in experiment

**Table 4.2.** Technical specifications of centrifugal pump

| | |
|---|---|
| Make: | Wilo-Star-RS 25/6 |
| Input: | 1-230 V, 50 Hz |
| Power: | 43/61/84 W, Single Phase |
| Speed: | 2480/ 2750/ 2840 R.P.M. |
| Maximum volume flow: | 4 $m^3$/h |
| Fluid temperature range | -10 ºC to 110 ºC |

### 4.4.4 Rotameter

The mass flow rate of circulating water was measured with the help of rotameter. It belongs to a class of flow meters called variable area meters. It measures flow rate by varying the cross-sectional area through which fluid flows. Rotameter was fitted in between outlet of pump and inlet of the PV/T system, to measure the flow rate of water. For the control of mass flow rate a ball valve was used in between the outlet of pump and inlet of rotameter.

### 4.4.5 Thermocouple

To measure the front surface temperature (glass) and rear surface temperature (Tedlar) of PV panel, K-type thermocouples were used. These thermocouples are reliable, has higher accuracy and temperature range than other surface thermocouples. In K-type thermocouple, two element junctions, (Chrome and Alumel) are used which are joined together to measure the temperature of the surface. The used K-type thermocouples have an accuracy of ±2.71% and temperature range between -150 ºC to 1350 ºC.

### 4.4.6 Temperature scanner logger

Using RTD's resistance versus temperature characteristics, the logger measures the resistance and hence temperature at the surface. For the experiment, temperature scanner CT716 (make: Countronics) was used which has 3 wire RTD and two wire thermocouple socket. The scanner logger displays the temperature by various RTDs and thermocouple sensors during the experimentation. This scanner logger device is compact and highly accurate. All temperature scanners were properly calibrated by the manufacturer (Countronics) during the make. In this system, temperature data is directly saved in readable format (.csv) which can be easily retrieved using USB pen drive. Fig. 4.15 shows the image of one of the temperature scanner logger used during the experimentation. The technical specifications and other details of used temperature scanner logger are given in Table 4.3.

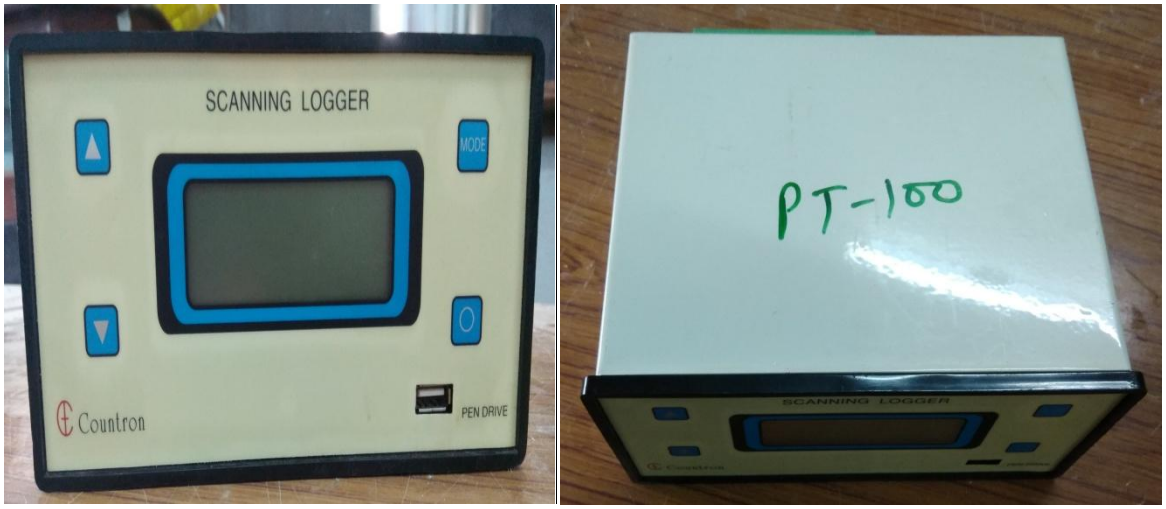


**Fig. 4.15.** Temperature scanner logger

**Table 4.3.** Technical specifications of temperature scanner logger

| | |
|---|---|
| Make and Model | Countronics, CT716 |
| RTD and thermocouple sensor type | PT 100 2W/3W and J/K/R thermocouple |
| Range for RTD | -100 to 600 ºC |
| Range for thermocouple | 0 to 1250 ºC |
| Accuracy for RTD | ±0.1 ºC ±1 ºC least significant digit for RTD |
| Accuracy for thermocouple | ±1 ºC ±1 ºC least significant digit for RTD |
| Power Supply | 230V AC ± 15%, 50/60 Hz |
| Installation | The RTD sensor should be connected using proper cables to minimize errors due to cable resistance. |
| Front facia | 96 mm × 192 mm |

### 4.4.7 Forward looking infrared camera

To achieve higher accuracy in the experiment, the temperature of front surface of PV panel (glazing glass) was measured with the help of FLIR T250 camera. This infrared camera is non contact device which detects the surface infrared radiation and convert it into electronic signal. These signals are then converted into the readable picture format (.jpeg) Fig. 4.16 shows the

FLIR camera used during the experiment. Technical specifications and other details are given in Table 4.4.


**Fig. 4.16.** FLIR camera used in experiment

**Table 4.4.** Technical specifications of FLIR camera

| | |
|---|---|
| Make and Model | FLIR, T250 |
| Resoultion | High quality, 200×150 IR |
| Thermal sensitivity | 80 m K |
| Touch screen LCD | 3.5 inch |
| Accuracy | ±2 ºC or ±2% ºC |
| Thermal sensitivity | 0.05 ºC at 30 ºC |

### 4.4.8 Voltmeter, Ammeter, Rheostat and Multimeter

Voltmeter, Ammeter and Rheostat are electronic instrument used to measure voltage, current and resistance respectively within the circuit. A multimeter is a device which measures all these three parameters. In the present experimental study, the short circuit current and open circuit voltage were measured with the help of digital multimeter. The load voltage and load current were measured with the help of analog voltmeter and analog ammeter respectively. The resistance during load current and load voltage was varied using rheostat. It is a device having variable

resistor which is used to control current. Fig. 4.17 shows the used electronic instruments and Table 4.5 gives their technical specifications.


**Fig. 4.17.** Multimeter, Ammeter and Voltmeter used in experiment

**Table 4.5.** Technical specifications of multimeter

| | |
|---|---|
| Make and Model | RISH max10 |
| Display | 3 ¾ digit |
| Counts | 3999 |
| DC Voltage range | 400 mV-1000 V |
| DC Voltage accuracy | ±0.5+2 |
| Dc current range | 40 mA-10 A |
| Dc current accuracy | ±0.8+2 |
| Power input | AAA (1.5 V×2) |
| Dimensions | 92 ×154 ×25 mm |

### 4.5 Error and uncertainty analysis in experiment

An uncertainty analysis is carried out on both electrical and thermal efficiencies from the energy balance point of view. The experimental uncertainties are calculated with the help of analysis of errors in the experimental through various instruments employed. During the measurement, the observed values on the instrument shall be indicated with the level of uncertainty in a measurement. In order to maintain high precision, the error within the measurement needs to be determined. The physical measurement of the instrument has two components: (1) A numerical value (in a specified system of units) giving the best estimate possible of the quantity measured and (2) the degree of uncertainty associated with this estimated value. Since different measuring instruments were used for the experimental measurement, the maximum error during the measurement can be calculated as the ratio of least count of the measuring instrument and minimum recorded value of the parameter. For the estimation of mathematical uncertainty within the calculations, the following equation is used [151]:

$$\omega_R = \left[\left(\frac{\partial R}{\partial x_1}\omega_1\right)^2 + \left(\frac{\partial R}{\partial x_2}\omega_2\right)^2 + \cdots \left(\frac{\partial R}{\partial x_n}\omega_n\right)^2\right]^{1/2} \qquad (4.1)$$

Where R is a function of 'n' independent linear parameters as $R = R(x_1, x_2, x_3 \ldots\ldots\ldots x_n)$.

Thus, using equation (4.1) the uncertainty has been calculated for the thermal and electrical efficiency of the system.

Thermal efficiency of the PV/T is depends on mass flow rate of fluid and inlet and outlet temperature of the PV/T. So the equation (4.1) solved for the all dependent variables in case of thermal efficiency and found resultant equation as:

$$\frac{\omega_R}{Q} = \left[\frac{a^2}{q^2} + \frac{b^2}{\left(T_{fin} - T_{out}\right)^2} - \frac{e^2}{\left(T_{fin} - T_{out}\right)^2}\right]^{1/2} \qquad (4.2)$$

Where $q = mc\,\Delta T$ and $T_{fin}$ and $T_{out}$ are the inlet and outlet temperature of the PV/T respectively. And *a, b, e* are the percentage errors in the measuring instruments.

Electrical efficiency of the PV depends up on current, voltage and solar radiation. So the equation (4.1) solved for the all dependent variables in case of electrical efficiency and found resultant equation as:

$$\frac{\omega_R}{\eta} = \left[\frac{a_1^2}{I^2} + \frac{b_1^2}{V^2} - \frac{e_1^2}{G^2}\right]^{1/2} \qquad (4.3)$$

Where I, V and G are the current, voltage and solar radiation respectively. And $a_1$, $b_1$, $e_1$ are the percentage errors in the measuring instruments.

The uncertainties related with the measuring instruments of the experimental setup are presented in Table 4.6.

**Table 4.6.** Uncertainties of measured and calculated parameters related to the experiment

| Parameter | Unit | Maximum uncertainty (in experiments) |
|---|---|---|
| PV/T Inlet and outlet temperature | °C | ±0.6 |
| EWHE Inlet and outlet temperature | °C | ±0.6 |
| Ambient temperature | °C | ±0.6 |
| PV panel temperature | °C | ±1.8 |
| Mass flow rate | kg/s | ±0.0006 |
| Solar radiation intensity | W/m$^2$ | ±6 |
| Open circuit voltage | V | ±0.005 |
| Short circuit current | A | ±0.015 |
| Electrical efficiency | % | ±0.37 |
| Thermal efficiency | % | ±1.94 |

## 4.6 Statistical analysis

To quantify the degree of agreement between the simulation (theoretical) results ($X_i$) and the experimental results ($Y_i$), the root mean square percent deviation ($e$) and correlation coefficient ($r$) have been evaluated by using the following expressions:

$$\text{Correlation coefficient } (r) = \frac{N\sum X_i Y_i - (\sum X_i)(\sum Y_i)}{\sqrt{(N\sum X_i^2 - (\sum X_i^2)^2}.\sqrt{N\sum Y_i^2 - (\sum Y_i^2)^2}} \qquad (4.4)$$

$$\text{Root mean square percent deviation, } e = \sqrt{\frac{\sum (e_i)^2}{N}} \qquad (4.5)$$

$$\text{Where } e_i = \left[\frac{X_i - Y_i}{X_i}\right] \times 100$$

## 4.7 Experimental methodology

Performance of coupled tube-and-sheet PV/T system with EWHE cooling has been evaluated on three consecutive days (09-11 Sep., 12-14 Sep. and 15-17 Sep.) with different flow rates in the month of September 2016. Experiments were conducted from 9$^{th}$ September to 17$^{th}$ September, 2016 for daily 6 hours duration from 10 a.m. to 4 p.m. During this study, system was kept closed between 4 p.m. to 9.45 a.m. of the next day, allowing the soil to get regenerated for rest of the day. Mass flow rate of cooling water through the PV/T and EWHE pipes was maintained at 0.017 kg/s, 0.025 kg/s and 0.033 kg/s for different respective days. Following this, the IPVTS system coupled with EWHE cooling was tested on 20$^{th}$ September at the mass flow rate of 0.033 kg/s. Measurement and recording of hourly data for the experimental set-up includes the following parameters; intensity of solar insolation, ambient air temperature and wind velocity, temperature at the inlet and outlet of PV/T system, temperature at inlet and outlet of EWHE system, temperature of water in the buried pipe at six different locations, depth-wise temperature of soil at six points, PV panel temperature with and without cooling, short circuit current, open circuit voltage, load current and load voltage.

## 4.8 Exergetic analysis of glazed PV/T system coupled with EWHE cooling

In order to optimize any system and to identify the efficiency of energy utilization within the system, first law analysis is a must. Apart from this, exergy, which is the work potential of the energy contained in the system, can be used to identify the grey areas for improvement [152-153]. The exergy or availability is the maximum useful work that can be extracted from a system at given condition with respect to surroundings (dead state). Thus, the exergy analysis of both PV/T (tube-and-sheet and IPVTS) systems coupled with EWHE was carried out and the corresponding equations are presented in this section. The second law analysis has been carried out using experimental data of each system. The exergetic analysis of the present system has been carried out in terms of exergy losses and exergy destructions. To perform the analysis, the exergy equations of PV/T system were developed and solved using MATLAB. It is important to mention here that the exergy equations for both tube-and-sheet and broad channel PV/T coupled with EWHE system are same.

### 4.8.1 Tube-and-sheet PV/T system

The exergy balance of PV/T system was carried out by taking it as a control volume and is given by equation (4.6) [153]:

$$\sum \dot{E}\, x_{input\ ,total} - \sum \dot{E}\, x_{output\ ,total} - \sum \dot{E}\, x_{loss,total} = 0 \qquad (4.6)$$

Where the total exergy loss in the system is equal to sum of internal and external exergy loss.

$$\sum \dot{E}\, x_{loss,total} = \sum \dot{E}\, x_{loss,int.} + \sum \dot{E}\, x_{loss,ext.} \qquad (4.7)$$

For the further discussion, the external exergy losses $\left(\sum \dot{E}\, x_{loss,ext.}\right)$ and internal exergy losses $\left(\sum \dot{E}\, x_{loss,int.}\right)$ are abbreviated as the exergy loss and exergy destruction respectively. The total exergy entering the PV/T collector from the solar radiation is given by equation (4.8) [154]

$$\sum \dot{E}\, x_{input\ ,total} = G(I)\, A_{PV/T} \left[1 - \frac{4}{3}\left(\frac{T_{amb}}{T_{Sun}}\right) + \frac{1}{3}\left(\frac{T_{amb}}{T_{Sun}}\right)^4\right] \qquad (4.8)$$

where $T_{Sun}$ is Sun temperature, taken as 5778 K.

The total exergy out of the PV/T, is calculated as the sum of thermal and electrical exergies and given by

$$\sum \dot{E}\, x_{output\ ,total} = \dot{E}x_{thermal} + \dot{E}x_{electrical} \qquad (4.9)$$

The thermal exergy rate is calculated as in equation (4.10)

$$\dot{E}x_{thermal} = \left[1 - \frac{T_{amb}}{T_{wo}}\right] \times Q_{thermal} \qquad (4.10)$$

$$\text{where } Q_{thermal} = \dot{m}_w C_w (T_{wo} - T_{wi})$$

The electrical exergy includes the difference between the electrical power output of PV/T and the consumed electrical power by pump and is given as in equation (4.11):

$$\dot{E}x_{electrical} = \dot{E}x_{power} - \dot{E}x_{pump} \qquad (4.11)$$

#### *4.8.1.1 The external exergy losses and destruction rate (internal exergy losses) of PV/T system*

The external exergy loss due to optical losses from PV/T surface is calculated as expressed in equation (4.12) [155]:

$$\dot{E}x_{loss,optical} = G(I)\, A_{PV/T}\left[1-\frac{4}{3}\left(\frac{T_{amb}}{T_{Sun}}\right)+\frac{1}{3}\left(\frac{T_{amb}}{T_{Sun}}\right)^{4}\right]-(\alpha\tau) \times G(I)\, A_{PV/T}\left[1-\frac{4}{3}\left(\frac{T_{amb}}{T_{Sun}}\right)+\frac{1}{3}\left(\frac{T_{amb}}{T_{Sun}}\right)^{4}\right] \quad (4.12)$$

The exergy loss due to heat loss from PV/T system to surroundings is calculated as per equation (4.13) [98].

$$\dot{E}x_{Q_{l,loss}} = \left(1-\frac{T_{amb}}{T_{cell}}\right) \times Q_l \quad (4.13)$$

where $Q_l$ is heat loss from PV/T system to surroundings and is calculated as per equation (4.14)

$$Q_l = U_T A_{PV/T}\ (T_{cell} - T_{amb}) \quad (4.14)$$

The exergy destruction due to pressure drop in PV/T system is estimated using equation (4.15)

$$\dot{E}x_{des,pressure} = \frac{T_{amb} \times \dot{m}_w \times \Delta P}{\rho \times T_{w,avg}} \quad (4.15)$$

The electrical exergy destruction is given by [155]:

$$\dot{E}x_{des,electrical} = I_{sc}V_{oc} - \left(\dot{E}x_{power} - \dot{E}x_{pump}\right) \quad (4.16)$$

The exergy destruction due to the temperature difference between the Sun and PV/T collector is given as in equation (4.17) [116]:

$$\dot{E}x_{des,Sun-PV/T} = (\alpha\tau) \times G(I)\, A_{PV/T}\left[1-\frac{4}{3}\left(\frac{T_{amb}}{T_{Sun}}\right)+\frac{1}{3}\left(\frac{T_{amb}}{T_{Sun}}\right)^{4}\right]-(\alpha\tau) \times G(I)\, A_{PV/T}\left(1-\frac{T_{amb}}{T_{cell}}\right) \quad (4.17)$$

The exergy destruction due to heat transfer from the PV/T surface to the cooling water is given as [155]:

$$\dot{E}x_{des,PV/T,W} = (\alpha\tau) \times G(I)\, A_{PV/T}\left(1 - \frac{T_{amb}}{T_{cell}}\right) - Q_l\left(1 - \frac{T_{amb}}{T_{cell}}\right) - Q_{thermal}\left(1 - \frac{T_{amb}}{T_{wo}}\right) - V_{oc} I_{sc} \quad (4.18)$$

Total exergy destruction of the PV/T system is

$$\dot{E}x_{des,total} = \dot{E}x_{des,pressure} + \dot{E}x_{des,electrical} + \dot{E}x_{des,Sun-PV/T} + \dot{E}x_{des,PV/T,W} \quad (4.19)$$

The external losses from the PV/T system are calculated as

$$\dot{E}x_{loss} = \dot{E}x_{loss,optical} + \dot{E}x_{Q_{l,loss}} \quad (4.20)$$

The exergetic efficiency of the PV/T system may be expressed as the ratio of total exergy output to the total exergy input as shown in equation (4.21).

$$\eta_{II\ law} = \frac{\dot{E}x_{output,total}}{\dot{E}x_{input,total}} \quad (4.21)$$

In this article, three approaches for estimating the exergetic efficiency of PV/T system are employed and the results obtained are compared. The adopted three approaches are as follows:

***Case (I)***. In the first case, the total exergy output and total exergy input is calculated using equation (4.9) and (4.8) respectively, and then are substituted in equation (4.21) to calculate the exergetic efficiency. The resulting expression in detailed form is expressed in equation (4.22).

$$\eta_{II\ law,case\,(I)} = \frac{Q_{thermal}\left(1 - \frac{T_{amb}}{T_{wo}}\right) + \dot{E}x_{power} - \dot{E}x_{pump}}{G(I)\, A_{PV/T}\left[1 - \frac{4}{3}\left(\frac{T_{amb}}{T_{Sun}}\right) + \frac{1}{3}\left(\frac{T_{amb}}{T_{Sun}}\right)^4\right]} \quad (4.22)$$

However, this case has some deficiencies. Firstly, it does not include the exergy loss components in the PV/T system, for example, exergy loss due to pressure drop in PV/T system. Secondly, it depicts significant error at lower solar irradiations and gives the value of exergetic efficiency near to the value of electrical efficiency of PV/T system at standard test conditions.

***Case (II)*** In this case, an attempt has been made to overcome the deficiencies of Case (I), while deriving the exergetic efficiency of the PV/T system [116]. Here, the total exergy losses are

evaluated as the sum of external exergy loss and exergy destruction, as per equation (4.7). The exergetic efficiency of case (II) is expected to be low as compared to case (I) due to the consideration of the possible losses into account.

$$\eta_{II\ law\ ,case\ (II)} = \left[1 - \frac{\dot{E}x_{loss} + \dot{E}x_{des}}{\dot{E}x_{input\ ,total}}\right] \qquad (4.23)$$

***Case (III)*** In this case, the exergetic efficiency of the PV/T system is calculated as per the standard definition of the second law efficiency, which is derived from the standard exergy balance equation for a steady flow system. The second law efficiency expression is given in equation (24)[156].

$$\eta_{II\ law\ ,case\ (III)} = \left[1 - \frac{\dot{E}x_{des}}{\dot{E}x_{input\ ,total}}\right] \qquad (4.24)$$

### 4.8.2 EWHE system

The total exergy per unit mass flow rate entering in to the EWHE system is given as [153]:

$$\Psi_{in} = h_{in} - h_{amb} - T_{amb}\,(s_{in} - s_{amb}) \qquad (4.25)$$

The total exergy output per unit mass flow rate of EWHE system is given as

$$\Psi_{out} = h_{out} - h_{amb} - T_{amb}\,(s_{out} - s_{amb}) \qquad (4.26)$$

The exergy destruction rate of EWHE is calculated as [157]

$$\dot{E}x_{des,EWHE} = \dot{m_w}(\Psi_{in} - \Psi_{out}) - Q_g\left(1 - \frac{T_o}{T_{soil}}\right) + \frac{T_{amb} \times \dot{m}_w \times \Delta P}{\rho \times T_{w,avg}} \qquad (4.27)$$

where $Q_g$ is the heat transferred from EWHE to soil

$$Q_g = \dot{m}_w C_w (T_{wi1} - T_{wo1}) \qquad (4.28)$$

In equation (4.27) the reference temperature ($T_0$) is taken as 25 °C (standard ambient temperature) and the values of specific enthalpy and specific entropy at inlet and outlet conditions (equation 4.25 and 4.26) are calculated using MATLAB by calling the required parameters from REFPROP v9.0.

The exergetic efficiency of EWHE calculates as

$$\eta_{II\ law\ ,EWHE} = \left(1 - \frac{\dot{E}x_{des\ ,EWHE}}{\dot{m}_w \Psi_{in}}\right) \tag{4.29}$$

### 4.8.3 PV/T coupled with EWHE system

Further, as discussed earlier two cases are employed for calculating the exergetic efficiency of the coupled system (EWHE+PV/T) and the results obtained are compared. The second law analysis of PV/T coupled with EWHE system has been carried out using the expression given in Case (II) and Case (III) of PV/T as discussed above. In the present work Case (I) has not been considered for the analysis owing to its deficiencies as discussed in Case (I) of PV/T.

***Case (II)*** In this case, the total exergetic efficiency of the coupled system (EWHE+PV/T) includes both exergy destructions and the external exergy losses and is expressed in equation (4.30).

$$\eta_{II\ law\ ,coupled\ \ system\ ,case\ (II)} = \left[1 - \frac{\left(\dot{E}x_{loss} + \dot{E}x_{des}\right)_{PV/T} + \dot{E}x_{des\ ,EWHE}}{\dot{E}x_{input\ ,total} + \dot{E}x_{pump}}\right] \tag{4.30}$$

***Case (III)*** In this case, the exergetic efficiency of the coupled system (PV/T+EWHE) is calculated as per the standard definition of the second law efficiency. This approach includes only the exergy destructions of PV/T and EWHE systems for calculating the exergetic efficiency of the coupled system.

$$\eta_{II\ law\ ,coupled\ \ system\ ,case\ (III)} = \left[1 - \frac{\dot{E}x_{des\ ,PV/T} + \dot{E}x_{des\ ,EWHE}}{\dot{E}x_{input\ ,total} + \dot{E}x_{pump}}\right] \tag{4.31}$$

# CHAPTER 5
# RESULTS AND DISCUSSION

## 5.0 Performance analysis of glazed PV/T systems coupled with EWHE and EAHE cooling

This chapter deals with performance analysis of glazed PV/T systems coupled with EWHE and EAHE systems. The developed mathematical models have been validated experimentally on an experimental set-up installed in Pilani, India. As discussed in the previous chapters, the present study deals with the analysis of two types of PV/T systems i.e. tube-and-sheet PV/T and broad channel IPVTS systems. Following the experiment, the simulation was also carried out for parametric study by developing mathematical model and validating it with experimental results. Performance of coupled tube-and-sheet PV/T system with EWHE cooling has been evaluated on three consecutive days (09-11 September, 12-14 September and 15-17 September) with different flow rates. In this section, the results of six days (09-11 September and 12-14 September) are discussed in details. Mass flow rate of cooling water through the tube-and-sheet PV/T and EWHE pipes was maintained at 0.017 kg/s, 0.025 kg/s and 0.033 kg/s for different respective days. Following this, the broad channel IPVTS system coupled with EWHE cooling was tested on 20$^{th}$ September at the mass flow rate of 0.033 kg/s. The results of analysis for PV/T coupled with EAHE system for combined power and space heating is also discussed in this chapter. For the same, the mathematical model was developed and validated with the results from the literature, and has already been discussed in Chapter 3. At the end, the experimental results based exergetic analysis for both tube-and-sheet PV/T and broad channel IPVTS systems coupled with EWHE was carried out using equations as given in Chapter 4.

## 5.1 Performance analysis of glazed tube-and-sheet PV/T system coupled with EWHE cooling

The experimental study was performed in realistic conditions at BITS Pilani, Pilani campus, Rajasthan. The simulated values of outlet temperatures of PV/T and EWHE, open-circuit voltage, short-circuit current, SCs temperature have been validated using the experimental results obtained by conducting daily 6-hours experimental study from 9$^{th}$ September to 17$^{th}$ September, 2016. The set of data which includes solar radiation and ambient temperature is taken for those

different days where the values are within the close range. The variation of ambient temperature and global solar radiation intensity during the test days are shown in Fig. 5.1. The ambient air temperature and solar radiation ranges between 30.9 °C to 36.9 °C and 534 W/m$^2$ to 980 W/m$^2$ respectively. The maximum deviation of ±6.33% was observed for ambient air temperature while for solar radiation, it was just ±1.96% during the experimentation. Hence it can be deduced that the experimental outdoor conditions are almost identical at any hour of operation and gives the relative performance of each day. The experiment was conducted for 0.017 kg/s, 0.025 kg/s and 0.033 kg/s flow rates.

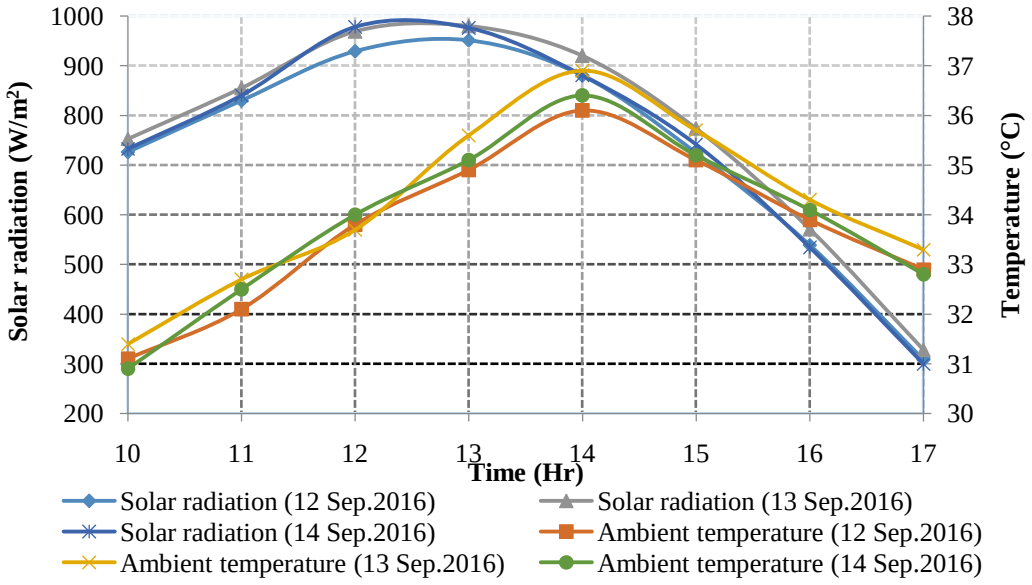


**Fig. 5.1.** Variation of solar radiation and ambient temperature during the test days

Hourly variation of PV panel temperature without cooling and with cooling at cooling water flow rates of 0.033 kg/s, 0.025 kg/s and 0.017 kg/s are shown in Fig. 5.2 (a), (b) and (c). From the experimental study, it was observed that the PV panel temperature without cooling ranges from 57 °C to 69 °C, 60 °C to 73 °C and 62 °C to 71 °C during 12 September, 13 September, and 14 September, 2016 respectively. On the other hand, the experimental results show that the PV panel temperature drops with EWHE cooling and ranges from 43.68 °C to 49.64 °C, 46.18 °C to 52.31 °C and 45.42 °C to 52.68 °C with 0.033 kg/s, 0.025 kg/s and 0.017 kg/s flow rates respectively. It is observed that during afternoon time, the PV panel temperature increases due to increase in solar radiation, which leads to decrease in the performance of PV system. The validation of the PV panel temperature is also carried out by comparing the results obtained from

FLIR thermography. Fig. 5.3 shows the thermal image of the PV panels during the experimentation. As mentioned in chapter 4, the mean square percent deviation (e) and correlation coefficient (r) criteria are tools to find the good agreement between theoretical and experimental results. As shown in Fig. 5.2, a fair agreement is observed between experimental and theoretical results. The mean square percent deviation (e) and correlation coefficient (r) are from 11.63% to 12.09% and from 0.9844 to 0.9864 respectively.

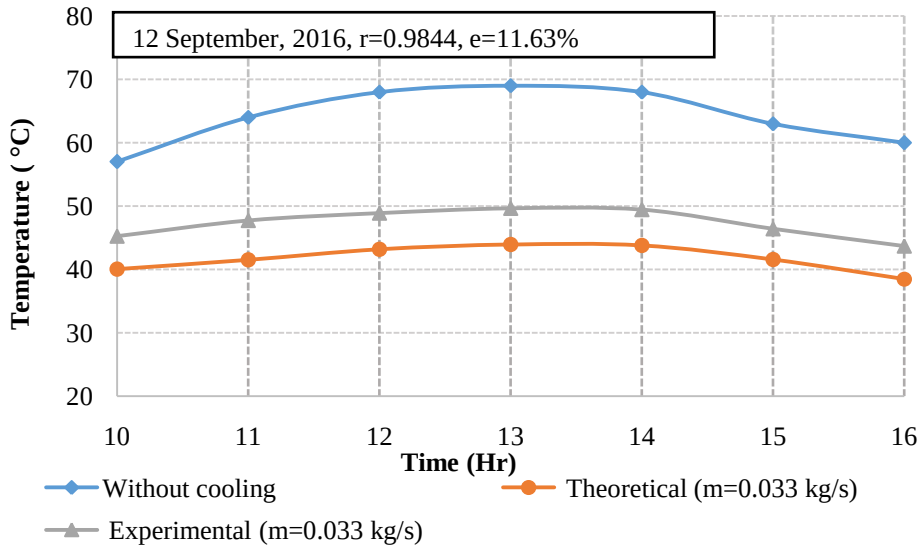


(a)

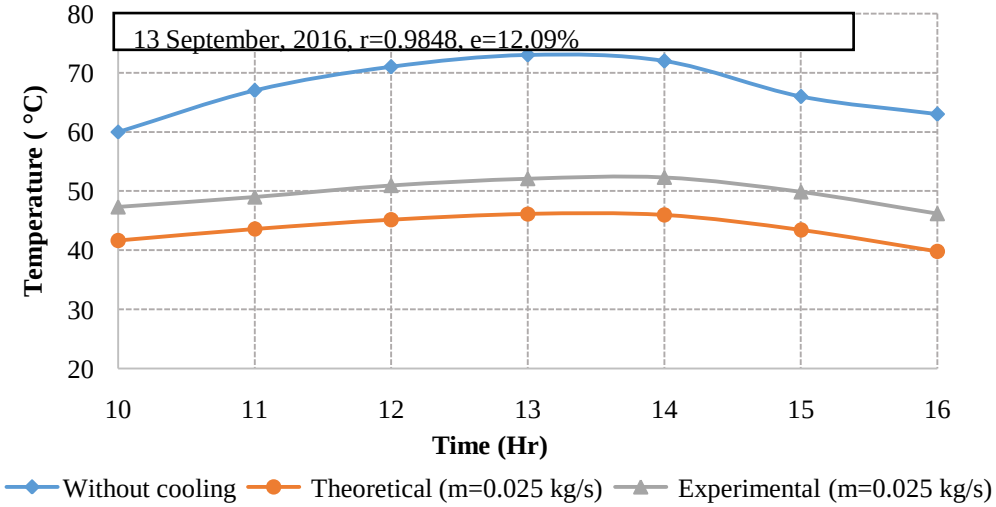


(b)

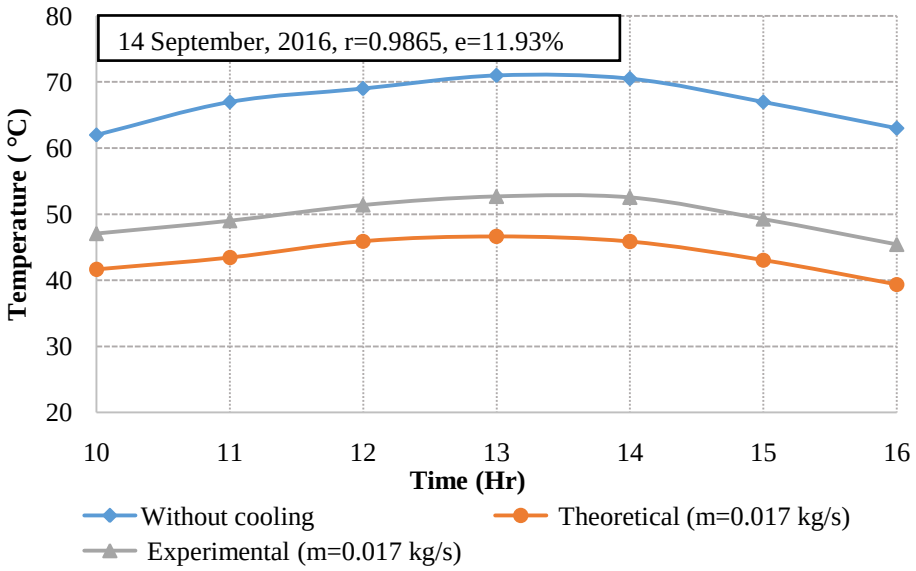


(c)

**Fig. 5.2 (a), (b) and (c)**. Simulated and experimental values of PV panel temperature during the test days for various flow rates

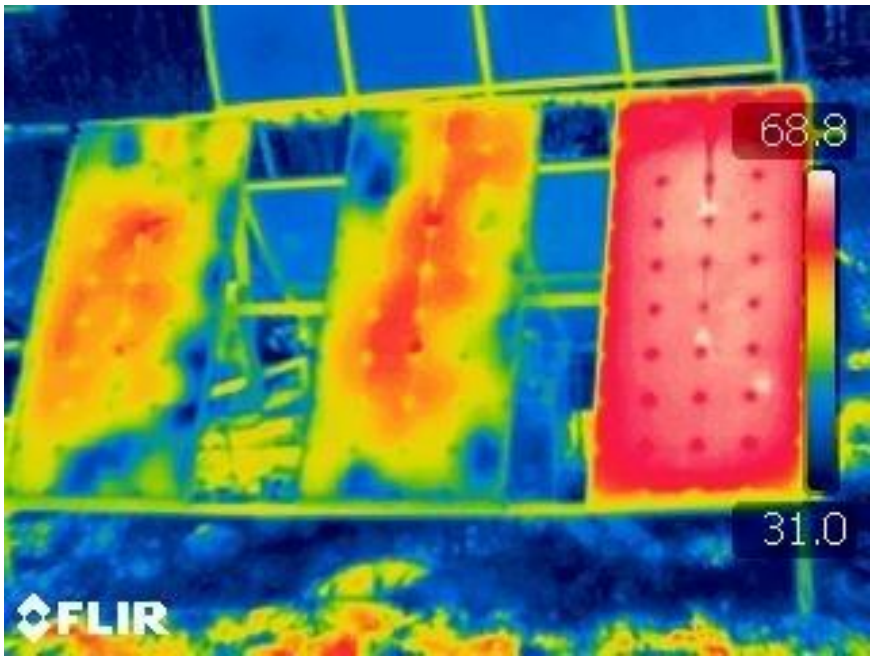


**Fig. 5.3.** PV panel temperature measured by FLIR

The hourly variation of experimental and theoretical results of the PV/T inlet and outlet temperature is shown in Fig. 5.4 (a), (b) and (c). It is important to mention here that the EWHE outlet temperature is inlet temperature of PV/T and outlet temperature of PV/T is inlet

temperature of EWHE in PV/T coupled with EWHE system. The analytical approach of using energy and mass balance is used to achieve theoretical results. However, in practical conditions, the outlet temperature of EWHE is slightly above as compared to theoretical values due to heat transfer to the connecting pipes from the surroundings. The results are represented in Fig. 5.4 (a), (b) and (c). Thus, the experimental PV/T outlet temperature is on a higher side as compared to the expected theoretical value. The maximum experimental PV/T outlet temperature at flow rates of 0.033 kg/s, 0.025 kg/s and 0.017 kg/s are 34.35 °C, 36.20 °C and 38.14 °C respectively. The PV/T inlet temperature (i.e. EWHE outlet) ranges between 30.2 °C to 30.7 °C for all the flow rates. The variation in PV/T outlet temperature also depends upon the intensity of the global solar radiation. From statistical analysis observed that the root mean square percent deviation (e) and correlation coefficient (r) are in a good agreement between experimental and theoretical results and the values are shown in Fig. 5.4 (a), (b) and (c).

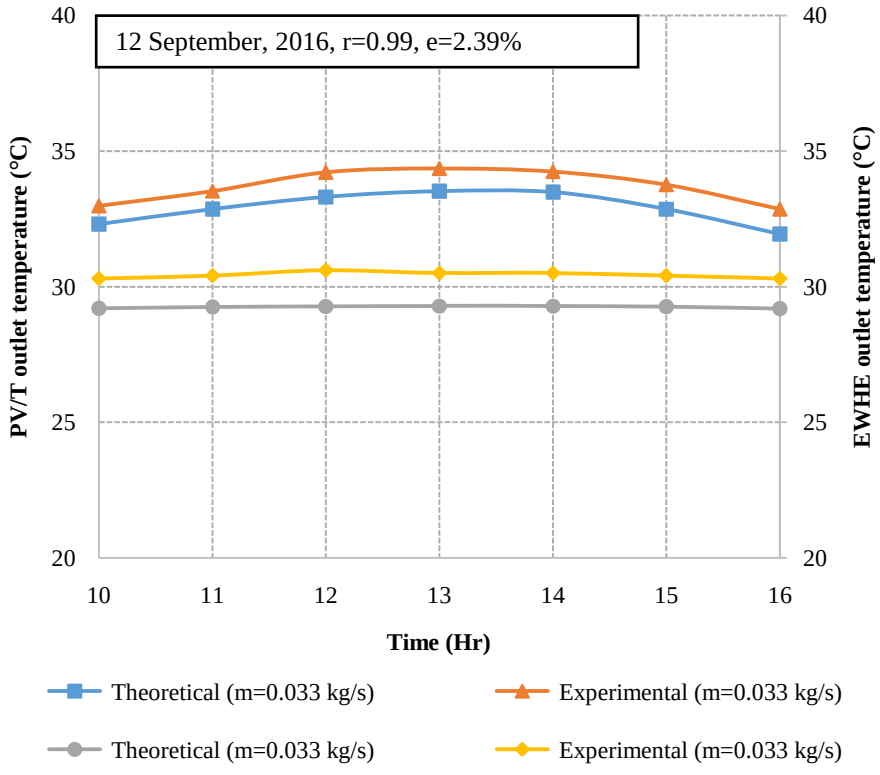


(a)

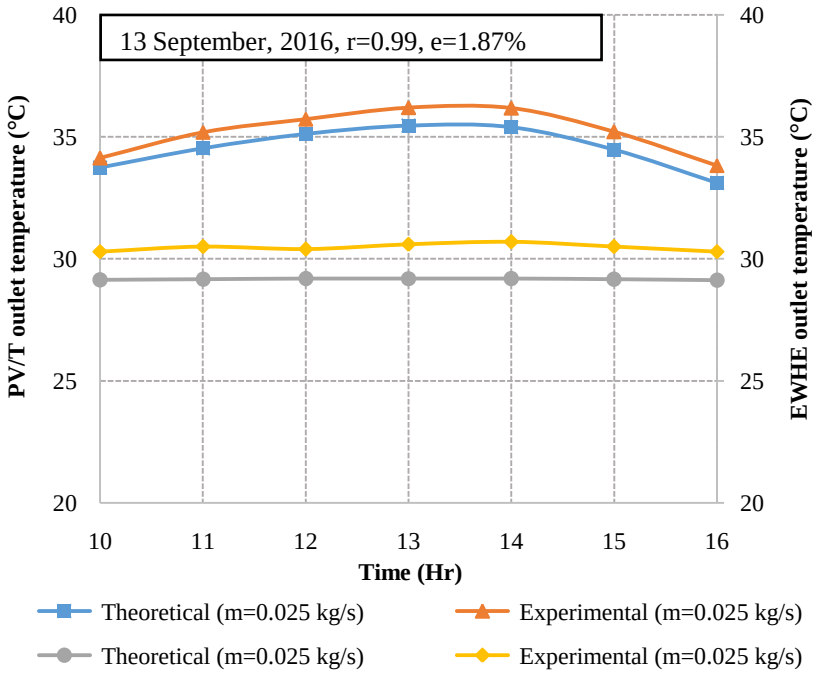


(b)

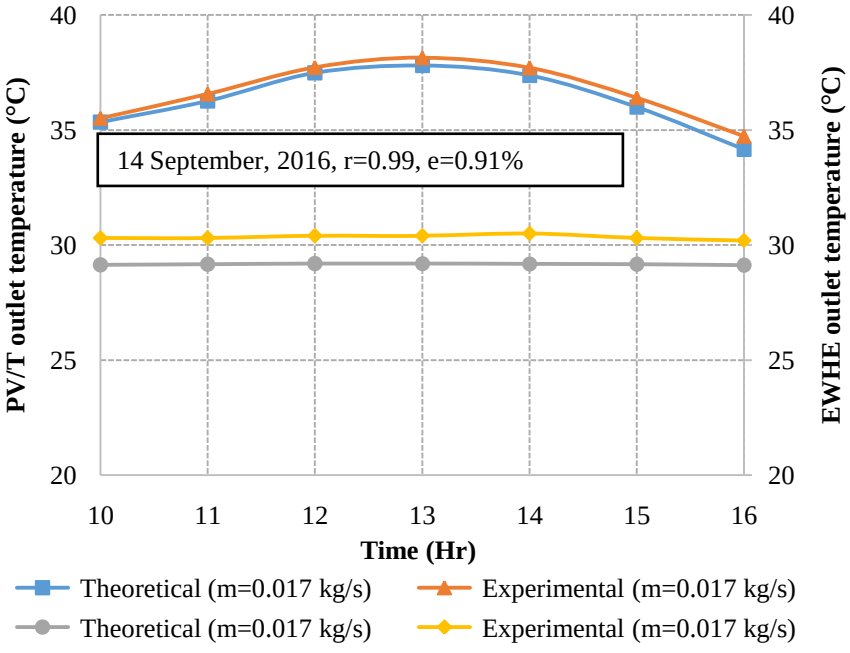


(c)

**Fig. 5.4 (a), (b) and (c)**. Simulated and experimental values of PV/T inlet and outlet temperature during the test days for various flow rates

Fig. 5.5 (a), (b) and (c) are represent the electrical efficiency of PV/T system with cooling and without cooling for different mass flow rates of cooling water. An electrical efficiency comparison was made for two scenarios first is when the PV panel was coupled with the thermal collector and second is PV panel without thermal collector. In the second case, i.e. PV panel without cooling, the electrical efficiency is observed to varying from 7.28% to 7.96% during all test days due to high cell temperature as mentioned earlier. While in first case PV panel with EWHE cooling, the experimental electrical efficiency is observed to vary from 8.27% to 8.52%, 8.15% to 8.41% and 8.14% to 8.44% for flow rates of 0.033 kg/s, 0.025 kg/s and 0.017 kg/s respectively during all test days. It can be concluded that the electrical efficiency of system is increased by 0.49% to 0.82% and 0.53% to 0.88% for 0.033 kg/s and 0.025 kg/s respectively, while it increases by 0.62% to 0.76% for 0.017 kg/s flow rate as compared to second case i.e. without cooling. It was observed that PV efficiency increases during the morning and evening period and decreases during peak sunshine hours. This is due to the change in the temperature of PV panel throughout the day. At higher temperature, the PV panel efficiency decreases. The experimental and theoretical hourly variation of PV/T collector thermal efficiency is shown in Fig. 5.6 (a), (b) and (c) for different flow rates of cooling water. It reveals that the experimental thermal efficiency ranges from 45.06% to 55.45%, 47.12% to 54.76% and 44.80% to 51.12% for flow rates of 0.033 kg/s, 0.025 kg/s and 0.017 kg/s respectively. The root mean square percent deviation (e) and correlation coefficient (r) obtained by validating with theoretical results are within the range from 10.07 to 11.65% and from 0.9497 to 0.9891 respectively.

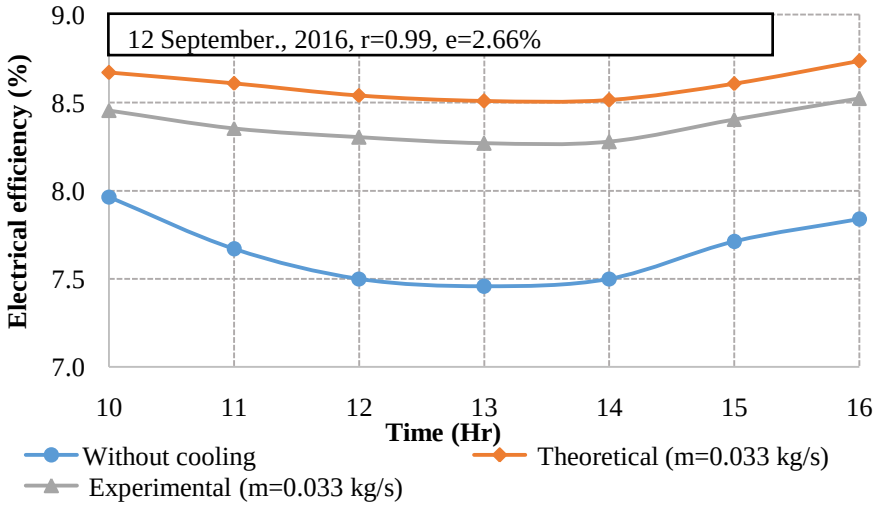


(a)

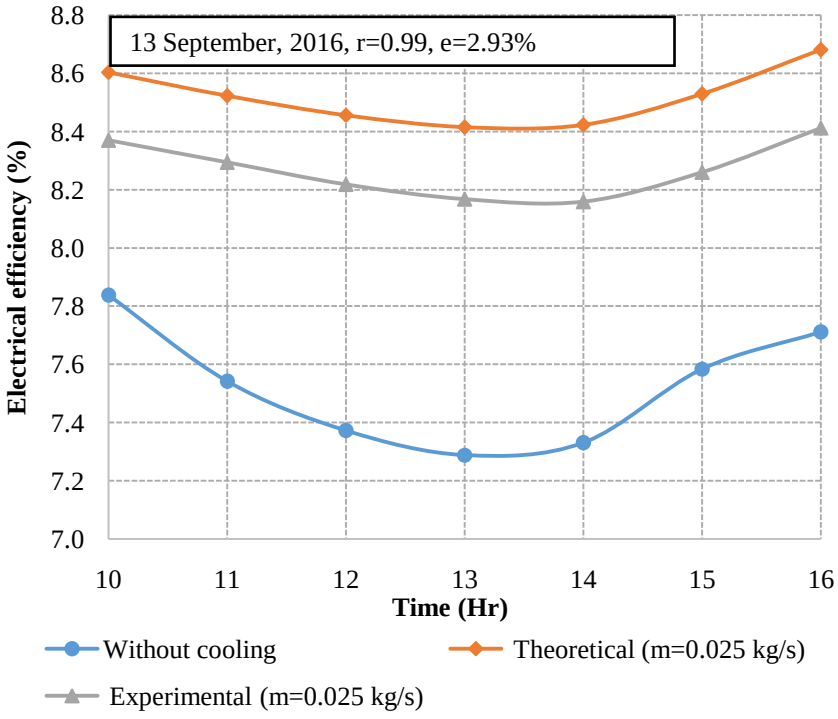


(b)

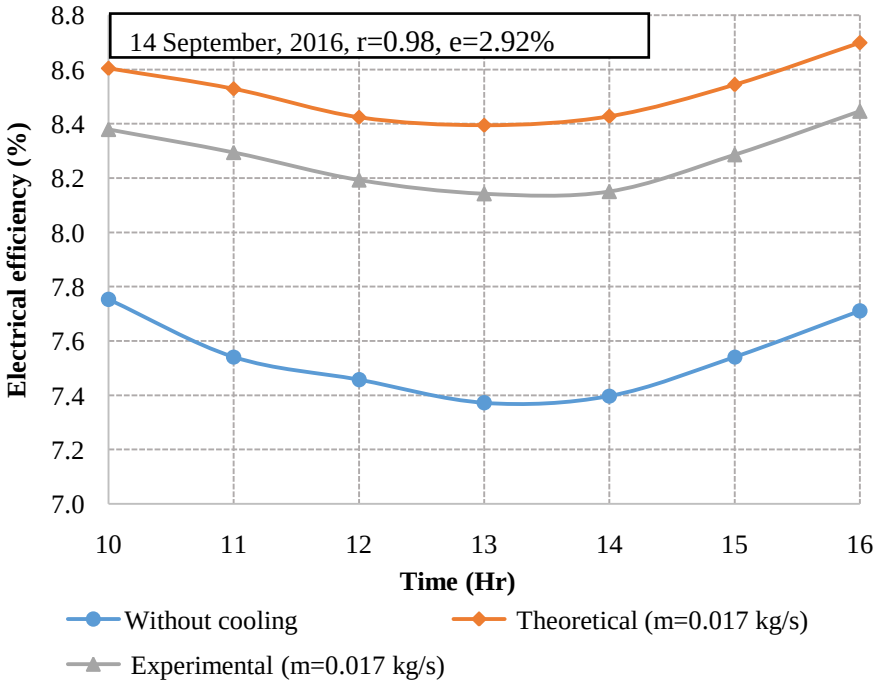


(c)

**Fig. 5.5 (a), (b) and (c).** Simulated and experimental values of electrical efficiency of PV during the test days for various flow rates

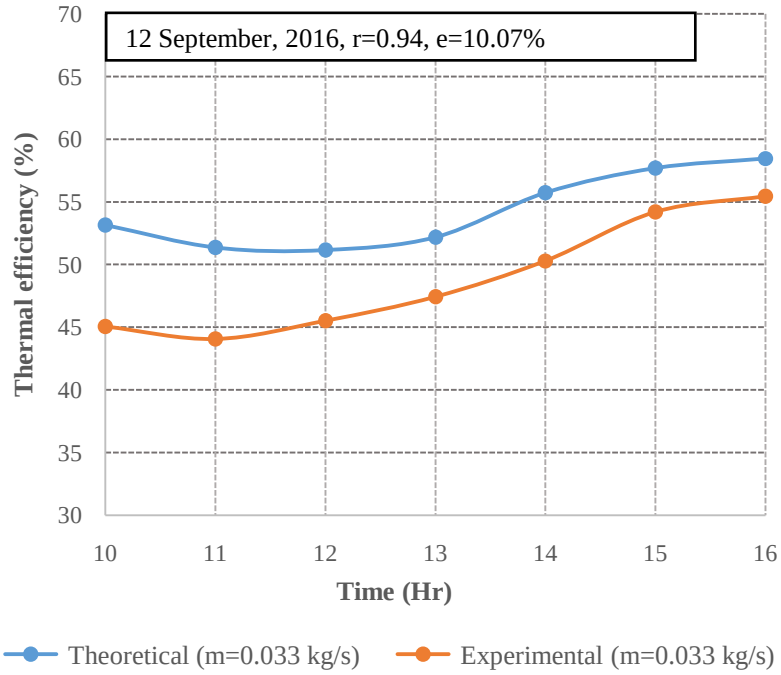
12 September, 2016, r=0.94, e=10.07%
Thermal efficiency (%)
70
65
60
55
50
45
40
35
30
10
11
12
13
14
15
16
Time (Hr)
Theoretical (m=0.033 kg/s)
Experimental (m=0.033 kg/s)

(a)

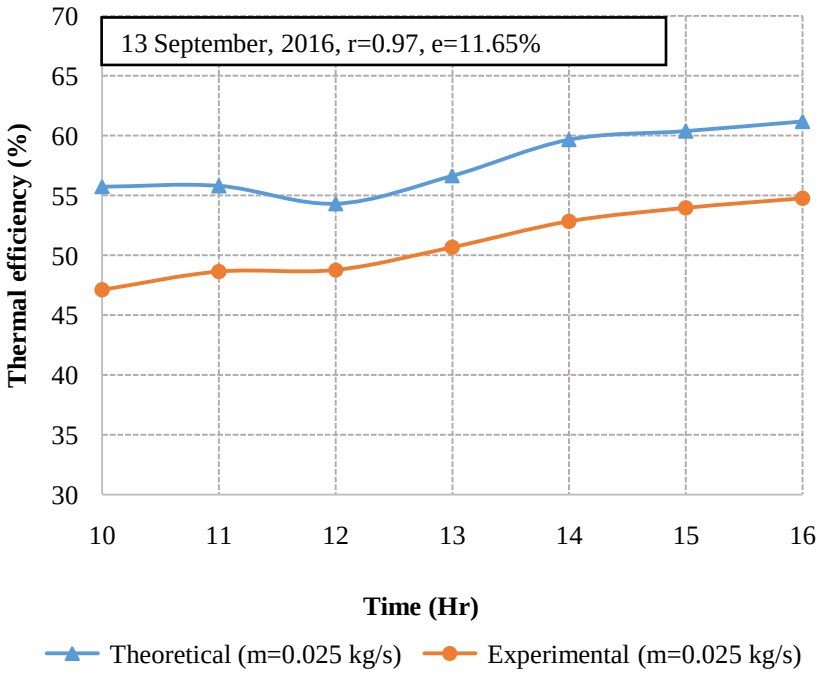
13 September, 2016, r=0.97, e=11.65%
Thermal efficiency (%)
70
65
60
55
50
45
40
35
30
10
11
12
13
14
15
16
Time (Hr)
Theoretical (m=0.025 kg/s)
Experimental (m=0.025 kg/s)

(b)

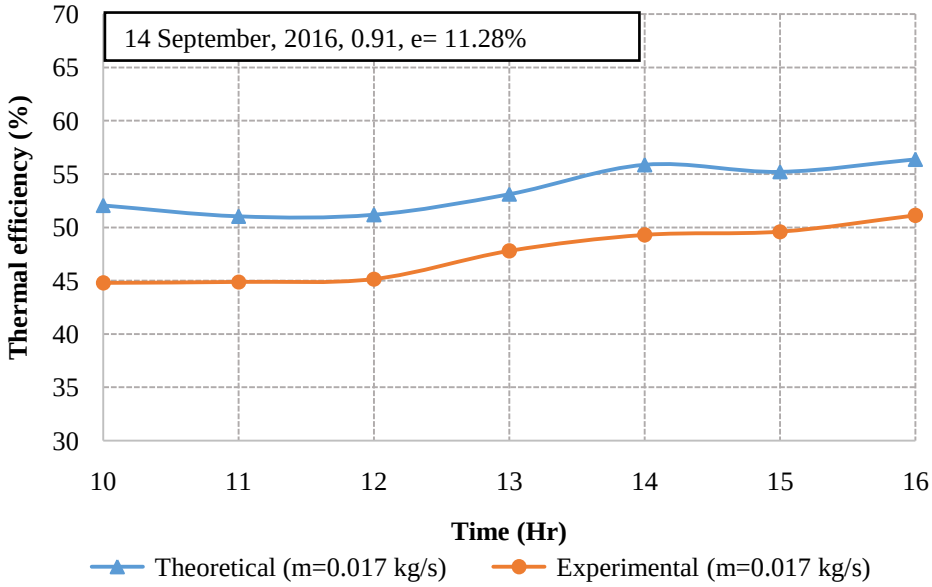


**Fig. 5.6 (a), (b) and (c).** Simulated and experimental values of thermal efficiency of PV/T during the test days for various flow rates

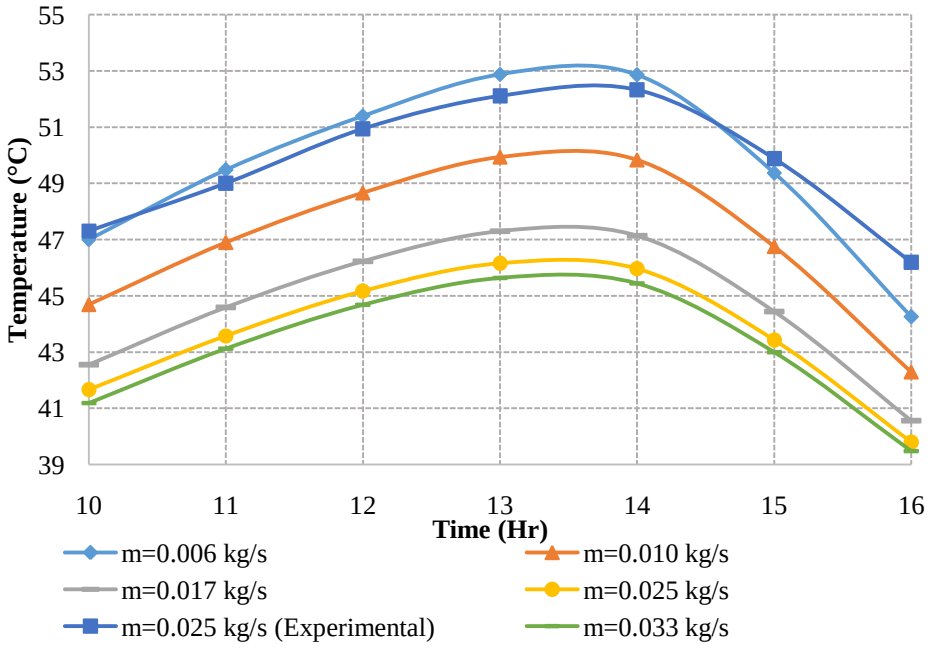


**Fig. 5.7**. PV Panel temperature for various flow rates of cooling water

The effect of the mass flow rate on the panel temperature along the EWHE pipe length of 80 m at same environmental conditions is plotted in Fig. 5.7. It was found that the panel temperature varies with different flow rates, i.e. 44.25 °C to 52.87 °C for 0.006 kg/s, 40.55 °C to 47.29 °C for

0.017 kg/s, and 39.47 °C to 45.63 °C for 0.033 kg/s. It was observed that the PV panel temperature reduced with increase in mass flow rate and becomes almost the same for 0.025 kg/s and 0.033 kg/s. This observation could be used for the practical applications, by considering 0.025 kg/s flow rate instead of higher one to achieve the similar results hence low pumping power requirement. With reduce PV panel temperature the thermal efficiency increases significantly with increase in flow rate of cooling water due to high heat removal rate from the PV/T system. This in turns increases the electrical efficiency because of the low cell temperature at high flow rates. Thus, in order to have maximum electrical and thermal efficiency of the PV/T system, the mass flow rate needs to be optimized within a suitable range.

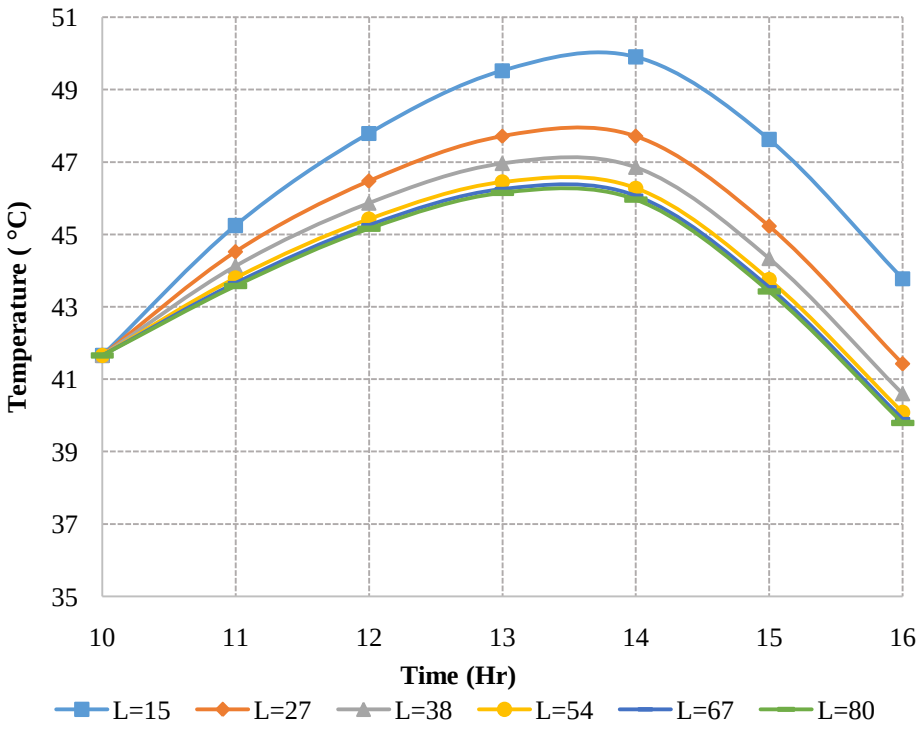


**Fig. 5.8**. PV Panel temperature for different EWHE pipe lengths with 0.025 kg/s flow rate

Furthermore, the hourly variation of PV panel temperature is simulated for the different pipe lengths of EWHE and presented in Fig. 5.8. It is found out that from 15 m to 80 m pipe length, the panel temperature reduces with increase in length. The maximum PV temperature drop occurs drastically at 38 m and beyond this the gradual drop is observed during peak sunshine hours. From this, it is evident that the pipe length of 38 m would be sufficient for such coupled systems. This system may be used for the arid and semi-arid regions of western Rajasthan which

receives high solar radiation, especially during summer period when the ambient temperature reach up to 50 °C. Also, there isn't any demand of hot water due to high ambient temperature. Thus, the proposed EWHE system will be a better solution to reject heat into geothermal sink i.e. earth. The experimentally recorded data for RTD temperature sensor $T_6$, buried at a depth of 3 m, reveals that the temperature of soil at this depth is not at all affected by the diurnal variation of ambient temperature and solar radiation, as shown in Table 5.1. It is clearly seen that for all the experimental days, the soil temperature ($T_6$) observed at a depth of 3 m are identical and varies from 29.03 °C to 29.08 °C. This temperature is almost 8 °C less than the ambient temperature.

**Table 5.1** Depth wise variation in temperature of soil layers

| **Position of temperature sensor** | | **Average soil temperature for whole day in ºC** | | |
|---|---|---|---|---|
| | | 12-September | 13-September | 14-September |
| Depth wise variation of soil temperature | $T_1$ at 0.5 m depth | 32.9 | 33.0 | 33.2 |
| | $T_2$ at 1.0 m depth | 32.0 | 32.2 | 32.2 |
| | $T_3$ at 1.5 m depth | 31.4 | 31.4 | 31.5 |
| | $T_4$ at 2.0 m depth | 30.5 | 30.6 | 30.6 |
| | $T_5$ at 2.5 m depth | 29.7 | 29.7 | 29.8 |
| | $T_6$ at 3.0 m depth | 29.0 | 29.0 | 29.0 |

## 5.2 Performance analysis of glazed broad water channel PV/T (IPVTS) system coupled with EWHE cooling

The experimental study was performed under realistic conditions at BITS Pilani, Pilani campus, Rajasthan. The simulated values of SCs temperature, short-circuit current, open-circuit voltage, outlet temperatures of IPVTS and EWHE have been validated experimentally by conducting 6-hours experimental study on 20$^{th}$ September, 2016. The experiment was conducted for the mass flow of 0.033 kg/s. Fig. 5.9 represents the hourly variation in the solar radiation and ambient air temperature during the test day. The solar radiation and ambient air temperature ranges between 494 W/m$^2$ to 953 W/m$^2$ and 31.2 °C to 37.7 °C respectively. The IPVTS panel temperature with and without EWHE cooling for flow rate of 0.033 kg/s is shown in Fig. 5.10. It is observed that the PV panel temperature without any cooling ranges between 60.4 °C to 74.5 °C. Whereas, the IPVTS panel temperature drops with EWHE cooling and ranges from 39.27 °C to 46.11 °C and 41.70 °C to 49.32 °C for experimental and theoretical studies respectively. The IPVTS panel

temperatures were observed to increase in the afternoon period due to increased solar radiation and ambient temperature, leading to a decrease in the overall performance of the IPVTS system. The root mean square percent deviation (e) and correlation coefficient (r) are effective tools to find agreement between the experimental and theoretical results. Fig. 5.10 shows a good agreement between theoretical and experimental results. The mean square percent deviation (e) ranges from 5.82% to 6.67% while, the correlation coefficient (r) was 0.984.

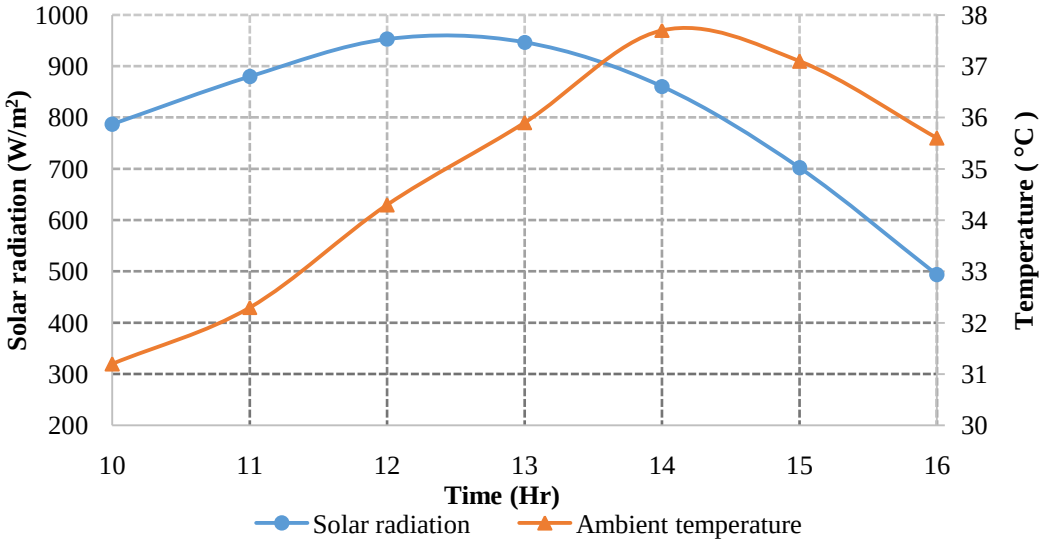


**Fig. 5.9** Variation of solar radiation and ambient air temperature during the test period

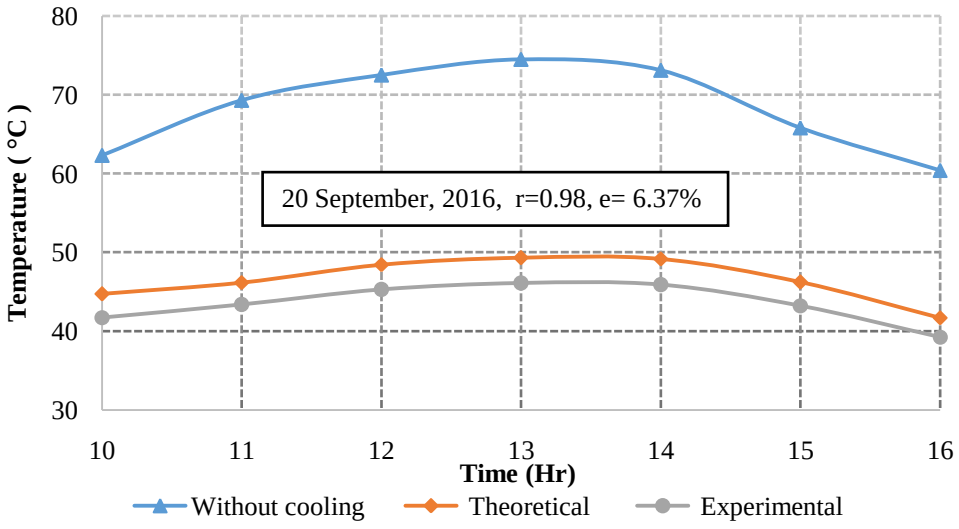


**Fig. 5.10**. Simulated and experimental values of IPVTS panel temperature during the test period

The theoretical and experimental results of the IPVTS inlet and outlet temperature is represented in Fig. 5.11. It is important to mention here that the outlet temperature of the EWHE is the inlet temperature of IPVTS and the IPVTS outlet temperature is an inlet temperature of EWHE in the coupled system. The theoretical results have been achieved by using the analytical approach of energy and mass balance. Although, during experimentation the outlet temperature of the EWHE was slightly higher than the theoretical values, due to heat transfer between the surroundings and connecting pipes. Thus, the experimental values of the IPVTS outlet temperature are also higher than theoretically calculated. The maximum experimental IPVTS outlet temperature at flow rates of 0.033 kg/s was observed to be 34.3 °C, while the IPVTS inlet temperature (i.e. EWHE outlet) varies between 30.3 °C to 30.7 °C during the test period. The IPVTS outlet temperatures also depended on the of the solar insolation intensity. The statistical analysis yields the root mean square percent deviation (e) and correlation coefficient (r) values, showing a good agreement between experimental and theoretical results as shown in Fig 5.11.

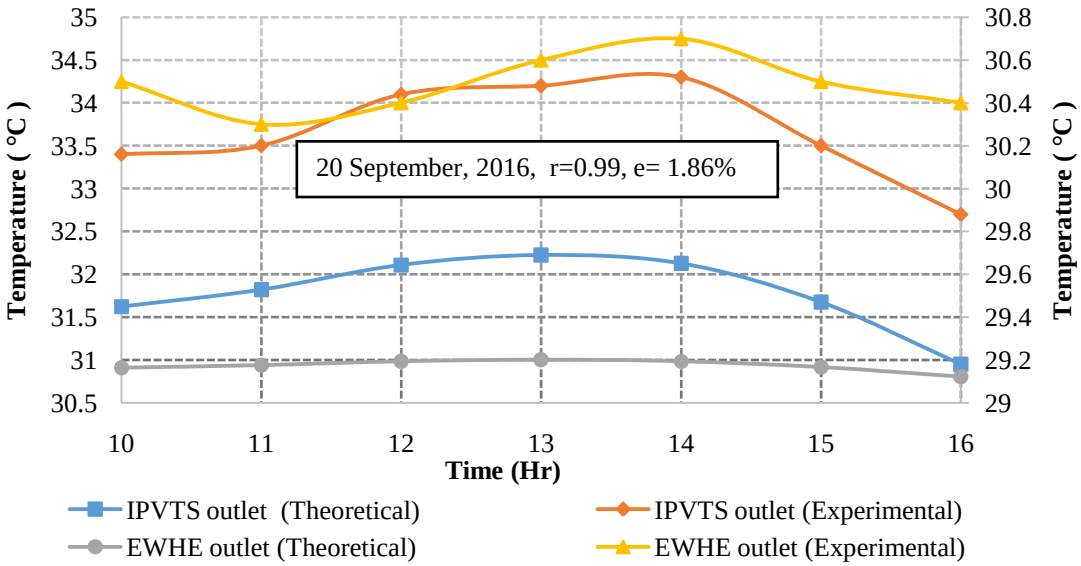


**Fig. 5.11**. Simulated and experimental values of IPVTS inlet and outlet temperature during the test period

The electrical efficiency of the IPVTS system with and without cooling for flow rate of 0.033 kg/s is shown in Fig. 5.12. The electrical efficiencies of the system with IPVTS cooling arrangement and a standalone PV panel were compared. The electrical efficiency of the standalone PV panel varied between 7.22% to 7.82% during the test period. The reason for this was found to be a high SCs temperature. Whereas, the electrical efficiency of the IPVTS panel

with EWHE cooling system was observed to be 8.28% to 8.60% and 8.42% to 8.68% for theoretical and experimental results respectively. It is observed that the electrical efficiency of the coupled system (IPVTS+EWHE) is increased by 0.78% to 1.05% and 0.86% to 1.19% for theoretical and experimental results respectively as compared to standalone PV panel efficiency. It was observed that the PV efficiency increases during the morning and evening periods, while, it decreases during the peak sunshine hours. The reason for this was found to be the change in PV temperature throughout the day. The PV panel efficiency drops at higher temperatures. The experimental and theoretical values of IPVTS collector thermal efficiency are represented in Fig. 5.13. It was observed that the thermal efficiency ranges from 40.92% to 48.11% and 46.55% to 57.01% for theoretical and experimental analysis respectively. The values of the root mean square percent deviation (e) and correlation coefficient (r) were $e = 11.90\%$ $r = 0.95$ which shows a good agreement between measured experimentally and theoretically calculated results.

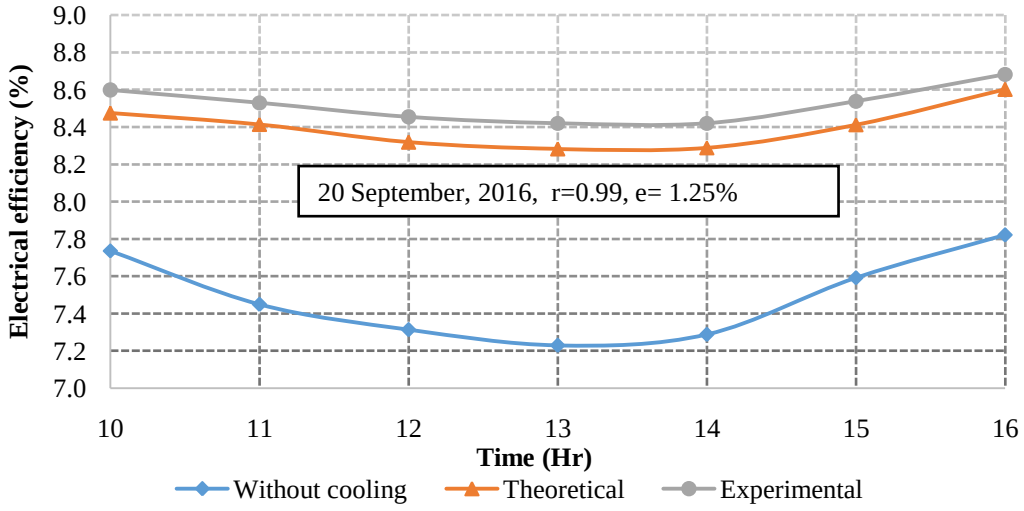


**Fig. 5.12**. Simulated and experimental values of electrical efficiency of IPVTS during test period

After an experimental validation for flow rate of 0.033 kg/s the analytical analysis has been carried out exhaustively for better understanding of the effect of different parameters on the panel temperature. The variation of IPVTS panel temperature with respect to various mass flow rates along the EWHE pipe length of 80 m at same environmental conditions is shown in Fig. 5.14. The IPVTS panel temperature ranges between 42.96 °C to 51.2 °C, 41.87 °C to 49.58 °C, 41.70 °C to 49.32 °C, 41.61 °C to 49.19 °C and 41.54 °C to 49.08 °C for the flow rates of 0.01 kg/s, 0.025 kg/s, 0.033 kg/s, 0.042 kg/s and 0.05 kg/s respectively. The IPVTS panel temperature

found to be decreased with an increase in flow rate of cooling water and becomes almost constant for the 0.033 kg/s, 0.042 kg/s and 0.05 kg/s flow rates. Hence 0.033 kg/s flow rate will give optimum results in the present study. With reduce PV panel temperature the thermal efficiency increases significantly with an increase in flow rate of cooling water due to high heat removal rate from the PV/T system. This in turns increases the electrical efficiency because of the low SCs temperature at high flow rates. Thus, in order to have a maximum electrical and thermal efficiency of the IPVTS system, the flow rate needs to be optimized within a suitable range.

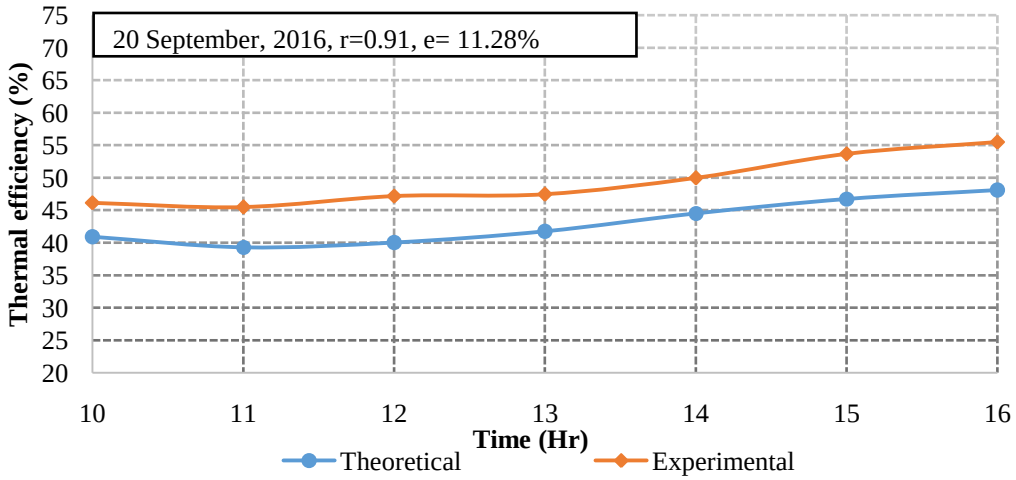


**Fig. 5.13**. Simulated and experimental values of thermal efficiency of IPVTS during the test day for various flow rates

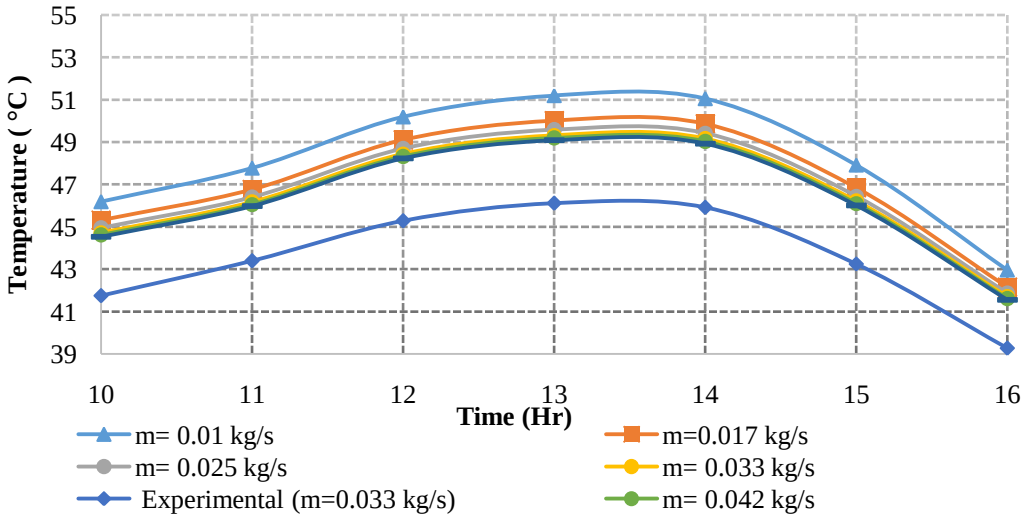


**Fig. 5.14**. IPVTS panel temperature for various flow rates of cooling water

Furthermore, the effect of the EWHE lengths on the IPVTS panel temperature at same ambient conditions is investigated also theoretically and represented in Fig. 5.15. It is found that the IPVTS panel temperature decreased with increase in EWHE pipe length from 15 m to 80 m. The maximum IPVTS panel temperature decreased for the 38 m length and beyond this the gradual drop is observed during afternoon time. From this, it is concluded that the pipe length of 38 m would be sufficient for such IPVTS+EWHE systems. The data recorded from temperature sensor T6, buried at a depth of 3 m shows no effect of variation of ambient temperature and solar radiation on the soil temperature at that depth. This data is presented in Table 5.2. It is evident that the soil temperature remained between 29.03 °C and 29.08 °C for experimental day. This temperature is almost 8.7 °C less than the ambient temperature.

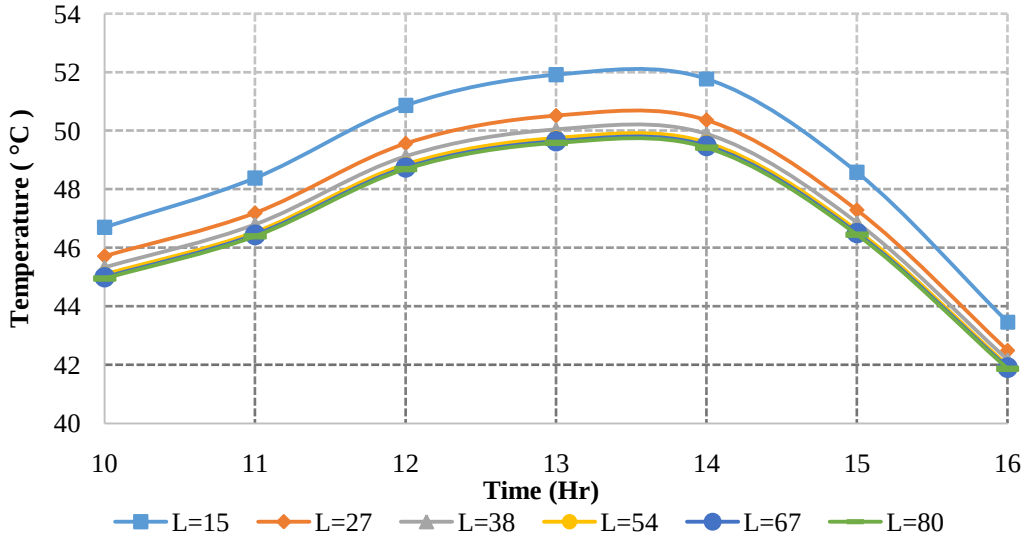


**Fig. 5.15**. IPVTS panel temperature for different EWHE pipe lengths with 0.025 kg/s flow rate

**Table 5.2.** Depth wise variation in temperature of soil layers

| **Position of temperature sensor** | | **Average soil temperature in ºC** 20-September, 2016 |
|---|---|---|
| Depth wise variation in temperature of soil layers | $T_1$ at 0.5 m depth | 33.7 |
| | $T_2$ at 1.0 m depth | 32.8 |
| | $T_3$ at 1.5 m depth | 31.9 |
| | $T_4$ at 2.0 m depth | 31.1 |
| | $T_5$ at 2.5 m depth | 30.2 |
| | $T_6$ at 3.0 m depth | 29.0 |

For the same day, the analysis has been performed for different channel depths of the IPVTS system, taking flow rate of 0.033 kg/s, the EAHE pipe length of 80 m. The variation of IPVTS temperature and IPVTS outlet temperature with various IPVTS channel depths are shown in Fig. 5.16 and Fig. 5.17 respectively. It is seen from the Fig. 5.16 that the IPVTS panel temperature ranges from 60.4 °C to 74.5 °C without any cooling. While in the case of EWHE cooling, the IPVTS panel temperature ranges from 39.15 °C to 45.55 °C, 40.12 °C to 47.02 °C, 40.96 °C to 48.27 °C and 41.69 °C to 49.36 °C with 10 mm, 20 mm, 30 mm and 40 mm channel depths, respectively. It was also observed that with an increase in channel depth, the Reynolds number decreases. This leads to a smaller Nusselt number and smaller convective heat transfer coefficient, resulting in less of a decrease in IPVTS panel temperature. Fig. 5.17 represents the IPVTS outlet temperature variation with channel depth. Similar to the previous case, here also with increase in channel depth, IPVTS outlet temperature decreases due to lower heat transfer. Therefore, it is essential to adopt an optimized channel depth for design of such a coupled system and for that, 10 mm could be taken as the optimum value.

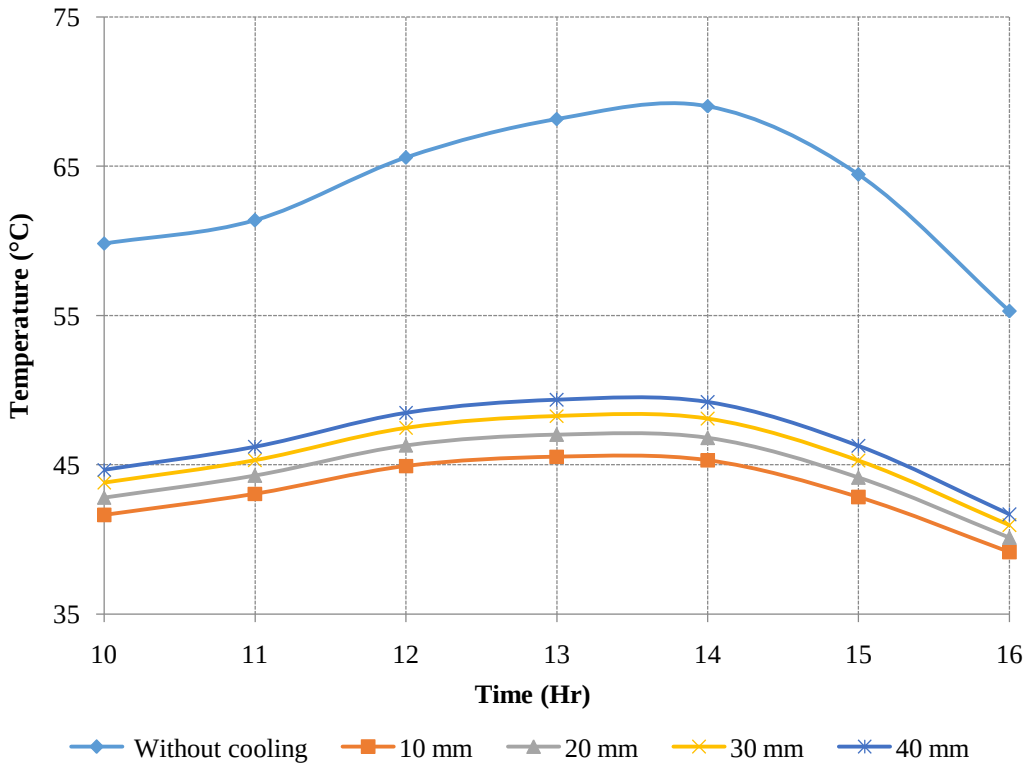


**Fig. 5.16**. IPVTS panel temperature for various channel depths with mass flow rate of 0.033 kg/s

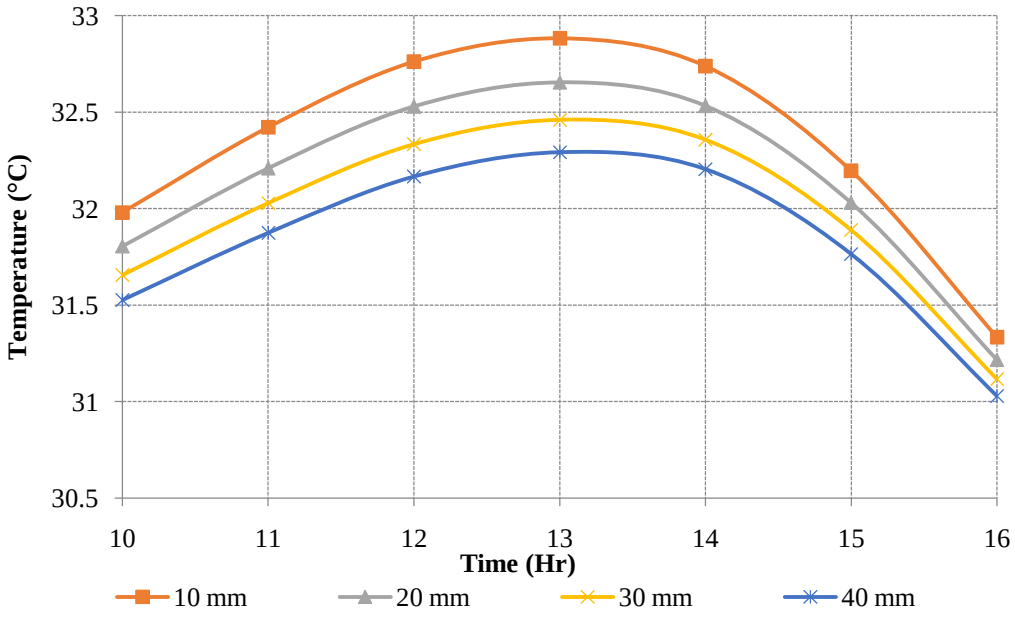


**Fig. 5.17**. IPVTS outlet temperature for various channel depths with mass flow rate of 0.033 kg/s

## 5.3 Performance analysis of rooftop glazed PV/T system coupled with EAHE cooling for combined electrical power and space heating

As discussed in chapter 3, one dimensional steady state analysis has been performed for rooftop PV/T with an EAHE system for the combined electrical power and space heating, by developing an algorithm using MATLAB software. The simulations have been performed for climatic conditions of Pilani, Ajmer (India) and Las Vegas (USA) which are semi-arid and arid regions. Based on the weather parameters like solar insolation, ambient temperature, etc., the daily performance evaluation is an effective test method to explain electrical and thermal performance of a PV/T coupled with EAHE system. In the present study, four days are selected in the month of November and December for each of the locations so that maximum efficiency could be achieved during peak winter period. Firstly, for these locations, SCs temperature, PV/T outlet temperature, EAHE outlet temperature and electrical efficiency of the PV/T system have been calculated for different mass flow rates. Following that, a parametric simulation is conducted for taking climatic conditions of Pilani as a base case to investigate the effects of various major operating parameters like PV/T channel depth, EAHE length and PV/T collector length.

The weather data, which include solar radiation and ambient temperature for locations of Pilani, Ajmer and Las Vegas, are shown in Fig. 5.18 (a), (b), (c) and (d).

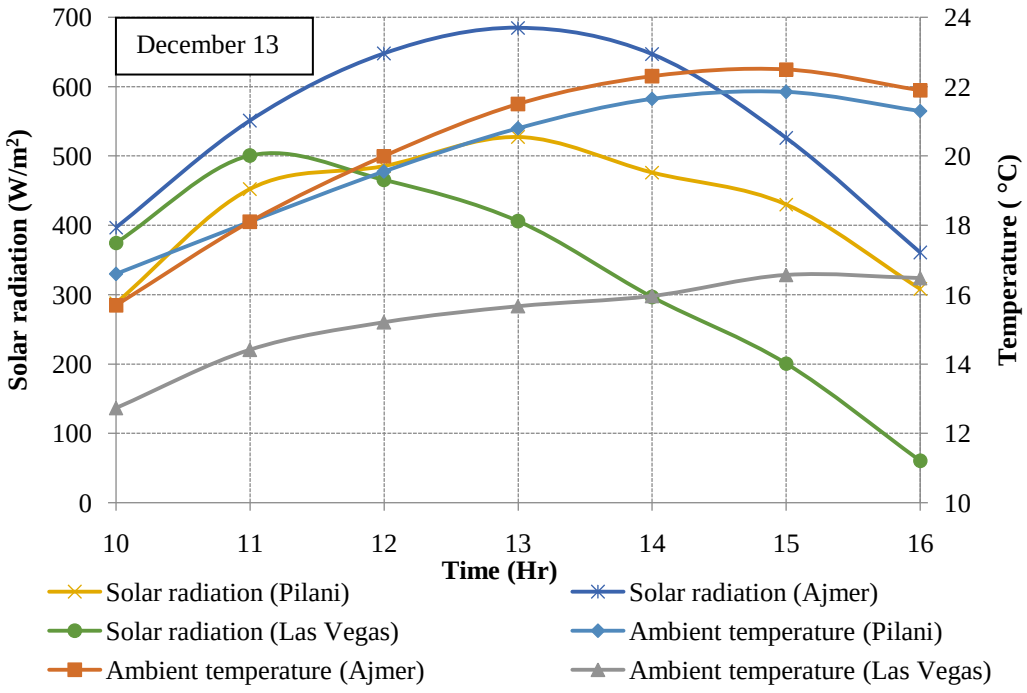


(a)

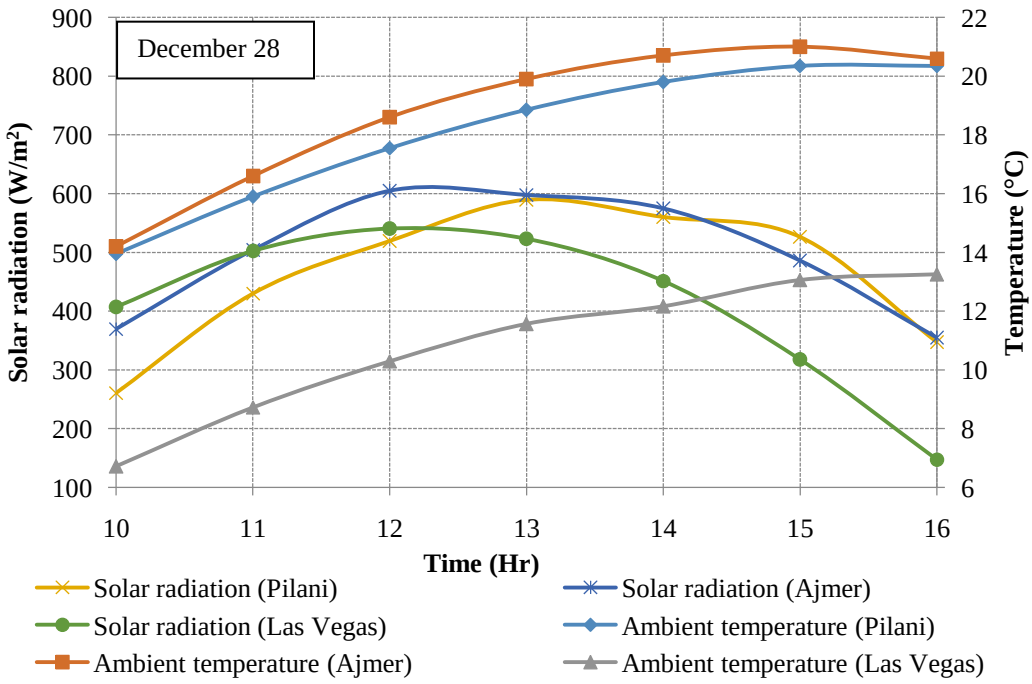


(b)

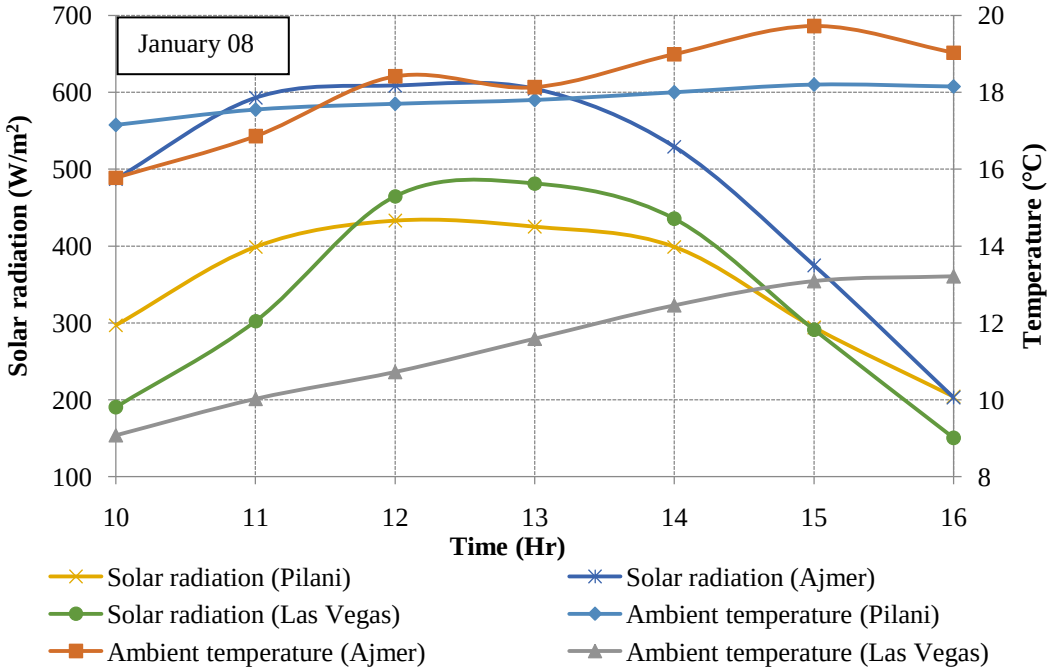


(c)

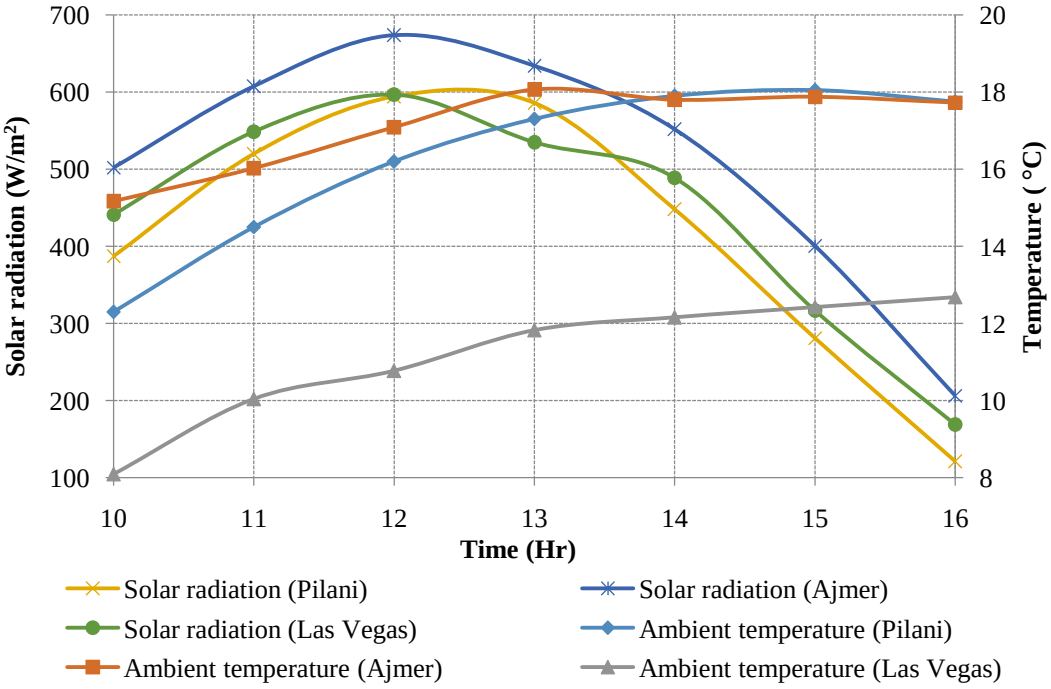


(d)

**Fig. 5.18** (a), (b), (c) and (d). Variation of solar radiation and ambient temperature for the conditions of Pilani, Ajmer and Las Vegas

It is important to mention here that the weather conditions for Pilani were taken from a Meteonorm file. While for Ajmer, the conditions were taken from a weather station at the government engineering college, Ajmer, and for Las Vegas, it was taken from the weather station of the Center For Energy Research, UNLV, Las Vegas. The ambient temperature and solar radiation for Pilani on 13 Dec., ranges between 12.3 °C to 18.1 °C and 121 W/m$^2$ to 594 W/m$^2$ respectively. For the same day, it varies from 15.2 °C to 18.1 °C and 206 W/m$^2$ to 674 W/m$^2$ for Ajmer and 8.1 °C to 12.7 °C and 168.9 W/m$^2$ to 596.6 W/m$^2$ for Las Vegas. It was observed that for all locations, the ambient temperature was lower than required for the human comfort level. It was further observed from Fig. 5.18 (a), (b), (c) and (d) that on 28 December, the maximum and minimum ambient temperature for Pilani, Ajmer and Las Vegas were 20.1 °C, 20.7 °C and 13.3 °C and 13.9 °C, 14.2 °C and 6.7 °C respectively.

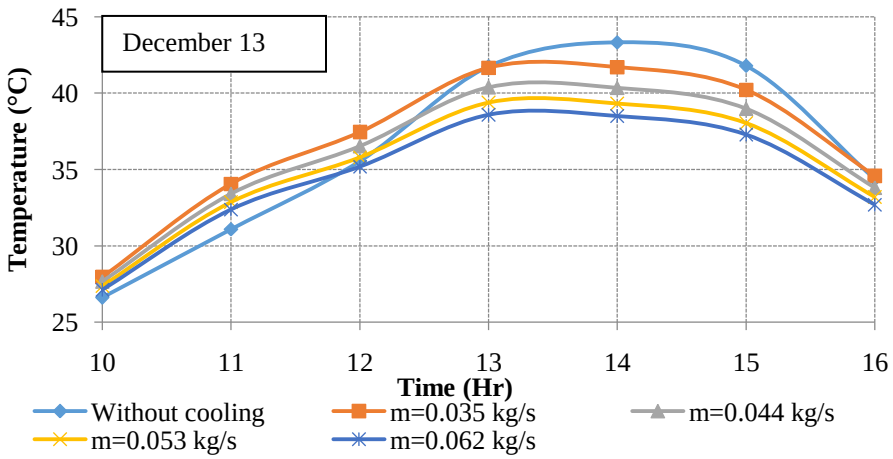


(a)

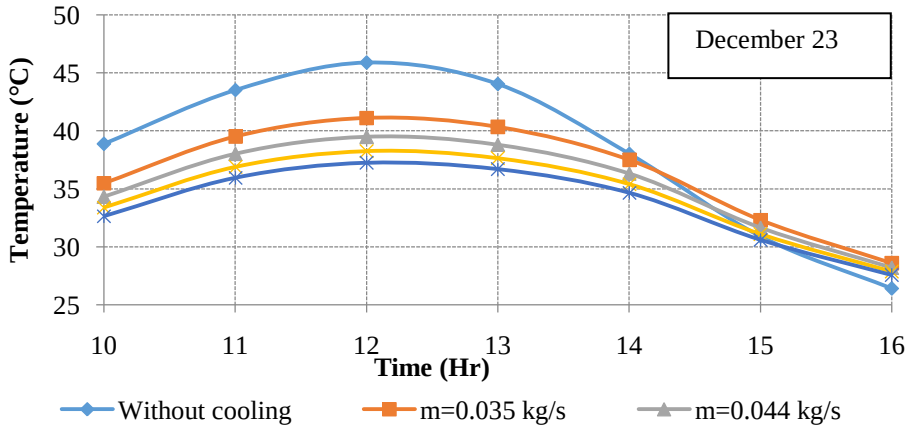


(b)

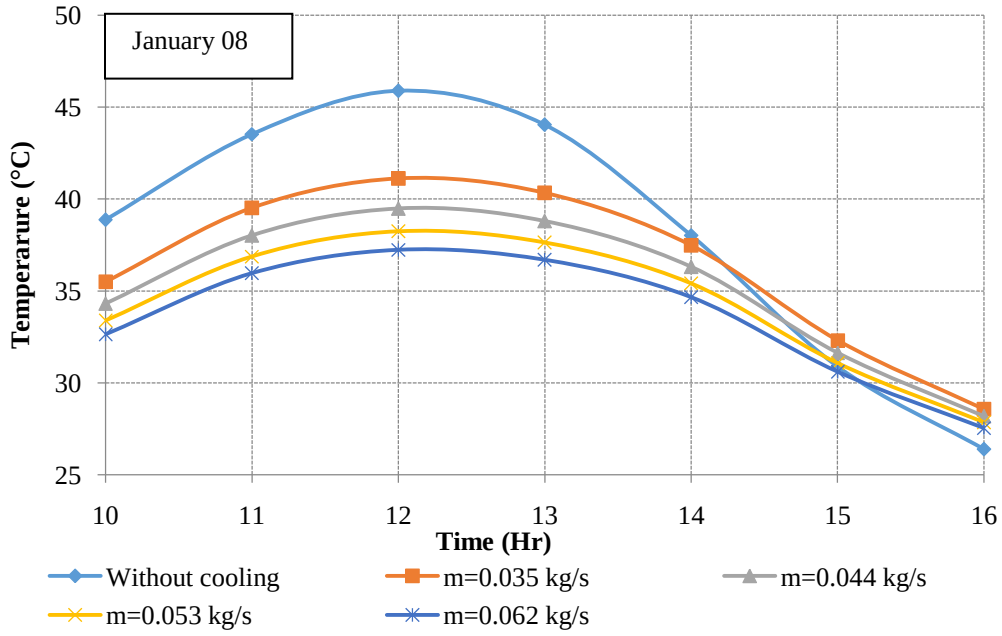


(c)

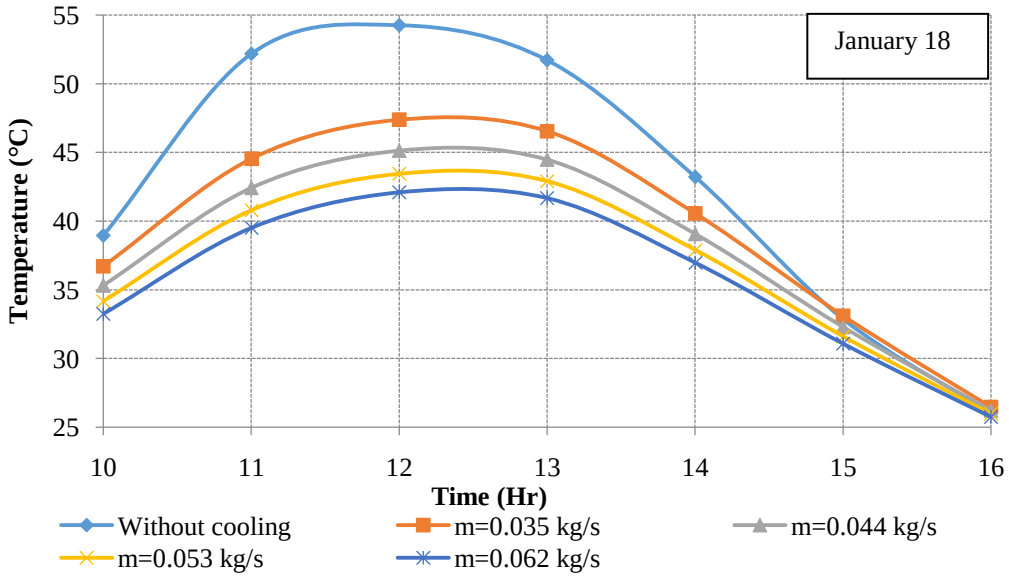


(d)

**Fig. 5.19** (a), (b), (c) and (d). SCs temperature with and without cooling for Pilani with different mass flow rates

The hourly variation of SCs temperature with and without cooling for mass flow rates of 0.035 kg/s, 0.044 kg/s, 0.053 kg/s and 0.062 kg/s are shown in Fig. 5.19-5.21 for all three conditions. For Pilani and Ajmer, the analysis has been carried out during PV operating hours (i.e. from 10

AM to 4 PM). In case of Las Vegas the operating hours were from 11 AM to 3 PM as before and after that the SCs temperature was less than 25 °C and didn't require any cooling. It was observed from simulations that for 18 January, the maximum SCs temperature without cooling goes up to 54.3 °C and 54.5 °C for the Pilani and Ajmer, respectively. While on 13 December, the maximum SCs temperature goes to 44.4 °C, for the Las Vegas. This indicates that even during the winter peak, there is certainly a need for cooling of the PV to maintain SCs temperature.

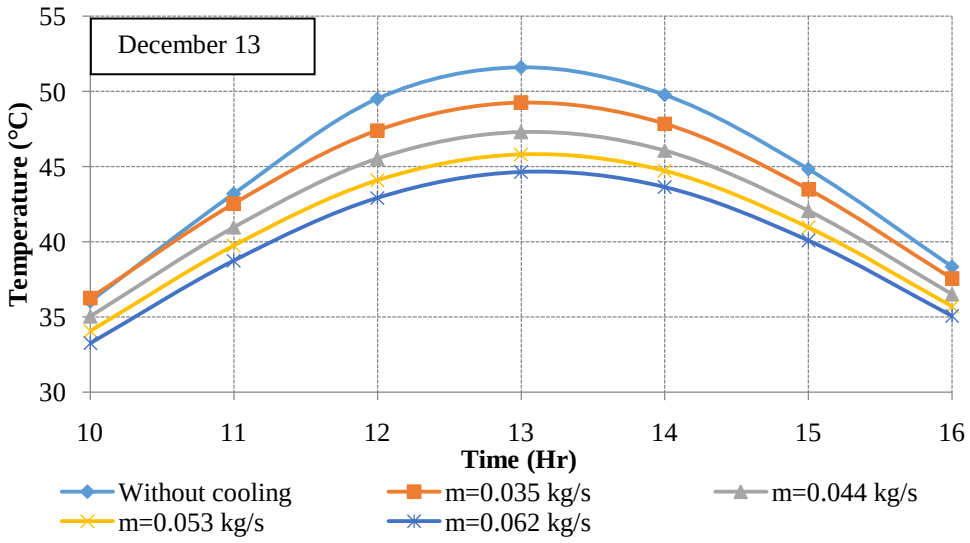


(a)

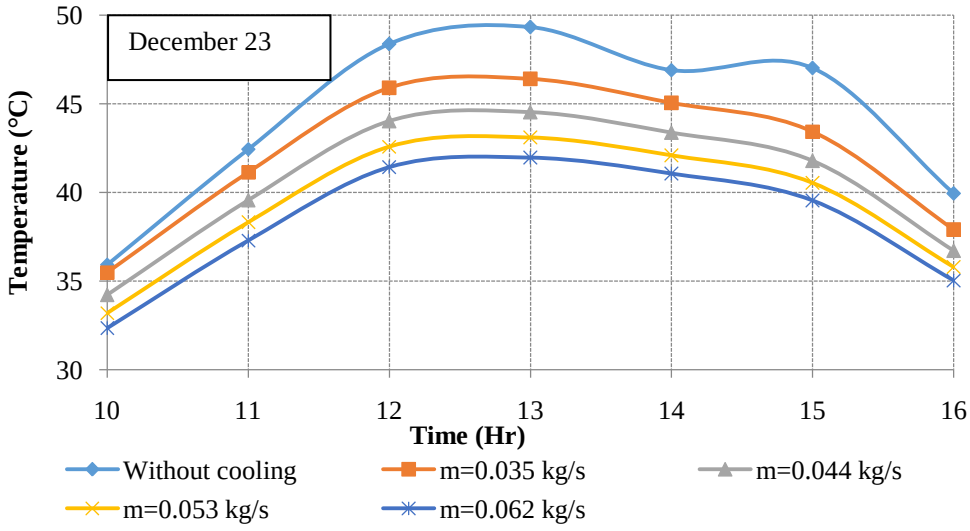


(b)

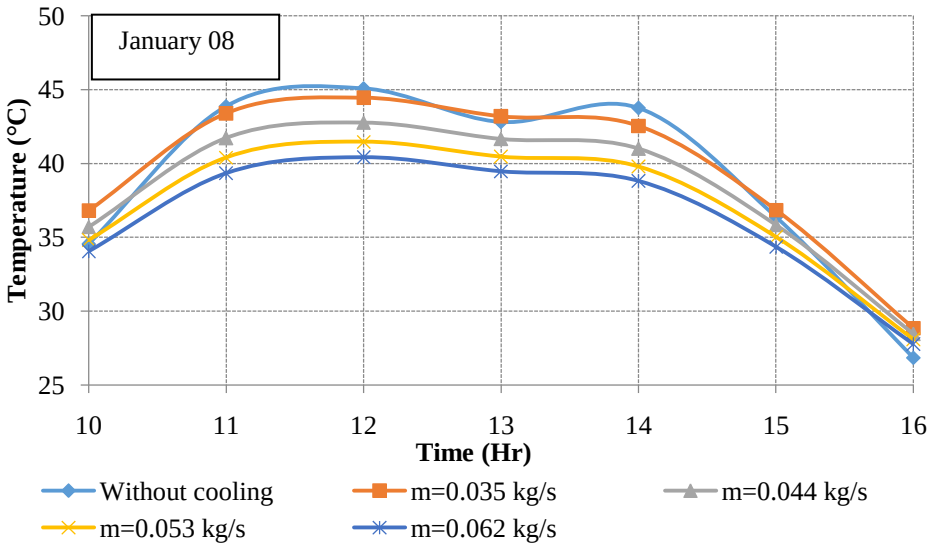


(c)

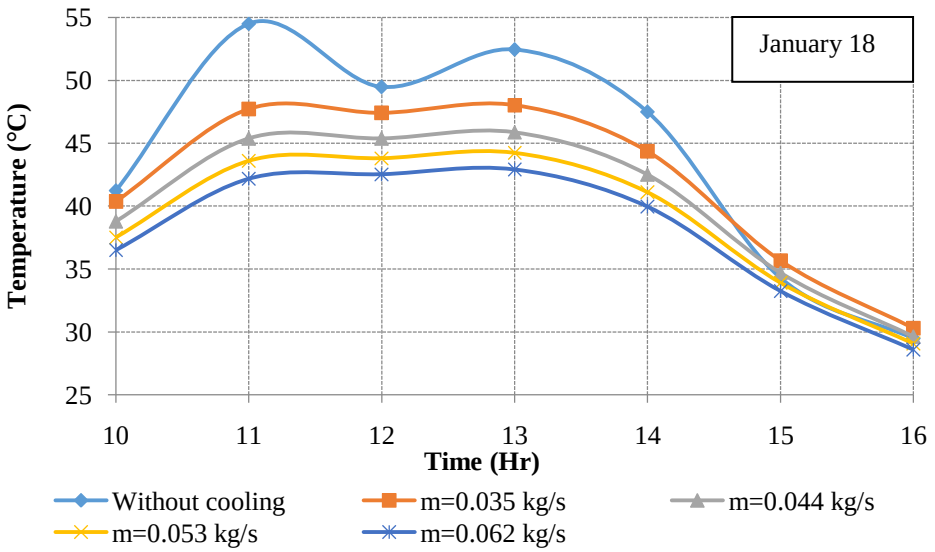


(d)

**Fig. 5.20** (a), (b), (c) and (d). SCs temperature with and without cooling for Ajmer with different mass flow rates

Further, the analysis showed that the SCs temperature ranges between 26.1 °C to 43.4 °C for Pilani and 29.1 °C to 44.2 °C for Ajmer with EAHE cooling for the flow rate of 0.053 kg/s, on January, 18. For December 13 at same mass flow rate, it lies between 25.6 °C to 35.6 °C for the case of Las Vegas conditions. Thus, it was inferred that for mass flow rate of 0.053 kg/s, the maximum SCs temperature drop was 11.4 °C, 10.9 °C and 8.8 °C for Pilani, Ajmer and Las Vegas, respectively. The temperature decreases significantly with the increase in mass flow rate

of air up to 0.053 kg/s, after which the temperature change is negligible (0.023 °C to 1.20 °C) from 0.053 kg/ and 0.062 kg/s.

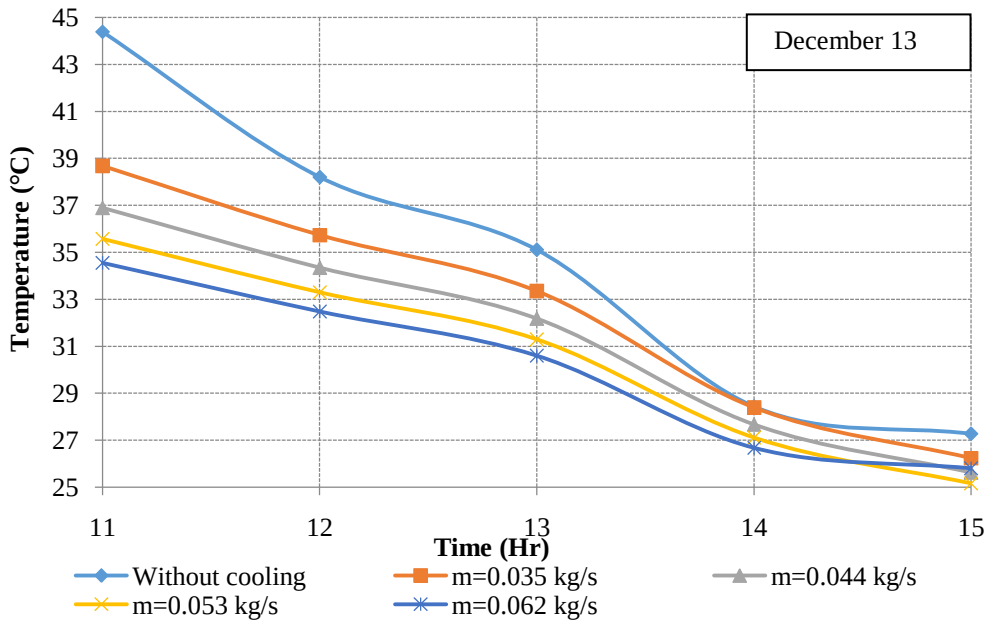


(a)

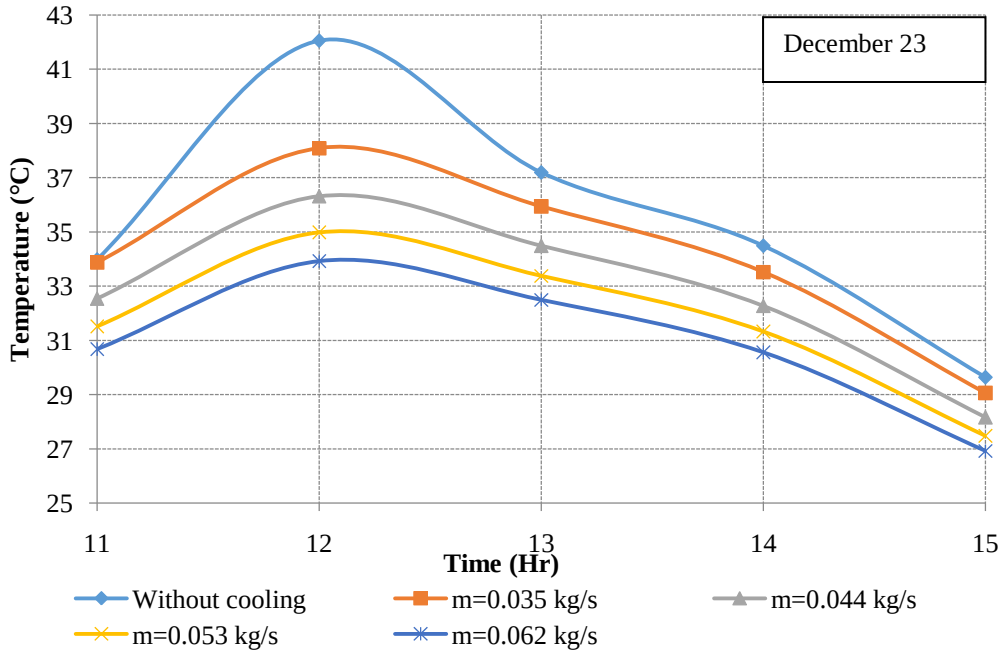


(b)

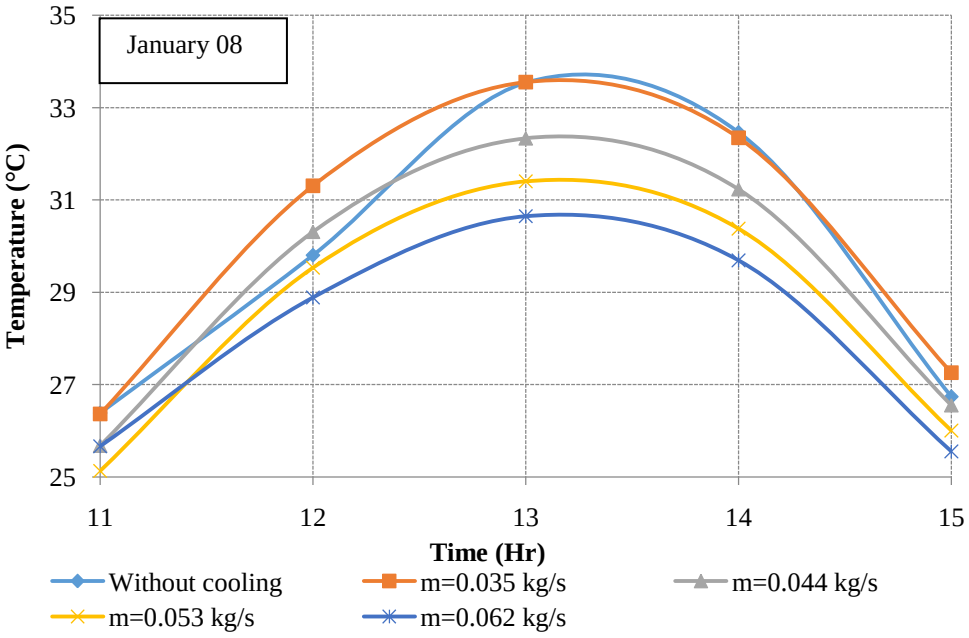


(c)

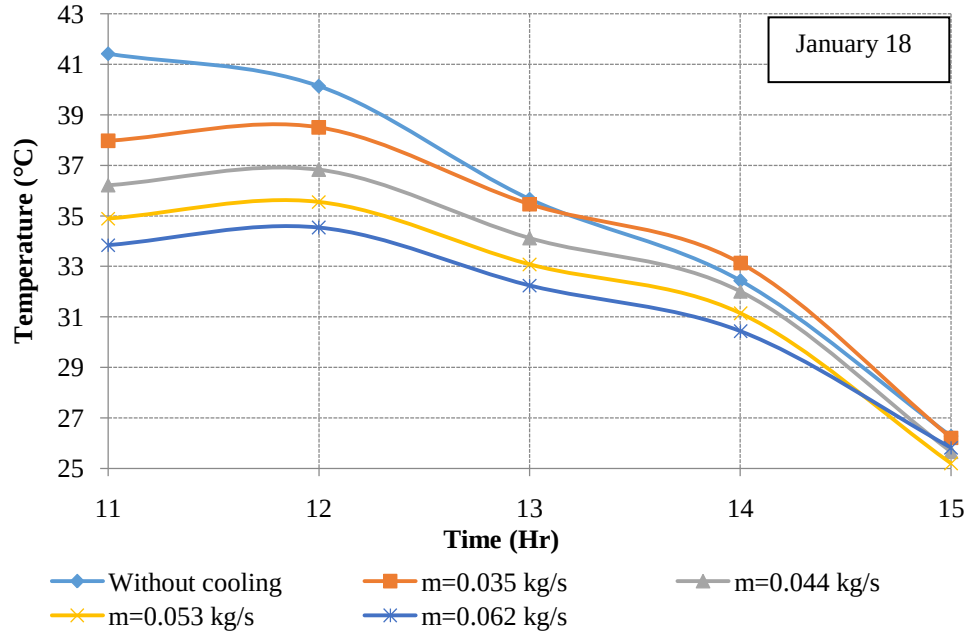


(d)

**Fig. 5.21 (a), (b), (c) and (d)**. SCs temperature with and without cooling for Las Vegas with different mass flow rates

The graphical representation of PV cell temperature based electrical efficiency with cooling and without cooling for all three locations is shown in Fig. 5.22-5.24. The electrical efficiency comparison has been carried out by taking cooling air channel and without any channel i.e. normal PV panel. It was observed that in case of without cooling, the cell electrical efficiency varies from 10.90% to 9.55%, 10.90% to 9.54% and 10.92% to 10.04% for Pilani, Ajmer and Las Vegas respectively during all test days. The reason for the same is mentioned above that, the efficiency decreases with enhance in operating SCs temperature.

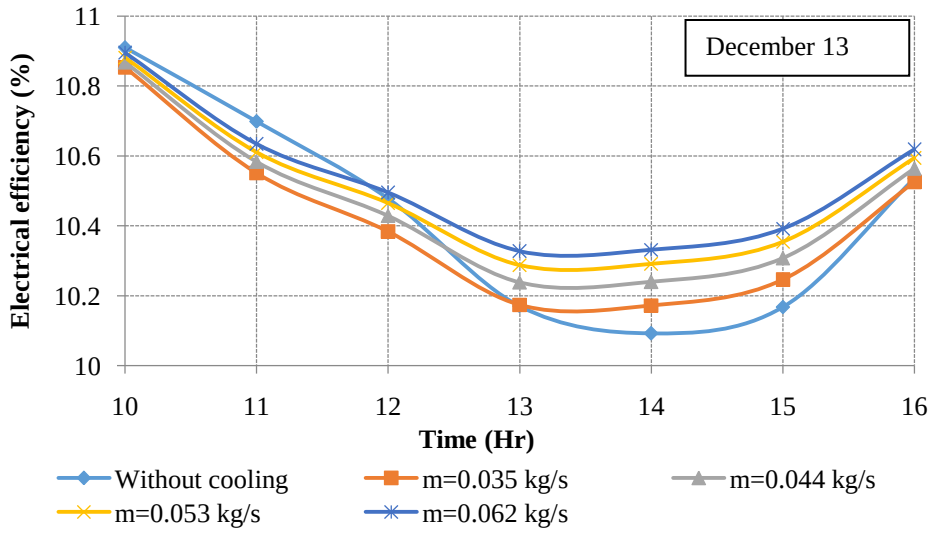


(a)

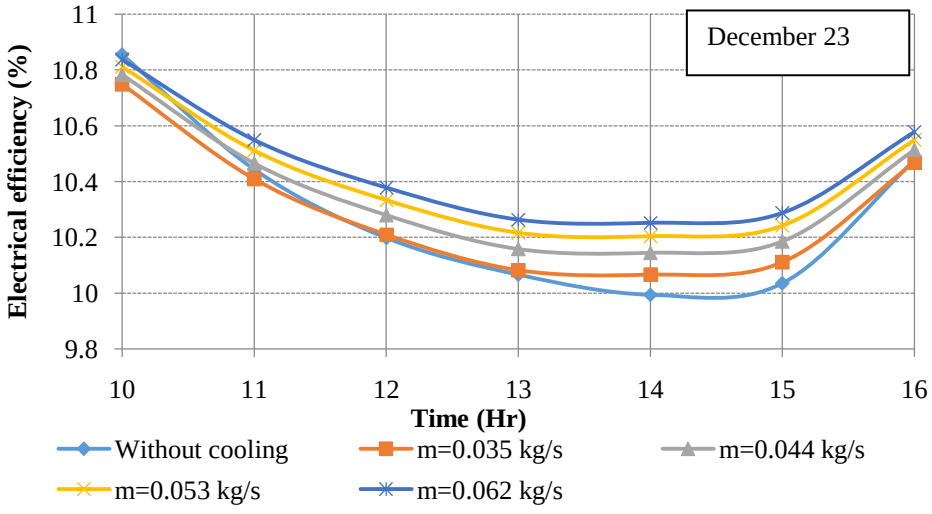


(b)

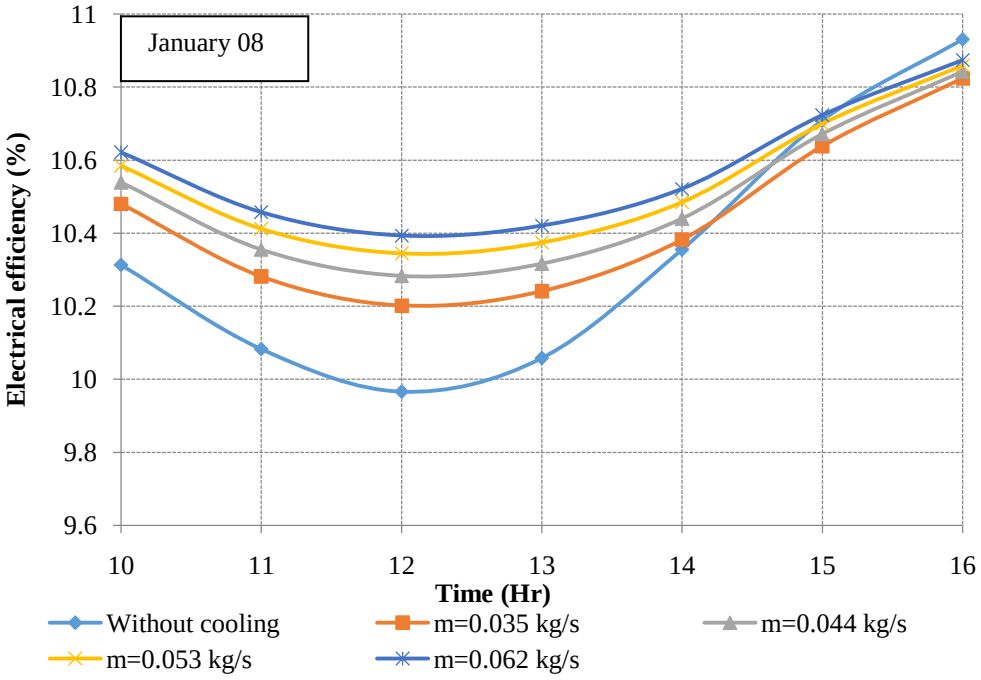


(c)

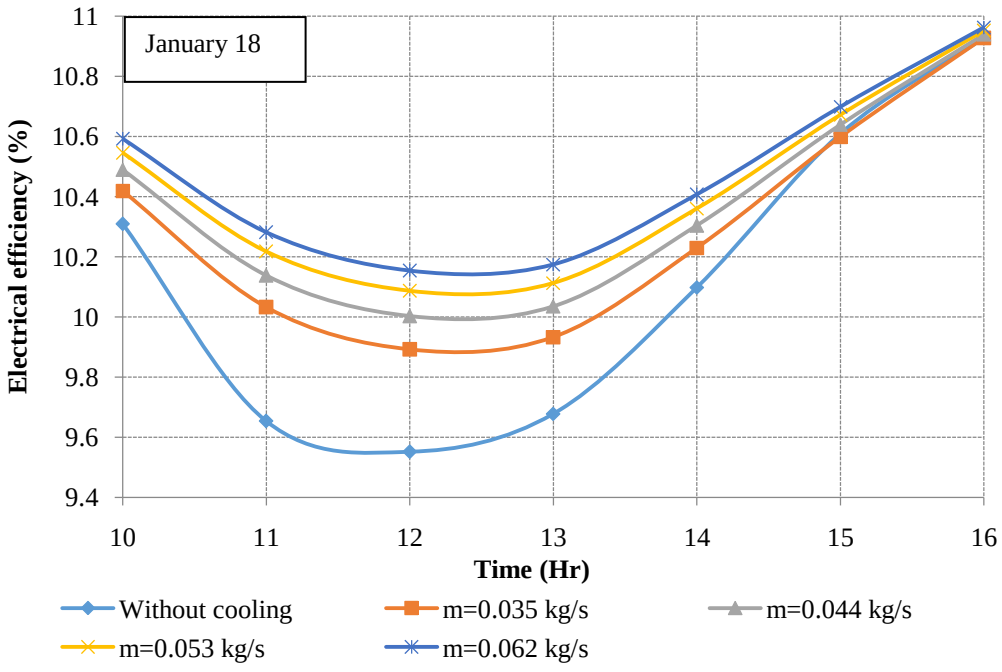


(d)

**Fig. 5.22 (a), (b), (c) and (d)**. Electrical efficiency of SCs with and without cooling for Pilani for various flow rates

For the chosen dates of respective locations, the cell electrical efficiency varies from 10.9% to 10.1%, 10.4% to 10.1% and 10.9% to 10.5% for Pilani, Ajmer and Las Vegas with EAHE cooling at mass flow rate of 0.053 kg/s. It was also observed that the with EAHE cooling, the maximum cell efficiency increased by 0.62%, 0.61% and 0.48% for the Pilani, Ajmer and Las Vegas respectively for mass flow rate of 0.053 kg/s. Thus, EAHE cooling is beneficial during winter season as it cools the PV and provides hot air for space heating. It was observed for Pilani and Ajmer that the cell efficiency was higher during the morning and evening and during peak sunshine hours, but it decreases which is mainly due to higher ambient temperature which eventually decreases the cell efficiency.

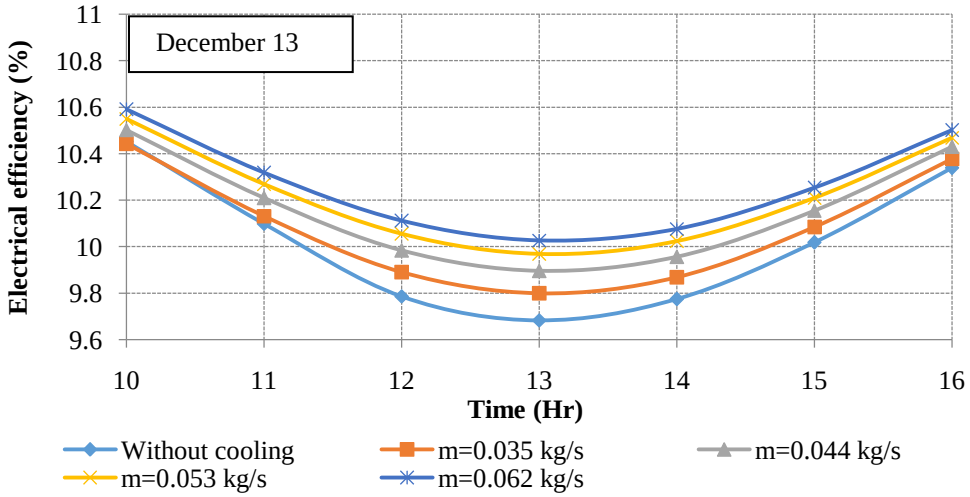


(a)

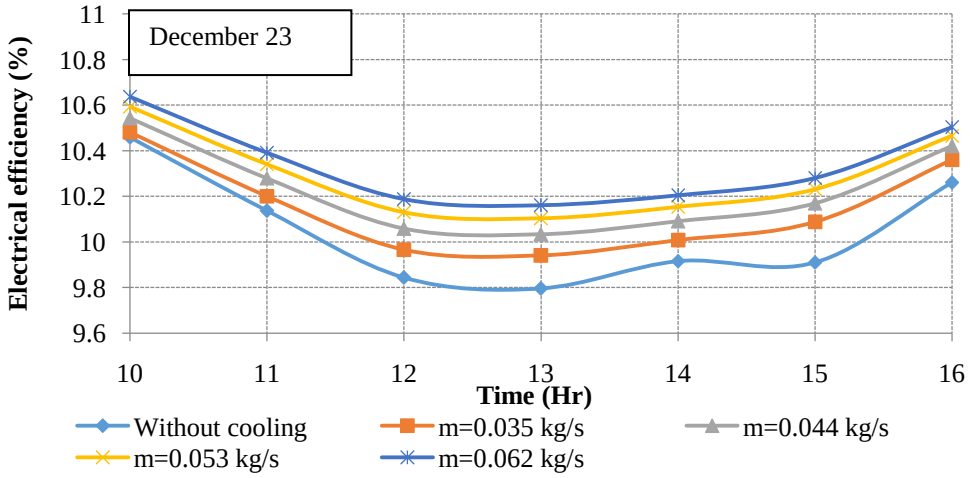


(b)

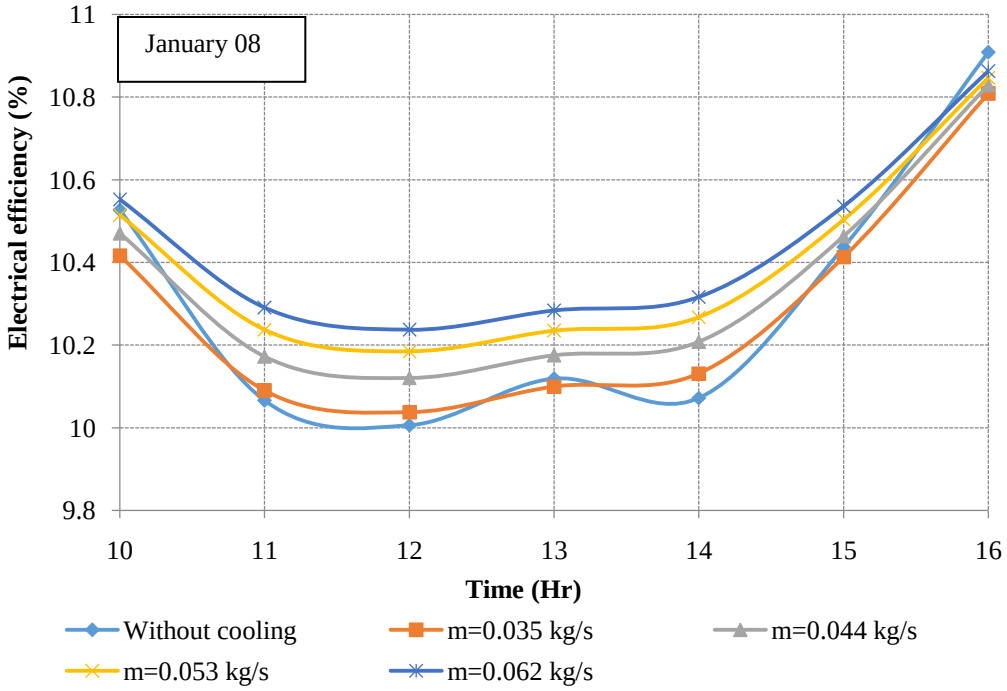


(c)

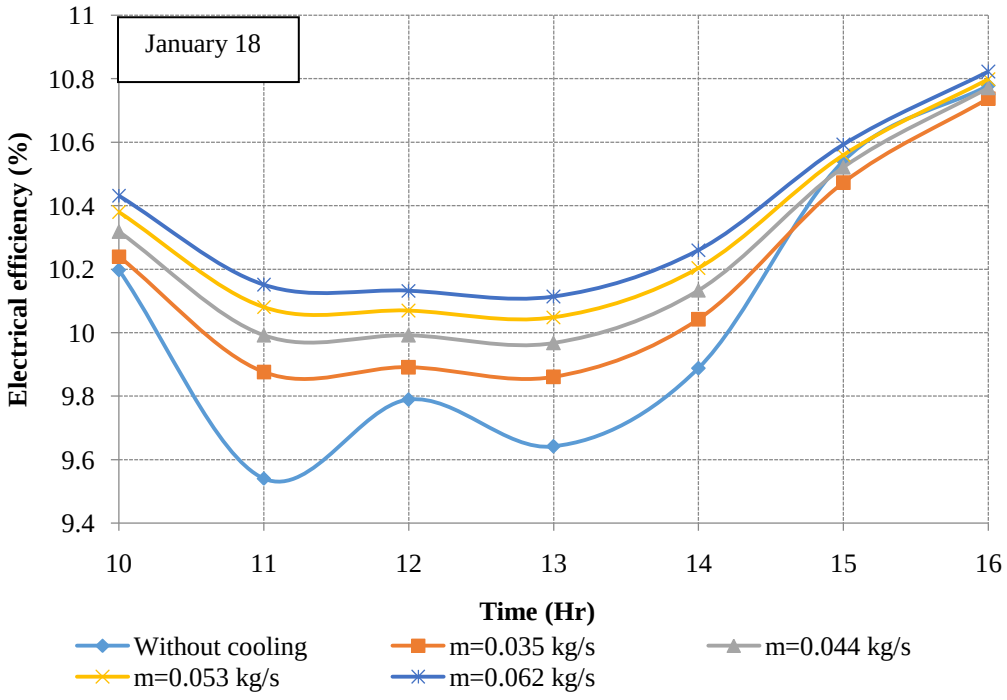


(d)

**Fig. 5.23 (a), (b), (c) and (d)**. Electrical efficiency of SCs with and without cooling for Ajmer for various flow rates

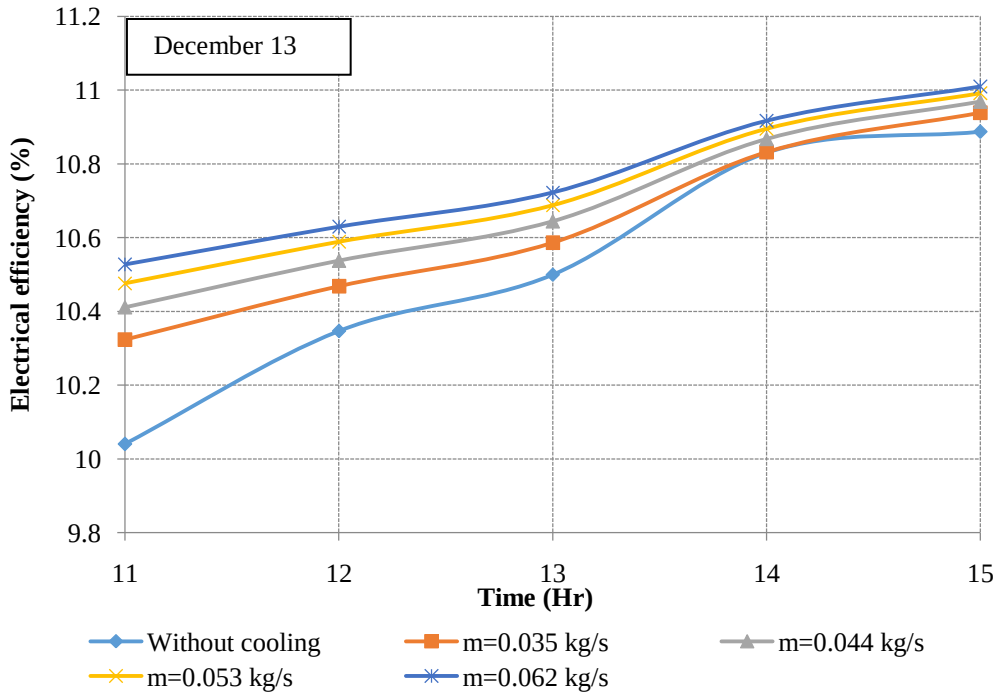
December 13
Electrical efficiency (%)
11.2
11
10.8
10.6
10.4
10.2
10
9.8
11
12
13
14
15
Time (Hr)
Without cooling
m=0.035 kg/s
m=0.044 kg/s
m=0.053 kg/s
m=0.062 kg/s

(a)

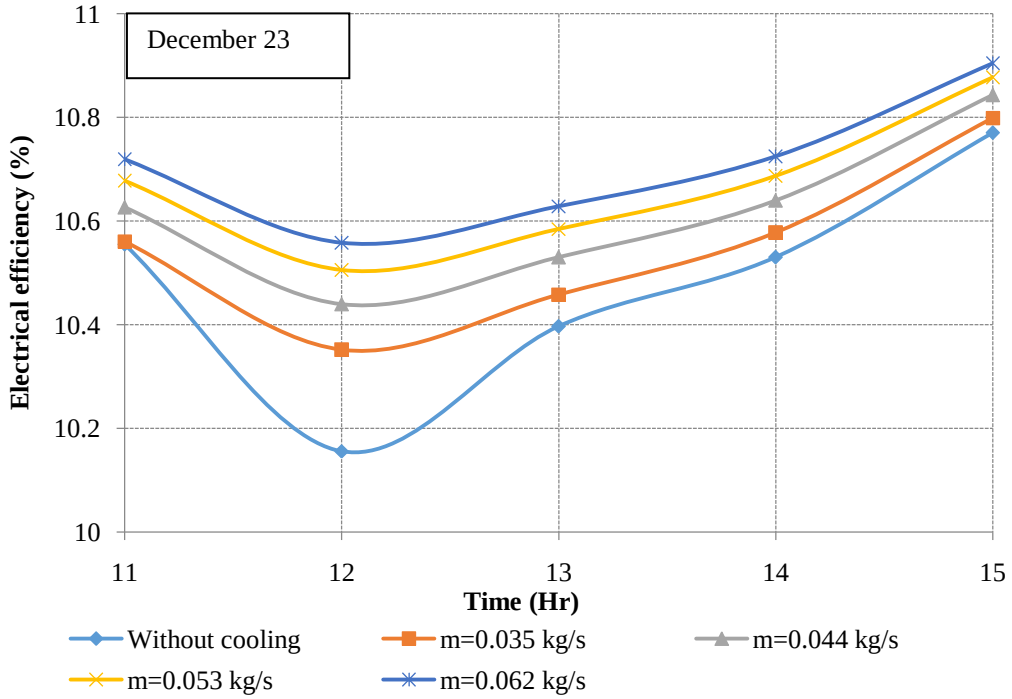
December 23
Electrical efficiency (%)
11
10.8
10.6
10.4
10.2
10
11
12
13
14
15
Time (Hr)
Without cooling
m=0.035 kg/s
m=0.044 kg/s
m=0.053 kg/s
m=0.062 kg/s

(b)

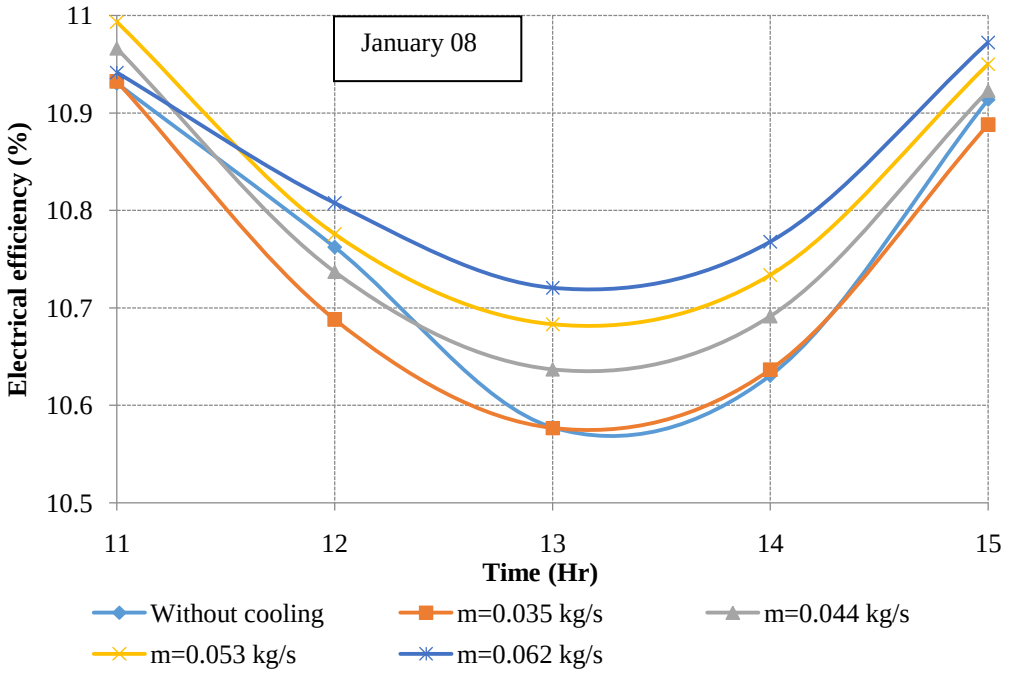


(c)

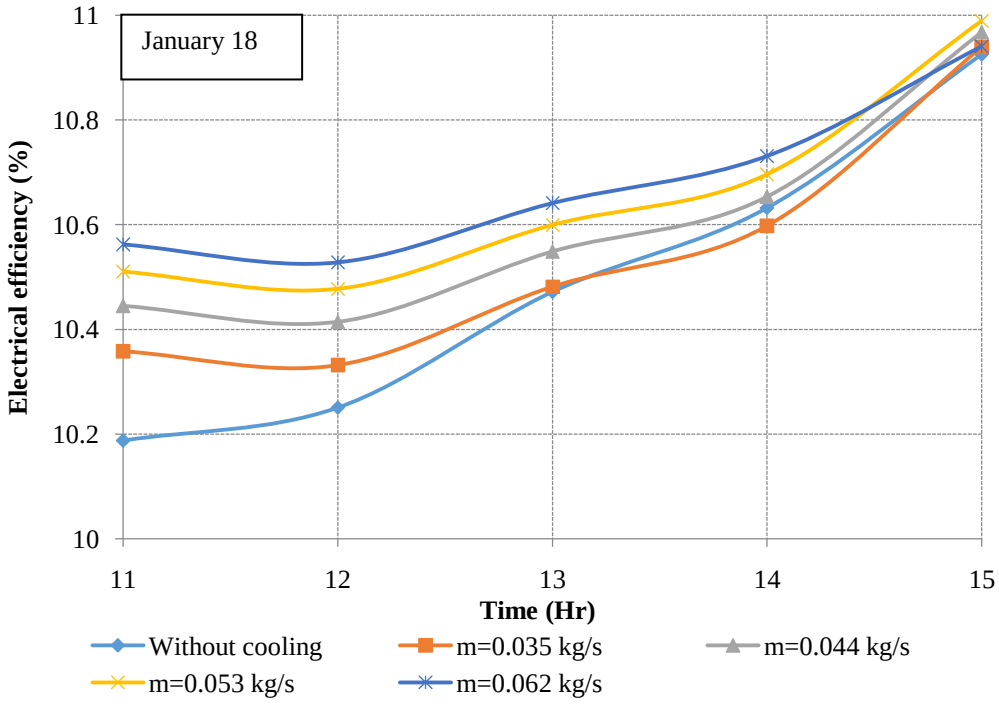


(d)

**Fig. 5.24 (a), (b), (c) and (d)**. Electrical efficiency of SCs with and without cooling for Las Vegas for various flow rates

The hourly variation of PV/T outlet air temperature and EAHE outlet air temperature for all three conditions during all analysis days are shown in Fig. 5.25-5.27. This is important to mention here that ambient temperature is same as the EAHE inlet temperature and outlet temperature of the EAHE is the inlet temperature of the PV/T system. From Fig. 5.25, it was observed that outlet temperature of the EAHE ranges from 23.8 °C to 24.9 °C and 24.3 °C to 24.5 °C for December 23 and January 08 with a flow rate of 0.053 kg/s for Pilani. On the other hand, the PV/T outlet temperature ranges from 24.7 °C to 29.7 °C and 24.9 °C to 29.8 °C for the same days with same flow rate. The outlet temperature of the EAHE and PV/T for Las Vegas are shown in Fig. 5.27. From Fig. 5.27 it was observed that the EAHE outlet temperature ranges from, 18.8 °C to 19.2 °C and 18.5 °C to 18.9 °C for December, 13 and January 08 with the flow rate of 0.053 kg/s. Whereas, the PV/T outlet temperature ranges from 19.5 °C to 23.4 °C and 20.5 °C to 22.6 °C for the same days with same flow rate. Fig. 5.25-5.27 show that the outlet temperature of EAHE air is almost constant irrespective of the time and duration for all three conditions. It was also observed that the temperature of air at the outlet of the PV/T system is higher than that obtained from only the EAHE system. Coupling the PV/T system with the EAHE system increased the air temperature by 5.6 °C, 5.9 °C and 5.1 °C for Pilani, Ajmer and Las Vegas, respectively, with a 0.053 kg/s flow rate on January 18. It can be concluded from this that the hybrid system of EAHE with PV/T not only decreases the cell temperature but also increases the air temperature which can be directly utilized for space heating. Using this coupled system, the heating load of the building could be reduced.

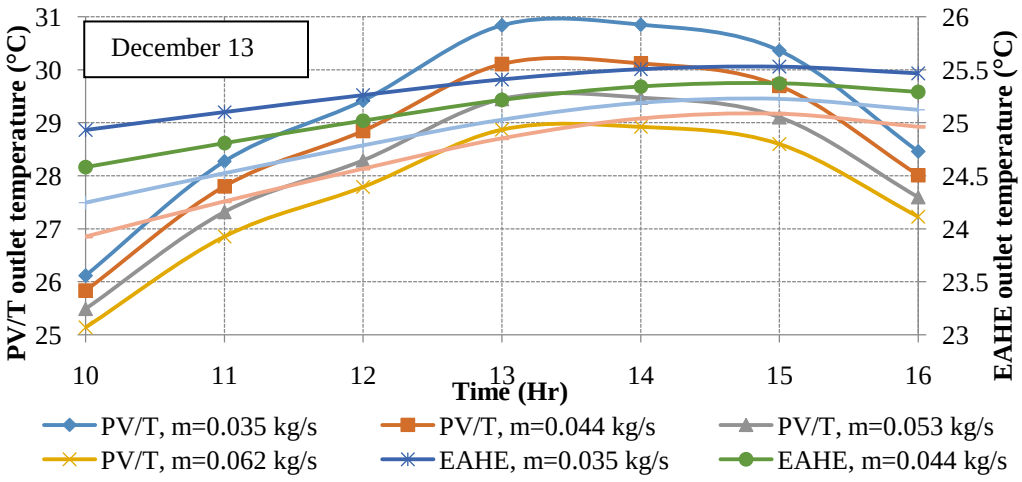


(a)

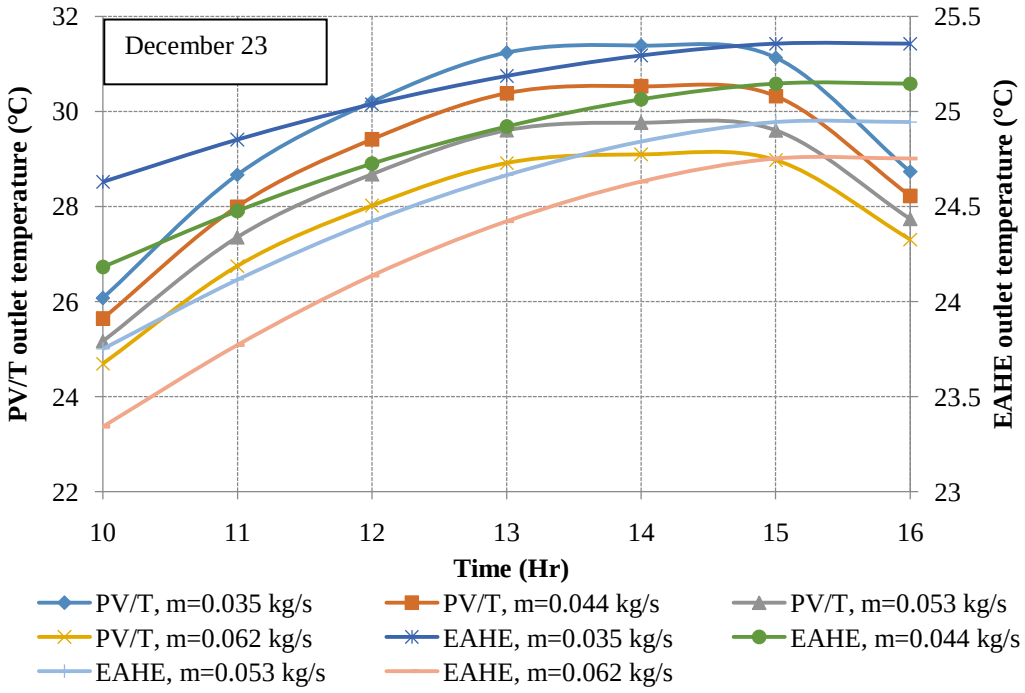
December 23
PV/T outlet temperature (°C)
EAHE outlet temperature (°C)
Time (Hr)
PV/T, m=0.035 kg/s
PV/T, m=0.044 kg/s
PV/T, m=0.053 kg/s
PV/T, m=0.062 kg/s
EAHE, m=0.035 kg/s
EAHE, m=0.044 kg/s
EAHE, m=0.053 kg/s
EAHE, m=0.062 kg/s

(b)

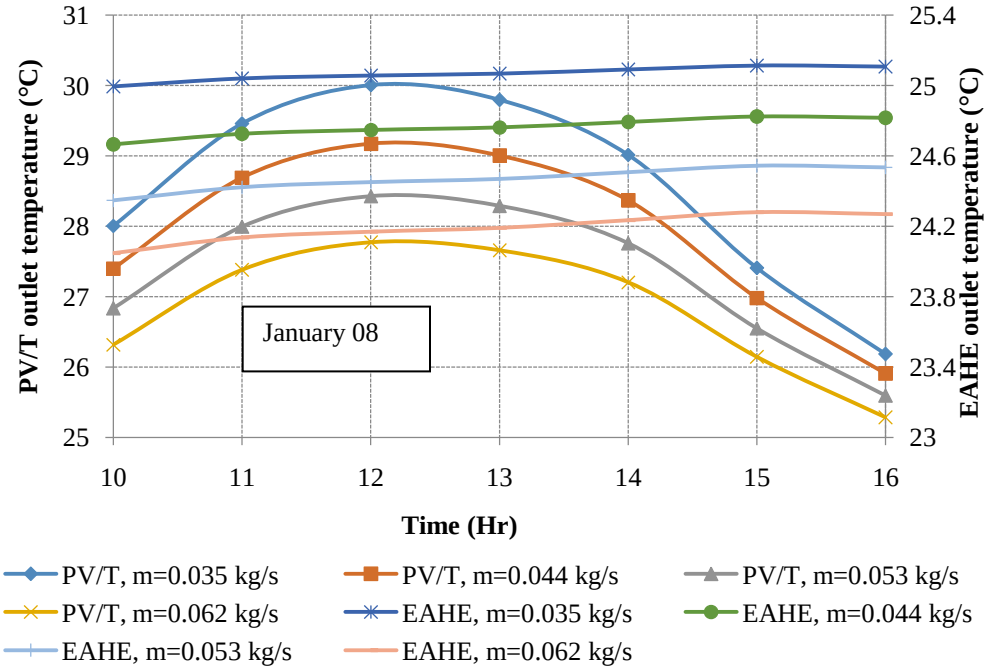
January 08
PV/T outlet temperature (°C)
EAHE outlet temperature (°C)
Time (Hr)
PV/T, m=0.035 kg/s
PV/T, m=0.044 kg/s
PV/T, m=0.053 kg/s
PV/T, m=0.062 kg/s
EAHE, m=0.035 kg/s
EAHE, m=0.044 kg/s
EAHE, m=0.053 kg/s
EAHE, m=0.062 kg/s

(c)

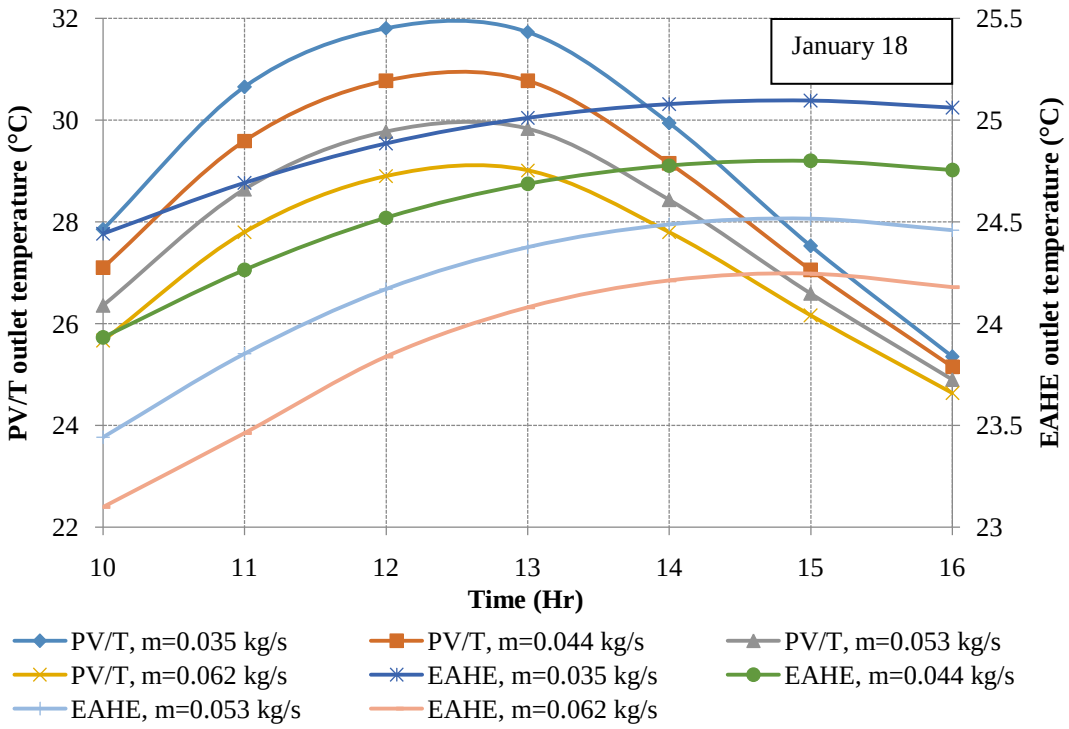


(d)

**Fig. 5.25 (a), (b), (c) and (d)**. EAHE and PV/T outlet temperature for Pilani for various flow rates

It was also observed from Fig.5.25-5.27 that at low flow rate, the outlet temperature of the PV/T and EAHE was higher as compared to that with higher flow rates. With increase in flow rates in EAHE system, although the convective heat transfer coefficients increase but the mean contact time between the soil and air decrease. Thus, the temperature reduction is greater in the case of low flow rates. In the case of the PV/T system, for lower flow rate the outlet temperature increases but also increases cell temperature. This is due to the fact that at lower flow rate, the Reynolds number reduced which also reduced the convective heat transfer coefficient. But at low flow rates, the time contact between the air and back surface of the PV panel increase, which increases the air temperature. Further, at lower flow rates, the surrounding losses from PV/T system increase causing reduction in heat transfer with the cooling medium (air), thus also increasing SCs temperature.

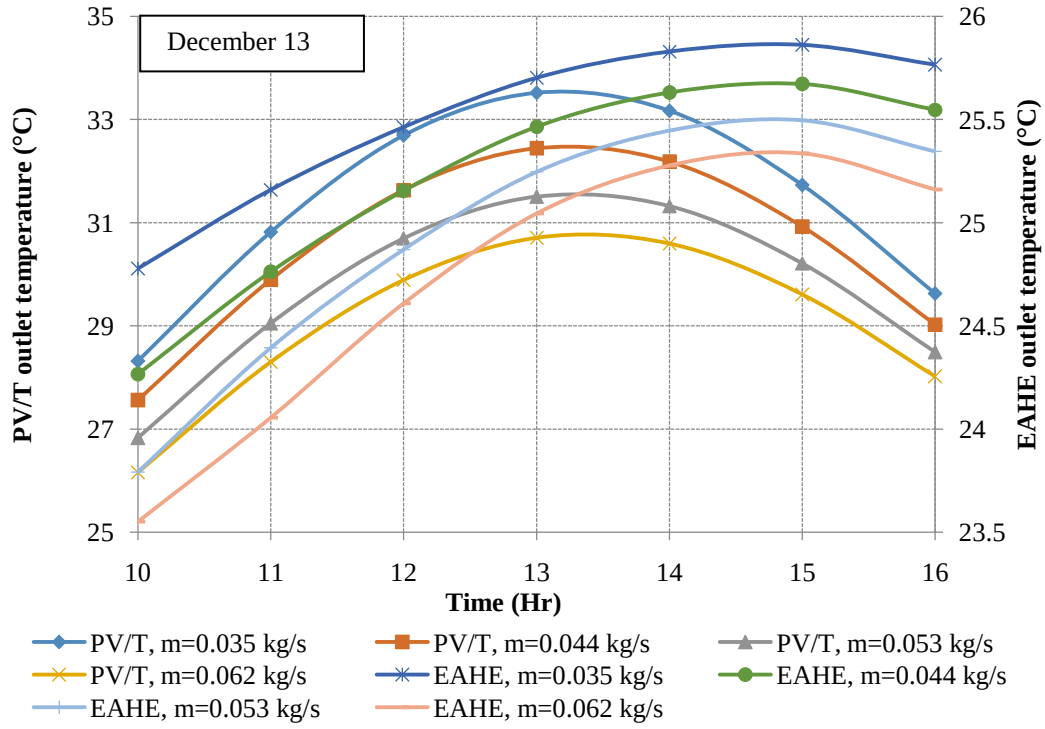
December 13
PV/T outlet temperature (°C)
EAHE outlet temperature (°C)
Time (Hr)
35
33
31
29
27
25
26
25.5
25
24.5
24
23.5
10
11
12
13
14
15
16
PV/T, m=0.035 kg/s
PV/T, m=0.044 kg/s
PV/T, m=0.053 kg/s
PV/T, m=0.062 kg/s
EAHE, m=0.035 kg/s
EAHE, m=0.044 kg/s
EAHE, m=0.053 kg/s
EAHE, m=0.062 kg/s

(a)

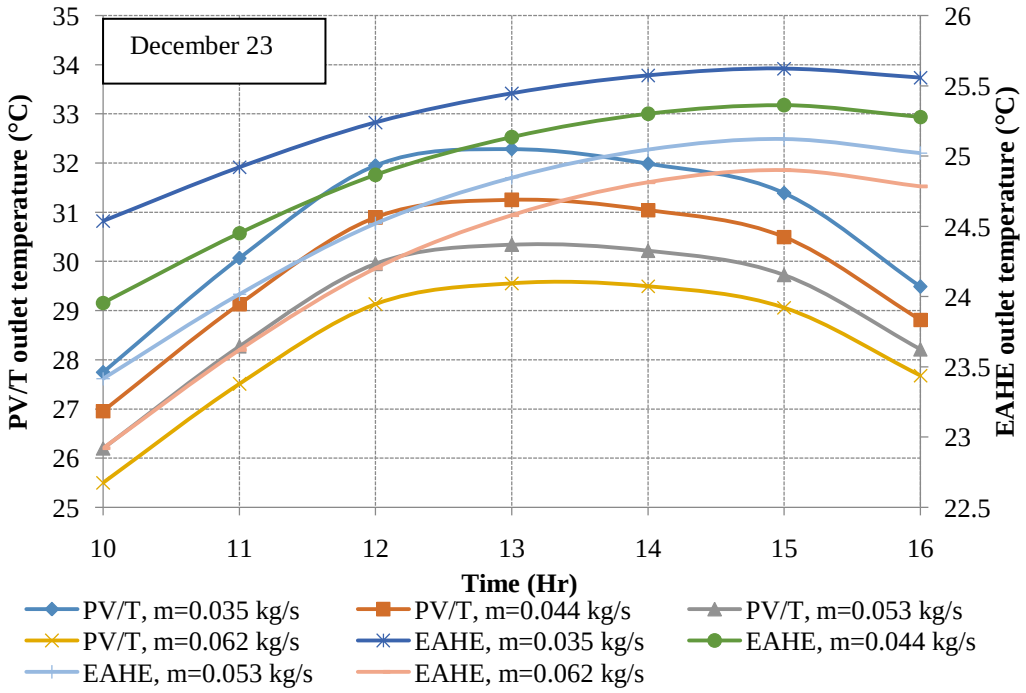
December 23
PV/T outlet temperature (°C)
EAHE outlet temperature (°C)
Time (Hr)
35
34
33
32
31
30
29
28
27
26
25
26
25.5
25
24.5
24
23.5
23
22.5
10
11
12
13
14
15
16
PV/T, m=0.035 kg/s
PV/T, m=0.044 kg/s
PV/T, m=0.053 kg/s
PV/T, m=0.062 kg/s
EAHE, m=0.035 kg/s
EAHE, m=0.044 kg/s
EAHE, m=0.053 kg/s
EAHE, m=0.062 kg/s

(b)

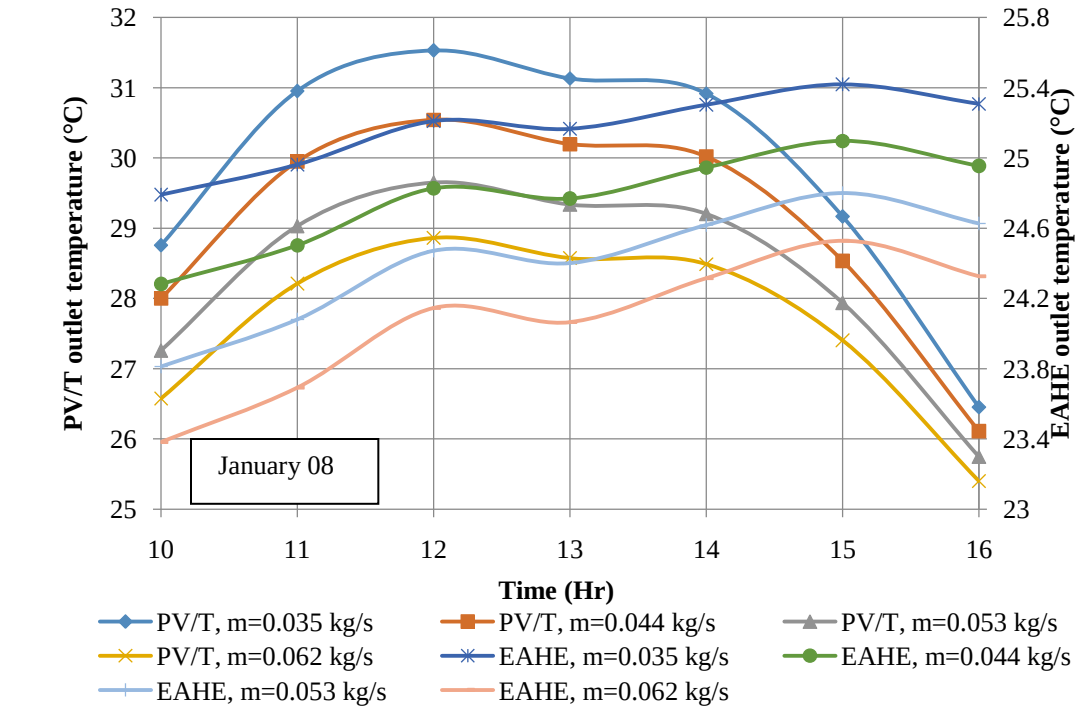


(c)

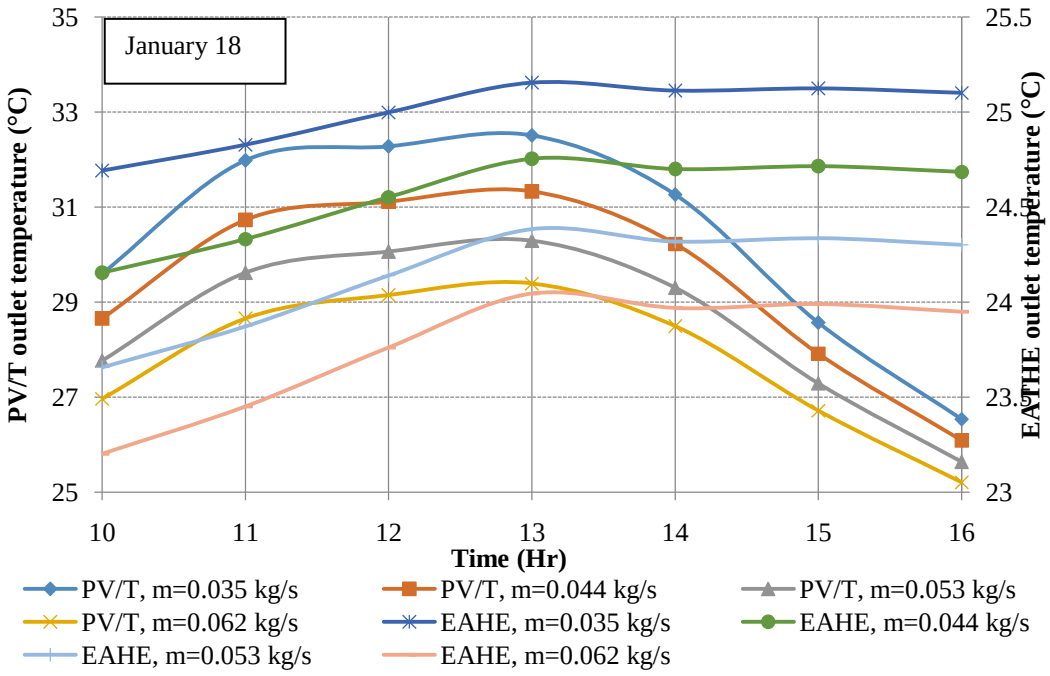


(d)

**Fig. 5.26 (a), (b), (c) and (d)**. EAHE and PV/T outlet temperature for Ajmer for various flow rates

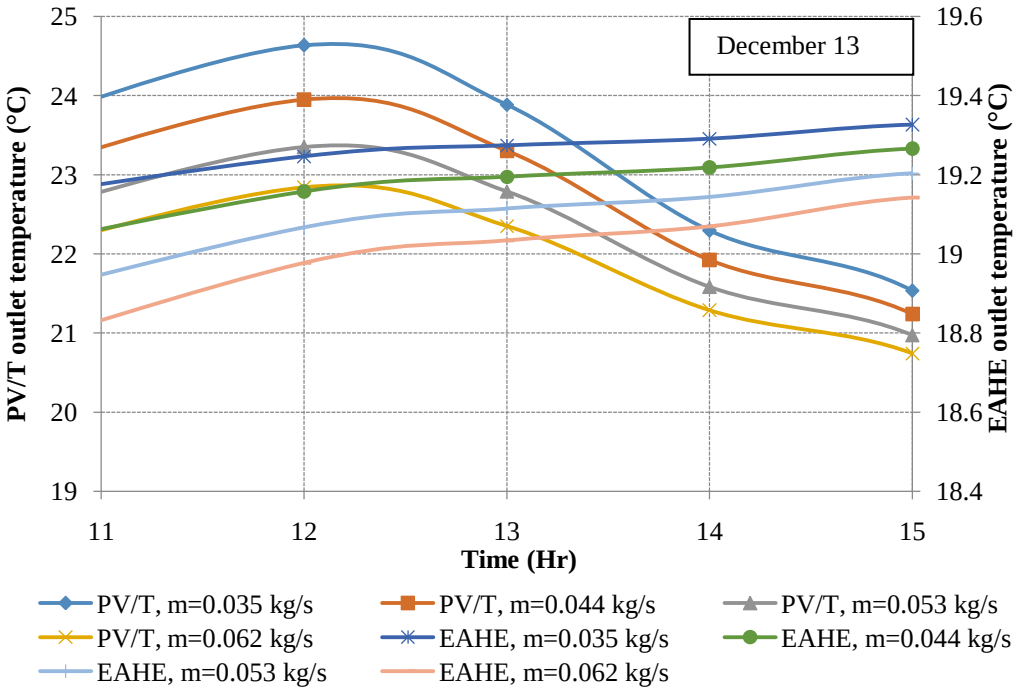
December 13
PV/T outlet temperature (°C)
EAHE outlet temperature (°C)
Time (Hr)
25
24
23
22
21
20
19
19.6
19.4
19.2
19
18.8
18.6
18.4
11
12
13
14
15
PV/T, m=0.035 kg/s
PV/T, m=0.044 kg/s
PV/T, m=0.053 kg/s
PV/T, m=0.062 kg/s
EAHE, m=0.035 kg/s
EAHE, m=0.044 kg/s
EAHE, m=0.053 kg/s
EAHE, m=0.062 kg/s

(a)

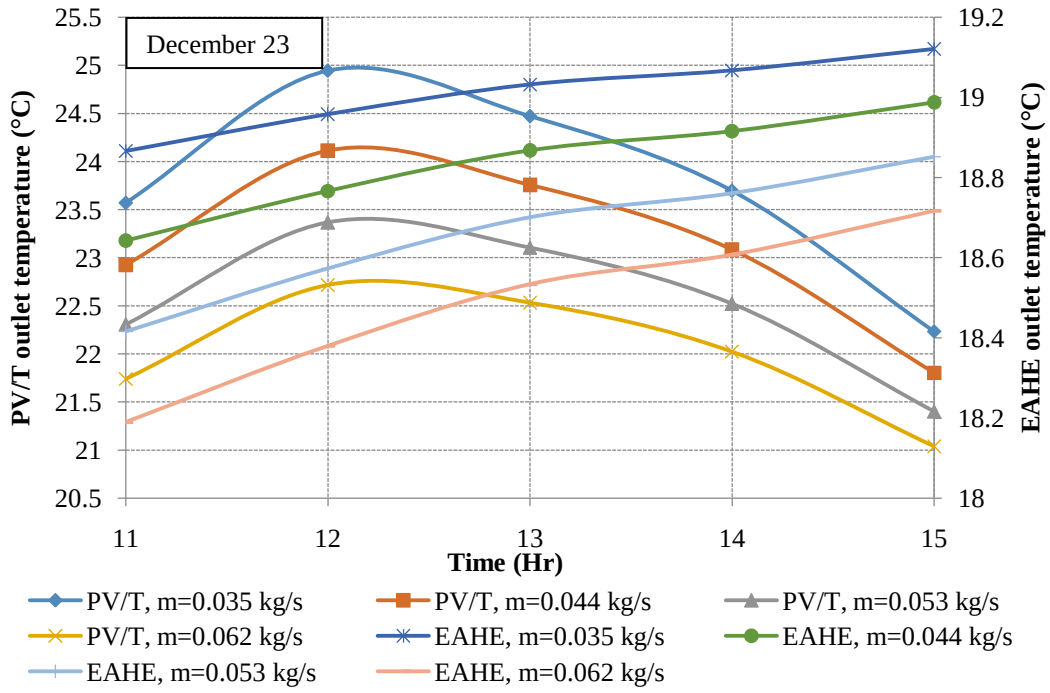
December 23
PV/T outlet temperature (°C)
EAHE outlet temperature (°C)
Time (Hr)
25.5
25
24.5
24
23.5
23
22.5
22
21.5
21
20.5
19.2
19
18.8
18.6
18.4
18.2
18
11
12
13
14
15
PV/T, m=0.035 kg/s
PV/T, m=0.044 kg/s
PV/T, m=0.053 kg/s
PV/T, m=0.062 kg/s
EAHE, m=0.035 kg/s
EAHE, m=0.044 kg/s
EAHE, m=0.053 kg/s
EAHE, m=0.062 kg/s

(b)

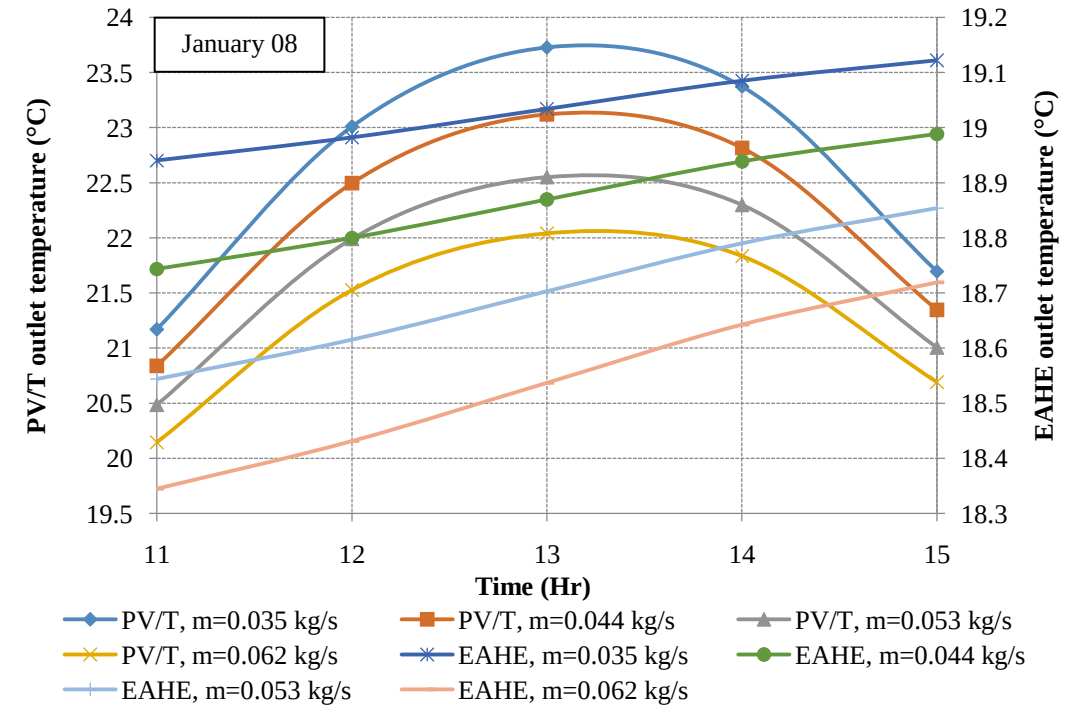


(c)

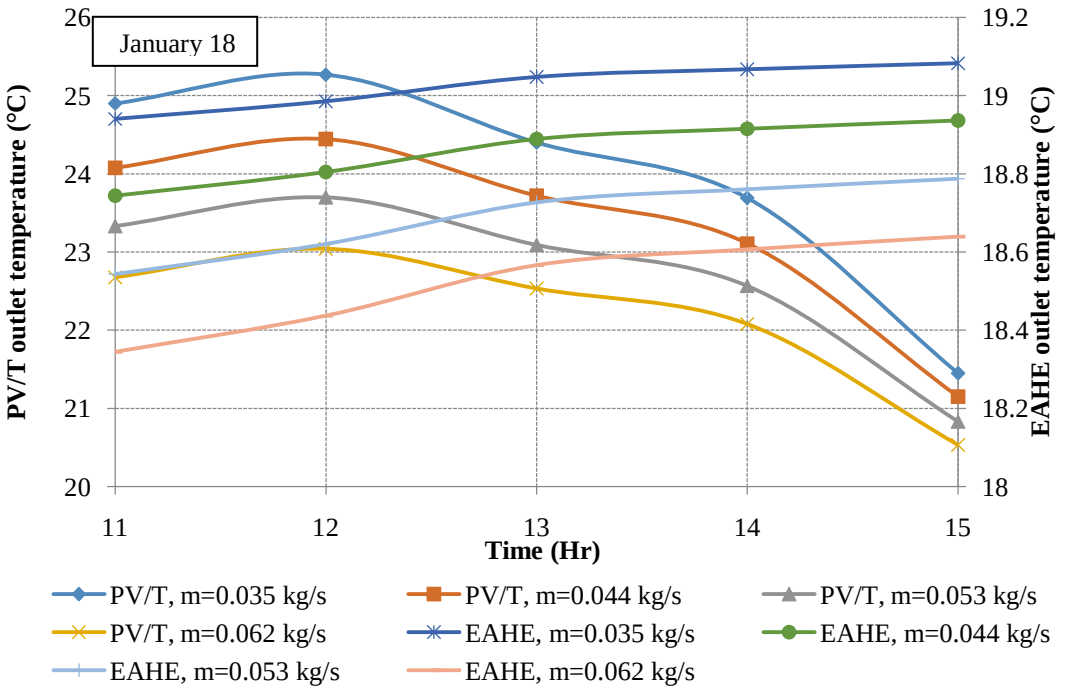


(d)

**Fig. 5.27 (a), (b), (c) and (d)**. EAHE and PV/T outlet temperature for Las Vegas for various flow rates

### 5.3.1 Parametric analysis of rooftop PV/T system coupled with EAHE cooling

The performance of the PV/T air collector coupled with the EAHE system depends upon various operating and design parameters like the EAHE pipe length, PV/T channel depth and PV/T collector length. Thus to estimate the effect of these parameters, a parametric analysis has been carried out for Pilani on January 18 and is presented in this section. For the same day, the analysis has been performed for different channel depths of the PV/T system, taking flow rate of 0.053 kg/s, the EAHE pipe length of 30 m and the PV/T collector area of 1.272 $m^2$. The variation of SCs temperature and PV/T outlet temperature with various PV/T channel depths are shown in Fig. 5.28 and Fig. 5.29 respectively. It is seen from the Fig. 5.28 that the SCs temperature ranges from 26.1 °C to 54.3 °C without any cooling. While in the case of EAHE cooling, the SCs temperature ranges from 25.8 °C to 39.8 °C, 26.0 °C to 43.4 °C, 26.3 °C to 48.9 °C and 26.6 °C to 52.8 °C with 5 mm, 10 mm, 20 mm and 30 mm channel depths, respectively. It was also observed that with an increase in channel depth, the Reynolds number decreases by a factor of 30. This leads to a smaller Nusselt number and smaller convective heat transfer coefficient, resulting in less of a decrease in SCs temperature. Fig. 5.29 represents the PV/T outlet temperature variation with channel depth. Similar to the previous case, here also with increase in channel depth, PV/T outlet temperature decreases due to lower heat transfer. Therefore, it is essential to adopt an optimized channel depth for design of such a coupled system and for that, 10 mm could be taken as the optimum value.

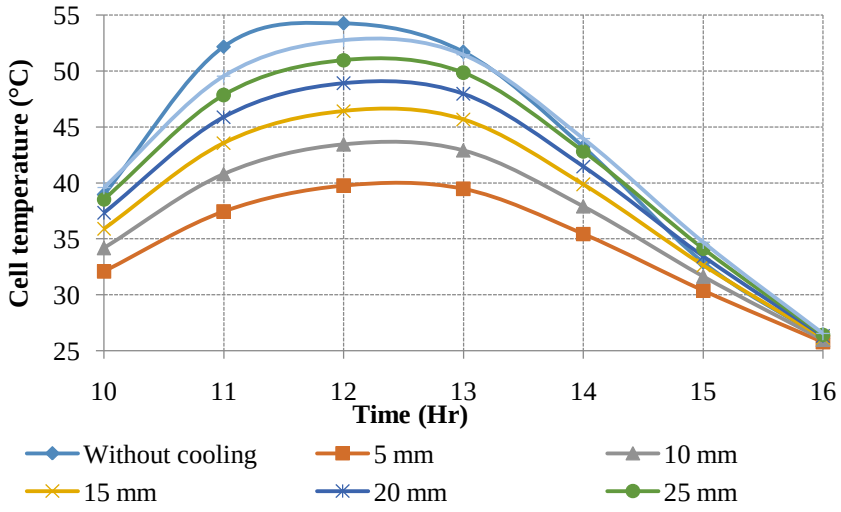


**Fig. 5.28**. SCs temperature for various channel depths with mass flow rate of 0.053 kg/s on January 18

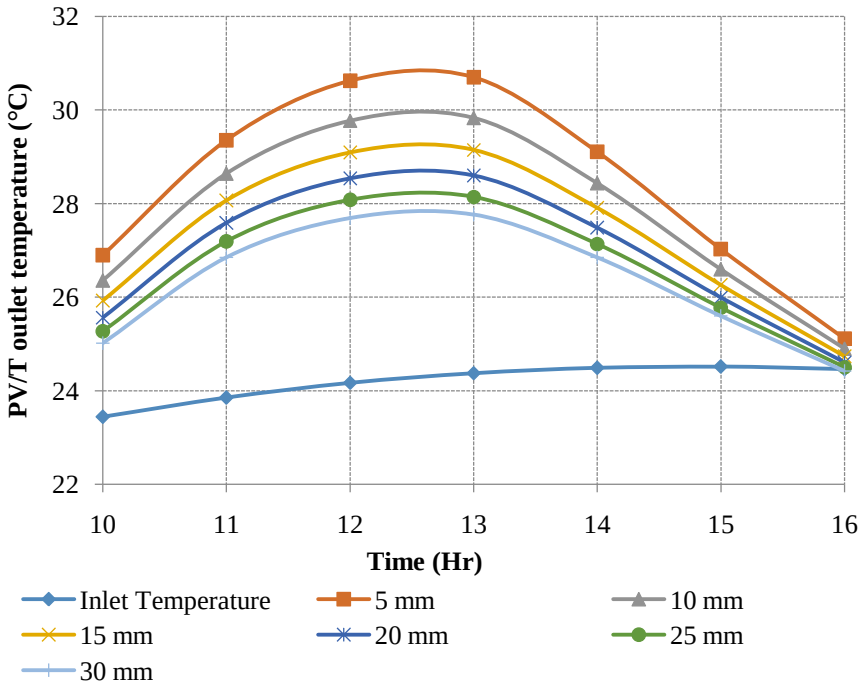


**Fig. 5.29**. PV/T outlet temperature for various channel depths with mass flow rate of 0.053 kg/s on January 18

Further the SCs temperature and PV/T outlet temperature for the different EAHE pipe lengths are shown in Fig. 5.30 and Fig. 5.31 respectively with flow rate of 0.053 kg/s and channel depth of 10 mm. It was observed that with increase in EAHE pipe length from 10 m to 60 m, the SCs temperature decreases eventually and the maximum drop occurred at a pipe length of 20 m after which the temperature remains constant. Further, the PV/T outlet temperature also increases with an increase in the EAHE pipe length and after 30 m, there was marginal increase in PV/T outlet temperature. Thus, in such coupled system, the pipe length of 30 m could be taken to obtain suitable range of PV cell temperatures and PV/T outlet temperatures. The SCs temperature and PV/T outlet temperatures for various PV/T collector lengths are shown in Fig. 5.32 and Fig. 5.33, respectively, with flow rate of 0.053 kg/s and channel depth of 10 mm. The SCs temperature ranges from 26.0 °C to 43.1 °C, 26.0 °C to 44.3 °C and 26.2 °C to 46.0 °C with PV/T collector lengths of 1 m, 1.8 m and 3.0 m, respectively. It was found that with an increase in PV/T collector length, the SCs temperature increases. Fig. 5.33 shows the PV/T outlet temperature variation for different collector lengths. It was observed that with an increase in collector length, the PV/T outlet increases due to higher heat transfer area and more contact time between the air and the collector. Fig. 5.32 and Fig. 5.33 also reflects the benefits of having a larger collector

length. This is due to the fact that, for 1 m length, the maximum PV/T outlet temperature was 28.9 °C while for 3 m it was 36.8 °C, which is 7.9 °C higher. Also at these lengths, the difference between cell temperatures was only 2.8 °C. Thus it was observed that large collector length (i.e. 3 m) is beneficial because with higher PV/T outlet temperature, the space heating of the building will be more and this decreases the heating load.

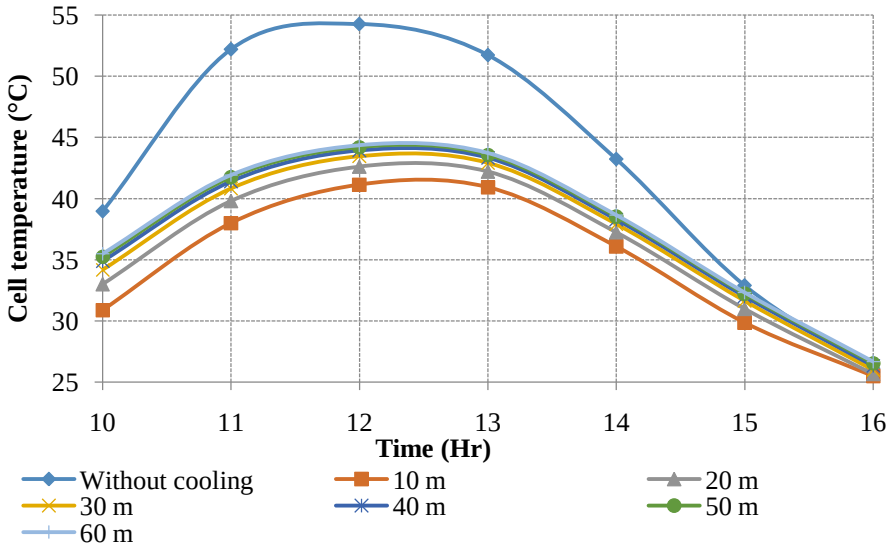


**Fig. 5.30**. SCs temperature for various EAHE pipe lengths with mass flow rate of 0.053 kg/s on January 18

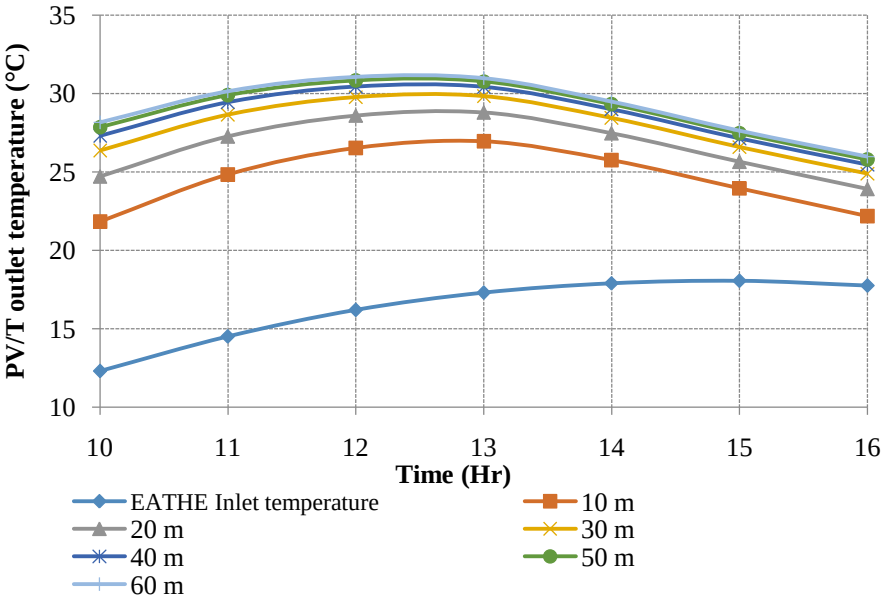


**Fig. 5.31**. PV/T outlet temperature for various EAHE pipe lengths with flow rate of 0.053 kg/s on January 18

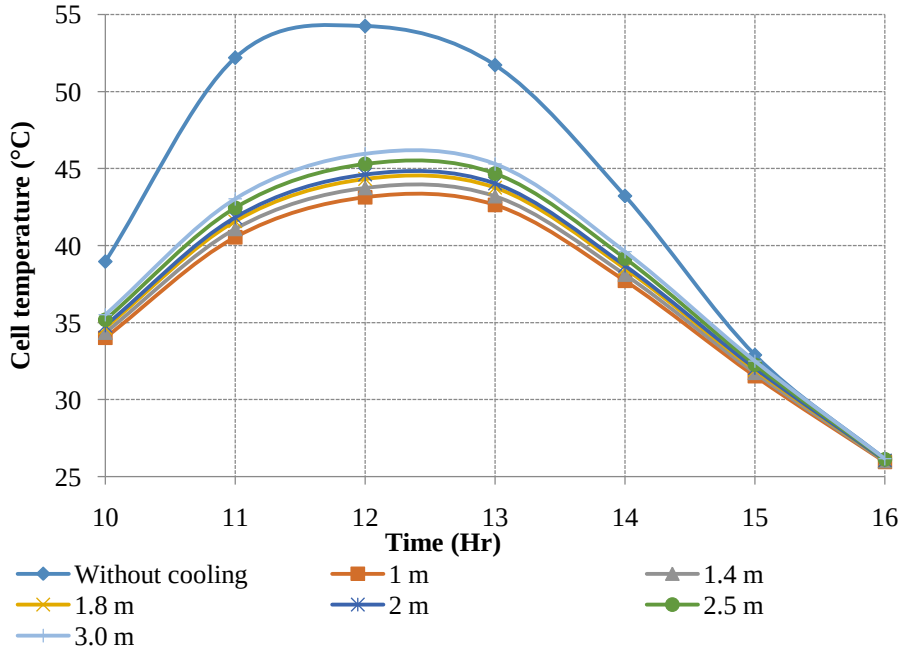


**Fig. 5.32**. SCs temperature for various PV/T collector lengths with mass flow rate of 0.053 kg/s on January 18

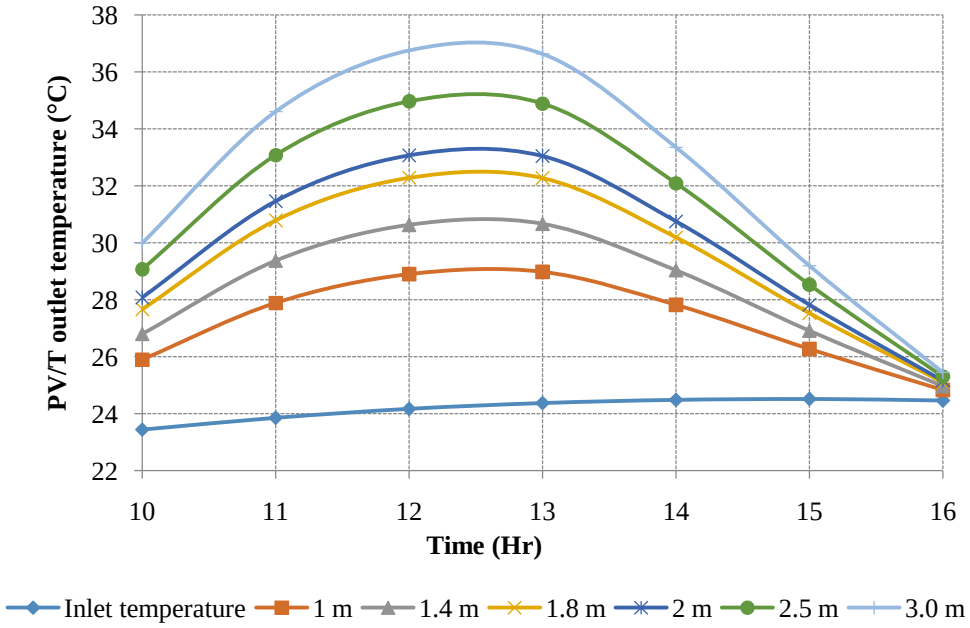


**Fig. 5.33**. PV/T outlet temperature for various PV/T collector lengths with mass flow rate of 0.053 kg/s on January 18

The heating capacity of the EAHE and PV/T was calculated using equation 3.64, chapter 3. In the case of the EAHE, the temperature difference (ΔT) is due to the inlet of EAHE (i.e. the ambient air) and the outlet of the EAHE (hot air). And in case of the PV/T, the temperature difference (ΔT) is due to inlet of the PV/T (i.e. the EAHE outlet) and the PV/T outlet. The average heating capacity of the EAHE coupled with PV/T is shown in Table 5.3 for Pilani, Ajmer and Las Vegas and was calculated on January 18 at a mass flow rate of 0.053 kg/s. Table 5.3 shows that the average heating capacity for Pilani was 405.40 Wh and 192.19 Wh for EAHE and PV/T systems respectively. Thus, by coupling the EAHE system with a PV/T system the heating capacity increased to 597.60 Wh. Similarly for Las Vegas, the heating capacity of the EAHE, the PV/T and the resulting overall heating capacity of the coupled system was 386.79 Wh, 184.70 Wh and 571.50 Wh, respectively. From this, it can be concluded that during winter season the EAHE system coupled with a PV/T system could be beneficial as the overall heating capacity is higher, the cell temperature is lower and thus improves the cell electrical efficiency.

**Table 5.3.** Heating capacity (Wh) of the EAHE and PV/T systems for all three locations with 0.053 kg/s flow rate in January 18

| **Time** | **Pilani** | | | **Ajmer** | | | **Las Vegas** | | |
|---|---|---|---|---|---|---|---|---|---|
| | **EAHE** | **PV/T** | **Total** | **EAHE** | **PV/T** | **Total** | **EAHE** | **PV/T** | **Total** |
| 10 AM | 571.73 | 155.50 | 727.24 | 435.99 | 210.09 | 655.08 | 530.71 | 180.63 | 711.35 |
| 11 AM | 479.92 | 255.36 | 735.29 | 402.92 | 306.25 | 709.18 | 438.42 | 255.26 | 693.68 |
| 12 AM | 408.98 | 298.74 | 707.72 | 361.98 | 315.93 | 677.91 | 403.34 | 270.75 | 670.10 |
| 13 PM | 363.07 | 290.99 | 654.07 | 324.49 | 314.95 | 639.45 | 354.42 | 232.73 | 587.16 |
| 14 PM | 338.03 | 210.41 | 548.44 | 334.49 | 265.72 | 600.21 | 339.19 | 203.02 | 542.22 |
| 15 PM | 331.77 | 110.89 | 442.66 | 331.80 | 157.58 | 489.38 | 326.73 | 109.08 | 435.82 |
| 16 PM | 344.29 | 23.47 | 367.76 | 337.18 | 71.18 | 408.37 | 314.74 | 41.43 | 356.17 |
| **Average** | 405.40 | 192.19 | 597.60 | 361.26 | 235.81 | 597.08 | 386.79 | 184.70 | 571.50 |

## 5.4 Exergetic analysis of tube-and-sheet PV/T and broad water channel PV/T system coupled with EWHE cooling

The exergetic analysis of both tube-and-sheets PV/T and broad channel IPVTS systems coupled with EWHE has been carried out and its results are presented in this section. The exergetic analysis has been carried out using experimental data of each system. The exergetic analysis of the present system has been carried out in terms of exergy losses and exergy destructions.

### 5.4.1 Tube-and-sheet PV/T system

The exergetic efficiencies are calculated for the experimental results obtained by conducting daily 6-hours experimental study from 9$^{th}$ September to 17$^{th}$ September, 2016. Measurements and recording of hourly data includes the wind speed, intensity of solar radiation, panels temperature with cooling and without cooling, ambient air temperature, inlet and outlet temperature of PV/T and EWHE, open circuit voltage, short circuit current, flow rate and temperature of water in the buried pipe at six different locations.

Performance of PV/T coupled with a EWHE system has been evaluated on periods of three consecutive days of September 2016 (09-11 September, 12-14 September and 15-17 September) with three flow rates. Fig. 5.34 shows the ambient conditions of Pilani, Rajasthan during test days and reveals that the solar radiation and ambient air temperature ranges between 498 W/m$^2$ to 960 W/m$^2$ and 29.8 °C to 36.3 °C respectively. It can be seen from the Fig. 5.34 that the maximum deviation in solar radiation and ambient air temperature for three days, during experimental duration was ±5.5% and 2.50% respectively, therefore, the ambient conditions were almost identical at any hour of operation. It ensures the identical outdoor ambient conditions in order to estimate the relative performance of each day. During the experimentation, three sets of mass flow rates i.e. 0.017 kg/s, 0.025 kg/s and 0.033 kg/s were taken. The measured energy consumption of pump for mass flow rate of 0.017 kg/s, 0.025 kg/s and 0.033 kg/s was found to be 4.3 W, 5.1 W and 5.8 W respectively.

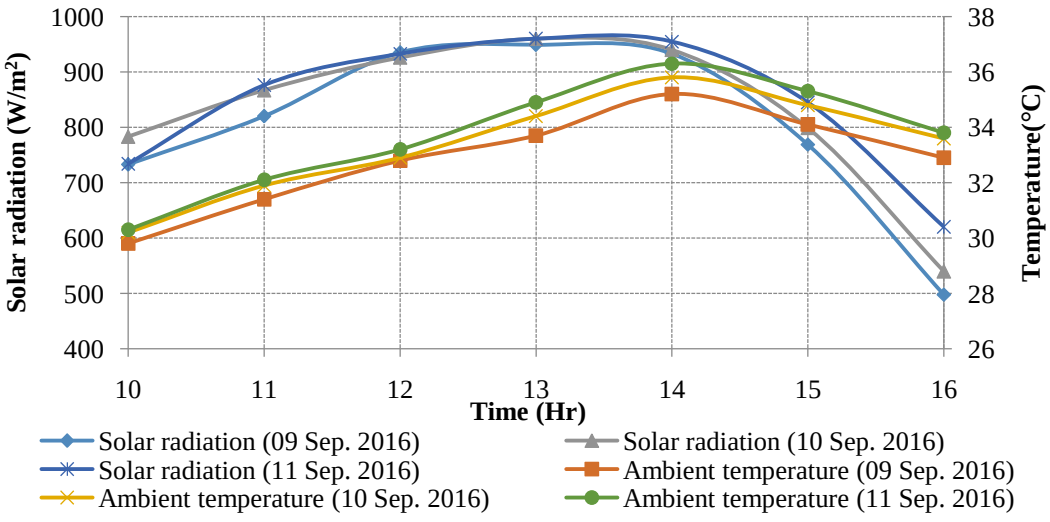


**Fig. 5.34.** Variation of solar radiation and ambient temperature during the test days

The overall exergy loss rate, which includes optical losses and heat losses of the PV/T system to surroundings, is shown in Fig. 5.35. It is noticeable from the Fig. 5.35 that with increase in solar radiation the overall exergy loss rate increases. Consequently, the losses for the whole day, first increases with increase in solar radiations and then decreases with reduction in radiation. This may be attributed to fact that rate of thermal exergy losses are proportional to SCs temperature, which in turn increases with increase in ambient temperature and solar radiation. It shows that the overall rate of losses ranges between 80.70 W to 150.26 W, 85.07 W to 152.46 W and 98.79 W to 153.86 W, on Sep., 09, Sep., 10 and Sep., 11, 2016 respectively. The external exergy losses can be minimized by reducing the cell temperature, which may be attainable by adoption of efficient cooling system for PV/T system similar to that adopted in this study. Further, reduction in exergy losses can be minimized by adoption of better quality insulation allowing reduction in overall loss coefficients. The optical losses are evident due to the non-black behaviour of the absorbing surfaces. Such losses can be reduced by employing better quality glazing with improved absorptivity and transmissivity.

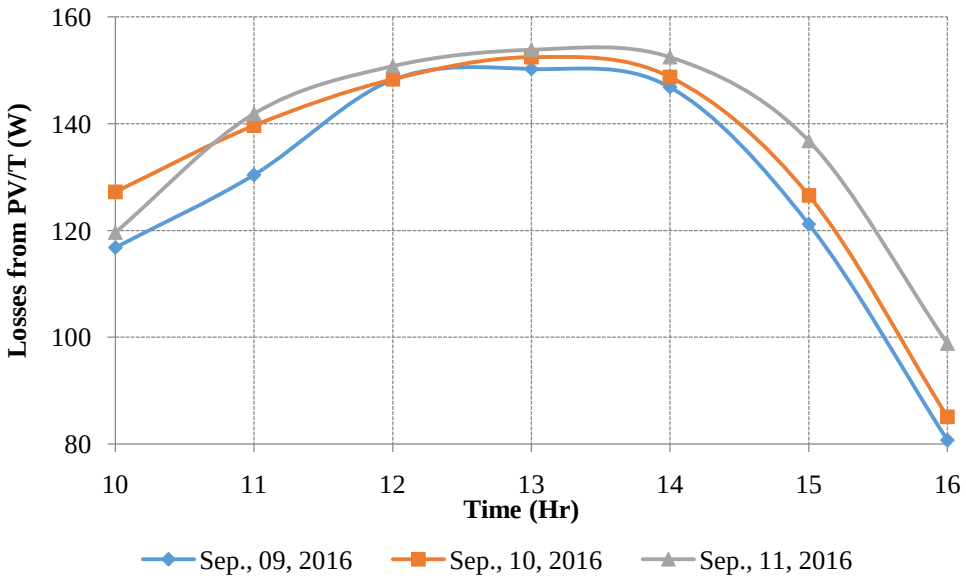


**Fig. 5.35.** Total exergy losses rate of PV/T during test days

Similarly, the overall exergy inlet rate and total exergy destruction rate of the PV/T system were calculated and its change per hour is shown in Fig. 5.36. The overall exergy inlet rate varied between 649.22 W to 1005.04 W, 565.52 W to 1005.16 W and 521.62 W to 993.81 W for mass slow rate of 0.017 kg/s, 0.025 kg/s and 0.033 kg/s respectively. It was observed that exergy inlet

rate increases with increase in solar radiation and thus exergy destruction rate will also increases. Fig. 5.36 also reveals that the total exergy destruction rate ranges between 402.37 W to 755.88 W for all experimental operation days. It is found from the analysis that the maximum exergy destruction occurs due to the large temperature difference between the Sun and PV/T collector. The exergy destruction rate due to heat transfer from PV/T surface to cooling water is also found to be significant. This can be reduced by adoption of efficient cooling system for PV/T. The electrical exergy destruction rate is found to be less significant. However, it can be reduced by improving the fill factor of the PV panel. By changing the mass flow rate from 0.017 kg/s to 0.033 kg/s the pressure drop in flow pipes increases, but a marginal increment in the exergy destruction rate due to pressure loss is observed. For the simplification, the exergy destruction rate owing to the pressure drop can be safely neglected.

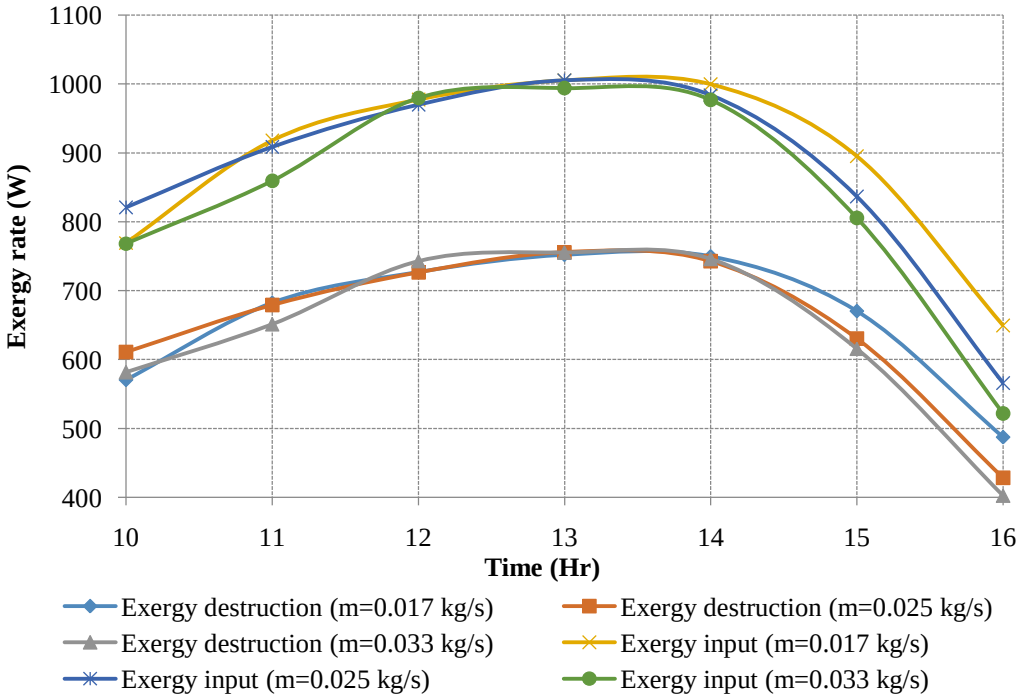


**Fig. 5.36.** Total exergy destruction rate and total exergy input rate of PV/T

Fig. 5.37 show the hourly variation of total exergetic efficiencies of PV/T system for three different flow rates of 0.017 kg/s, 0.025 kg/s and 0.033 kg/s. As shown in Fig. 5.37 the exergetic efficiency for Case I varied from 9.80% to 10.37%, 9.41% to 10.17% and 9.16% to 10.04% for the flow rate of 0.017 kg/s, 0.025 kg/s and 0.033 kg/s respectively, while exergetic efficiency for Case II ranges from 9.73% to 10.31%, 9.26% to 10.08% and 9.05% to 9.89% for the same flow

rates. It is observed that exergetic efficiency of Case I is little greater than that of Case II at same mass flow rate. This may be because the Case I does not includes the exergetic losses and destructions rates. It was also observed that the exergetic efficiency is lower for flow rate of 0.033 kg/s and 0.025 kg/s as compared to flow rate of 0.017 kg/s.

The PV/T exergetic efficiency for Case III is shown in Fig. 5.38, which includes only exergy destructions or internal losses. The PV/T exergetic efficiency for Case III decreases with increases of solar radiation and ambient temperature. It is observed that the efficiency of Case III is much higher than that of Case I and Case II and it ranges between 24.95% to 25.85%, 24.30% to 25.57% and 23.97% to 25.08% for flow rate of 0.017 kg/s, 0.025 kg/s and 0.033 kg/s respectively. For higher flow rate the outlet temperature of PV/T does not increase much, thus causes the decrease in thermal exergy efficiency. However, this increases the electrical exergetic efficiency as cell temperature decrease at high flow rate.

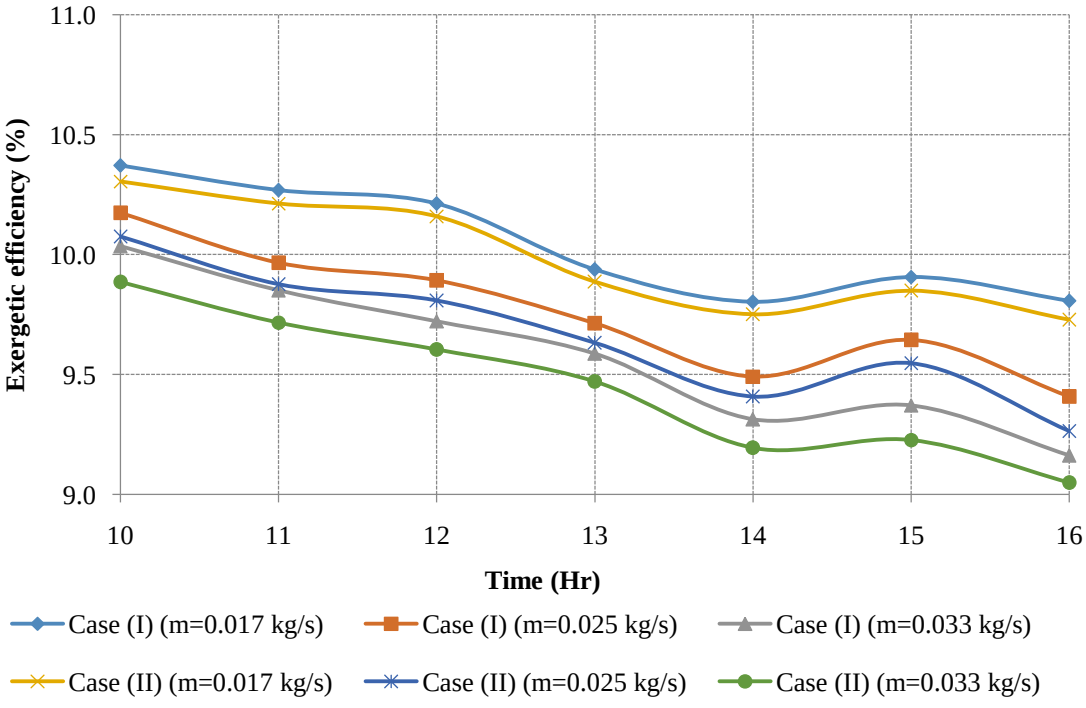


**Fig. 5.37.** PV/T exergetic efficiency in case (I) and case (II) for different flow rates

The exergetic efficiency and exergy destruction rate of EWHE system for different flow rates is represented graphically in Fig. 5.39. According to the Fig. 5.39 the exergy destruction rate was higher for 0.017 kg/s flow rate that for 0.025 kg/s and 0.033 kg/s and ranges between 3.37 W to 10.01 W for all flow rates. It is also observed that the exergetic efficiency of EWHE is higher for

flow rate of 0.033 kg/s as compared to flow rate of 0.017 kg/s and 0.025 kg/s. The maximum exergetic efficiency values for the flow rate of 0.017 kg/s, 0.025 kg/s and 0.033 kg/s are obtained as 60.01%, 67.78% and 72.45% respectively. The causes of the exergy destruction in the EWHE system include the pump and underground water piping (i.e. EWHE). It is observed from the analysis that the highest exergy destruction occurs in underground water piping because of the friction and also in the pump. The friction losses in pipe can be minimized by selecting the pipe with the better finishing or lower friction coefficient.

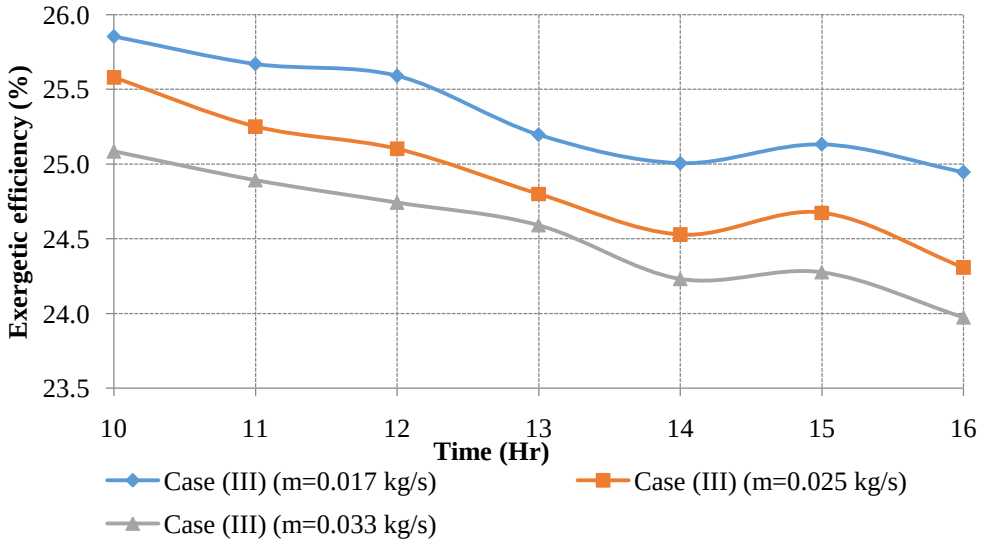


**Fig. 5.38.** Exergetic efficiency of PV/T in case (III) for different flow rates

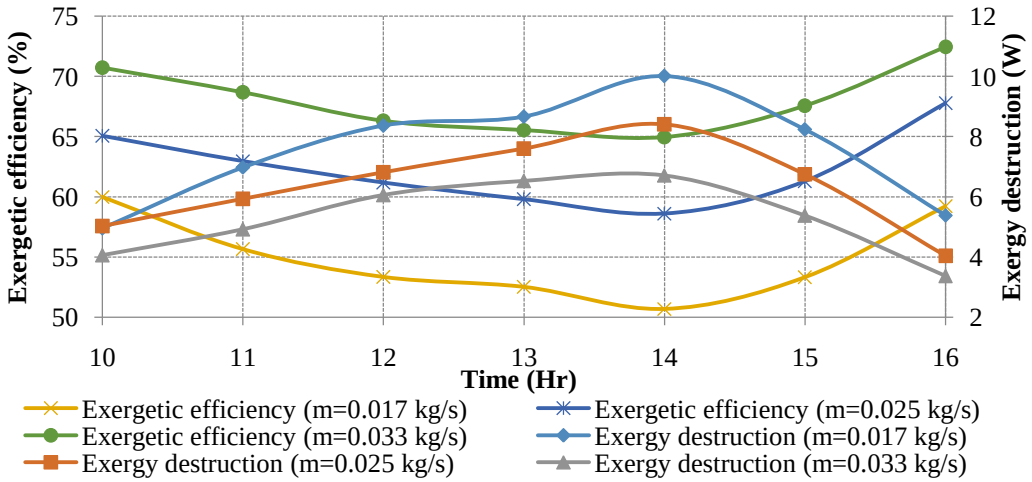


**Fig. 5.39.** Total exergetic efficiency and exergy destruction of EWHE system for different flow rates

The total exergetic efficiency of the coupled system (EWHE+PV/T) in Case (II) is shown in Fig. 5.40 and reveals that the exergetic efficiency of the coupled system was lower for higher flow rate of 0.033 kg/s as compared to lower flow rate of 0.017 kg/s and 0.025 kg/s. The difference between total exergetic efficiency for flow rate of 0.017 kg/s and 0.025 kg/s is merely from 0.07% to 0.14%. Fig. 5.41 shows the total exergetic efficiency for the coupled system using Case III. It is found out that the exergetic efficiency for Case III is more than that of Case II by 15.12% to 15.46% for 0.017 kg/s flow rate and by 14.91% to 15.41% for 0.025 kg/s flow rate and by 14.87% to 15.12% for flow rate of 0.033 kg/s. This is due to fact that Case III includes only internal exergy losses (i.e. exergy destructions) not includes the external exergy losses. It is observed that exergetic efficiency of coupled system was higher in the morning due to lower solar radiation. While during peak sunshine hours it decreased up to 8.95% and 23.99% in case II and case III respectively due to higher solar radiation. During evening, the trend is similar that of morning period. It is also seen form Fig. 5.40 and Fig. 5.41 that the exergetic efficiencies of coupled system were minimum around 2 P.M. due to increase in exergy destruction or irreversibility rates of PV/T because of increase in temperature difference due to higher solar insolation. From the above exergeticanalysis and experimental results, it is observed that theelectrical power output of PV/T system is increased with EWHE cooling as compared to without cooling, hence current coupled system could be efficient and suitable for the purpose of the PV/T cooling.

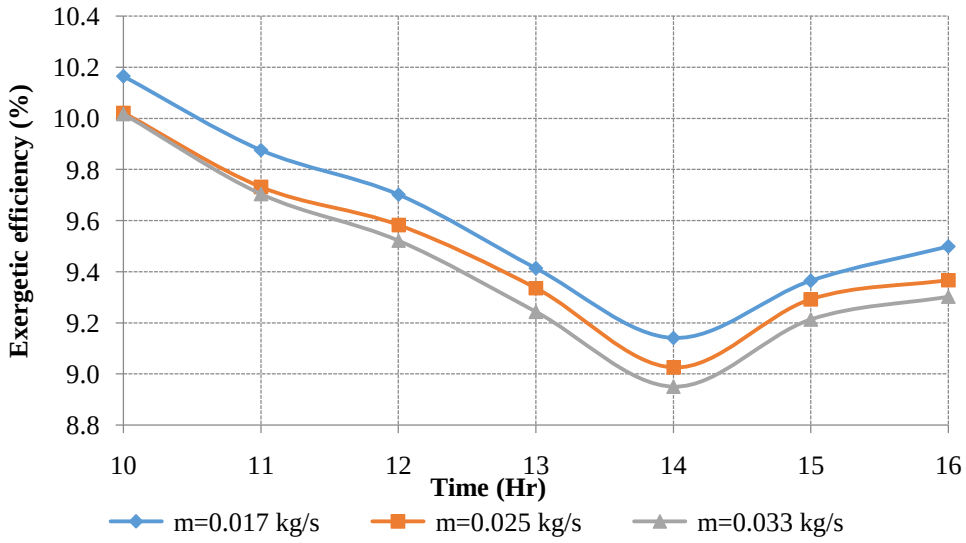


**Fig. 5.40**. Exergetic efficiency of coupled system (PV/T+EWHE) in case (II) for different flow rates

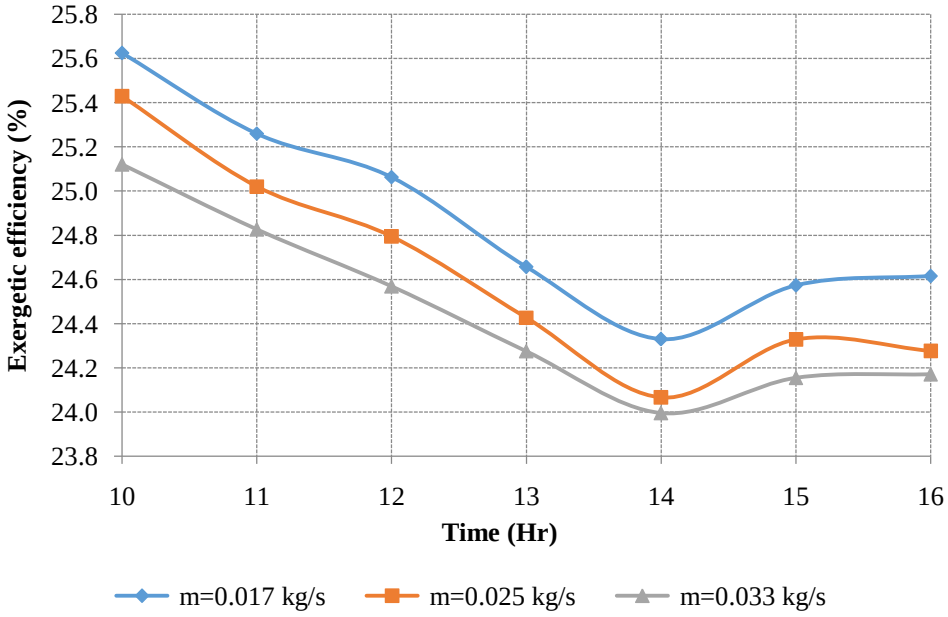


**Fig. 5.41.** Exergetic efficiency of coupled system (PV/T+EWHE) in case (III) for different flow rates

### 5.4.2 Broad water channel PV/T system (IPVTS)

The experiments were performed under realistic conditions at BITS Pilani, Pilani campus, Rajasthan on 20$^{th}$ September, 2016. Measurements and recording of hourly data includes the intensity of solar radiation, panel's temperature with cooling and without cooling, ambient air temperature, inlet and outlet temperature of PV/T and EWHE, open-circuit voltage, short- circuit current, flow rate and temperature of water in the buried pipe at six different locations.The experiment was conducted only for the mass flow of 0.033 kg/s.

The calculated overall exergy inlet rate, external exergy losses rate and exergy destructions rate of IPVTS system are shown in Fig. 5.42. The external losses, which include heat loss from the IPVTS system to the surroundings and optical losses from the IPVTS system are calculated using equations. The exergy inlate rate was calculated to be from 583.62 W to 1126.20 W. The external exergy losses and exergy destruction rate ranges between 84.90 W to 165.65 W and 451.08 W to 867.19 W respectively. An increase in the exergy loss rate was also observed due to increase in solar radiation and IPVTS panel temperature. Similarly, the exergy inlet rate was also observed to increase with solar radiation, also causing the electrical exergy rate to increase. The maximum exergy destruction occurs owing to the large temperature difference between the

IPVTS collector and Sun, as demonstrated by the analysis. A significant exergy destruction rate is observed owing to heat transfer from IPVTS surface to cooling water due to high temperature difference. The electrical exergy destruction rate can be minimized by improving the fill factor of the PV panel.

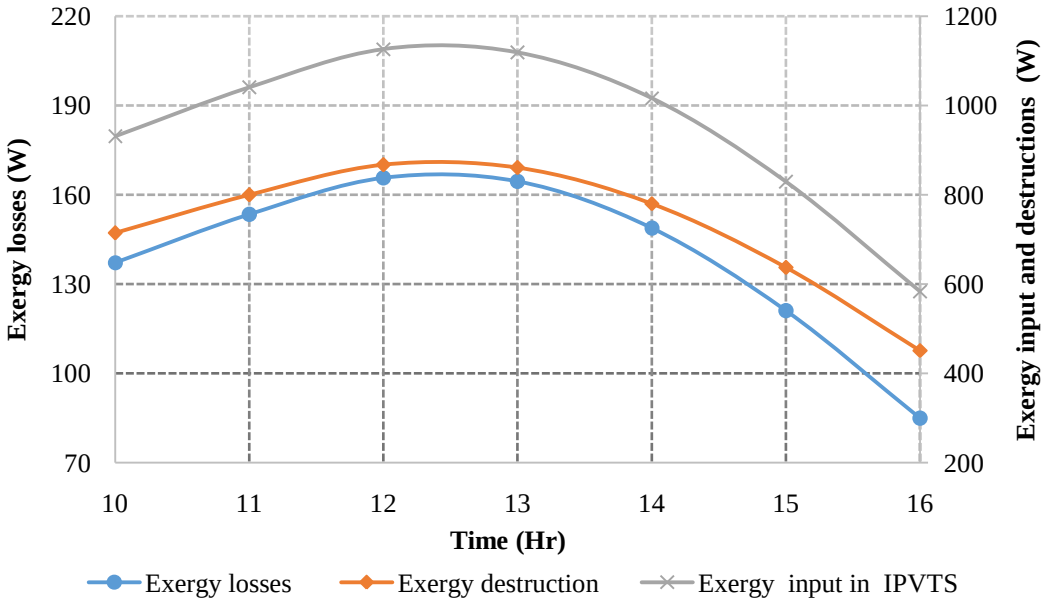


**Fig. 5.42.** Total exergy input, exergy losses and exergy destructions rate of IPVTS

The hourly variation of experimental exergetic efficiencies of IPVTS system for Case I, Case II and Case III have been calculated using equations and represented in Fig 5.43. The exergetic efficiency for Case I and Case II ranges from 8.50% to 8.75% and 8.16% to 8.54% respectively. A slight increase in the exergetic efficiency was observed in Case I for the same mass flow rate of cooling water. The reason for this was found to be a lack of inclusion of exergetic losses and destructions rate in Case I. The IPVTS exergetic efficiency for Case III is also shown in Fig. 5.43, which includes only exergy destructions or internal losses. The IPVTS exergetic efficiency for Case III decreases with increases of solar radiation and ambient temperature. It is observed that the efficiency of Case III is much higher than that of Case I and Case II and it ranges between 22.71% and 23.28%. The experimental exergy destruction rate and exergetic efficiency of EWHE system is calculated and represented in Fig. 5.44. The exergy destruction rate and exergetic efficiency are found to be 9.24 W to 15.35 W and 60.84% to 66.08% respectively. The irreversibility in pump and underground water piping (i.e. EWHE) are the causes for the exergy destruction in the EWHE system. As established by the analysis, the higher exergy destruction

occurs in underground water piping because of friction. The frictional losses in pipe can be minimized by selecting a pipe with better finishing or lower friction coefficient. Fig. 5.45 depicts the experimental exergetic efficiency and total exergetic destruction of the IPVTS coupled with EWHE system in Case II and Case III. It is observed that the the exergetic efficiency of the coupled system is found to be 8.39% to 8.69% in Case II.

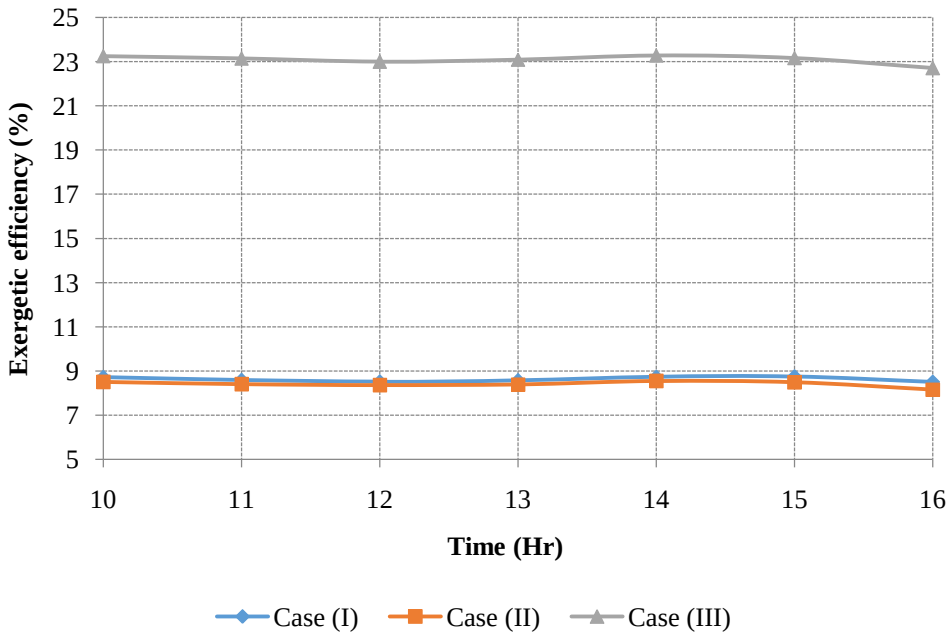


**Fig. 5.43.** IPVTS exergetic efficiency in Case (I), Case (II) and Case (III)

Fig. 5.45 also shows that the exergetic efficiency for Case III is more than that of Case II by 14.35% to 14.63 for flow rate of 0.033 kg/s. This is due to fact that Case III includes only internal exergy losses (i.e. exergy destructions) not includes the external exergy losses. It is observed that exergetic efficiency of coupled system was higher in the morning due to lower solar radiation. While during peak sunshine hours it decreased up to 8.39% and 22.87% in case II and case III respectively due to higher solar radiation. During evening, the trend is similar that of the morning period.

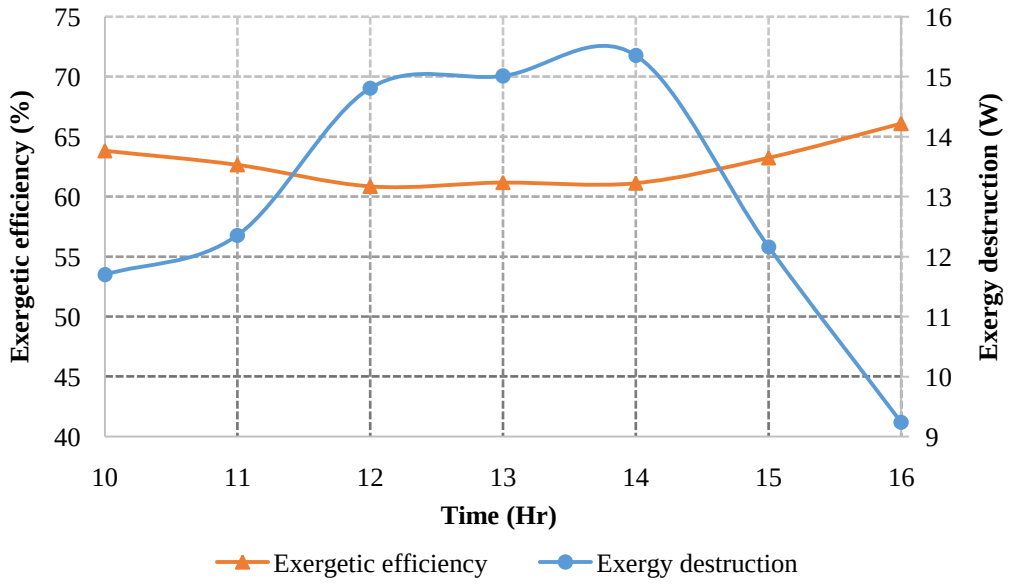


**Fig. 5.44.** Total exergetic efficiency and exergy destruction of EWHE system

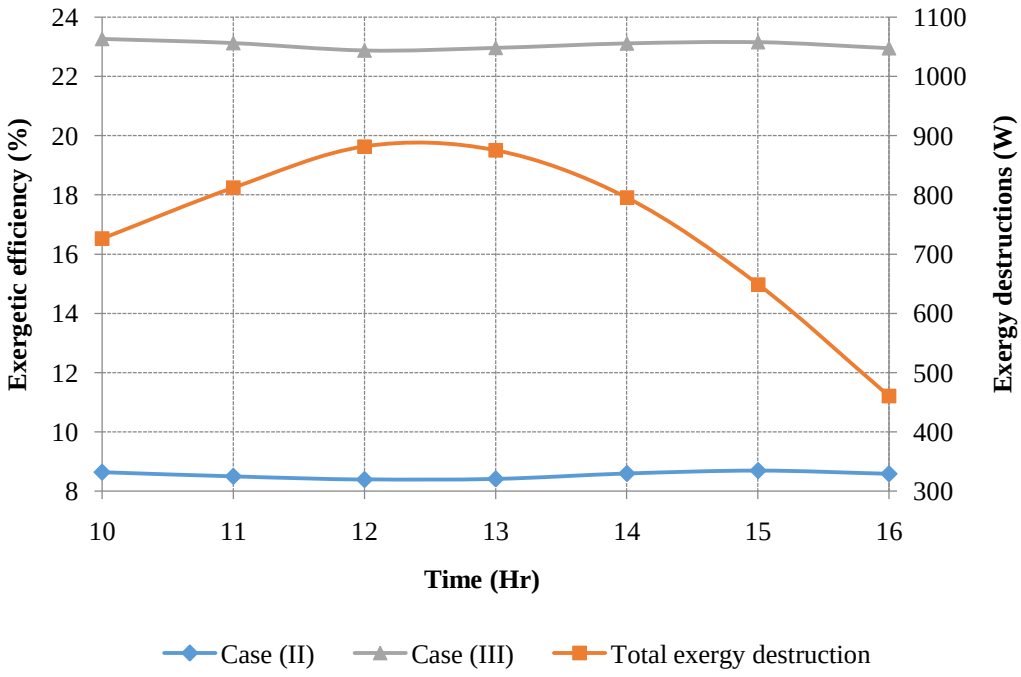


**Fig. 5.45**. Exergetic efficiency in Case (II) and Case (III) and total exergy destruction of coupled system (IPVTS+EWHE)

# CHAPTER 6

# CONCLUSION AND FUTURE SCOPE OF THE WORK

In the present work a novel cooling technique for PV and CPV systems termed as EWHE is designed and tested for the semi-arid region. A detailed TRNSYS modelling and simulation has been carried out to understand the transient behaviour of the unglazed PV/T and glazed CPV/T systems coupled with EWHE cooling. The TRNSYS software has inbuilt models which do not allow the user to perform parametric variation, but in PV/T collector only tube-and-sheet type model is available. Hence, to carry out the parametric variation, with different types of PV/T collectors a detailed mathematical modelling has been done for glazed tube-and-sheet PV/T and broad water channel PV/T systems coupled with EWHE cooling and is simulated using MATLAB software. The simulation results are compared and validated with experimental results obtained on an experimental set-up installed in Pilani, India. Further to identify the grey areas of the improvement and to utilize the maximum energy, exergetic analysis of coupled (EWHE+PV/T) systems has been carried out in terms of exergy losses and exergy destructions. At the end a theoretical analysis has been done on rooftop PV/T air collector coupled with EAHE system to evaluate its applicability for combined electrical power and space heating. The outcome of the simulation and experimental based studies, and major conclusions are summarized as below.

## 6.1 Conclusions

### 6.1.1 Modelling and simulation of unglazed PV/T system coupled with EWHE cooling

- The simulation results show that the maximum PV panel temperature reached up to 79.31 °C without any cooling. On the other hand, when PV panels are coupled with EWHE cooling system, the panel temperature drops to 46.29 °C.
- The performance of unglazed PV/T system coupled with EWHE cooling for various pipe materials i.e. GI, HDPE, steel is compared. From the analysis, it is observed that there is marginally variation in the performance of the system for different pipe materials. So it is concluded that among three materials which are considered for the analysis, HDPE pipe

may be used for practical applications because of economical reasons.

- In case of without cooling, the electrical efficiency was 9% for most of the time due to high SCs temperature. Further with EWHE cooling the efficiency is maintained at 11% for 0.022 kg/s and 0.026 kg/s flow rates. It can be concluded that the electrical efficiency of the system is increased by 2% for 0.022 kg/s and 0.026 kg/s, while it increases by 1% for 0.006 kg/s and 0.01 kg/s flow rates as compared to without any cooling.
- From the simulation results of variation in pipe lengths it is observed that with increase in pipe length the PV temperature decreases and power output increases. Results showed that maximum drop in PV temperature have observed from 10 m to 50 m length as 60 °C to 42.89 °C. However for the length of 60 m the PV temperature is 41.59 °C which is little higher as compared to 50 m pipe length. Similar trend has been observed for the PV power output.
- Further analysis shows that with increase the pipe diameter the PV/T outlet temperature decreases gradually over a period of time but at the peak simulation hour the PV temperature for all the pipe diameters exhibits similar temperature drop. Thus smaller pipe diameter i.e. 12 mm may be used for the practical applications.

### 6.1.2 Modelling and simulation of the CPV/T system coupled with EWHE cooling

- The simulation results show that at 3 Suns, the maximum CPV temperature goes to 416.36 °C in case of without any cooling. In case of EWHE cooling scenario, the CPV temperature decreases drastically and is obtained as 85.28 °C for the mass flow rate of 0.022 kg/s. The mass flow rate of 0.022 kg/s is considered to be optimum flow rate as it may be used for the practical applications.
- With increase in CR the maximum CPV panel temperature increases from 290.68 °C to 793.39 °C for CR variation of 2 to 6 Suns respectively.
- The simulation of CPV/T with EWHE shows the positive results in the improvement of the system. Such system may be used for the semi-arid regions of western Rajasthan which receives high solar insolation for more than 325 days in a year. This system will be very much helpful in summer as outside temperature reach up to 48 °C, leaving very

small scope for utilization of thermal energy. The excess waste heat, thus easily dissipated with the help of geothermal cooling principle.

### 6.1.3 Simulation and experimental study for tube-and-sheet PV/T system coupled with EWHE cooling

- As discussed in detail in chapter 5, it has been observed that there is good agreement between the theoretical PV panel temperature, PV/T outlet temperature, EWHE outlet temperature and electrical and thermal efficiency and the results obtained by the experimental study.
- For the PV/T with EWHE system, it was observed that the PV panel temperature is reduced with increase in mass flow rate and becomes almost same for 0.025 kg/s and 0.033 kg/s. This outcome can be used for the practical applications, by considering 0.025 kg/s flow rate to achieve the similar results with reduced pumping power.
- Results showed that the PV panel temperature drops drastically with EWHE cooling from 73 °C (without cooling) to 52.10 °C for the mass flow rate of 0.025 kg/s.
- For the lower mass flow rates, the PV/T outlet temperature increases but at the same time PV panel temperature is also increasing. This is due to fact that the cooling water gains heat from surroundings due to more time available for heat transfer, lower thermal resistance from the surrounding side as compared to the thermal resistance from the PV panel side. Thus, the lower mass flow rates (0.017 kg/s) is not that much beneficial as compared to flow rate of 0.025 kg/s.
- The electrical efficiency of the PV/T system is higher in the morning due to lower ambient temperatures and gradual increase of solar radiation. While during peak solar radiation hours and higher ambient temperatures leads to higher PV panel temperature and hence lower PV panel efficiency. During evening, the trend is similar to that of the morning period.
- The EWHE pipe length of 38 m would be sufficient for the proposed system.
- The analysis of experimental results confirms that the EWHE system is quite effective for the cooling of PV panels as it increases the electrical efficiency of PV system.

### 6.1.4 Exergetic analysis of tube-and-sheet PV/T system coupled with EWHE cooling based on experimental data

- The total exergy loss rate of the PV/T system is found directly proportional to solar radiation and SCs temperature and it increases with increase in solar radiation and SCs temperature. The overall exergy loss rate was found to be in the range of 85.07 W to 152.46 W and 98.79 W to 153.86 W, on Sep., 10 and Sep., 11, 2016, respectively.
- The total exergy destruction rate ranges between 428.06 W to 755.88 W for both experimental operation days. The exergy destruction owing to the large temperature difference between Sun and PV/T system is found to be the highest followed by the destruction due to the heat transfer from the PV/T surface to cooling fluid. The electrical exergy destruction rate is observed to less significant, whereas the exergy destruction due to pressure drop is found to be insignificant.
- The exergetic efficiency of the PV/T system for Case I is observed to be maximum i.e. 10.37%, while exergetic efficiency for Case II reached a maximum of 10.31% for the same flow rates. The exergetic efficiency in Case I is found to be a little higher than Case II as the former does not include the exergy losses. Whereas in Case III the second law efficiency goes up to 25.85% and 25.58% for flow rate of 0.017 kg/s and 0.025 kg/s, respectively. This gives a higher value of total exergetic efficiency as compared to Case I and Case II.
- The exergetic efficiency of the coupled system (EWHE+PV/T) in Case III was more than that of Case II by 15.12% to 15.46% for 0.017 kg/s flow rate and by 14.91% to 15.41% for 0.025 kg/s flow rate.

### 6.1.5 Simulation and experimental study of broad water channel PV/T system (IPVTS) coupled with EWHE cooling

- As discussed in detail in chapter 5, it has been observed that the theoretical values of IPVTS panel temperature, EWHE and IPVTS outlet temperature and thermal and electrical efficiencies shows a good agreement with the values measured through the experimental study.

- The maximum IPVTS panel temperature was found to be 74.5 °C without any cooling while it decreased drastically with EWHE cooling and ranges between 39.27 °C to 46.11 °C for the flow rate of 0.033 kg/s.
- The reduction in IPVTS panel temperature with the increase in the flow rate of cooling water was found to be identical for 0.033 kg/s and 0.042 kg/s for the coupled system. Thus, by considering 0.033 kg/s flow rate. Thus 0.033 kg/s is optimum flow rate.
- The electrical efficiency of the standalone PV panel varied between 7.22% and 7.82% during the test period. The reason for this was found to be a high SCs temperature. Whereas, the electrical efficiency of the IPVTS panel with EWHE cooling system was observed to be 8.28% to 8.60% and 8.42% to 8.68% for theoretical and experimental results respectively.
- The analysis establishes the effectiveness of the EWHE system in cooling the PV panels due to increase in the electrical efficiency of the same. The proposed coupled system could be used for the semi-arid regions of North-West India, which are blessed with huge solar radiation.

### 6.1.6 Exergetic analysis of broad water channel PV/T system (IPVTS) coupled with EWHE cooling based on experimental data

- The total exergy loss rate of the IPVTS are found directly proportional to solar radiation and SCs temperature and it increases with increase in solar radiation and SCs temperature. The overall exergy loss rate ranges between 84.90 W to 165.65 W.
- The exergetic efficiency for Case I and Case II ranges from 8.50% to 8.75% and 8.16% to 8.54% respectively. A slight increase in the exergetic efficiency was observed in Case I for the same mass flow rate of cooling water. The reason for this was found to be a lack of inclusion of exergetic losses and destructions rate in Case I. Whereas in Case III the exergetic efficiency found out to be 22.71% to 23.25% for the flow rate of 0.033 kg/s. This gives a higher value of total exergetic efficiency as compared to Case I and Case II.
- The exergetic efficiency of the coupled system (EWHE+PV/T) in Case III was also more than that of Case II by 14.35% to 14.62% for 0.033 kg/s flow rate.

### 6.1.7 Simulation of rooftop PV/T air collector coupled with EAHE system for combined electrical power and space heating

- The increase in mass flow rate shows favourable effect on decreasing the SCs temperature but it has unfavourable effect on PV/T outlet air temperature for space heating, which required higher temperature during winter period. With higher mass flow rates, additional heating will be required for such heating applications in such situations.
- Results showed that during winter season, the maximum SCs temperature goes up to 54.3 °C, 54.5 °C 44.4 °C for Pilani, Ajmer and Las Vegas, respectively, in the case without cooling and 43.4 °C, 44.2 °C and 35.6 °C with cooling for respective locations, at a 0.053 kg/s flow rate.
- The heating capacity of the EAHE ranges from 331.77 Wh to 571.73 Wh, 324.49 Wh to 435.99 Wh and 314.74 Wh to 530.71 Wh for Pilani, Ajmer and Las Vegas, respectively, at a flow rate of 0.053 kg/s. When coupled with a PV/T, the heating capacity increases from 367.76 Wh to 735.29 Wh, 408.37 Wh to 709.18 Wh and 356.17 Wh to 711.35 Wh for the respective locations. Thus the coupled system has a higher heating capacity and a lower PV/T operating temperature which eventually leads to an increase in a peak electrical efficiency of 0.62%.
- For such a coupled system, the EAHE pipe length of 30 m is sufficient
- The electrical and thermal performance of this coupled system depends upon channel depth. Hence, it is quite important to optimize channel depth for its design. For the present analysis, channel depth of 10 mm gives good results.
- This system could be beneficial for Pilani (India), Ajmer (India) and Las Vegas (USA) to reduce the SCs temperature and space heating as even during winter season, maximum SCs temperature goes up to 55 °C.

## 6.2 Future scope of work

- Experimental study may be carried out for the unglazed PV/T and glazed CPV/T systems coupled with EWHE cooling.
- The economic analysis and life cycle analysis can be recommended for further work, which will be required before commercialization of the system.

- Experimental study may be carried for the rooftop PV/T air collector with EAHE system for combined electrical power and space heating.
- Transient parametric study of PV/T air collector coupled with EAHE system for its intermittent operation is something which may be investigated and optimized.
- Coupling of BIPV/T system and EAHE system may be thought of to enhance the heating potential of the EAHE system so that system could be used to maintain thermal comfort conditions in cold countries during winters.

# REFERENCES


[1] V.S. Reddy, S.C. Kaushik, N.L. Panwar, Review on power generation scenario of India, Renew. Sustain. Energy Rev. 18 (2013) 43–48.

[2] Key world energy statistics, Int. Energy Agency. (2017). https://www.iea.org/publications/freepublications/publication/KeyWorld2016.pdf.

[3] Executive summary, Minist. Power Cent. Electr. Auth. New Delhi. (2017). http://www.cea.nic.in/reports/monthly/executivesummary/2017/exe_summary-01.pdf.

[4] Renewables Trends from excerpts from Renewable Information, Int. Energy Agency. (2015). www.iea.org/statistics/topics/electricity.

[5] Annual Report, Minist. New Renew. Energy. (2016). http://mnre.gov.in/file-manager/annual-report/2015-2016/EN/Chapter 1/chapter_1.htm.

[6] P. Würfel, U. Würfel, Physics of Solar Cells: From Basic Principles to Advanced Concepts, John Wiley & Sons, 2009.

[7] R. D. Rugescu, Solar Energy, Intech publishing Croatia, 2010, ISBN: 978-953-307-052-0.

[8] Photovoltaic Module Qualification Plus Testing, Natl. Renew. Energy Lab. (2013). https://www.nrel.gov/docs/fy14osti/60950.pdf.

[9] Ryan Mayfield, Calculating Current Ratings of Photovoltaic Modules, ECM. (2012). http://www.ecmweb.com/green-building/calculating-current-ratings-photovoltaic modules.

[10] P. Pérez-Higueras, E. Muñoz, G. Almonacid, P.G. Vidal, High Concentrator PhotoVoltaics efficiencies: Present status and forecast, Renew. Sustain. Energy Rev. 15 (2011) 1810–1815.

[11] A. Ummadisingu, M.S. Soni, Concentrating solar power–technology, potential and policy in India, Renew. Sustain. Energy Rev. 15 (2011) 5169–5175.

[12] C. Sangani, C. Solanki, Experimental evaluation of V-trough (2 suns) PV concentrator system using commercial PV modules, Sol. Energy Mater. Sol. Cells. 91 (2007) 453–459.

[13] E. Skoplaki, J. a. Palyvos, On the temperature dependence of photovoltaic module electrical performance: A review of efficiency/power correlations, Sol. Energy. 83 (2009) 614–624.

[14] K. Nishioka, T. Takamoto, T. Agui, M. Kaneiwa, Y. Uraoka, T. Fuyuki, Annual output estimation of concentrator photovoltaic systems using high-efficiency InGaP/InGaAs/Ge triple-junction solar cells based on experimental solar cell's characteristics and field-test meteorological data, Sol. Energy Mater. Sol. Cells. 90 (2006) 57–67.

[15] V.M. Puri, Heat and mass transfer analysis and modeling in unsaturated ground soils for buried tube systems, Energy Agric. 6 (1987) 179–193.

[16] ASHRAE, Handbook of application. Atlanta Ga. American Society of Heating Refrigerating and Air Conditioning engineers Inc., in: 1985.

[17] D. Reay, R. McGlen, P. Kew, Heat pipes: Theory, design and applications, Butterworth-Heinemann, 2013.

[18] G.P. Peterson, An introduction to heat pipes, John Wiley & Sons, Canada, 1994.

[19] R. Singh, A. Akbarzadeh, M. Mochizuki, Operational characteristics of a miniature loop heat pipe with flat evaporator, Int. J. Therm. Sci. 47 (2008) 1504–1515.

[20] G.F. Russell, Uniform surface temperature heat pipe and method of using the same, US Patent 4,320,246, 1982.

[21] A. Akbarzadeh, T. Wadowski, Heat pipe based cooling systems for photovoltaic cells under concentrated solar radiation, Appl. Therm. Eng. 16 (1996) 81–87.

[22] A. Cheknane, B. Benyoucef, A. Chaker, Performance of concentrator solar cells with passive cooling, Semicond. Sci. Technol. 21 (2006) 144–147.

[23] W.G. Anderson, P.M. Dussinger, D.B. Sarraf, S. Tamanna, Heat Pipe Cooling of Concentrating Photovoltaic Cells, in: 33rd, Photovoltaic Spec. Conf., IEEE, 2008: pp. 1–6.

[24] H.-J. Huang, S.-C. Shen, H.-J. Shaw, Design and Fabrication of a Novel Hybrid-Structure Heat Pipe for a Concentrator Photovoltaic, Energies. 5 (2012) 4340–4349.

[25] D. Il Lee, S.W. Baek, Development of a Heating System Using CPV Technology and

Heat Pipes, Environ. Prog. Sustain. Energy. 0 (2015) 1–11.

[26] M.A.Farahat, Photovoltaic cells by cooling, in: 39th Int. Univ. Power Eng. Conf., IEEE, 2004: pp. 623–628.

[27] C.R. Russell, Optical concentrator and cooling system for photovoltaic cells, US Patent RE30,584, 1981.

[28] H.C. Koehler, Cooling photovoltaic (PV) cells during concentrated solar radiation in specified arrangement in coolant with as low electric conductivity as possible, US Patent, DE19904717, 2000.

[29] Y.A. Abrahamyan, V.I. Serago, et al. Aroutiounian, V M, The efficiency of solar cells immersed in liquid dielectrics, Sol. Energy Mater. Sol. Cells. 73 (2002) 367–375.

[30] Y. Wang, Z. Fang, L. Zhu, Q. Huang, Y. Zhang, Z. Zhang, The performance of silicon solar cells operated in liquids, Appl. Energy. 86 (2009) 1037–1042.

[31] L. Zhu, Y. Wang, Z. Fang, Y. Sun, Q. Huang, An effective heat dissipation method for densely packed solar cells under high concentrations, Sol. Energy Mater. Sol. Cells. 94 (2010) 133–140.

[32] L. Liu, L. Zhu, Y. Wang, Q. Huang, Y. Sun, Z. Yin, Heat dissipation performance of silicon solar cells by direct dielectric liquid immersion under intensified illuminations, Sol. Energy. 85 (2011) 922–930.

[33] X. Han, Y. Wang, L. Zhu, Electrical and thermal performance of silicon concentrator solar cells immersed in dielectric liquids, Appl. Energy. 88 (2011) 4481–4489.

[34] L. Zhu, R.F. Boehm, Y. Wang, C. Halford, Y. Sun, Water immersion cooling of PV cells in a high concentration system, Sol. Energy Mater. Sol. Cells. 95 (2011) 538–545.

[35] H. Xiang, Y. Wang, L. Zhu, X. Han, Y. Sun, Z. Zhao, 3D numerical simulation on heat transfer performance of a cylindrical liquid immersion solar receiver, Energy Convers. Manag. 64 (2012) 97–105.

[36] X. Han, Y. Wang, L. Zhu, The performance and long-term stability of silicon concentrator solar cells immersed in dielectric liquids, Energy Convers. Manag. 66 (2013) 189–198.

[37] Y. Sun, Y. Wang, L. Zhu, B. Yin, H. Xiang, Q. Huang, Direct liquid-immersion cooling

of concentrator silicon solar cells in a linear concentrating photovoltaic receiver, Energy. 65 (2014) 264–271.

[38] G. Xin, Y. Wang, Y. Sun, Q. Huang, L. Zhu, Experimental study of liquid-immersion III – V multi-junction solar cells with dimethyl silicon oil under high concentrations, Energy Convers. Manag. 94 (2015) 169–177.

[39] M.W. Edenburn, J.R. Burns, Shading analysis of a photovoltaic-cell string illuminated by a parabolic-trough concentrator, NASA STI/Recon Tech. Rep. N. 83 (1982) 21537.

[40] K. Araki, H. Uozumi, M. Yamaguchi, a simple passive cooling structure and its heat analysis for 500 X, In Photovoltaic Specialists Conference, 2002. Conference Record of the Twenty-Ninth IEEE, pp. 1568-1571. IEEE.

[41] T. Chou, Z. Shih, H. Hong, C. Han, K. Chiang, Investigation of the Thermal Performance of High-Concentration Photovoltaic Solar Cell Package, in: Int. Conf. Electron. Mater. Packag., IEEE, 2007: pp. 1–6.

[42] E. Kermani, S. Dessiatoun, A. Shooshtari, M.M. Ohadi, Experimental investigation of heat transfer performance of a manifold microchannel heat sink for cooling of concentrated solar cells, in: Electron. Components Technol. Conf. ECTC. 59th, 2009, IEEE, 2009: pp. 453–459.

[43] C. Min, C. Nuofu, Y. Xiaoli, W. Yu, B. Yiming, Z. Xingwang, Thermal analysis and test for single concentrator solar cells, J. Semicond. 30 (2009) 44011.

[44] B. Ramos-Alvarado, P. Li, H. Liu, A. Hernandez-Guerrero, CFD study of liquid-cooled heat sinks with microchannel flow field configurations for electronics, fuel cells, and concentrated solar cells, Appl. Therm. Eng. 31 (2011) 2494–2507.

[45] E. Di Maio, R. Mastrullo, A.W. Mauro, D. Toto, Thermal management of a multiple mini-channel heat sink by the integration of a thermal responsive shape memory material, Appl. Therm. Eng. 62 (2014) 113–122.

[46] S.K. Natarajan, T.K. Mallick, M. Katz, S. Weingaertner, Numerical investigations of solar cell temperature for photovoltaic concentrator system with and without passive cooling arrangements, Int. J. Therm. Sci. 50 (2011) 2514–2521.

[47] C.K.K. Lee S.S., Lai s.o., A Study on Cooling of Concentrator Photovoltaic Cells using

CFD, in: 2012 Int. Conf. Innov. Manag. Technol. Res. (ICIMTR), Malacca, Malaysia, IEEE, 2012: pp. 21–22.

[48] R.J. Linderman, Z.S. Judkins, M. Shoecraft, M.J. Dawson, Thermal Performance of the SunPower Alpha-2 PV Concentrator, IEEE J. Photovoltaics. 2 (2012) 196–201.

[49] F. Gualdi, O. Arenas, A. Vossier, A. Dollet, V. Aimez, R. Arès, Determining passive cooling limits in CPV using an analytical thermal model, in: 9TH Int. Conf. Conc. Photovolt. Syst., AIP Publishing, 2013: pp. 10–13.

[50] L. Collin, O.J. Arenas, R. Arès, L.G. Fréchette, A. Concentrated, Thermal Resistance and Heat Spreading Characterization Platform for Concentrated Photovoltaic Cell Receivers, IEEE Trans. Components, Packag. Manuf. Technol. 3 (2013) 1673–1682.

[51] K.S. Reddy, S. Lokeswaran, P. Agarwal, T.K. Mallick, Numerical Investigation of Micro-channel based Active Module Cooling for Solar CPV System, Energy Procedia. 54 (2014) 400–416.

[52] T. Liao, B. Lin, Z. Yang, Performance characteristics of a low concentrated photovoltaic–thermoelectric hybrid power generation device, Int. J. Therm. Sci. 77 (2014) 158–164.

[53] Y. Wu, S. Wu, L. Xiao, Performance analysis of photovoltaic – thermoelectric hybrid system with and without glass cover, Energy Convers. Manag. 93 (2015) 151–159.

[54] S. Sarangi, K.K. Bodla, S. V. Garimella, J.Y. Murthy, Manifold microchannel heat sink design using optimization under uncertainty, Int. J. Heat Mass Transf. 69 (2014) 92–105.

[55] K. Yang, C. Zuo, A novel multi-layer manifold microchannel cooling system for concentrating photovoltaic cells, Energy Convers. Manag. 89 (2015) 214–221.

[56] R. Kandasamy, X. Wang, A. Mujumdar, Application of phase change materials in thermal management of electronics, Appl. Therm. Eng. 27 (2007) 2822–2832.

[57] F.L. Tan, C.P. Tso, Cooling of mobile electronic devices using phase change materials, Appl. Therm. Eng. 24 (2004) 159–169.

[58] S. Maiti, S. Banerjee, K. Vyas, P. Patel, P.K. Ghosh, Self regulation of photovoltaic module temperature in V-trough using a metal–wax composite phase change matrix, Sol. Energy. 85 (2011) 1805–1816.

[59] L. Tan, Y. Kwok, A. Date, A. Akbarzadeh, Numerical Analysis of Natural Convection Effects in Latent Heat Storage Using Different Fin Shapes, Int. J. Energy Sci. 1 (2011) 162–168.

[60] L. Tan, B. Singh, A. Date, A. Akbarzadeh, Sustainable Thermoelectric Power System Using Concentrated Solar Energy and Latent Heat Storage, in: Int. Conf. Power Energy, IEEE, 2012: pp. 2–5.

[61] M.Y.H. Othman, B. Yatim, K. Sopian, M.N. Abu Bakar, Performance analysis of a double-pass photovoltaic/thermal (PV/T) solar collector with CPC and fins, Renew. Energy. 30 (2005) 2005–2017.

[62] S. Jian, S. Mingheng, Numerical Simulation of Electric-Thermal Performance of A Solar Concentrating Photovoltaic / Thermal System, In Power and Energy Engineering Conference, 2009. APPEEC 2009. Asia-Pacific (pp. 1-4). IEEE.

[63] E. Cuce, P.M. Cuce, Improving thermodynamic performance parameters of silicon photovoltaic cells via air cooling, Int. J. Ambient Energy. (2013) 1–7.

[64] F. Al-Amri, T.K. Mallick, Alleviating operating temperature of concentration solar cell by air active cooling and surface radiation, Appl. Therm. Eng. 59 (2013) 348–354.

[65] F. CHENLO, M. CID, A linear concentrator photovoltaic module: analysis of non-uniform illumination and temperature effects on efficiency, Sol. Cells. 20 (1987) 27–39.

[66] W.E. Horne, Solar energy system, US Patent 5,269,851, 1993.

[67] J.B. Lasich, Cooling circuit for receiver of solar radiation, US Patent 7,076,965, 2006.

[68] M. Kolhe, D. Bin, E. Hu, Water Cooled Concentrated Photovoltaic System, Int. J. Smart Grid Clean Energy. 2 (2012) 2–6.

[69] K.-K. Chong, W.-C. Tan, Study of automotive radiator cooling system for dense-array concentration photovoltaic system, Sol. Energy. 86 (2012) 2632–2643.

[70] D. Correia, A.M. Shulenberger, J. Braig, Concentrated Photovoltaic and Thermal Solar Energy Collector, US Patent 8,455,755, 2013.

[71] L. Tan, X. Ji, M. Li, C. Leng, X. Luo, H. Li, The experimental study of a two-stage photovoltaic thermal system based on solar trough concentration, Energy Convers.

Manag. 86 (2014) 410–417.

[72] M. Kuo, W. Lo, S. Member, A Combination of Concentrator Photovoltaics and Water Cooling System to Improve Solar Energy Utilization, IEEE Trans. Components, Packag. Manuf. Technol. 50 (2014) 2818–2827.

[73] M. Chaabane, H. Mhiri, P. Bournot, Performance Optimization of Water-Cooled Concentrated Photovoltaic System Performance Optimization of Water-Cooled Concentrated Photovoltaic System, Heat Transf. Eng. 37 (2016) 78–81.

[74] J.S. Coventry, Performance of a concentrating photovoltaic/thermal solar collector, Sol. Energy. 78 (2005) 211–222.

[75] G. Mittelman, A. Kribus, O. Mouchtar, A. Dayan, Water desalination with concentrating photovoltaic/thermal (CPVT) systems, Sol. Energy. 83 (2009) 1322–1334.

[76] P.J. Sonneveld, G.L. a. M. Swinkels, B. a. J. Van Tuijl, H.J.J. Janssen, J. Campen, G.P. a. Bot, Performance of a concentrated photovoltaic energy system with static linear Fresnel lenses, Sol. Energy. 85 (2011) 432–442.

[77] T. Kerzmann, L. Schaefer, System simulation of a linear concentrating photovoltaic system with an active cooling system, Renew. Energy. 41 (2012) 254–261.

[78] C.L. Ong, W. Escher, S. Paredes, A.S.G. Khalil, B. Michel, A novel concept of energy reuse from high concentration photovoltaic thermal (HCPVT) system for desalination, Desalination. 295 (2012) 70–81.

[79] M. Li, X. Ji, G.L. Li, Z.M. Yang, S.X. Wei, L.L. Wang, Performance investigation and optimization of the Trough Concentrating Photovoltaic/Thermal system, Sol. Energy. 85 (2011) 1028–1034.

[80] X. Xu, M.M. Meyers, B.G. Sammakia, B.T. Murray, Thermal Modeling of Hybrid Concentrating PV / T Collectors with Tree-shaped Channel Networks Cooling System, in: 13th IEEE Intersoc. Conf. onThermal Thermomechanical Phenom. Electron. Syst. (ITherm), IEEE, 2012: pp. 1131–1138.

[81] C. Renno, F. Petito, Design and modeling of a concentrating photovoltaic thermal (CPV/T) system for a domestic application, Energy Build. 62 (2013) 392–402.

[82] R. Künnemeyer, T.N. Anderson, M. Duke, J.K. Carson, Performance of a V-trough photovoltaic/thermal concentrator, Sol. Energy. 101 (2014) 19–27.

[83] H. Helmers, A.W. Bett, J. Parisi, C. Agert, Modeling of concentrating photovoltaic and thermal systems, Prog. Photovoltaics Res. Appl. 22 (2014) 427–439.

[84] G. Kosmadakis, D. Manolakos, G. Papadakis, Simulation and economic analysis of a CPV / thermal system coupled with an organic Rankine cycle for increased power generation, Sol. Energy. 85 (2011) 308–324.

[85] N. Xu, J. Ji, W. Sun, L. Han, H. Chen, Z. Jin, Outdoor performance analysis of a 1090 Â point-focus Fresnel high concentrator photovoltaic / thermal system with triple-junction solar cells, Energy Convers. Manag. 100 (2015) 191–200.

[86] M.I. Hussain, G.H. Lee, Experimental and numerical studies of a U-shaped solar energy collector to track the maximum CPV / T system output by varying the fl ow rate, Renew. Energy. 76 (2015) 735–742.

[87] H.M. Bahaidarah, B. Tanweer, P. Gandhidasan, S. Rehman, A Combined Optical, Thermal and Electrical Performance Study of a V-Trough PV System—Experimental and Analytical Investigations, Energies. 8 (2015) 2803–2827.

[88] H. Baig, N. Sellami, D. Chemisana, J. Rosell, T.K. Mallick, Performance analysis of a dielectric based 3D building integrated concentrating photovoltaic system, Sol. Energy. 103 (2014) 525–540.

[89] H. Baig, N. Sellami, T.K. Mallick, Performance modeling and testing of a Building Integrated Concentrating Photovoltaic ( BICPV ) system $, Sol. Energy Mater. Sol. Cells. 134 (2015) 29–44.

[90] L.M. Candanedo, A. Athienitis, K.-W. Park, Convective Heat Transfer Coefficients in a Building-Integrated Photovoltaic/Thermal System, J. Sol. Energy Eng. 133 (2011) 21002.

[91] C.M. Jubayer, P. Karava, E. Savory., Building-Integrated Photovoltaic / Thermal Systems – Numerical Prediction of Exterior Convective Heat Transfer Coefficients and Parametric Analysis, in: Int. High Perform. Build. Conf., Purdue University, 2010.

[92] D. Babic, D.B. Murray, A. a. Torrance, Mist jet cooling of grinding processes, Int. J. Mach. Tools Manuf. 45 (2005) 1171–1177.

[93] A. Royne, C.J. Dey, Design of a jet impingement cooling device for densely packed PV cells under high concentration, Sol. Energy. 81 (2007) 1014–1024.

[94] J. Barrau, A. Perona, A. Dollet, J. Rosell, Outdoor test of a hybrid jet impingement / micro-channel cooling device for densely packed concentrated photovoltaic cells, Sol. Energy. 107 (2014) 113–121.

[95] a. Al-Alili, Y. Hwang, R. Radermacher, I. Kubo, A high efficiency solar air conditioner using concentrating photovoltaic/thermal collectors, Appl. Energy. 93 (2012) 138–147.

[96] A.A. Hegazy, Comparative study of the performances of four photovoltaic/thermal solar air collectors, Energy Convers. Manag. 41 (2000) 861–881.

[97] A. Tiwari, M.S. Sodha, A. Chandra, J.C. Joshi, Performance evaluation of photovoltaic thermal solar air collector for composite climate of India, Sol. Energy Mater. Sol. Cells. 90 (2006) 175–189.

[98] A.S. Joshi, A. Tiwari, G.N. Tiwari, I. Dincer, B. V. Reddy, Performance evaluation of a hybrid photovoltaic thermal (PV/T) (glass-to-glass) system, Int. J. Therm. Sci. 48 (2009) 154–164.

[99] S.C. Solanki, S. Dubey, A. Tiwari, Indoor simulation and testing of photovoltaic thermal (PV/T) air collectors, Appl. Energy. 86 (2009) 2421–2428.

[100] P. Barnwal, A. Tiwari, Thermodynamic performance analysis of a hybrid Photovoltaic-Thermal (PV/T) integrated greenhouse air heater and dryer, Int. J. Exergy. 6 (2009) 111–130.

[101] F. Sarhaddi, A. Farahat, S., Ajam, H. and Behzadmehr, Exergetic optimization of a solar photovoltaic thermal (PV/T) air collector, Int. J. Energy Res. 35 (2011) 813–827.

[102] D. Kamthania, S. Nayak, G.N. Tiwari, Performance evaluation of a hybrid photovoltaic thermal double pass facade for space heating, Energy Build. 43 (2011) 2274–2281.

[103] M. Gholampour, M. Ameri, Design Considerations of Unglazed Transpired Collectors: Energetic and Exergetic Studies, J. Sol. Energy Eng. 136 (2014) 31004.

[104] S. Singh, S. Agarwal, G.N. Tiwari, D. Chauhan, Application of genetic algorithm with multi-objective function to improve the efficiency of glazed photovoltaic thermal system

for New Delhi (India) climatic condition, Sol. Energy. 117 (2015) 153–166.

[105] S. Nižetić, F. Grubišić- Čabo, I. Marinić-Kragić, A.M. Papadopoulos, Experimental and numerical investigation of a backside convective cooling mechanism on photovoltaic panels, Energy. 111 (2016) 211–225.

[106] B.J. Huang, T.H. Lin, W.C. Hung, F.S. Sun, Performance evaluation of solar photovoltaic / thermal systems, Sol. Energy. 70 (2001) 443–448.

[107] Y. Tripanagnostopoulos, T.H. Nousia, M. Souliotis, P. Yianoulis, hybrid photovoltaic / thermal solar systems, Sol. Energy. 72 (2002) 217–234.

[108] H.A. Zondag, D.W. de Vries, W.G.J. van Helden, R.J.C. van Zolingen, A.A. van Steenhoven, The yield of different combined PV-thermal collector designs, Sol. Energy. 74 (2003) 253–269.

[109] G. Vokas, N. Christandonis, F. Skittides, Hybrid photovoltaic–thermal systems for domestic heating and cooling—A theoretical approach, Sol. Energy. 80 (2006) 607–615.

[110] T.T. Chow, W. He, J. Ji, Hybrid photovoltaic-thermosyphon water heating system for residential application, Sol. Energy. 80 (2006) 298–306.

[111] S. Dubey, G.N. Tiwari, Thermal modeling of a combined system of photovoltaic thermal (PV/T) solar water heater, Sol. Energy. 82 (2008) 602–612.

[112] S. Kumar, A. Tiwari, Design, fabrication and performance of a hybrid photovoltaic/thermal (PV/T) active solar still, Energy Convers. Manag. 51 (2010) 1219–1229.

[113] J.I. Bilbao, A.B. Sproul, EXPERIMENTAL RESULTS OF A PVT-WATER MODULE DESIGN FOR DEVELOPING COUNTRIES, in: Proceeding 50th Annu. Conf. Aust. Sol. Energy Soc., 2012: pp. 1–11.

[114] G. Li, G. Pei, M. Yang, J. Ji, Experiment Investigation on Electrical and Thermal Performances of a Semitransparent Photovoltaic / Thermal System with Water Cooling, Int. J. Photoenergy. 2014 (2014) 1–19.

[115] G. Evola, L. Marletta, Exergy and thermoeconomic optimization of a water-cooled glazed hybrid photovoltaic/thermal (PVT) collector, Sol. Energy. 107 (2014) 12–25.

[116] J. Yazdanpanahi, F. Sarhaddi, M. Mahdavi Adeli, Experimental investigation of exergy efficiency of a solar photovoltaic thermal (PVT) water collector based on exergy losses, Sol. Energy. 118 (2015) 197–208.

[117] S. Nižetić, D. Čoko, A. Yadav, F. Grubišić-Čabo, Water spray cooling technique applied on a photovoltaic panel: The performance response, Energy Convers. Manag. 108 (2016) 287–296.

[118] T.N. Anderson, M. Duke, G.L. Morrison, J.K. Carson, Performance of a building integrated photovoltaic/thermal (BIPVT) solar collector, Sol. Energy. 83 (2009) 445–455.

[119] B. Agrawal, G.N. Tiwari, Life cycle cost assessment of building integrated photovoltaic thermal (BIPVT) systems, Energy Build. 42 (2010) 1472–1481.

[120] B. Agrawal, G.N. Tiwari, Optimizing the energy and exergy of building integrated photovoltaic thermal (BIPVT) systems under cold climatic conditions, Appl. Energy. 87 (2010) 417–426.

[121] T. Yang, A.K. Athienitis, A study of design options for a building integrated photovoltaic/thermal (BIPV/T) system with glazed air collector and multiple inlets, Sol. Energy. 104 (2014) 82–92.

[122] Y. Wang, S. Ke, F. Liu, J. Li, G. Pei, Performance of a building-integrated photovoltaic / thermal system under frame shadows, Energy Build. 134 (2017) 71–79.

[123] N. Gupta, A. Tiwari, G.N. Tiwari, Exergy analysis of building integrated semitransparent photovoltaic thermal (BiSPVT) system, Eng. Sci. Technol. an Int. J. 20 (2016) 41–50.

[124] M.J. Huang, P.C. Eames, B. Norton, Thermal regulation of building-integrated photovoltaics using phase change materials, Int. J. Heat Mass Transf. 47 (2004) 2715–2733.

[125] M.J. Huang, P.C. Eames, B. Norton, Phase change materials for limiting temperature rise in building integrated photovoltaics, Sol. Energy. 80 (2006) 1121–1130.

[126] A. Hasan, S.J. McCormack, M.J. Huang, B. Norton, Evaluation of phase change materials for thermal regulation enhancement of building integrated photovoltaics, Sol. Energy. 84 (2010) 1601–1612.

[127] P.H. Biwole, P. Eclache, F. Kuznik, Phase-change materials to improve solar panel's performance, Energy Build. 62 (2013) 59–67.

[128] M.S. Sodha, D. Buddhi, R.L. Sawhney, Optimization of pipe parameters of an underground air pipe cooling system, Energy Convers. Manag. 34 (1993) 465–470.

[129] G. Sharan, R. Jadhav, Performance of single pass earth tube heat exchanger: An experimental study, Indian Inst. Manag. Ahmedabad. IIMA (2003) 1-18.

[130] F. Al-Ajmi, D.L. Loveday, V.I. Hanby, The cooling potential of earth–air heat exchangers for domestic buildings in a desert climate, Build. Environ. 41 (2006) 235–244. doi:10.1016/j.buildenv.2005.01.027.

[131] R. Kumar, A.R. Sinha, B.K. Singh, U. Modhukalya, A design optimization tool of earth-to-air heat exchanger using a genetic algorithm, Renew. Energy. 33 (2008) 2282–2288.

[132] A. Chel, G.N. Tiwari, Performance evaluation and life cycle cost analysis of earth to air heat exchanger integrated with adobe building for New Delhi composite climate, Energy Build. 41 (2009) 56–66.

[133] V. Bansal, R. Misra, G. Das Agrawal, J. Mathur, Performance analysis of earth–pipe–air heat exchanger for summer cooling, Energy Build. 42 (2010) 645–648.

[134] S. Jakhar, R. Misra, V. Bansal, M.S. Soni, Thermal performance investigation of earth air tunnel heat exchanger coupled with a solar air heating duct for northwestern India, Energy Build. 87 (2015) 360–369.

[135] S. Jakhar, R. Misra, M.S. Soni, N. Gakkhar, Parametric simulation and experimental analysis of earth air heat exchanger with solar air heating duct, Eng. Sci. Technol. an Int. J. 19 (2016) 1059–1066.

[136] P.D. me. Joen, Christophe T, Liu Liping, Comparison of Earth-Air and Earth-Water Ground Tube Heat Exchangers for Residentialal Application, in: Int. Refrig. Air Cond. Conf. Purdue Univ., 2012: pp. 2194–10.

[137] A. Chel, A. Janssens, M. De Paepe, Thermal performance of a nearly zero energy passive house integrated with the air-air heat exchanger and the earth-water heat exchanger, Energy Build. 96 (2015) 53–63.

[138] S.B. Shah, Z.A. Lentz, E. van Heugten, R.D. Currin Jr, I. Singletary, Tempering ventilation air in a swine finishing barn with a low-cost earth-to-water heat exchanger, J. Renew. Sustain. Energy. 9 (2017) 23901.

[139] R. Misra, V. Bansal, G. Das Agarwal, J. Mathur, T. Aseri, Evaluating Thermal Performance and Energy Conservation Potential of Hybrid Earth Air Tunnel Heat Exchanger in Hot and Dry Climate—In Situ Measurement, J. Therm. Sci. Eng. Appl. 5 (2013) 31006.

[140] V. Bansal, R. Misra, G. Das Agrawal, J. Mathur, Performance analysis of earth–pipe–air heat exchanger for winter heating, Energy Build. 41 (2009) 1151–1154.

[141] M. Li, G.L. Li, X. Ji, F. Yin, L. Xu, The performance analysis of the trough concentrating solar photovoltaic/thermal system, Energy Convers. Manag. 52 (2011) 2378–2383.

[142] A.S. Joshi, A. Tiwari, Energy and exergy efficiencies of a hybrid photovoltaic-thermal (PV/T) air collector, Renew. Energy. 32 (2007) 2223–2241.

[143] J.A. Duffie, W.A. Beckman, Solar engineering of thermal processes, John Wiley & Sons, 2013.

[144] D.L. Evans, Simplified method for predicting photovoltaic array output, Sol. Energy. 27 (1981) 555–560.

[145] T. Schott, Operation temperatures of pv modules: a theoretical and experimental approach, in: EC Photovolt. Sol. Energy Conf. 6, 1985: pp. 392–396.

[146] D. Atheaya, A. Tiwari, G.N. Tiwari, Experimental validation of a fully covered photovoltaic thermal compound parabolic concentrator system, Eng. Sci. Technol. an Int. J. 19 (2016) 1845–1856.

[147] J.P. Holman, Heat transfer 9th Edition, New York, Boston, McGraw-Hill, Inc. (2002) 168–169.

[148] F.P. Incropera, D.P. De Witt, Fundamentals of heat and mass transfer, John Wiley & Sons, 2009.

[149] A. Tiwari, M.S. Sodha, Performance evaluation of solar PV/T system: An experimental validation, Sol. Energy. 80 (2006) 751–759.

[150] A. Tiwari, M.S. Sodha, A. Chandra, J.C. Joshi, Performance evaluation of photovoltaic thermal solar air collector for composite climate of India, Sol. Energy Mater. Sol. Cells. 90 (2006) 175–189.

[151] J.P. Holman, W.J. Gajda, Experimental methods for engineers, McGraw-Hill New York, 1994.

[152] N. Gakkhar, M.S. Soni, S. Jakhar, Second law thermodynamic study of solar assisted distillation system: A review, Renew. Sustain. Energy Rev. 56 (2016) 519–535.

[153] I. Dincer, M.A. Rosen, Exergy: energy, environment and sustainable development, second edition, Elsevier, Oxford., 2012.

[154] R. Petela, Exergy of undiluted thermal radiation, Sol. Energy. 74 (2003) 469–488.

[155] F. Sarhaddi, S. Farahat, H. Ajam, A. Behzadmehr, Exergetic Optimization of a Solar Photovoltaic Array, J. Thermodyn. (2009) 1–11.

[156] Y.A. Cengel, M.A. Boles, Thermodynamics: an engineering approach, New York, Boston, McGraw-Hill, Inc. (2003)

[157] H. Esen, M. Inalli, M. Esen, K. Pihtili, Energy and exergy analysis of a ground-coupled heat pump system with two horizontal ground heat exchangers, Build. Environ. 42 (2007) 3606–3615.

# List of Publications and Awards

**International Journals**

1. **Sanjeev Jakhar,** Manoj S. Soni, Robert F Boehm, "Thermal modelling of a rooftop photovoltaic/thermal system with earth air heat exchanger for combined power and space heating", Journal of Solar Energy Engineering, (ASME), Volume 140 (3), March 2018, Pages 031011-15, ISSN:0199-6231 **(Impact factor: 1.19, SCI ).**

2. **Sanjeev Jakhar** and Manoj S. Soni, "Experimental and theoretical analysis of glazed tube-and-sheet photovoltaic/thermal system with earth water heat exchanger cooling", Energy conversion and management (Elsevier), Volume 153, December 2017, Pages 576-588, ISSN: 0196-8904 **(Impact factor: 5.589, SCI ).**

3. **Sanjeev Jakhar**, Manoj S. Soni, Nikhil Gakkhar, An integrated photovoltaic thermal solar (IPVTS) system with earth water heat exchanger cooling: Energy and exergy analysis" Solar Energy (Elsevier), Volume 157, November 2017, Pages 81-93, ISSN: 0038-092X **(Impact factor: 4.018, SCI).**

4. **Sanjeev Jakhar,** Manoj S. Soni, Nikhil Gakkhar, "Exergy analysis of a photovoltaic thermal system with earth water heat exchanger cooling system based on experimental data", International journal of exergy (Inderscience), Volume 23, Issue 4, September 2017, Pages 367-387, ISSN online: 1742-8300 **(Impact factor: 1.377, SCI).**

5. **Sanjeev Jakhar,** M.S. Soni, Nikhil Gakkhar, "Historical and recent development of concentrating photovoltaic cooling technologies", Renewable and Sustainable Energy Reviews (Elsevier), Volume 60, July 2016, Pages 41-59, ISSN: 1364-0321 **(Impact factor: 8.052, SCI).**

6. **Sanjeev Jakhar**, M.S. Soni, Nikhil Gakkhar, "Parametric modeling and simulation of photovoltaic panels with earth water heat exchanger cooling" Geothermal Energy (Springer), 2016, 4.10, ISSN: 2195-9706 **(Impact factor: 1.188, SCIE).**

7. **Sanjeev Jakhar**, M.S. Soni, Nikhil Gakkhar, "Performance analysis of earth water heat exchanger for concentrating photovoltaic cooling", Energy Procedia (Elsevier), Volume 90, 2016, pages 145-153, ISSN: 1876-6102 **(Scopus Indexed).**

8. **Sanjeev Jakhar,** M.S. Soni, Nikhil Gakkhar, "Performance analysis of photovoltaic panels with earth water heat exchanger", MATEC web of Conferences, Volume 55, 2016, pages 1-6, ISSN: 2261-236X **(Scopus Indexed).**

9. **Sanjeev Jakhar,** M.S. Soni, Nikhil Gakkhar, "Modelling and simulation of concentrating photovoltaic system with earth water heat exchanger", Energy Procedia (Elsevier), Volume 109, 2017, pages 78-85, ISSN: 1876-6102 **(Scopus Indexed).**

**International Conferences**

1. Sravan Raj P**.,** Soni M.S. and **Jakhar Sanjeev**, A review on Photovoltaic/Thermal and Concentrated Photovoltaic/Thermal hybrid solar technology. International Congress on Renewable Energy (ICORE)-2014, "*Powering National Growth Through Solar", Manekshaw Centre, Parade Road, Delhi Cantonment, New Delhi, December 8 - 9, 2014 pp: 282-289.*

## Awards:

- Awarded prestigious Building Energy Efficiency Higher & Advanced Network (BHAVAN) Internship Program, 2017 from the Department of Science and Technology (DST), the government of India and the Indo-US science and technology forum for the research visit for the duration of three months (June, 2017 to August, 2017) in the University of Nevada, Las Vegas, USA.
- Awarded DAAD (German Academic Exchange Service) fellowship for the research visit (November, 2016 to December, 2016) in the IWF, Technical University Braunschweig, Germany.
- Awarded a travel grant from the Department of Science and Technology (DST) Govt. Of India, New Delhi for the presenting a research paper in the International conference on Renewable Energy and Smart Grid in Bangkok, Thailand (20th to 22nd March 2016).

## About the candidate (Sanjeev Jakhar)

Sanjeev Jakhar is working as a Ph.D. research scholar in Mechanical Engineering Department, Birla Institute of Technology and Science Pilani (BITS), Pilani Campus, Rajasthan, India since August, 2013. He is a graduate in the discipline of Mechanical Engineering from University of Rajasthan, Jaipur, India in 2009, post-graduate in Mechanical Engineering with specialization in Thermal Engineering from Jai Narain Vyas University (MBM engineering college), Jodhpur, India in 2013 and pursuing PhD in renewable energy from BITS Pilani, Pilani campus, India. He has published various research papers in internationals journals of repute, one book, and many technical papers in international conferences. His areas of research interest are in solar PV and CPV cooling, Geothermal cooling and Solar water distillation, etc.

## About the Supervisor (Dr. Manoj Kumar Soni)

Dr. Manoj Soni is B.E. Mechanical, M.E. Thermal Power, Ph.D. in Energy Efficiency. He has @22 yrs teaching and research experience. He served as a faculty at VNIT, Nagpur 1995-2002. He joined BITS Pilani as a faculty in 2002. He is coordinator of Centre for Renewable Energy and Environment Development at BITS, Pilani.

His research interest includes solar thermal, thermal engineering, renewable energy and energy efficiency. He has total 28 publications in international journals and international conferences. He has submitted one patent. He is guiding four PhD students and has guided over 50 PG and UG thesis. He has developed a course named "Energy Technology" under National Mission Project on Education through ICT: Developing suitable pedagogical methods for various classes intellectual calibers and research in e-learning - anchored by IIT Kharagpur.

As a research team member, he visited PT Indo Bharat Rayon,Indonesia in 2011. In 2015 he was awarded scholarship under university immersion scheme of BITS and visited University of South Florida, Tampa, USA.

With special interest in spirituality, he intertwined spirituality and thermodynamics. His most coveted lecture on Spiritual thermodynamics is very well appreciated by the students, academicians and industrial personnel. He delivered this lecture at USF, Tampa also.

He is actively involved in industrial collaborations in Work Integrated Programs Division as coordinator of various collaborative programs: B.Tech Power and Process Engg, BS Engg Design, M.Tech Engineering Management, M.Tech Embedded Systems for NTPC, THDC, ESSAR Power, Tata Power, JSW, Aditya Birla Group, Vedanta, L&T, Mahindra & Mahindra. He has conducted training programs on *Steam and Power Balance*, *Boiler Technology*, and *Power Plant Performance Calculations* for the executives of Grasim Industries at various locations.

He is FIE, and Life member of International Solar Energy Society, and Energy and Fuels Users Association of India. He is associate member of Solar Cookers International, USA and Senior Member, Universal Association of Mechanical and Aeronautical Engineers.

His web page is http://universe.bits-pilani.ac.in/pilani/mssoni/profile